Carbon Nanomaterial based Flexible Pressure/Strain Sensors for Wearable Electronics

THESIS

Submitted in partial fulfillment of the requirements for the degree of

DOCTOR OF PHILOSOPHY

by

Suraj Baloda

ID No. 2018PHXF0445P

Under the supervision of

Prof. Navneet Gupta

and

Under the co-supervision of

Dr. Sumitra Singh

BIRLA INSTITUTE OF TECHNOLOGY AND SCIENCE

PILANI (RAJASTHAN) INDIA

March 2024

BIRLA INSTITUTE OF TECHNOLOGY AND SCIENCE

DEPARTMENT OF ELECTRICAL AND ELECTRONICS ENGINEERING

PILANI- CAMPUS PILANI (RAJASTHAN) INDIA

CERTIFICATE

This is to certify that the thesis entitled **"Carbon Nanomaterial based Flexible Pressure/Strain Sensors for Wearable Electronics"** submitted by **Suraj Baloda,** ID. No. **2018PHXF0445P** for an award of Ph.D. of the Institute embodies his original work under my supervision.

Signature of the Supervisor

Name **Prof. (Dr.) Navneet Gupta**

Designation **Professor, Department of Electrical & Electronics Engineering Birla Institute of Technology and Science, Pilani, Pilani-Campus Rajasthan, INDIA**

Date 20/03/2024

Signature of the Co-Supervisor

Name **Dr. Sumitra Singh**

Designation **Principal Scientist, Semiconductor Sensors and Microsystems Group, CSIR- Central Electronics Engineering Research Institute (CEERI), Pilani, Rajasthan, INDIA**

Date 20/03/2024

BIRLA INSTITUTE OF TECHNOLOGY AND SCIENCE

DEPARTMENT OF ELECTRICAL AND ELECTRONICS ENGINEERING

PILANI- CAMPUS PILANI (RAJASTHAN) INDIA

DECLARATION

I hereby declare that this submission is solely my original work. To the best of my knowledge and belief, it does not include any content previously published or authored by another individual, nor does it incorporate material that has substantially contributed to the conferral of any other academic degree or diploma from a university or other institution of higher learning.

I further authorize the Birla Institute of Technology and Science (BITS), Pilani to reproduce this thesis, either in whole or in part, through photocopying or any other means. This authorization extends to fulfilling requests from other institutions or individuals exclusively for scholarly research purposes.

Signature 

Name **Suraj Baloda**

Date 20/03/2024

ACKNOWLEDGEMENT

I would like to express my sincere gratitude to all those who have contributed to completing this thesis. First and foremost, I am grateful to my supervisors, Prof. Navneet Gupta and Dr. Sumita Singh, for their unwavering support, guidance, and expertise throughout the entire research process. Their combined insights and encouragement played a crucial role in shaping the direction and quality of this thesis.

I am highly thankful to my Doctoral Advisory Committee members, Prof. Rajkumar Gupta and Prof. Arnab Hazra, for their insightful feedback and constructive criticism. Their expertise greatly enriched the quality of this research. I am indebted to Dr. T Eshwar, Senior Scientist, Semiconductor Device Fabrication Group, CSIR-CEERI, Pilani, for his insightful suggestions and devoted time to this work. I thank Central Analytical Laboratory, BITS Pilani, for providing access to characterization facilities. Financial support from the Council of Scientific and Industrial Research (CSIR), India government, through fellowship grant number 09/719(0102)/2019-EMR-I, allowed me to focus on my research without financial constraints.

I am grateful to the EEE department, BITS-Pilani, for providing the necessary resources and facilities to conduct this research. The academic environment and resources offered by the department were instrumental in the successful completion of this thesis. I am thankful to Prof. Praveen Kumar A. V. (Convener-Departmental Research Committee), Dr. Sujan Yenuganti, Dr. Meetha V. Shenoy, and other faculty colleagues of the EEE department for their constant motivation and encouragement. Special thanks to Prof. V. Ramgopal Rao, Vice-Chancellor of BITS Pilani, and Prof. Sudhirkumar Barai, Director BITS Pilani, Pilani campus, for allowing me to pursue my research successfully.

I am grateful to my friends and colleagues, Dr. Surjeet Chachal, Dr. Anil Kumar, Dr. Ankita Dixit, Jeevan Kittur, Premsai Regalla, Sudhir Kumar Mitharwal for being with me during my research days. At the same time, I am grateful to all the staff members, especially Mahesh Chandra Saini of the EEE department, for their support.

Last but not least, I would like to give love and thanks to my parents, Mr Shivpal Singh and Mrs Kavita Devi, for their unwavering support and understanding throughout this academic endeavor. Thanks to my wife Ritika Choudhary for her enormous sacrifice to support my work. I deeply value the cooperation and support from my brother Manish Baloda, my mother-in-law Mrs Prem, father-in-law Mr. Satyapal Choudhary and other family members.

Suraj Baloda

(2018PHXF0445)

Dedicated

to

My Son RIVANSH

ABSTRACT

This thesis explores the design, fabrication, and application of flexible strain, pressure and dry electrodes utilizing carbon nanomaterials for wearable electronics. Recent years have witnessed the emergence of wearable electronics, characterized by soft, bendable, and stretchable properties that conform to diverse surfaces. The advancements in flexible sensors and dry electrodes find relevance in bio-signal detection for health monitoring systems. Unlike traditional rigid and planar sensors and dry electrodes, which struggle with the soft and curvilinear nature of the human body, flexible and wearable sensors have garnered attention. These sensors offer the capability for personalized, continuous, long-term, and real-time bio-signal measurements without causing discomfort to the patient.

The fabrication of wearable sensors predominantly relies on the utilization of flexible materials, including flexible polymers as substrate and nanomaterials and conductive polymers as active elements. Among the various wearable sensors, flexible strain, pressure sensors, and dry electrodes have gained extensive research interest due to potential applications in human motion detection, health monitoring, wrist pulse and respiratory rate monitoring, electrophysiological signal detection and human-machine interfaces. Carbon nanomaterials, such as graphene and carbon nanotubes, present unique properties that make them ideal candidates for developing highly sensitive flexible sensors and dry electrodes. Flexible sensors and dry electrodes represent simple devices with easy operation, amenable to fabrication through cost-effective and scalable methods. Despite notable advancements, the primary challenge remains the development of wearable sensors that exhibit high sensitivity, low and large working range, and attributes such as durability, bio-compatibility, conformability, re-usability, and wearability comfort. Addressing these multifaceted requirements is vital for achieving continuous and long-term bio-signal monitoring.

We have reported the fabrication of graphene nanoplatelets (GNP)/ Polydimethylsiloxane (PDMS) based flexible resistive strain sensor by a simple, low-cost screen printing method and demonstrated its potential applications in health monitoring. The GNP/PDMS strain sensor exhibits good strain sensitivity, stretchability up to 65% with a gauge factor of 62.5. The proposed sensor effectively detects subtle strains and monitors various human movements, such as wrist

pulse and finger bending movements. Further, we employed a low-pressure chemical vapor deposition (LPCVD) technique on copper foil to produce high-quality multilayer graphene, subsequently transferred onto a flexible PDMS substrate. Raman spectroscopy and FESEM analysis confirmed the graphene's multilayer structure and high quality, while XPS analysis further reinforced its excellent quality. Additionally, we have fabricated dry electrodes using a spray-coating method by depositing reduced graphene oxide (rGO) on a PDMS substrate. The rGO-PDMS dry electrodes demonstrate the ability to capture and relay weak electrophysiological signals, such as ECG and EMG, without significant attenuation or distortion. Experimental results show that when compared to conventional wet Ag/AgCl electrodes, the fabricated rGO-PDMS electrodes measure higher-quality ECG signals with improved SNR while offering similar contact quality and electrode-skin impedance despite being a dry electrode. The fabricated rGO-PDMS electrodes demonstrated excellent performance and applicability, making them suitable for wearable long-term health monitoring devices.

Further, we have fabricated pressure sensors using MWCNT/PDMS composites with varying MWCNT contents. These sensors mechanical and electrical properties have been thoroughly assessed. The MWCNT/PDMS composite pressure sensors exhibit remarkable sensitivity (0.02715–0.08283 kPa^{-1}) across a broad pressure range from 0.1 to 100 kPa. Furthermore, the strain-sensing properties of the MWCNT composite demonstrate high reliability through a cyclic stretching test, with consistent performance over 1000 repetitive cycles. The fabricated flexible pressure sensor as wearable electronic skin is successfully applied to human skin for monitoring human wrist pulse.

Finally, we present a novel electronic glove (e-glove) based on SWCNT/PDMS for Human-Machine Interface (HMI) applications. The fabrication process and a detailed mechanical and electrical performance analysis are discussed. The e-glove serves as a strain sensor, and its potential applications in detecting finger gestures are explored. The SWCNT/PDMS strain sensor exhibits a high gauge factor of 73, indicating sensitivity suitable for precise finger gesture detection. The e-glove records strain distribution when gripping or releasing soft objects. Experimental results validate the successful control of a robot finger through the integration of SWCNT/PDMS strain sensors onto the e-glove.

Table of Contents

Certificate ----------**i**

Declaration----------ii

Acknowledgements----------**iii**

Abstract ----------**vi**

Table of Contents ----------**viii**

List of Figures----------**xi**

List of Tables ----------**xviii**

List of Symbols and Abbreviations ----------**xix**

Chapter: 1
Introduction

1.1 Background and Motivation ----------1
1.2 Challenges and Issues----------6
1.3 Objectives ----------7
1.4 Thesis Structure ----------8
References ----------9

Chapter: 2
Literature Review

2.1 Introduction to flexible sensors ----------13
2.2 Flexible strain sensors ----------14
2.3 Flexible pressure sensors ----------18
2.4 Performance parameters of flexible strain and pressure sensors ----------20

2.4.1 Sensitivity and stretchability ----------22
2.4.2 Working range ----------23
2.4.3 Stability and durability ----------23
2.4.4 Linearity ----------24
2.4.5 Hysteresis ----------24
2.4.6 Response and recovery time ----------24

2.5 Graphene ----------26
2.6 Graphene synthesis ----------27

2.6.1 Chemical vapor deposition (CVD) ----------28
2.6.2 Mechanical exfoliation ----------29

2.6.3 Chemical exfoliation ----------30
2.6.4 Epitaxial growth ----------31

2.7 Carbon nanotubes ----------32
2.8 Applications of flexible strain/pressure sensors in wearable electronics ----------33

2.8.1 Human motion detection and health monitoring ----------34
2.8.2 Electronic skin (E-Skin) ----------37
2.8.3 Electrophysiological signal detection ----------40
2.8.4 Human-machine interface ----------45
2.9 Conclusions ----------47
References ----------48

Chapter: 3
PDMS and Graphene: Development, Synthesis and Characterizations

3.1 Materials ----------60
3.2 Polydimethylsiloxane (PDMS): a flexible substrate ----------60
3.3 Development of PDMS substrate ----------62
3.4 Mechanical properties of developed PDMS substrate ----------64
3.5 Reduced Graphene Oxide (rGO) synthesis ----------67
3.6 Multilayer graphene growth by low-pressure CVD (LPCVD) method ----------69
3.7 Fabrication of multilayer graphene/PDMS-based flexible strain sensor ----------70
3.8 Conclusion ----------73
References ----------74

Chapter: 4

Graphene-based Flexible Sensors: Design, Development and Applications

4.1 Graphene nanoplatelets (GNP)-based piezoresistive strain sensor ----------77
4.2. GNP fabrication on PDMS ----------78
4.2.1 Measurement of GNP-based strain sensor ----------81
4.2.2 GNP-based wrist pulse sensor ----------82
4.2.3 GNP-based strain sensor under bending ----------83
4.2.4 GNP-based resistive touch sensor ----------85
4.3 Multilayer graphene/PDMS-based flexible sensor for human motion detection-------86
4.4 Graphene-based dry electrodes ----------87
4.4.1 Fabrication of rGO -PDMS dry electrodes ----------88
4.4.2 Impedance measurement and electrode modelling ----------90
4.4.3 Electrocardiogram acquisition ----------93
4.4.4 Electromyogram acquisition ----------95
4.4 Conclusion ----------96
References ----------97

Chapter: 5

Carbon Nanotubes-based Flexible Sensors: Design, Development and Applications

5.1 MWCNTs-based flexible pressure sensor ----------102
5.2. Fabrication of MWCNTs/PDMS pressure sensor ----------104
5.2.1 Mechanical tests of fabricated MWCNTs/ PDMS composites ----------105
5.2.2 Piezo-resistive Properties of MWCNTs/PDMS composite in cyclic loading---------- 108
5.2.3 Measurements of MWCNT/PDMS pressure sensor ----------110
5.2.4 Response of MWCNTs/PDMS pressure sensor for wrist pulse monitoring ---------- 114

5.3. SWCNTs-based flexible strain sensor ----------115
5.3.1 Fabrication of SWCNTs/PDMS strain sensor ----------117
5.3.2 Fabrication of electronic glove ----------120
5.3.3 Development of robotic hand ----------121
5.3.4 Electrical performance of SWCNTs/PDMS strain sensor ----------122
5.3.5 Human robotic hand interaction and glove-based controllers ----------123
5.3.6 Finger motion detection using electronic glove ----------126
5.3.7 SWCNTs/PDMS strain sensor for HMI application ----------129
5.4 Conclusions ----------130
References ----------130

Chapter: 6

Conclusion and Future Work

6.1 Conclusion----------135
6.2 Future work ----------138

List of Patents/Publications ----------140
Biography of Candidate ----------141
Biography of Supervisor ----------142
Biography of Co-Supervisor ----------143

List of Figures

Figure 1.1. Illustrates the diverse applications of wearable electronic devices ----------1

Figure 1.2. Illustrates the diverse bio-signals emanating from the human body, along with pertinent epidermal and wearable electronics designed to detect these signals, facilitating wireless and remote healthcare for early diagnosis ----------4

Figure 2.1. Applications of recently developed flexible strain sensors ----------14

Figure 2.2. Applications of recently developed flexible pressure sensors ----------18

Figure 2.3. Schematic illustration of three common transduction mechanisms and representative devices: (a) piezoresistivity, (b) capacitance, and (c) piezoelectricity ----------19

Figure 2.4. Various performance parameters of flexible strain/pressure sensors ----------22

Figure 2.5. Schematic representation of single-layer graphene depicting the lattice arrangement of atoms (a) in-plane view and (b) stacked view of graphene layers ----------26

Figure 2.6. Flowchart illustrating the processes of graphene synthesis ----------27

Figure 2.7. Shows (a) a Schematic of a common setup for chemical vapor deposition of graphene and (b) the growth mechanism of graphene on Cu substrates by CVD ----------28

Figure 2.8. (a) Scotch tape-based mechanical exfoliation of graphene layer from bulk graphite. (b) Normal-force and shear-force-based mechanical exfoliation----------30

Figure 2.9. Schematic illustration of chemical exfoliation of graphene from graphite ----------31

Figure 2.10. Epitaxial growth of graphene by thermal decomposition of SiC, together with the structural model of bilayer graphene on SiC, the blue broken line is the buffer layer -----31

Figure 2.11. (a) Formation of three main types of carbon nanotube structures from a graphene layer, a_1 and a_2 denote unit vectors, while (n,m) denote chiral indices used to describe the exact chiralities of every nanotube: armchair shape, zigzag shape, and chiral shape and (c) representation of single-walled CNT (SWCNT) and multi-walled CNT (MWCNT)------33

Figure 2.12. Detection of human motions with the strain sensor attached to the human finger and elbow joints: (a) photographs showing the bending test of the finger, (b) the corresponding relative resistance change of the sensor in response to the finger bending, (c) the corresponding relative resistance change of the sensor in response to the different finger-bending angles, (d–f) photographs showing the bending test of the elbow, (g) the corresponding relative resistance change of the sensor in response to the sensor in response to the elbow bending ----------35

Figure 2.13. Motion responses strain sensor to (a) weak pulse signals, (b) individual pulse waveforms, (c) facial smiling expressions, (d) breathing responses of different intensities in the human body, (e) neck (inclined), (f) finger bending at different angles), (g) reciprocating elbow bending at different angles, and (h) human knee bending ----------36

Figure 2.14. Highly stretchable and fully transparent pressure sensor under discriminable strain: (a) Schematic illustration of device design (b) Transmittance curves of the sensor (c) under folding, twisting, and stretching conditions (d) Conformability of the sensor on human hands ----------38

Figure 2.15. Fabrication process of GET. (A, B) Graphene was grown on copper foil using an atmospheric pressure chemical vapor deposition system (APCVD), (C) Less than 500 nm thick PMMA was spin-coated on graphene, (D) Copper was etched away, (E) Graphene/PMMA (Gr/PMMA) was transferred onto the tattoo paper, with PMMA touching the paper and graphene facing up, (F) Gr/PMMA was cut by a mechanical cutter plotter, (G) Extraneous Gr/PMMA was peeled off from the tattoo paper, (H) Mounting GET on the skin like a temporary transfer tattoo, (I) GET on skin----------39

Figure 2.16. (a) Schematic showing the various sequences of depolarization and repolarization of the heart; (b) A typical electrocardiogram (ECG) waveform and its characteristic patterns (P and T waves, PR and ST segments, PR and QT intervals, and the QRS complex) -----41

Figure 2.17. (a) Photograph of an uncompressed graphene sponge electrode and SEM images (top-view) of the electrodes, (b) the ECG signals measured by the graphene sponge and conventional (Ag/AgCl) electrode, (c) Demonstration of the GS electrode connection to the wrist by anti-allergic tape to measure ECG without any gel or electrolyte ----------43

Figure 2.18. (a) Image of the fabricated electrode (inset: electrode wound around the forearm), (b) skin under the PDMS-based dry electrode after seven days of use, (c) skin under the Ag/AgCl electrode after two days of use ----------43

Figure 2.19. (a) Stability of LIG/PDMS electrodes, (b) ECG signals collected after different ultrasonic treatment cycles----------44

Figure. 2.20. (a) Schematic illustration of the preparation and structure of smart textile fibers with a "steel-concrete" layered structure. (b) Synchronized control of a robotic hand by human hand movements based on wearable smart textile sensors ----------46

Figure. 2.21. (a) An optical image of the e-glove system in contact with the human chest for recording ECG signals, (b) ECG signals measured for eight continuous cycles from the chest at unstretched and 15% stretched, showing reduced amplitude under stretched conditions with noise introduction, (c) Characteristic peaks of the ECG waveform, encompassing P, Q, R, S, and T waves,(d) Photographs highlight the integration of the e-glove with a wired interactive robotic hand, (e) Real-time demonstrations of human–machine interactions are captured through photographs, showcasing the control of the robotic hand via the opening and closing of a human finger equipped with the e-glove ----
----------47

Figure 3.1. Chemical structure of polydimethylsiloxane ----------62

Figure 3.2. Optical photographs of the fabrication steps of PDMS Substrate (a) mixed silicon elastomer base and silicon elastomer curing agent (b) Teflon boat (c) silicon wafer on Teflon boat (d) drop mixed solution on wafer (e) peel of PDMS (f) obtained flexible PDMS substrate ----------63

Figure 3.3. Field emission scanning electron microscopy (FESEM) images of obtained PDMS ---
----------63

Figure 3.4. (a) Design of the acrylic moulds for the mechanical testing of PDMS with their parameters (b) fabricated plain PDMS ----------64

Figure 3.5. Mark-10 instrument setup for tensile testing ----------65

Figure 3.6. Typical tensile stress-strain curves for PDMS Samples with different amounts of crosslinking ----------66

Figure 3.7. Raman spectrum of rGO synthesized using modified Hummer's method ----------68

Figure 3.8. Field emission scanning electron microscopy (FESEM) of the reduced graphene oxide: (a) at the 30 μm scale and (b) at the 500 nm scale ----------68

Figure 3.9. Temperature profile as a function of the time of graphene growth by the LPCVD system----------70

Figure 3.10. Schematic of graphene transfer process using a simple wet transfer method and multilayer graphene/PDMS-based flexible strain sensor fabrication ----------71

Figure 3.11. Raman spectra of transferred graphene with the laser wavelength of 532 nm -------72

Figure 3.12. FESEM image of the transferred graphene on the PDMS substrate ----------72

Figure 3.13. Obtain XPS spectra of transferred graphene ----------73

Figure 4.1. Optical photographs of fabricated GNP/PDMS strain sensor at (a) stretchable, (b) foldable, (c) twistable, (d) demonstration of fabricated GNP strain sensor having stretchability up to 65%----------79

Figure 4.2. Obtained Raman spectra of fabricated GNP/PDMS ----------80

Figure 4.3. FESEM images of (a) purchased GNP, (b) fabricated GNP on PDMS, (c) fabricated GNP on Carbon fiber with 100 μm scale, and (d) fabricated GNP on Carbon fiber with 1 μm scale ----------80

Figure 4.4. Experimental strain sensor setup where the inset shows the attached GNP sensor, (b) $\Delta R/R_0$ versus strain curves of the GNP/PDMS strain sensor. Relative resistance changed when the strain was applied from zero to 25 %, (c, d) graphene-based strain sensor showing the significant change in resistance upon stretching and releasing for one cycle and two cycles with time ----------81

Figure 4.5. Wrist pulse response with different substrates (a) GNP/PDMS pulse sensor; the top inset has two single pulses (b) GNP/PET pulse sensor; the top inset is a single pulse, (c)

GNP/Polyimide pulse sensor; the top inset is a single pulse, (d) GNP/Carbon fiber pulse sensor; the top inset has two single pulses ----------83

Figure 4.6. The GNP sensor shows relative change in resistance under different finger bending angles 0◦, 30◦ and 90◦. (a) corresponding signals of the bending of the finger, (b) unbending of the finger, (c) bending of flexible piper, (d) signals of PET/GNP strain sensor, (e) step response of each finger bending figure (6a and 6b) at different angles ----------84

Figure 4.7. Real-time monitoring of resistance responses of GNP/PDMS for press/release of an index finger on GNP/PDMS sensor with various press/release times (a) 1 sec, (b) 1.5 sec, (c) 2 sec, (d) 4 sec, (e) 8 sec, (f) after undergoing intensive loading-unloading cycles for 5-sec press/release time for longer period ----------86

Figure 4.8. Application of the strain sensor for human motion detection: (a) recognition of elbow bending, (b) recognition of finger bending and (c) recognition of wrist bending.----------87

Figure 4.9. The steps of fabrication of the rGO-PDMS dry electrodes: (A) Teflon mould (B) silicon wafer on Teflon mould (C) PDMS mixture spread on the wafer and a male snap button placed at the centre of the wafer (D, E) peel of PDMS with the male snap button (F) back-view and (G) front-view of obtained rGO-PDMS dry electrode ----------89

Figure 4.10. FESEM image of rGO/PDMS dry electrode at 1μm scale bars showing rGO flakes deposited over PDMS----------90

Figure 4.11. (A) Measured electrode impedance for the Ag/AgCl and fabricated rGO-PDMS electrodes and its (B) Nyquist plot form ----------91

Figure 4.12. (A) The electrode skin interface and its circuit model, (B) simplified circuit model and (C) circuit models for the measurements performed ----------92

Figure 4.13. (A) The electronic ECG data acquisition system and the (B) 3-electrode configuration were used for the simultaneous ECG measurement using wet Ag/AgCl and dry rGO PDMS electrodes----------93

Figure 4.14. ECG signals were recorded using (A) Ag/AgCl electrodes and (B) fabricated rGO-PDMS dry electrodes ----------94

Figure 4.15. Obtained ECG cycle using the rGO-PDMS dry electrodes ----------95

Figure 4.16. EMG signals were measured using (A) Ag/AgCl electrodes and (B) fabricated rGO-PDMS dry electrodes ----------96

Figure 5.1. The schematic shows the fabrication procedure of the MWCNTs/PDMS pressure sensor ----------104

Figure 5.2. FESEM images showing (a) purchased MWCNTs at 500-nm scale bars, (b) MWCNTs at 200-nm scale bars with an average diameter and length of 25 nm and 20 μm, respectively, and (c) fabricated MWCNT/PDMS composite ----------105

Figure 5.3. MWCNTS/PDMS composites for tensile and pressure sensor testing ----------106

Figure 5.4. Tensile stress–strain curves for MWCNT/PDMS samples with their weight percentage ----------106

Figure 5.5. Variation of Young's modulus for PDMS and MWCNT/PDMS composites with varying CNT wt% ----------107

Figure 5.6. Variation of the electric resistance $\Delta R/R_0$ with time for the MWCNTs/PDMS composites for 1000 loading-unloading cycles ----------109

Figure 5.7. The pressure sensor testing setup: Yantrika dead weight tester ----------110

Figure 5.8. Typical geometry of an MWCNT/PDMS pressure sensor circular shape with 30-mm diameter, (b) pressure sensors undeflected and deflected position when pressure applied ----------111

Figure 5.9. (a) Stainless steel-based isolated diaphragm, and (b) fabricated pressure sensor for measurement----------111

Figure 5.10. Piezo-resistive response of MWCNT/PDMS composites pressure sensor with an intermediate MWCNTs concentration of 2–10 wt%----------112

Figure 5.11. Shows the effect of CNT weight percentages increases the sensitivity ----------114

Figure 5.12. Response of MWCNTs/PDMS pressure sensor for wrist pulse monitoring --------115

Figure 5.13. Shows recorded Raman spectra of SWCNTs ----------118

Figure 5.14. FESEM image of SWCNTs at 400-nm scale bars with an average diameter of 40 nm ----------119

Figure 5.15. Optical photographs of fabricated SWCNTs/PDMS-based flexible strain sensor (a) stretchable, (b), twistable and (c) foldable ----------119
Figure 5.16. Optical photographs of the e-glove fabrication process: (a) acrylic adhesive double-sided tape onto the latex glove, (b) thin copper tape with liquid PDMS on the acrylic tape, and (c) the latex glove with SWCNTs/PDMS flexible strain sensors ----------120
Figure 5.17. The procedure followed for assembling the hand ----------121
Figure 5.18. Shows the linear relationship between the variable resistance and the applied strain----------122
Figure 5.19. Fatigue test of the SWCNTs/PDMS strain sensor under repeated loading and unloading cycles----------123
Figure 5.20. A generic voltage divider circuit to measure unknown resistance ----------125
Figure 5.21. Electrical assembly of the glove-controlled robotic hand ----------125
Figure 5.22. Strain data from the e-glove with different fingers bending ----------127
Figure 5.23. The resistance changes while holding and releasing the smiley face squeeze ball placed within the fingers of the glove----------128
Figure 5.24. (a-f) Photographs were taken while showcasing real-time human-machine interactions of a robotic hand using an SWCNTs/PDMS-based electronic glove-controlled opening and closing of a human finger ----------129

List of Tables

Table 2.1 Resistive-based strain sensors: sensor materials, fabrication methods and applications.

Table 2.2 Resistive-based pressure sensors: sensor materials, fabrication methods and applications.

Table 2.3 Flexible strain and pressure sensors: key performance parameters.

Table 3.1 Mechanical properties of PDMS Samples with different amounts of Crosslinking.

Table 4.1 Equivalent circuit model parameters of the electrode-skin interfaces formed.

Table 5.1. Mechanical properties of MWCNT/PDMS composites.

Table 5.2. Comparison of recently reported carbon nanotube-based flexible pressure sensors.

Table 6.1. Summary of the developed flexible sensors, dry electrodes, materials, fabrication methods, performance parameters and applications developed and discussed in this thesis.

List of Symbols and Abbreviations

E	Young's modulus
ε	strain
σ	stress
S	sensitivity
ΔR	change in resistance
R_0	initial resistance
$\Delta R/R_0$	Relative resistance
δP	variation of the applied pressure
Ag	Silver
AgCl	Silver Chloride
Au	Gold
BGBs	Braided graphene belts
CB	Carbon Black
CNFs	Carbon nanofibers
CNT	Carbon nanotubes
CVDs	Crdiovascular diseases
D	Dicrotic wave
dB	Decibels
DI	De-ionised
ECG	Electrocardiogram
EEG	Electroencephalogram
EMG	Electromyogram
ESI	Electrode-skin interface
E-skin	Electronic skin
GF	Gauge factor
GNP	Graphene nanoplatelets
GO	Graphene oxide
HMI	Human-machine interface
LPCVD	Low-pressure chemical vapor deposition

MCG	Molybdenum-carbide-graphene
MWCNT	Multi-wall carbon nanotubes
NFs	Nanofibers
NWF	Nonwoven fabric
OLEDs	Organic light-emitting diodes
P	Percussion Wave
PAN	Polyacrylonitrile
PANI	Polyaniline
PDMS	Polydimethylsiloxane
PEDOT	Poly(3,4-ethylenedioxythiophene)
PET	Polyethylene terephthalate
PI	Polyimide
PSS	Polystyrene Sulfonate
rGO	Reduced graphene oxide
Sccm	Standard cubic centimetres per minute
SDGs	Sustainable development goals
SEM	Scanning electron microscopy
SNR	Signal-to-noise ratio
SR	Silicon rubber
SWCNT	Single-wall carbon nanotubes
T	Tidal wave
Ti	Titanium
TPU	Thermoplastic polyurethane
WPU	Waterborne polyurethane
XPS	X-ray photoelectron spectroscopy
ZnO	Zinc oxide

Chapter: 1 Introduction

1.1 Background and Motivation

Wearable electronics have gained significant attention in recent years, driven by the growing emphasis on human health monitoring and advancements in biomedical devices [1]. These wearable devices are vital in monitoring human movements and health status, delivering precise and reliable information. One prominent example of wearable devices is continuously tracking an individual's wrist pulse and heartbeat, enabling people to monitor their health conditions without hospitalization. As an innovative technology in flexible and stretchable electronics, this newly developed wearable electronics is rapidly emerging. It demonstrates various applications across diverse fields due to its ability to compress, twist, and conform to complex, non-planar surfaces [2]. These applications are shown in figure 1.1, include large-area electronics, electronic skin, drug delivery systems, piezoelectric and triboelectric nanogenerators, supercapacitors, flexible displays, wearable sensors, health monitoring, optoelectronics, and flexible antennas [3-9].

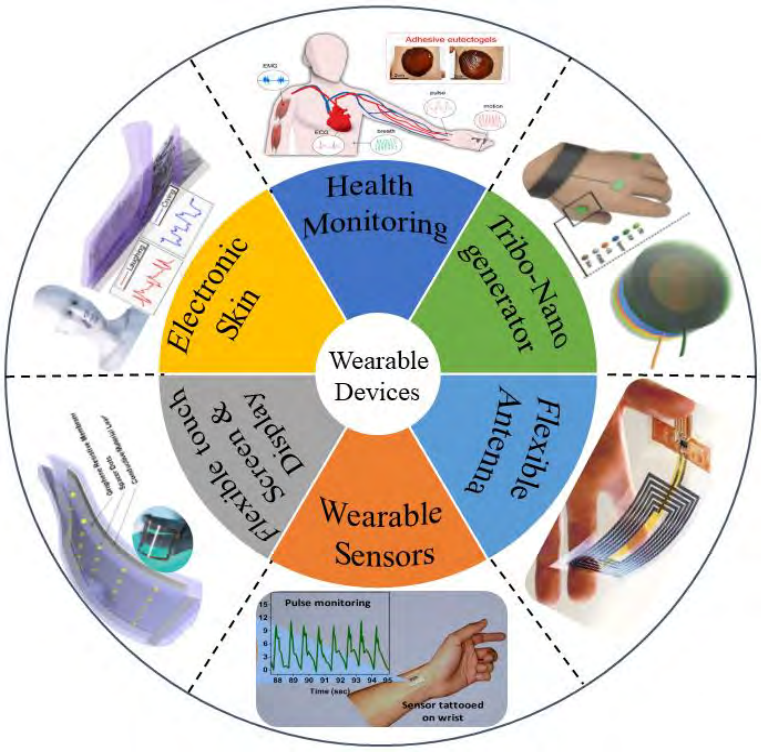

Figure 1.1. Illustrates the diverse applications of wearable electronic devices [3-8].

The concept of flexible and stretchable electronics can be traced back to the early 2000s when researchers began exploring new materials and fabrication techniques to create electronics that could conform to irregular shapes or be stretched without losing functionality. Early attempts focused on flexible devices such as transistors and transducers by forming organic thin film or transferring inorganic thin film on plastic substrates like polyimide and flexible printed circuit boards [10]. Organic electronics, which utilize organic (carbon-based) materials for conducting and semiconducting components, played a crucial role in developing flexible and stretchable electronics. Organic thin-film transistors (OTFTs) and organic light-emitting diodes (OLEDs) enabled the creation of flexible displays and sensors [11].

In the late 2000s, researchers began to focus on making electronics not only flexible but also stretchable. Materials like elastomers and conductive polymers were used to create stretchable circuits and sensors [12]. These innovations found applications in wearable health monitoring devices and fitness trackers. Advancements in microfabrication techniques allowed for the development of flexible electronics based on silicon materials. Thin silicon wafers were integrated onto flexible substrates, enabling high-performance flexible sensors and displays [13]. Companies started developing prototypes and commercial products like flexible OLED displays.

The 2010s saw a surge in wearable technology, driven by the development of flexible and stretchable electronics. Products like fitness trackers, smart bracelets, smartwatches, and electronic skin patches became popular, providing users with real-time health monitoring, fitness tracking, and other applications [14]. Flexible and stretchable electronics have also found applications in healthcare, where they can be integrated into medical devices, such as wearable biosensors and smart bandages. These innovations have the potential to revolutionize patient monitoring and healthcare delivery. The fashion industry has embraced the concept of "smart textiles," which incorporate flexible and stretchable electronics into clothing and accessories. These garments can change color, display patterns, or even provide climate control. Research and development in flexible and stretchable electronics is going on. Innovations in materials, fabrication techniques and miniaturization were expected to continue driving progress in this field. Integrating artificial intelligence and machine learning with these wearable technologies are a growing trend, promising more intelligent and personalized functionalities.

The emerging field of wearable electronics offers efficient, affordable, easy-to-use, practical, and rapid solutions for monitoring health metrics, enhancing personal fitness, and seamlessly integrating technology into daily life. Wearable devices have evolved gradually in the form of accessories, integrated clothing, body attachments and body inserts. Recent advances in electronic devices have broadened the scope of flexible electronics from earlier flexible/stretchable, foldable storage devices to the more advanced stretchable and wearable devices that lie outside the operational scope of conventional rigid material-based electronics. By integrating them with complex curved surfaces and maintaining their functionality even when subjected to deformation, they open a new route for applications for close monitoring and recording various vital signals such as those found in structural and human health monitoring, electronic skin patches, human-machine interface, and real-time motion tracking [15-17]. For wearable electronics, since sensors should be easily attached to the irregular surfaces of the sensed objects with good curvature, the high flexibility of sensors is highly demanding in different kinds of sensing applications. Wearable, flexible and stretchable sensors are of low fabrication cost, light weight, non-invasive, and non-irritating devices that continuously measure a person's physiological signals in real-time [18].

In this thesis, the work focuses on the fabrication of flexible strain/pressure sensors, which have recently gained attention for diverse applications. These applications include human motion detection, health monitoring, E-skin, physiological signal detection, drug delivery, motion capture technology, and human-machine interface. The fabrication of flexible strain/pressure sensors typically involves integrating conductive nanomaterials with flexible substrates. Flexible polymers are the substrate or platform material, while conductive materials function as active components or sensing elements. The flexible substrates often include polyethylene terephthalate (PET), polyimide, polydimethylsiloxane (PDMS), ecoflex, fabric, and paper [19-20]. On the other hand, conductive nanomaterials, such as graphene, carbon nanotubes, metallic nanowires, and nanoparticles, are utilized as active materials for flexible sensors [21-23].

Carbon nanomaterials have played a revolutionary role in the development of flexible strain/ pressure sensors for wearable technology. Their exceptional properties, such as intrinsic flexibility, remarkable stretchability, extensive surface area, fast electron mobility, good

piezoresistivity, and high mechanical flexibility, make them ideal candidates for wearable sensors [24]. Furthermore, carbon nanomaterial-based wearable sensors offer several advantages over traditional sensors based on metals or semiconductors, including high flexibility, stretchability, simple fabrication processes, lightweight design, and many more [25]. Various structures are available within the realm of carbon nanomaterials, with graphene and carbon nanotubes being the most prominent options for flexible sensors. The distinguishing feature of these carbon nanomaterial-based flexible sensors is their ability to monitor substantial strain variations, primarily achieved through adjustments in the percolation network within the polymer/conductive fillers composite.

The human body continuously generates diverse bio-signals comprising electrophysiological, physiological, and biochemical [26]. Electrophysiological signals, such as Electrocardiography (ECG), Electroencephalography (EEG) and Electromyography (EMG), provide critical insights into the electrical activity of biological cells, tissues, and organs, including the heart and brain. Figure 1.2 depicts various medical applications wherein skin-conformal wearable devices are employed to detect biosignals.

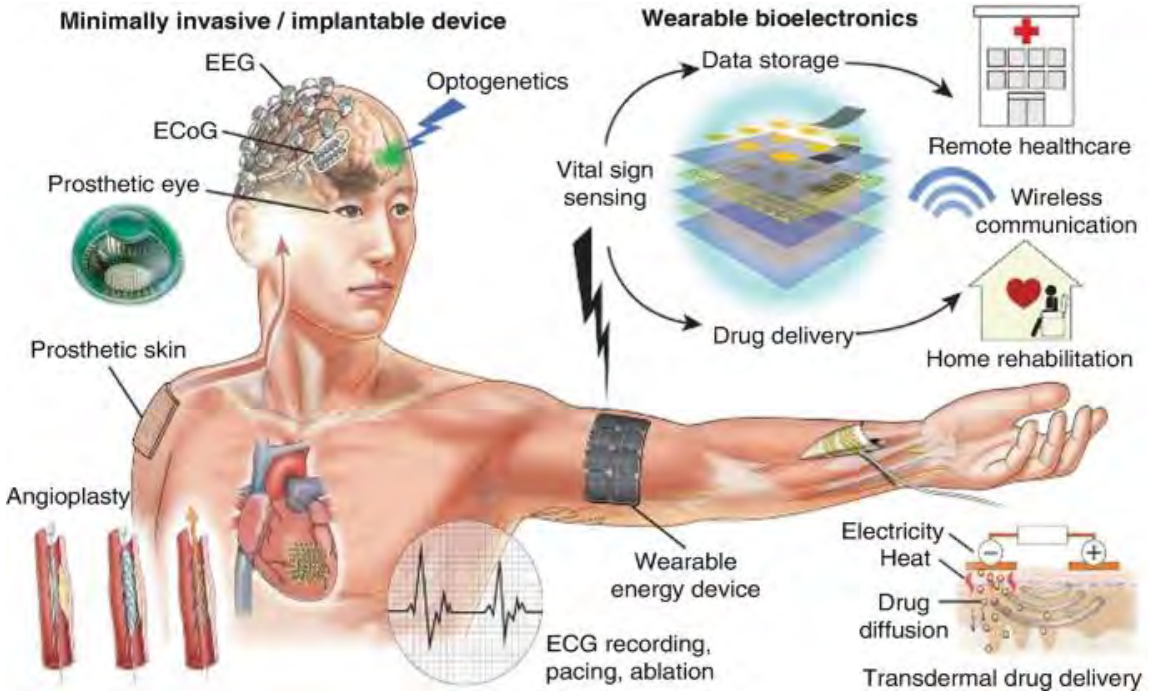

Figure 1.2. Illustrates the diverse bio-signals emanating from the human body, along with pertinent epidermal and wearable electronics designed to detect these signals, facilitating wireless and remote healthcare for early diagnosis [27].

ECG serves as a visual representation of the heart's electrical signals, aiding in understanding the functioning of the heart and detecting cardiovascular conditions. Physiological signals include measurements like respiratory rate, wrist pulse, pressure, strain, and temperature, while biochemical signals involve parameters like glucose and pH levels. These signals collectively offer a wealth of information for monitoring and understanding the functioning of the body and overall health status. The continuous monitoring of these bio-signals could help to detect abnormalities and lead to the detection of diseases at an early stage.

United Nations Sustainable Development Goals (SDGs) are a blueprint for achieving a more sustainable future by 2030. SDG-3 provides guidelines that ensure healthy lives and promote well-being at all ages. SDG-3 emphasizes making high-quality care accessible to all. The development of lightweight, simple-to-use biomedical devices for the safe and effective diagnosis and treatment of diseases would enable the same. As per the World Health Organization (WHO) [28], noncommunicable diseases (NCDs) cause the death of 41 million individuals annually, accounting for 71% of global mortality. Notably, cardiovascular diseases (CVDs) stand out as the primary cause of NCD-related deaths, claiming 17.9 million lives each year worldwide. India's population is predicted to surpass China's around 2027, making India the nation with the largest population. These changing demographics will directly impact the worldwide primary healthcare sector. It necessitates new methods of ensuring the availability of the most essential and fundamental health care services aimed at early detection, diagnosis and prevention of ailments and promoting good health. The mortality rate from CVDs could be significantly reduced if individual's biopotentials, such as the electrocardiogram (ECG), are monitored and analyzed regularly. Continuous and real-time monitoring of heart activities would play an important role in the early diagnosis and treatment of cardiovascular diseases. In particular, ECG recordings are widely used for the early detection and management of heart problems. Electrophysiological sensors, also known as electrodes, are widely used to detect and record ECG signals.

Conductive materials form the basis of electrodes strategically positioned on the human body to capture electrophysiological signals, and their precise placement is crucial for obtaining accurate measurements while minimizing noise and artefacts. Proper skin preparation is essential to optimize signal quality. Advanced signal processing techniques are commonly applied to

analyze the collected electrical activity data, aiding medical professionals in making informed diagnoses and decisions about patient care. Commercial Ag/AgCl electrodes excel in delivering high-quality short-term measurements for precise diagnostics across various medical conditions. Their focus on short-term use limits accessibility for prolonged monitoring [29]. Additionally, these electrodes utilize electrolytic gels, posing risks of skin irritation and potential allergic reactions. Their single-use nature is further compounded by gel evaporation over time. In response to these challenges, significant efforts have been invested in developing alternative solutions for long-term bio-signal monitoring. The exploration of high-performance flexible dry electrodes, which can establish excellent contact without gels or skin preparation, has gained interest [30]. The criteria of reusability, flexibility, softness, adhesion, and biocompatibility have emerged as pivotal attributes.

In light of these considerations, carbon nanomaterials like carbon nanotubes and graphene emerge as promising materials for bioelectrode design when integrated into polymeric matrices. Their exceptional electrical conductivity, biocompatibility, and conformity make them a compelling choice. Graphene-based dry electrodes have garnered significant attention for ECG monitoring applications in recent years. This is due to graphene's remarkable specific surface area and electrical conductivity, outstanding mechanical properties and thermal stability, which have opened doors to innovation in this field [31]. There is an increasing scope for flexible dry electrodes, which can be used to record and monitor various bio-signals generated in the human body for continuous and personalized health monitoring, irrespective of the patient's location.

1.2 Challenges and Issues

The primary challenge in achieving continuous and long-term monitoring of electrophysiological signals lies in fabricating dry electrodes that possess flexibility, high conductivity, biocompatibility, conformability, reusability, and resistance to motion artefacts and sweat. The pursuit of both high conductivity and exceptional conformability in flexible dry electrodes is crucial for establishing close, reliable skin contact and maintaining consistently low skin-electrode impedance. This, in turn, enables the detection of high-quality electrophysiological signals.

Fabricating flexible strain/pressure sensors with high sensitivity, a wide range of operations, high stretchability, durability, and scalability are the foremost challenges. However, advancements in materials and fabrication techniques have made it possible to overcome these challenges. The high sensitivity in a low strain/pressure regime is essential for monitoring tiny movements and vital signals accurately, especially in wearable health monitoring devices like those used for measuring wrist pulse rate, heart rate, and other physiological parameters. These sensors find applications in wearable electronics, human-machine interfaces, and structural health monitoring, paving the way for safer and more intuitive interactions with technology and improved structural safety. However, long-term stability, calibration, and integration challenges must be overcome to realize their potential fully.

1. 3 Objectives

This work intends to fabricate a flexible strain/pressure sensor and flexible dry electrodes using carbon nanomaterials specifically designed to be compatible with wearable electronic devices. The scope of this work involves employing a cost-effective and straightforward fabrication process, focusing on the development of a piezoresistive strain/pressure sensor and flexible dry electrodes tailored for wearable electronic applications. Thus, in order to pursue this work, the research work is divided into the following objectives:

1. To synthesize advanced carbon nanomaterials comprising graphene/CNTs as an active material for pressure/strain sensors.
2. Design and development of flexible Polydimethylsiloxane (PDMS) substrate for pressure/strain sensor.
3. Deposition and characterization of suitable graphene/CNTs-based electrodes.
4. Design and fabrication of various types of flexible and stretchable pressure/strain sensors for wearable electronics.
5. Performance analysis of the developed device for different real-time sensing applications.

1.4 Thesis Structure

The thesis is organized into six chapters as follows.

Chapter 1: Introduction

This chapter presents the background of the study, and it will summarise the importance of flexible and stretchable electronics and their promising applications, particularly wearable health monitoring devices. Also, this chapter presents the current challenges and issues related to flexible and wearable sensors, the motivations behind and the objectives of the thesis, followed by the detail of the thesis structure.

Chapter 2: Literature Review

This chapter deals with a comprehensive literature survey concerning flexible strain/pressure sensors, dry electrodes and their potential application, such as human motion detection, health monitoring, electronic skin and human-machine interface. Also, this chapter discusses materials, methods and sensor parameters proposed for fabricating these sensors and current issues relating to the development of wearable devices.

Chapter 3: PDMS and Graphene: Development, Synthesis and Characterizations

This chapter discusses the development of flexible PDMS substrate, synthesis of multilayer graphene and reduced graphene oxide (rGO). The synthesis rGO was achieved using a modified Hummer's method, and multilayer graphene was produced using the low-pressure chemical vapor deposition method. Also, the multilayer graphene on copper foil transferred onto a flexible PDMS substrate using the wet transfer method. In order to verify the properties and surface morphology of developed materials, various characterization techniques were used.

Chapter 4: Graphene-based Flexible Sensors: Design, Development and Applications

This chapter presents the fabrication of GNP/PDMS-based flexible strain sensor and discusses its potential application in real-time monitoring of small and large-scale human motions.

This chapter also discusses the fabrication of rGO/PDMS-based flexible dry electrodes by spray coating method for electrophysiological signal monitoring. The electrical properties and biocompatibility of rGO//PDMS dry electrodes are presented. Electrophysiological signals obtained from flexible rGO//PDMS dry electrodes are compared with the conventional wet Ag/AgCl electrodes.

Chapter 5: Carbon Nanotubes-based Flexible Sensors: Design, Development and Applications

This chapter presents the fabrication of multi-walled carbon nanotubes/ polydimethylosiloxane composite based flexible pressure sensor for wearable electronic-skin application. Electrical, mechanical characterization and stability of MWCNT/PDMS pressure sensors are studied. A simple electronic glove based on SWCNT/PDMS composite strain sensors for human-machine interface and its ability to control a robotic hand is presented.

Chapter 6: Conclusion and Future Scope

This chapter summarizes the outcomes of this research and provides some insight into the future scope to the area of wearable electronics.

References

[1] C. Wang et al., "Advanced carbon for flexible and wearable electronics," *Advanced M*aterials, vol. 31, no. 9, p. 1801072, 2019.

[2] S. Choi et al., "Recent advances in flexible and stretchable bio-electronic devices integrated with nanomaterials," *Advanced Materials*, vol. 28, no. 22, pp. 4203-4218, 2016.

[3] S. Wang et al., "Self-adhesive, stretchable, biocompatible, and conductive nonvolatile eutectogels as wearable conformal strain and pressure sensors and biopotential electrodes for precise health monitoring," *ACS Applied Materials & Interfaces*, vol. 13, no. 17, pp. 20735-20745, 2021.

[4] C.M. Chiu et al., "A smart glove with integrated triboelectric nanogenerator for self-powered gesture recognition and language expression," *Science and Technology of Advanced Materials*, vol. 20, no. 1, pp. 964-971, 2019.

[5] A. Scidà et al., "Application of graphene-based flexible antennas in consumer electronic devices," *Materials Today*, vol. 21, no. 3, pp. 223-230, 2018.

[6] V. Kedambaimoole et al., "Laser-induced direct patterning of free-standing Ti3C2–MXene films for skin conformal tattoo sensors," *ACS sensors*, vol. 5, no. 7, pp. 2086-2095, 2020.

[7] Y. Liu, M. Pharr, and G.A. Salvatore, "Lab-on-skin: a review of flexible and stretchable electronics for wearable health monitoring," *ACS nano*, vol. 11, no. 10, pp. 9614-9635, 2017.

[8] E. Roh et al., "Stretchable, transparent, ultrasensitive, and patchable strain sensor for human–machine interfaces comprising a nanohybrid of carbon nanotubes and conductive elastomers," *ACS nano*, vol. 9, no. 6, pp. 6252-6261, 2015.

[9] Y. Lee and J.H. Ahn, "Graphene-based transparent conductive films," *Nano*, vol. 8, no. 03, p. 1330001, 2013.

[10] K. Takei, "History of Flexible and Stretchable Devices," *in Flexible and Stretchable Medical Devices*, pp. 1-6, 2018.

[11] H. Zhu et al., "Printable semiconductors for backplane TFTs of flexible OLED displays," *Advanced Functional Materials*, vol. 30, no. 20, p. 1904588, 2020.

[12] D. Corzo, G. Tostado-Blázquez, and D. Baran, "Flexible electronics: status, challenges and opportunities," *Frontiers in Electronics*, vol. 1, p. 594003, 2020.

[13] S. Gupta, W.T. Navaraj, L. Lorenzelli, and R. Dahiya, "Ultra-thin chips for high-performance flexible electronics," *npj Flexible Electronics*, vol. 2, no. 1, p. 8, 2018.

[14] A. Channa et al., "The rise of wearable devices during the COVID-19 pandemic: A systematic review," *Sensors*, vol. 21, no. 17, p. 5787, 2021.

[15] K. Guk et al., "Evolution of wearable devices with real-time disease monitoring for personalized healthcare," *Nanomaterials*, vol. 9, no. 6, p. 813, 2019.

[16] B. Zazoum, K.M. Batoo, and M.A.A. Khan, "Recent advances in flexible sensors and their applications," *Sensors*, vol. 22, no. 12, p. 4653, 2022.

[17] W. Wu, "Stretchable electronics: functional materials, fabrication strategies and applications," *Science and Technology of Advanced Materials*, vol. 20, no. 1, pp. 187-224, 2019.

[18] A. Nag, S.C. Mukhopadhyay, and J. Kosel, "Wearable flexible sensors: A review," *IEEE Sensors Journal*, vol. 17, no. 13, pp. 3949-3960, 2017.

[19] Y. Zhang et al., "Highly sensitive, low hysteretic and flexible strain sensor based on ecoflex-AgNWs-MWCNTs flexible composite materials," *IEEE Sensors Journal*, vol. 20, no. 23, pp. 14118-14125, 2020.

[20] I. Miranda et al., "Properties and applications of PDMS for biomedical engineering: A review," *Journal of functional biomaterials*, vol. 13, no. 1, p. 2, 2021.

[21] N. Wen et al., "Emerging flexible sensors based on nanomaterials: Recent status and applications," *Journal of Materials Chemistry A*, vol. 8, no. 48, pp. 25499-25527, 2020.

[22] M. Gong, L. Zhang, and P. Wan, "Polymer nanocomposite meshes for flexible electronic devices," *Progress in Polymer Science*, vol. 107, p. 101279, 2020.

[23] M.D. Ho, Y. Ling, L.W. Yap, Y. Wang, D. Dong, Y. Zhao, and W. Cheng, "Percolating network of ultrathin gold nanowires and silver nanowires toward 'invisible' wearable sensors for detecting emotional expression and apexcardiogram," *Advanced Functional Materials*, vol. 27, no. 25, p. 1700845, 2017.

[24] G. Speranza, "Carbon nanomaterials: Synthesis, functionalization and sensing applications," *Nanomaterials*, vol. 11, no. 4, p. 967, 2021.

[25] X. Wang, E.G. Lim, K. Hoettges, and P. Song, "A Review of Carbon Nanotubes, Graphene and Nanodiamond Based Strain Sensor in Harsh Environments," *C*, vol. 9, no. 4, p. 108, 2023.

[26] M. Kim et al., "Emerging Bio-Interfacing Wearable Devices for Signal Monitoring: Overview of the Mechanisms and Diverse Sensor Designs to Target Distinct Physiological Bio-Parameters," *Advanced Sensor Research*, vol. 2, no. 4, p. 2200049, 2023.

[27] M. Ha, S. Lim, and H. Ko, "Wearable and flexible sensors for user-interactive health-monitoring devices," *Journal of Materials Chemistry B*, vol. 6, no. 24, pp. 4043-4064, 2018.

[28] World Health Organization, "Noncommunicable Diseases," *who.int*, Available: https://www.who.int/news-room/fact-sheets/detail/noncommunicablediseases (accessed on 17 January 2022).

[29] H. Kim et al., "Advances in soft and dry electrodes for wearable health monitoring devices," *Micromachines*, vol. 13, no. 4, p. 629, 2022.

[30] Q. Liu, J. Zhou, Q. Zeng, D. Sun, B. Yu, L. Yang, Z. Zhang, J. Wu, and Y. Zhang, "Flexible Dry Epidermal Electrophysiological Electrodes Based on One-Dimensional Platinum-Coated Silver Nanowires," *ACS Applied Nano Materials*, 2023.

[31] X. Chen, L. Zhang, and S. Chen, "Large area CVD growth of graphene," *Synthetic Metals*, vol. 210, pp. 95-108, 2015.

Chapter: 2 Literature Review

This chapter presents a comprehensive literature survey, offering an in-depth analysis of the current state of the art in flexible sensors. This chapter focuses on two types of sensors: flexible strain sensors and flexible pressure sensors that detect bio-signals such as wrist pulse, human motions, respiratory rate, electrocardiogram (ECG) and surface electromyogram (sEMG). A literature survey has also been conducted for recently developed sensors and devices based on graphene and carbon nanotubes for wearable electronics applications. The aim is to present a thorough review of the existing research and developments in wearable electronics, highlighting key advancements and breakthroughs. Within this chapter, detailed literature review is presented, encompassing flexible strain/pressure sensors and flexible dry electrodes for human motion detection, structural health monitoring, electrophysiological signals detection and human-machine interfaces.

2.1 Introduction to flexible sensors

Flexible sensors have garnered significant interest and are a groundbreaking technological innovation with various applications in wearable electronics. Unlike traditional rigid sensors, flexible sensors are designed to conform to the shape and movement of objects, surfaces, or even the human body. These sensors are typically composed of flexible and stretchable materials, such as graphene, carbon nanotubes, or polymers, which enable them to detect a range of physical parameters, including strain, pressure, temperature, and other additional parameters [1,2]. The versatility of flexible sensors makes them ideal for applications like human motion detection, health monitoring, wearable technology, electronic skin (e-skin), and human-machine interfaces [3-5]. In addition to flexible sensor types, flexible strain sensors and dry electrodes have attracted considerable attention for monitoring various bio-signals, including human movements, wrist pulses, blood pressure, respiratory rates, and electrophysiological signals [6,7]. Whether integrated into wearable technology, healthcare devices, robotics, or even smart infrastructure, flexible sensors introduce a new dimension of adaptability, sensitivity, and user comfort.

2.2 Flexible strain sensors

Flexible strain sensors represent a pivotal advancement in sensor technology, offering the ability to precisely measure and monitor mechanical deformation by changing their electrical properties. Flexible strain sensors are critical in enhancing safety, performance, and efficiency. Their capacity to provide real-time, high-precision data on strain and deformation position them at the forefront of industries like healthcare, manufacturing and automation [8, 9]. Flexible strain sensors have several tremendous applications, including mobile health monitoring, soft robotics, human motion detection, motion capture techniques, drug delivery, monitoring performance of sportspersons, human-machine interfaces, etc.[10, 11]. These flexible sensors are utilized in wearable electronic devices due to being lightweight, ultrathin, highly flexible and stretchable [12]. Various applications of recently developed flexible strain sensors are illustrated in the figure. 2.1.

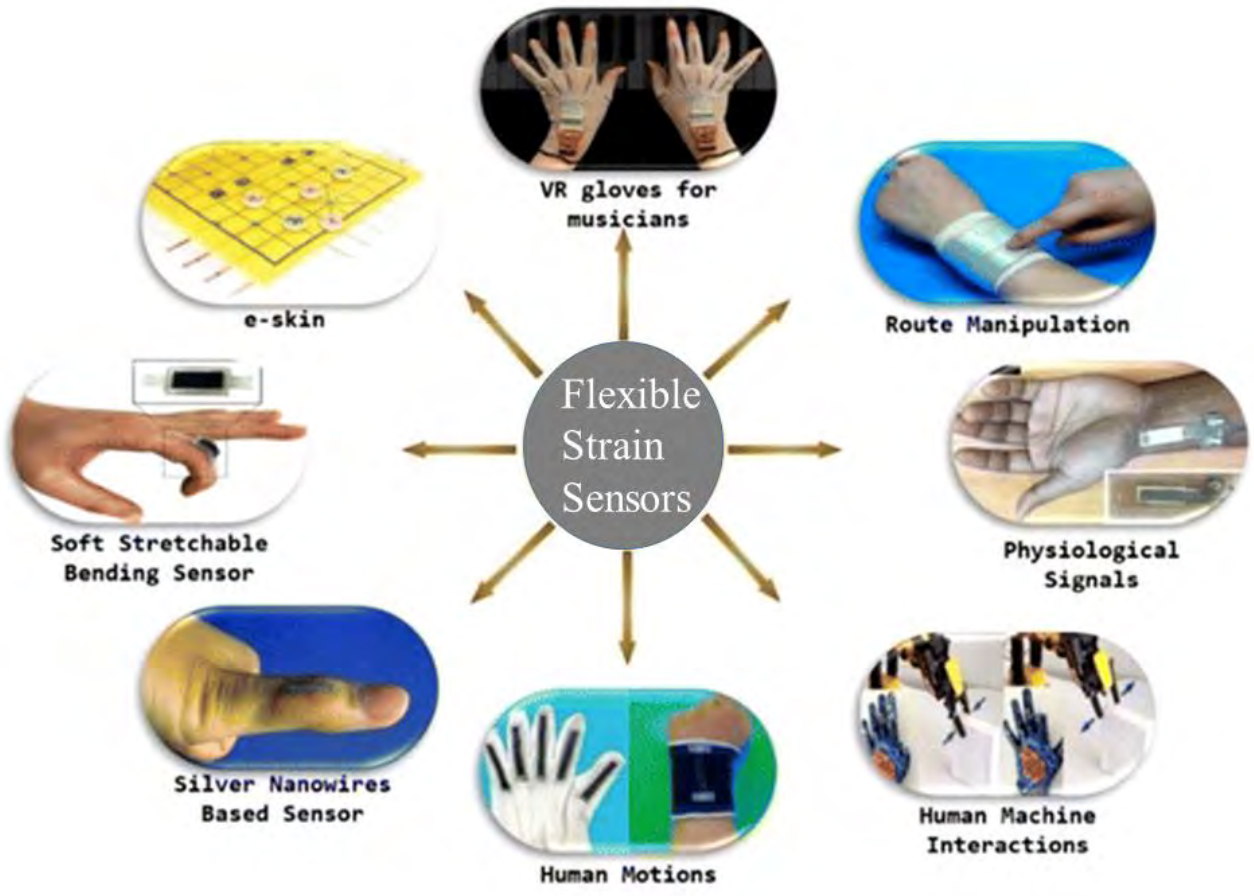

Figure 2.1. Applications of recently developed flexible strain sensors [12].

There are various strain sensors; based on the working mechanism, strain sensors are classified into optical, resistive, capacitive, piezoelectric and triboelectric [13]. Optical strain sensors, also known as fiber optic strain sensors or fiber Bragg grating (FBG) sensors, operate based on detecting strain or deformation in a material by measuring the changes in the optical properties of a fiber optic sensor. These sensors offer exceptional precision and stability in measuring strain [14]. They are ideal for applications that demand accurate, fine-tuned strain monitoring, such as structural health monitoring, aerospace, civil engineering, and industrial settings [15]. Optical sensors can be relatively expensive, require specialized expertise for installation, are somewhat fragile, and may be less suitable for high-strain applications.

Piezoelectric strain sensors operate on the principle of piezoelectricity, a property exhibited by certain materials where they generate an electrical charge in response to mechanical deformation [16]. These sensors are commonly used to measure strain, pressure, and acceleration. These sensors are renowned for their remarkable sensitivity to mechanical deformation, making them a top choice for applications that require precise dynamic strain measurements. Their wide frequency range and rapid response time make them invaluable for impact testing, vibration analysis, and acoustics. However, they are not well-suited for static or quasi-static mechanical deformations as they can exhibit "creep" behavior, leading to changes in output over time [17].

Capacitive strain sensors work on the principle of changes in capacitance resulting from mechanical deformation. These sensors offer high sensitivity, enabling them to detect the smallest changes in distance between their capacitor plates with remarkable precision. Their wide linear measurement range makes them versatile for static and dynamic applications. They exhibit good long-term stability and low hysteresis, contributing to reliable and accurate measurements over time [18]. However, these sensors can be sensitive to temperature, humidity, and other environmental changes, which can introduce measurement errors [19].

Triboelectric strain sensors, based on the triboelectric effect, operate by generating an electrical charge through the contact and separation of two materials with different triboelectric properties [20]. Triboelectric sensors are self-powered, which means that they can generate electrical energy from mechanical strain without the need for external power sources or batteries.

These self-powered sensors harness the energy generated during mechanical deformation, making them ideal for remote or energy-constrained applications. However, the calibration of triboelectric sensors can be intricate, as it requires precise control of environmental variables and the selection of materials, as the output depends on these factors [21].

Among these, the resistive-type strain sensors show a potential prospect in the strain sensing field due to their simple preparation methods and the advantages of tunable sensing performance. Resistive strain sensors, often referred to as strain gauges, operate on the principle of changing electrical resistance in response to mechanical deformation or strain in a material. They are widely used for measuring strain, stress, and deformation in various applications. Typically, achieving a flexible strain sensor with high sensitivity, fast response time, and a wide detection range is crucial. However, traditional strain sensors based on semiconductors and metal foils exhibit low sensitivity (GF s for metallic foils are typically between 2 to 5) [22], a maximum strain capability of less than 5%, and poor flexibility, which cannot meet the requirements for wearable electronics applications. Therefore, there is a demand for flexible strain sensors possessing a large strain range and high sensitivity.

Flexible strain sensors typically consist of active sensing materials combined with flexible and stretchable substrates. These active materials are commonly found in the form of composites, thin films, conductive yarns/fabrics, conducting micro-/nanomaterials and polymers [23, 24]. When stretched or compressed, the electrical resistance of the conductive network changes in response to the applied mechanical strain. The variations in resistance during stretching result from geometric alterations, such as changes in length and cross-sectional area, as well as intrinsic resistive properties of the active materials, tunnelling effects, and disconnection mechanisms. The resistance reversibly returns to its initial values after releasing strain from tensile or compressive states. Several research groups have focused on developing flexible strain sensors based on novel materials to meet the various applications in the field of wearable electronics. Various techniques have been developed to fabricate flexible strain sensors and proposed a suitable sensing mechanism, explaining the change in sensor resistance with externally applied strain. The sensor materials, fabrication methods and applications of some reported resistive-based flexible strain sensors are summarized in Table 2.1.

Table 2.1 Resistive-based strain sensors: sensor materials, fabrication methods and applications.

Sensor Materials	Fabrication method	Stretchability (%)	Gauge Factor	Applications	Ref.
rGO/TPU composites	electrospinning and ultrasonication	100	11 in (10 %) 79 in (100 % strain)	human motion monitoring	[25]
PDMS/ CB	solution mixing-casting molding method	50	15.75	human motion detection	[26]
PDMS/CNFs/GNPs	hybridization method	50	5.83	wearable sensors and e-skins	[27]
Ecoflex/conducting wool yarns (GNPs/CB)	solution mixing method	200	7.75	human movements	[28]
MWCNTs/PDMS	pickering emulsion mechanism	40	7.22	human-machine interfaces	[29]
FGF/PDMS	drop cast method	70	15 to 29	health-monitoring	[30]
GnPs film inside a PDMS	mechanical transfer of GnPs	------	27.7–164.5	human-machine interface	[31]
GE/AgNPs/TPU	in situ reduction method	1000	7 at 50%, 476 at 500% strain	human motions detection	[32]
Ecoflex and rGO/DI	template methods	31.6	400	detection of acoustic vibration and human vocalization	[33]
carbon nanotubes (CNTs) into elastic bands (EB)	swelling-ultrasonication treatment	780–920	129	human-machineinterfaces	[34]
graphene pellets and thermoplastic polyurethane (TPU) pellets	3D printing	100	11 strain of 10% and 80 strain of 100%	3D printed wearable devices.	[35]
PDMS and SWCNTs/CB/SR composite	solution mixing-casting molding method	120	1.25	human motion monitoring	[36]
Graphene Foam and PDMS	template-assisted method	30	47.74−98.66	human motion monitoring	[37]
braided graphene belts (BGBs) and dragon skin	template-assisted method	60	175.16	human movement detection	[38]

2.3 Flexible pressure sensors

Flexible pressure sensors have captured considerable interest due to their remarkable properties, such as exceptional flexibility, high sensitivity, and lightweight for electronic skin (E-skin) and wearable, flexible sensing devices [39]. They excel in applications where traditional rigid pressure sensors fall short, such as wearable devices, medical applications, automotive systems, and smart textiles. By accurately measuring changes in pressure, flexible pressure sensors can provide critical data for many purposes, from monitoring vital signals in healthcare to enhance the safety and efficiency of automotive airbags.

Figure 2.2. Applications of recently developed flexible pressure sensors [40].

Various studies have investigated the utilization of piezoresistivity, capacitance, and piezoelectricity as transduction mechanisms for converting pressure stimuli into electrical signals. Building upon these three fundamental transduction principles, extensive research efforts have been directed towards improving the characteristics of flexible pressure sensors. The capacitive flexible pressure sensor operates on the principle of a parallel plate capacitor and offers several advantages, including high sensitivity, rapid response times, and a broad dynamic range. Its underlying working mechanism involves modifying the capacitance of the sensor by adjusting the separation distance between the parallel plates when an external force is applied [41]. The following equation determines the capacitance:

$$C = \varepsilon A/d \qquad \textbf{...(2.1)}$$

where ε is the dielectric constant, A represents the overlapping area, and d is the distance between two electrodes. When applying pressure is perpendicularly to the electrodes, d changes, leading to a variation in the capacitance, whereas A changes with shear force. Figure 2.3 illustrates the three common transduction mechanisms.

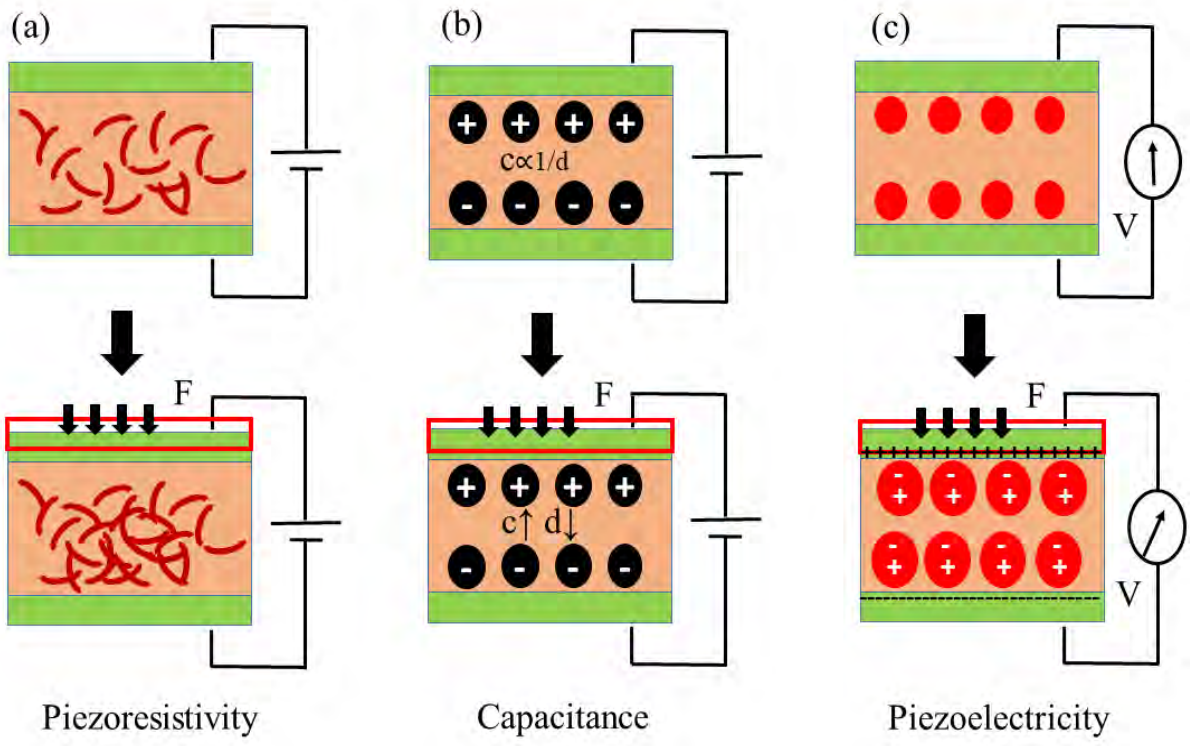

Figure 2.3. Schematic illustration of three common transduction mechanisms and representative devices: (a) piezoresistivity, (b) capacitance, and (c) piezoelectricity.

Flexible piezoelectric pressure sensors have garnered significant attention from researchers due to their straightforward materials preparation, cost-effectiveness, easy electrical signal acquisition, and other notable advantages. These sensors primarily consist of piezoelectric-sensitive materials that convert mechanical energy into electrical energy and vice versa. Their transduction mechanism can be described as follows: when subjected to external pressure, the functional material undergoes deformation, separating positive and negative charges. On opposite surfaces of the material, positive and negative charges align in opposing directions, creating a potential difference within the material. These potential differences are then examined to determine the impact of external forces [42].

Piezoresistive-based sensors function by inducing deformation in a composite material when subjected to external force. This deformation indirectly alters the material's arrangement and contact with conductive fillers, leading to a consistent change in the composite's resistance. Consequently, piezoresistive sensors are favored for their simplicity, low power consumption, extensive pressure testing capabilities, and straightforward manufacturing processes [43]. As a result, they have gained substantial attention and are extensively researched compared to capacitive and piezoelectric pressure sensors [44]. Various techniques have been developed to fabricate flexible pressure sensors and propose a suitable sensing mechanism, explaining the change in sensor resistance with externally applied pressure. The sensor materials, fabrication methods, and applications of some reported resistive-based flexible pressure sensors are summarized in Table 2.2.

2.4 Performance parameters of flexible strain and pressure sensors

The feasibility of the commercial employment of sensors depends on their performance, including sensitivity and stretchability, working range, stability and durability, linearity, hysteresis, response and recovery time, etc. Evaluating these performance parameters is essential when selecting a flexible strain or pressure sensor to ensure it meets the requirements for suitable applications. Various sensor technologies and designs can perform well or have limitations within these parameters. Therefore, it's essential to think carefully when fabricating flexible sensors.

Table 2.2 Resistive-based pressure sensors: sensor materials, fabrication methods and applications.

Sensor Materials	Fabrication method	Working range	Sensitivity (kPa^{-1})	Applications	Ref.
GNP/SR composites	foaming and micromanufacturing method	60% strain	8.45 and 195.02	human motion detection	[45]
PEDOT/NWF composites	in-situ dipping and solution deposition techniques.	< 5 kPa	21.162	healthcare monitors	[46]
gradient rGO wrinkles	coating and chemical treatment	100–200 Pa	178	human motion detection.	[47]
CB/MXene/SR/fiber nanocomposites	dip coating and moulding	0.1–1700 kPa	2.08	human-computer interaction	[48]
CB/TPU foam	freeze-drying process.	80% strain	GF of 1.55	human motions detection	[49]
CNT wrapped PDMS	emulsion polymerization and CNT coating	1 to 20 kPa	0.111	physiological signal detection	[50]
PDMS with ZnO nanotetrapods	spin coating and casting method	less than 14 N	70.8 mV/N.	hand gesture	[51]
PVDF/ZnO	electrospinning, epitaxially growth	1.8 to 451 kPa	3.12 mV kPa^{-1}	physiological monitoring	[52]
MWCNT/PDMS composite	solution mixing-casting and micro molding method	<0.5 kPa	15.1	healthcare monitoring and E-skin	[53]
ACNT/Gr/PDMS	CVD, solution mixing-casting	<0.3 kPa	19.8	E-skin	[54]
VACNT/PDMS	T-CVD process, spin-coating	<5 kPa	0.3	human motions	[55]
MWCNTs/PU	mixed solution template method	(0–47.77 kPa	66.89	physiological signals detection	[56]

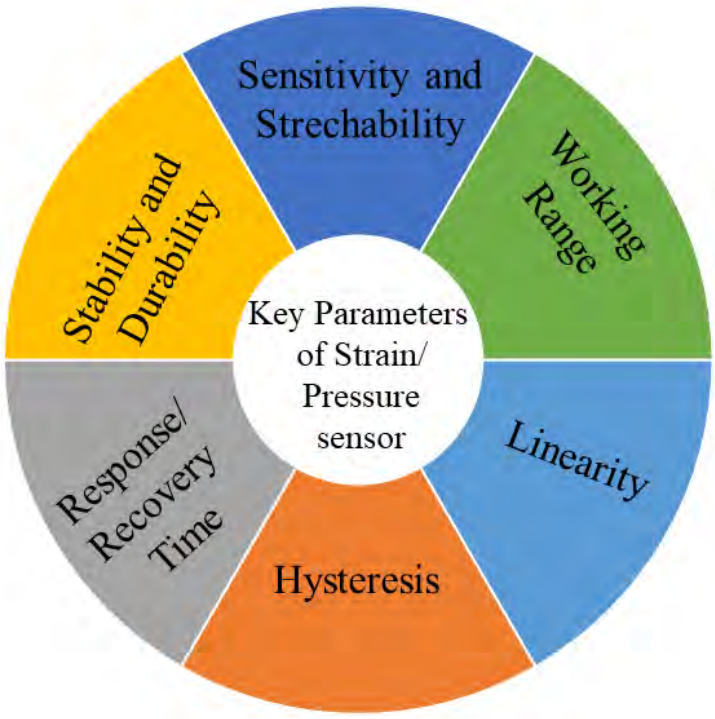

Figure 2.4. Various performance parameters of flexible strain/pressure sensors.

2.4.1 Sensitivity and stretchability

Sensitivity refers to a sensor's ability to detect and respond to changes in strain or pressure. It is typically represented by the slope of the relative variation of electrical signals, such as resistance and capacitance, in response to applied strain or pressure. Sensitivity is often quantified using the Gauge Factor (GF), which can be expressed as $GF = \Delta R / (\varepsilon \times R_0)$ for piezoresistive-type sensors or $GF = \Delta C / (\varepsilon \times C_0)$ for capacitive-type sensors [57]. A higher sensitivity indicates that the sensor can detect smaller variations in the applied strain or pressure. Here, ΔR represents the change in resistance, R_0 is the initial resistance, C_0 is the initial capacitance, and ε is the strain. Generally, piezoresistive-type sensors tend to exhibit higher sensitivity compared to capacitive-type sensors. For piezoresistive-type sensors, the GF is typically dependent on the structure of the percolation network formed by conductive fillers within the polymer matrix. When these sensors deform, the junctions between fillers may disconnect, leading to an increase in resistance and a rapid increase in GF. The properties of the fillers, such as their dispersion state, concentration, and shapes, can significantly influence the network's structure. Typically, fillers with a high aspect ratio are preferred due to their ability to facilitate the construction of an effective network.

The stretchability of flexible strain/pressure sensors refers to their ability to deform or stretch while maintaining functionality and sensing capabilities. Stretchable sensors can adapt various shapes and sizes, which is particularly useful for applications where the sensor must conform to curved or dynamic surfaces or experience mechanical strain or deformation. This stretchability is a key characteristic of flexible sensors, allowing them to withstand and measure changes in shape or pressure without damage or loss of performance. Polymer-based strain/pressure sensors generally have higher stretchability than conventional metal or semiconductor-based sensors [58]. Polymer materials are well-known for their inherent flexibility and ability to stretch without losing structural integrity. This feature makes them well-suited for applications where the sensor needs to adapt various shapes and experience mechanical strain without breaking or losing sensitivity.

2.4.2 Working range

The working range of a flexible sensor refers to the range of pressure and strain values within which the sensor can accurately and reliably measure and provide data. It typically includes the minimum and maximum values the sensor can detect while maintaining its performance and accuracy. The working range is an important parameter when choosing a sensor for a specific application, as it ensures that the sensor can effectively capture the desired data within the required pressure and strain parameters. The range of a flexible strain or pressure sensor specifies the minimum and maximum values of strain or pressure it can accurately measure. Sensors with a wide detection or working range can handle broader applications.

2.4.3 Stability and durability

Stability and durability are critical characteristics of a flexible pressure and strain sensor, describing its long-term performance and consistency over time. Sensor stability refers to its ability to maintain performance and accuracy over an extended period without significant deviations or fluctuations. A stable sensor will produce consistent and reliable measurements, even when exposed to changing environmental conditions or mechanical stress. On the other hand, sensor durability pertains to its capacity to withstand various mechanical stress, environmental factors, or wear and tear without significantly losing performance or structural integrity. A durable sensor can endure prolonged use and challenging conditions without degradation.

2.4.4 Linearity

The linearity of a flexible pressure and strain sensor refers to how closely the sensor's output corresponds to a straight-line relationship to the applied pressure or strain across its working range. In other words, it assesses how accurately the sensor's response follows a linear trend. Ideally, a linear sensor would produce output values that increase or decrease proportionally with the applied pressure or strain, resulting in a straight-line relationship when plotted on a graph [59]. However, some sensors may exhibit non-linearity, which means their output deviates from a perfect linear relationship.

2.4.5 Hysteresis

Hysteresis measures the difference in output when the sensor is subjected to the same strain or pressure loading and unloading cycles. Hysteresis is typically expressed as a percentage or error and represents the maximum difference in output between ascending and descending measurements at the same pressure or strain point. Lower hysteresis indicates better repeatability. Hysteresis is a critical exponent for stretchable strain sensors, which means the deviation between the electrical signal during the strain increasing and releasing period. Large hysteresis behavior results in inaccurate sensing performance upon dynamic loading.

2.4.6 Response and recovery time

A sensor's response and recovery times are important considerations in various applications, which involve dynamic or transient events, where accurate and timely data acquisition is crucial. Response time refers to the time it takes for the sensor to detect and respond to a change in pressure or strain and provide a stable output. It measures how quickly the sensor can register an alteration in the applied pressure or strain and accurately reflect it in its output signal. A shorter response time is often desirable, especially in real-time monitoring applications. Recovery time refers to when the sensor returns to its baseline state or the original output value after the applied pressure or strain has been removed or returned to its initial state. A shorter recovery time is important for applications where the sensor needs to adapt to dynamic pressure or strain conditions and quickly provide accurate readings once the conditions stabilize. In our study, we have focused on key performance parameters, including sensitivity and working range, response time, cyclic stability, linearity and hysteresis.

Table 2.3 Flexible strain and pressure sensors: key performance parameters.

Sensor Materials	Sensitivity	Working range	Response Time	Stability (cycles)	Ref.
CNTs/graphene/WC composite aerogels	0.25 kPa^{-1}	4.2 to 10 kPa	120 ms	>800	[60]
graphene/Ecoflex	gauge factor of 1078.1	strain range (50∼300%).	140 ms	3000	[61]
UHCS-PDMS	260.3 kPa^{-1} at 1 Pa	1 to 10,000 Pa	60 ms	5000	[62]
CNT-GNP hierarchical networks	gauge factor 197 at 10% strain)	high stretchability (≥ 50%)	----------	1000	[63]
MXene/PEDOT:PSS Composite Aerogel	26.65 kPa^{-1} within (0−2 kPa),	0 to 12 kPa	106 ms	500	[64]
PEDOT /PAAMPSA film	164.5 kPa^{-1}	0 to 100 kPa	19ms	1500	[65]
MWCNTs/WPU	GF of 2000	range of 120%,	90 ms	1000	[66]
porous graphene foam	1.16 kPa^{-1}	0.06 to 2.82 kPa	150 ms	100000	[67]
RGD spinosum/ MXene/PDMS	507 kPa^{-1}	0 to 40 kPa	60 ms	5000	[68]
MCG-based paper sensors	gauge factor of 73	in the range of 10%.	126 ms	1200	[69]
PEDOT: PSS fibers	0.34 kPa^{-1}	82 to 600 Pa.	47 ms	500	[70]
PDMS/Ti/Au	2.32 kPa^{-1}	>1 kPa	2.5 ms	250	[71]
PANI/PAN NFs	1.71 $V N^{-1}$	0.1 N to 1 N	66 ms	3000	[72]
PEDOT:PSS/ CNT@PDA@PDMS (PCPP) sensor	0.04-1.97 kPa^{-1}	0 to 100 kPa	170 ms	5000	[73]
PEDOT:PSS/ PDMS bimorph	642.5 kPa^{-1}	0 to 15 kPa	200 µs	10000	[74]
BTO/PVDF nanofibers	3.95 $V N^{-1}$	0 to 3 N	------	7400	[75]

2.5 Graphene

Graphene consists of a single layer of carbon atoms arranged in a hexagonal lattice, forming a two-dimensional monatomic layered structure (see Figure 2.5). This structure is composed of sp^2- hybridized carbon atoms. Graphene has unique properties such as high thermal conductivity (3000-5000 W/mK), high current density ($2.8x10^8$ A/cm^2), ultra-high electronic mobility (15000–200000 cm^2/(V.s)), ballistic transport, optical transmittance, high chemical and thermal stability and superhydrophobicity at the nanometer scale [76-78]. Furthermore, graphene exhibits excellent mechanical properties, with high tensile strength (~130 GPa), Young's modulus of (~0.5–1) TPa, and remarkable stretching ability [79], making it an ideal material for flexible and stretchable devices. In addition to these attributes, graphene possesses a wide optical absorption spectrum (ranging from 300 to 1400 nm), excellent transparency of (~97%) in the visible wavelength range, piezo and thermo-resistive response, and electrical sensitivity towards biochemical substances [80,81], This versatility positions graphene as a highly promising multifunctional material for flexible devices. Moreover, graphene's outstanding physical, mechanical, and electronic properties open up opportunities for various sensing applications, including optical, magnetic, strain, chemical, biomedical, and electrochemical sensors.

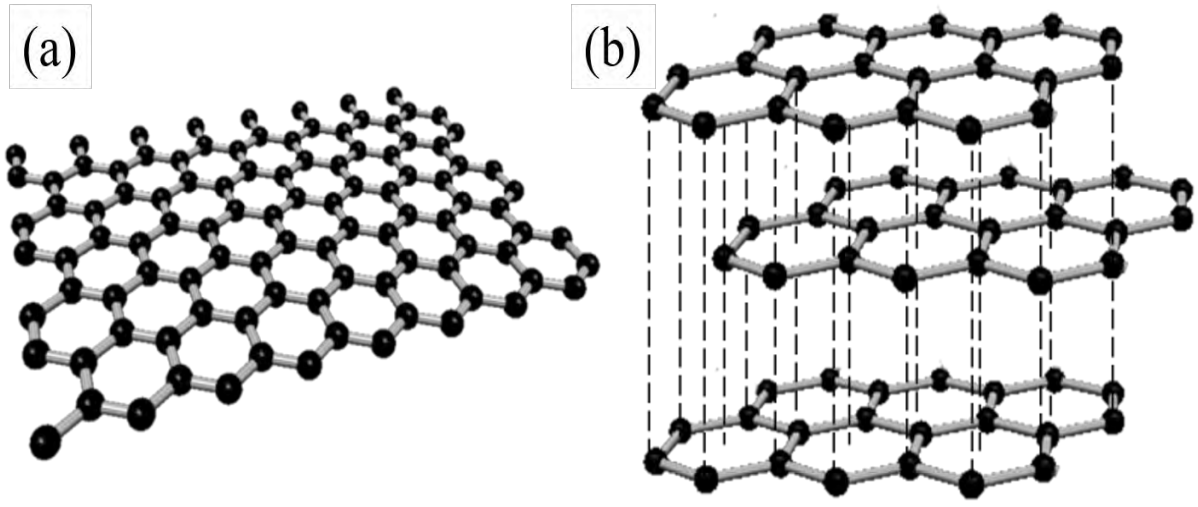

Figure 2.5. Schematic representation of single-layer graphene depicting the lattice arrangement of atoms (a) in-plane view and (b) stacked view of graphene layers [82].

2.6 Graphene synthesis

Graphene synthesis involves creating single or multi-layers of carbon atoms arranged in a hexagonal lattice, mimicking the structure of naturally occurring graphene. Graphene synthesis can be accomplished through two main approaches: "top-down" and "bottom-up." In the top-down approach, graphene is derived from larger structures like bulk graphite and then exfoliated into single-layer sheets, often employing mechanical or chemical methods. The bottom-up approach involves building graphene atom by atom, typically through chemical vapor deposition (CVD), where carbon-containing gases are decomposed on a substrate. Top-down methods are preferred for research and small-scale high-quality graphene production, while bottom-up methods, like CVD, are suitable for large-scale and industrial applications. The choice of approach depends on specific requirements and considerations, including scalability and cost. Over the past decade, various methods have been established and employed to produce graphene. Novoselov and his colleagues were credited with the groundbreaking discovery of graphene in 2004 [83]. They were the first to unveil a method for synthesizing graphene through exfoliation. After this discovery, significant efforts were made to develop new techniques to achieve efficient and large-scale graphene production. The flowchart in figure 2.6 provides an overview of various graphene synthesis methods.

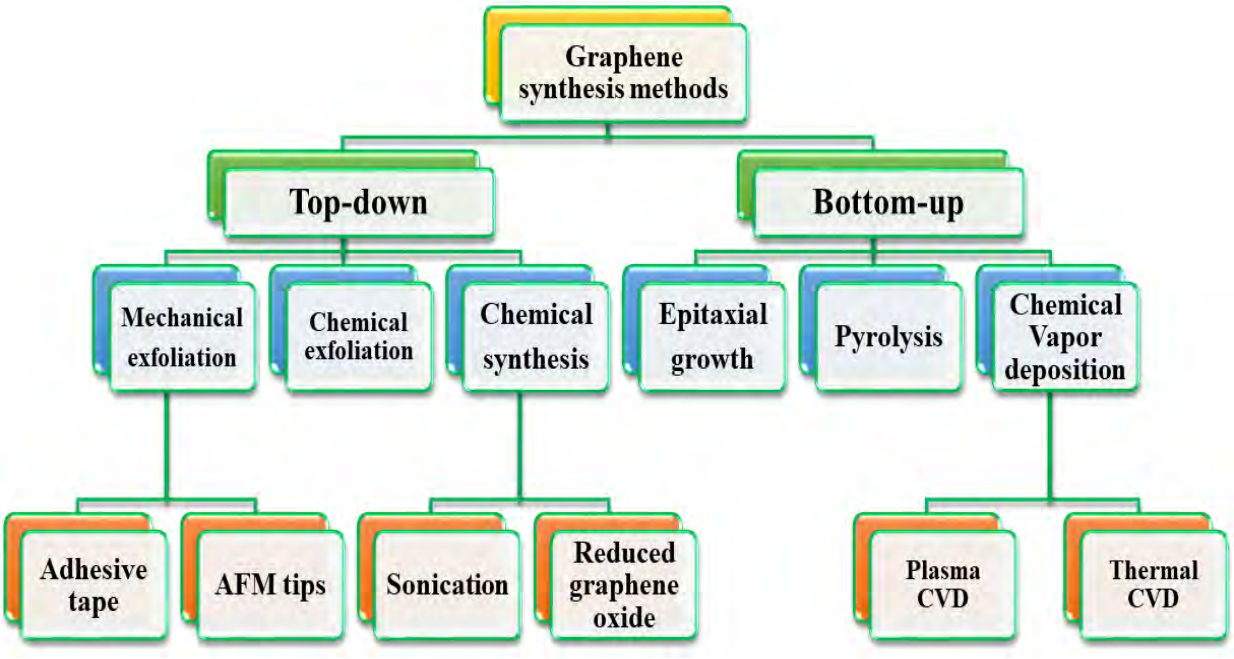

Figure 2.6. Flowchart illustrating the processes of graphene synthesis.

There are various graphene synthesis methods, such as mechanical exfoliation, chemical exfoliation, chemical synthesis, epitaxial growth and CVD method, each offering advantages and limitations. Here are some of the most commonly employed techniques.

2.6.1 Chemical vapor deposition (CVD)

CVD is one of the most widely used methods for synthesizing high-quality graphene. In this process, a carbon-containing gas, often methane or ethylene, is introduced into a furnace at high temperatures. The deposition of high-quality graphene from the CVD process is typically carried out in the presence of a metal catalyst, with common choices including Nickel (Ni) and copper (Cu). The carbon atoms arrange themselves into a graphene layer on the metal surface. After synthesis, the graphene can be transferred to other substrates for various applications. Figure 2.7 illustrates a schematic of a commonly used CVD experimental setup and growth mechanism for producing single-layer graphene with a Cu catalyst.

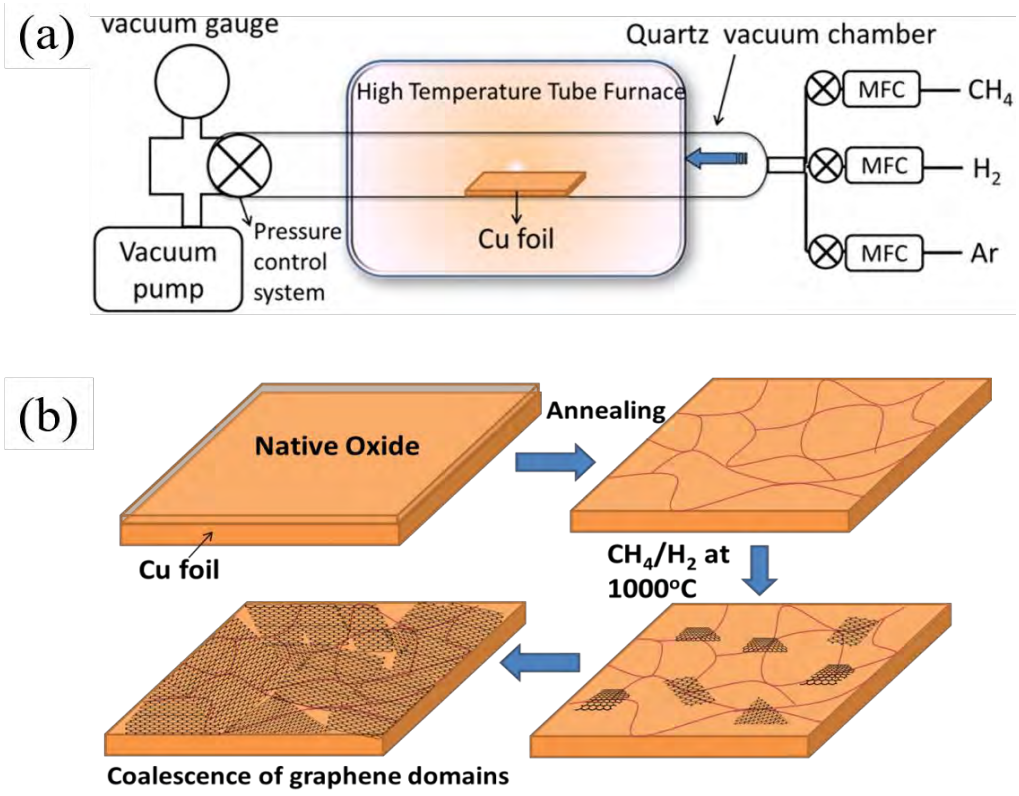

Figure 2.7. Shows (a) a Schematic of a common setup for chemical vapor deposition of graphene and (b) the growth mechanism of graphene on Cu substrates by CVD [82, 84].

Jeongjin Kim et al. proposed a well-established process for the nickel (Ni)-catalyzed growth of a single- or rotated graphene layer conducted above 800 K. Their study also investigated the role of gold (Au) catalysis in carbon segregation and graphene formation on an Au/Ni (111) surface alloy, along with the influence of the size of Ni domains on an Au/Ni(111) surface alloy [85]. In a recent study by Seung-Il Kim et al. [86], a 3-inch-wide quartz tube was employed within the CVD system. This setup enabled the synthesis of large-area, monolayer graphene on a 15 × 10 cm Cu foil. To ensure temperature uniformity in the CVD chamber and achieve consistent graphene growth, the Cu foil was securely wrapped and loaded into a 2-inch quartz tube. Throughout the annealing and growth stages, the temperature for graphene growth was carefully controlled, with adjustments made in 25 °C increments, ranging from 900 °C to 1050 °C, while maintaining all other growth parameters constant. Subsequently, the as-grown graphene, produced under various temperature conditions, was transferred onto a 300 nm SiO_2/Si substrate.

Furthermore, Bohr-Ran Huang et al. reported that a self-assembled low-pressure chemical vapor deposition (CVD) system was used for graphene synthesis. High-purity argon served as a carrier gas for methanol as a carbon source. The copper foil substrates were prepared and placed in the system. Various growth conditions were tested, including temperature, gas composition, and growth period [87].

2.6.2 Mechanical exfoliation

In this process, graphene can be peeled from the bulk graphite layer by layer. In general, there are two primary forces are employed to exfoliate graphite into graphene flakes. The first force is the normal force, which counteracts the van der Waals forces between graphene sheets, facilitating exfoliation. An illustrative example of this is the Scotch tape method. The second force applied is shear force, in which graphene layers slide relative to each other, leading to cleavage. An example of shear force-driven graphene exfoliation can be found in the ball milling process, where mechanical action promotes layer separation (as depicted in figure 2.8). Although the graphene produced by this method is of superior quality and purity, the method is not suitable for large-scale production. Also, poor transfer technique does not allow for reliable and reproducible construction of a sensor platform.

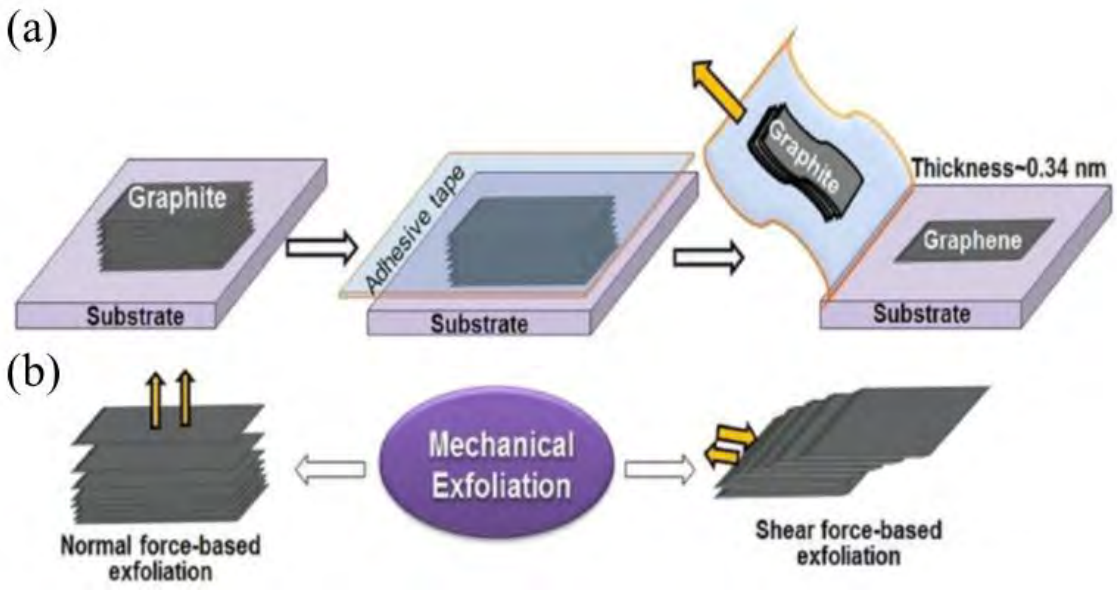

Figure 2.8. (a) Scotch tape-based mechanical exfoliation of graphene layer from bulk graphite. (b) Normal-force and shear-force-based mechanical exfoliation [88].

2.6.3 Chemical exfoliation

Chemical Exfoliation of graphene is a widely used method rooted in the well-known Hummers method to modify the properties of graphene and its oxide forms (e.g., graphene oxide, reduced graphene oxide). It initiates with graphite, featuring its well-known layered carbon structure. The initial stage is the conversion of graphite into graphite oxide (GO). This is achieved by applying strong oxidizing agents like sulfuric acid and potassium permanganate and introducing oxygen-functional groups, such as epoxides, hydroxyls, and carboxyls, onto graphene sheets. GO exhibits an expanded interlayer spacing and diminished electrical conductivity compared to its graphite precursor. The GO is further treated with reducing agents like hydrazine, sodium borohydride, or ascorbic acid. These agents remove oxygen-containing functional groups from graphene oxide to produce reduced graphene oxide (rGO). This stage involves the careful reduction of GO, effectively eliminating oxygen functional groups and reinstating the coveted sp^2 carbon-carbon bonding within the graphene layers. rGO exhibits superior electrical conductivity compared to GO, making it suitable for various electronic and electrical applications.

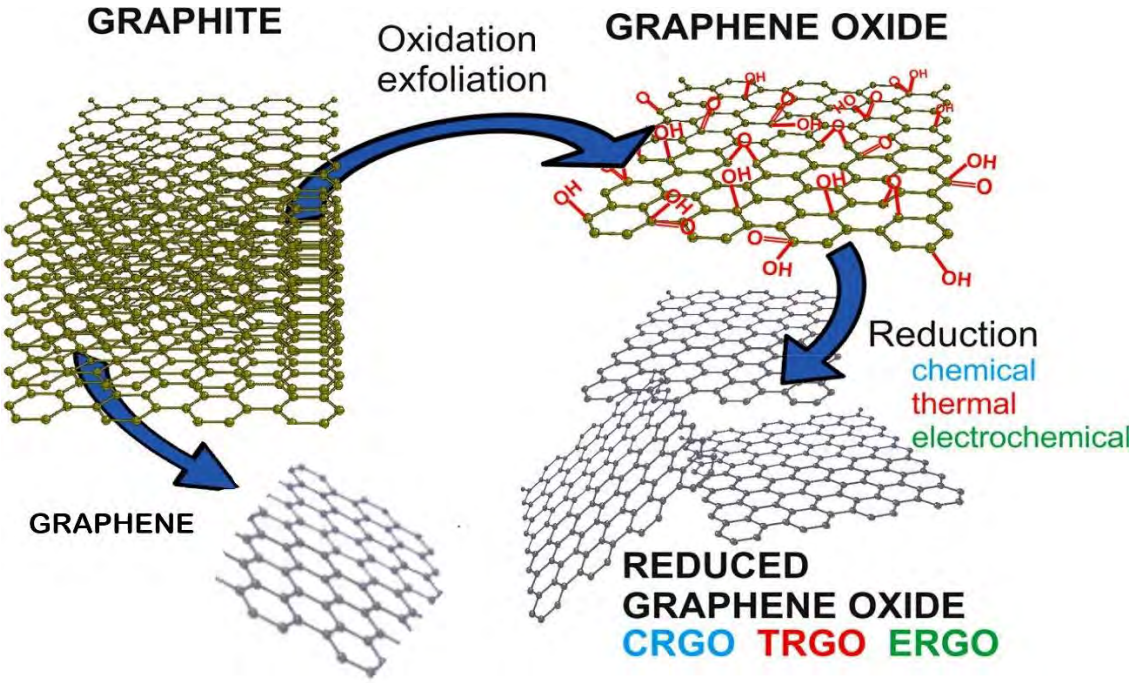

Figure 2.9. Schematic illustration of chemical exfoliation of graphene from graphite [89].

2.6.4 Epitaxial growth

Graphene can be grown on a silicon carbide substrate by heating it to high temperatures in an inert atmosphere. The silicon atoms sublime, leaving behind a carbon-rich surface that forms single or multi-layer graphene. This method is well-suited for producing high-quality epitaxial graphene. It does not require the complicated process of transferring the graphene layer on other substrates and is compatible with electronic device applications.

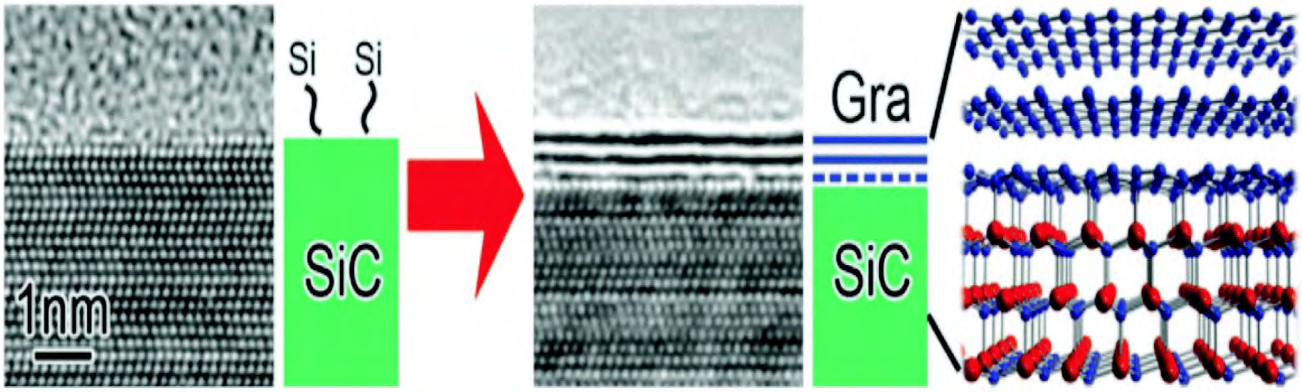

Figure 2.10. Epitaxial growth of graphene by thermal decomposition of SiC, together with the structural model of bilayer graphene on SiC, the blue broken line is the buffer layer. [90].

In our study, graphene was synthesized using physical and chemical methods. We employed a modified Hummer's method to chemically exfoliate graphite flakes, resulting in reduced Graphene Oxide (rGO). The rGO was dispersed in N-Methyl pyrrolidone (NMP) to create an rGO-NMP suspension, which was subsequently applied to the PDMS surface using the spray-coating technique. This approach allows for easy scalability and ensures the reproducibility of the deposited material. Additionally, we achieved the growth of multi-layer graphene through the low-pressure chemical vapor deposition (LPCVD) method, followed by its transfer onto the PDMS substrate.

2.7 Carbon nanotubes

Carbon nanotubes (CNTs) have a unique structure, high thermal conductivity, and extraordinary electrical and mechanical properties. It was discovered by S. Iijima in 1991 [91]. As shown in figure 2.11, CNTs, cylindrical nanostructures composed of carbon atoms, can be divided into two categories based on two fundamental characteristics: the number of walls and chirality. Based on the number of walls, it is further classified into two types, i.e., single-walled CNTs composed of a single rolled graphene sheet and multi-walled CNTs formed by rolling up two or more graphene sheets. The turning of the graphene layer depends on the chiral vector ($\overrightarrow{Ch}$) and chiral angle (θ). The chiral vector is defined by unit vectors and given as ($\vec{C}h$) =n $\overrightarrow{a1}$+ m $\overrightarrow{a2}$ where n and m are chiral indices. Based on chirality and chiral angle (θ), CNTs can be further divided into three different types: zigzag (n, 0), θ=0˚, armchair (n, n), θ=30˚and chiral (helical) CNT (n, m), 0˚<θ<30˚[92].

CNTs have attracted much attention due to their large surface area, piezoresistivity and electrochemical properties, making them a promising smart sensor material. CNTs are nanometer-sized fibers with extremely high aspect ratio, Young's modulus (1 TPa) and tensile strength (100 GPa), good current carrying ability (109 A/cm^2), and thermal conductivity (3500 W/mK) [93]. The electronic properties of nanotubes are a strong function of their atomic structure. Furthermore, mechanical deformation or chemical functionalization of the surface can induce changes in the conductance of a nanotube. The small size of CNTs allow them to be used as extremely small sensors sensitive to the nanotube's chemical and mechanical environments. These properties represent great potential for developing flexible sensors with high stress, strain and low operating

voltage for applications such as interactive electronics, structural health monitoring, smart clothing, robotic systems with advanced sensing capabilities, and human motion detection.

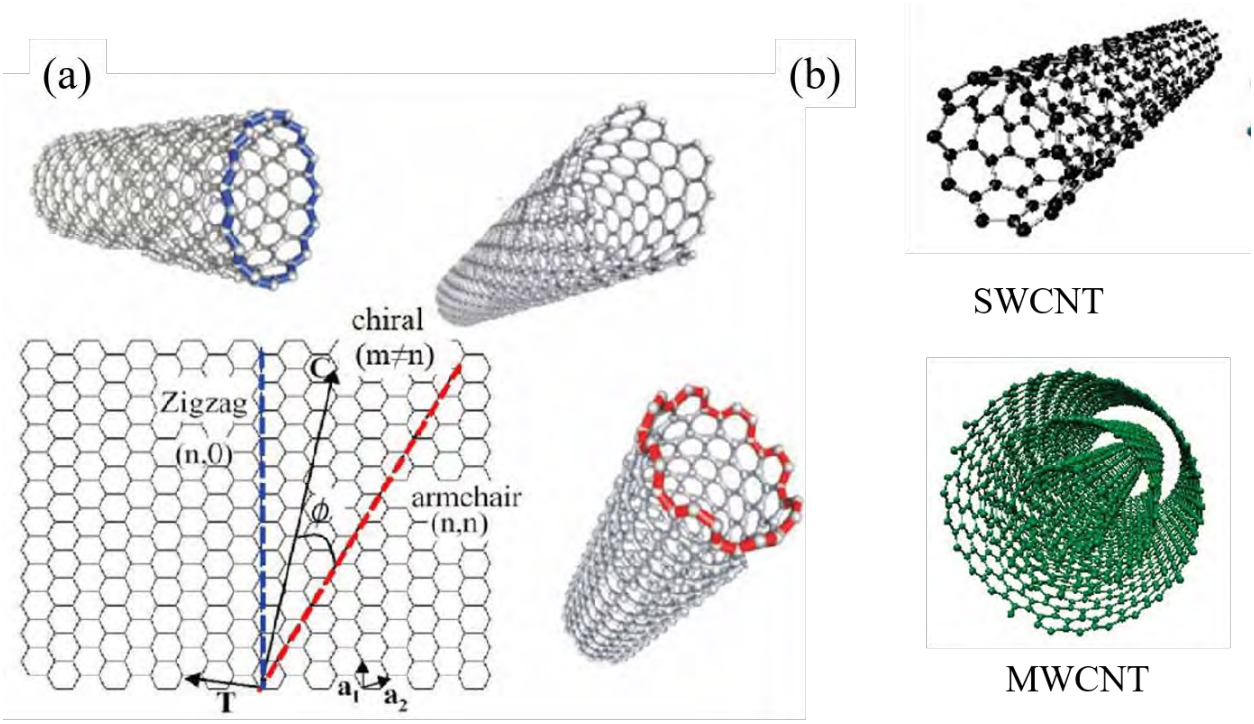

Figure 2.11. (a) Formation of three main types of carbon nanotube structures from a graphene layer, a_1 and a_2 denote unit vectors, while (n,m) denote chiral indices used to describe the exact chiralities of every nanotube: armchair shape, zigzag shape, and chiral shape and (c) representation of single-walled CNT (SWCNT) and multi-walled CNT (MWCNT) [94].

2.8 Applications of flexible strain/pressure sensors in wearable electronics

Carbon nanomaterials are a diverse group of materials composed primarily of carbon atoms arranged in various nanostructured forms. Carbon nanomaterials, particularly CNT and graphene-based flexible sensors, exhibit unique properties such as high sensitivity, wide sensing range, mechanical robustness, low power consumption, excellent repeatability, biocompatibility, flexibility, and bendability, which have tremendous applications in wearable electronics. These applications have gained considerable interest in recent years owing to their tremendous promise, including interactive electronics, structural health monitoring, smart clothing, E-skin, smart textiles, robotic systems with advanced sensing capabilities, electrophysiological signal detection and human motion detection. This section will present some of the applications that align with the targets in our research work.

2.8.1 Human motion detection and health monitoring

Human motion detection and health monitoring devices are crucial in helping individuals to track and manage the health of their well-being. They provide real-time data on various health parameters, such as heart rate, blood pressure, and sleep patterns, providing valuable information for the early detection of potential health issues. Integrating flexible sensors in these devices is paramount, enhancing adaptability to body contours for optimal comfort and precision in capturing data related to shape changes and deformations.

There has been a growing demand for real-time monitoring of human activities in recent years. In contrast to traditional metallic or semiconducting strain sensors with limited stretchability, flexible sensors based on graphene and carbon nanotubes now provide a broader range of strain compatibility. These sensors can be applied on various body parts to track the deformation movements of the body continuously. This monitoring capability extends to vigorous activities like limb bending or stretching and more delicate motions such as emotional expressions and swallowing.

Hua Xu et al. [95] highlighted the impressive capabilities of a graphene-based sensor characterized by high sensitivity, multifunctionality, and wearability. The flexible sensor is fabricated using a reduced oxide graphene film onto a porous inverse opal acetylcellulose film. The resulting sensor can effectively monitor a range of human motions and simultaneously measure ion concentrations in sweat. The sensor proved effective in human motion detection, such as finger bending, wrist bending, head rotation, and various small-scale throat motions. Similarly, Xiaoxu Xie et al. [96] presented a highly sensitive and stretchable strain sensor based on a spirally layered composite yarn and the synergistic effect of carbon nanotube (CNT) and reduced graphene oxide (rGO). Their work showcased the sensor's ability to monitor various human activities, including eye motion, pronunciation, facial expressions, finger bending, and knee movements. In another study, Shan Wang et al. [97] demonstrated a dry and self-adhesive strain sensor composed of a sensing layer and an adhesive layer prepared by solution processing. The sensing layer, made of non-adhesive waterborne polyurethane (WPU) composites of rGO and CNTs, accurately monitored both small- and large-scale body movements, encompassing joint and muscle motions. The adhesive strain sensors effectively monitored body movements with significant or subtle strains, covering the motions of fingers, wrists, knees, ankles, and muscles.

Qi Li et al. [98] described a scalable and highly efficient template method to enhance the sensitivity of a strain sensor based on a CNT/PDMS nanocomposite. The strain sensor successfully detected the bending of fingers and elbows, demonstrating its potential applications as a wearable human body motion monitor, as shown in figure 2.12.

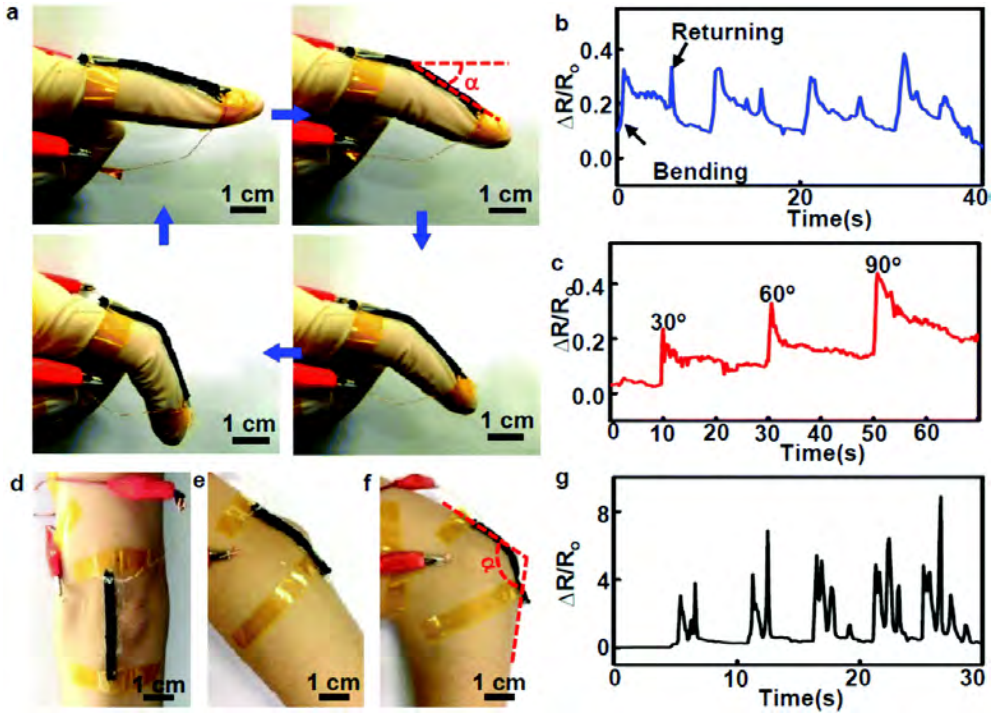

Figure 2.12. Detection of human motions with the strain sensor attached to the human finger and elbow joints: (a) photographs showing the bending test of the finger, (b) the corresponding relative resistance change of the sensor in response to the finger bending, (c) the corresponding relative resistance change of the sensor in response to the different finger-bending angles, (d–f) photographs showing the bending test of the elbow, (g) the corresponding relative resistance change of the sensor in response to the sensor in response to the elbow bending [98].

Mengzhu Wang et al. [99] developed a simple wearable resistive pressure sensor utilizing multi-walled carbon nanotubes (MWCNTs) and graphene nanoflakes (GNFs) on an ultra-deformable flexible substrate (PDMS). The strain sensor effectively captured subtle pulse signals, facial smiles, varied-intensity breathing responses, and different angles of finger bending and reciprocating elbow movements, as shown in figure 2.13. The remarkable performance of this sensor has paved the way for diverse applications in human motion detection, encompassing even minor variations in pulse and respiration.

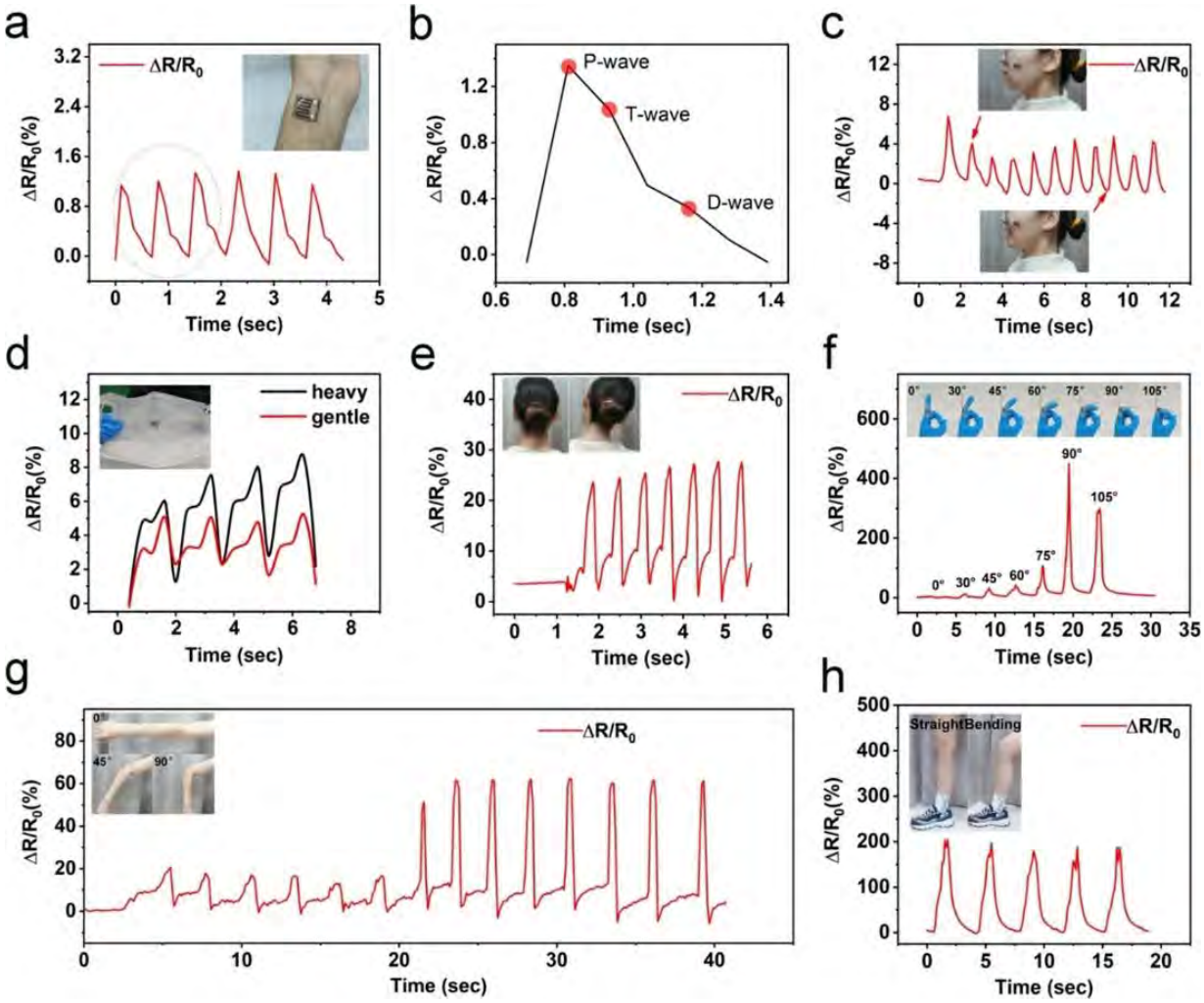

Figure 2.13. Motion responses strain sensor to (a) weak pulse signals, (b) individual pulse waveforms, (c) facial smiling expressions, (d) breathing responses of different intensities in the human body, (e) neck (inclined), (f) finger bending at different angles), (g) reciprocating elbow bending at different angles, and (h) human knee bending [99].

The studies we mentioned include many different human movements, but some specific motions or situations are tricky to monitor accurately. One challenge is ensuring the sensors stay in place during long periods of use, especially when people are moving a lot. Additionally, Composite strain sensors face a limitation in the form of sensor variation caused by uneven distribution of conductive materials within the elastomeric matrix. This problem becomes more pronounced as sensors decrease in size.

2.8.2 Electronic skin (E-Skin)

Skin is the largest sensory organ and receives information from external stimuli. Human body signals have been monitored using wearable devices, which are gradually replaced by electronic skin (e-skin). E-skin is a flexible, stretchable and self-healing electronic device that mimics human skin. It possesses thin, soft, and stretchable qualities, closely resembling the properties of natural skin. It can easily fit on the surface of human skin or robots to feel external environmental stimuli, such as pressure, temperature, and object shape, to achieve haptic perception. Electronic skin devices are typically composed of various types of sensors that mimic the sensing capabilities of human skin. These sensors detect pressure and force, allowing the electronic skin to sense touch and pressure changes. Designing and preparing e-skin presents a significant challenge due to the conventional use of rigid planar electronics, while the functionality of e-skin demands flexibility. To address this, researchers have explored various nanomaterials such as nanofibers, nanowires, nanotubes, and graphene in the fabrication of e-skins.

Detecting physiological signals is crucial for identifying health abnormalities, significantly expanding human health monitoring and diagnostics possibilities. Zhu et al. [100] reported a sensor based on chemical vapor deposited (CVD)-graphene for noninvasive and real-time monitoring of cardiovascular parameters. The study demonstrated that when this sensor is closely knit to human skin, it can accurately detect and distinguish wrist pulses among various age groups before and after physical activity. Human skin can detect and differentiate information such as temperature, surface roughness or smoothness, touch, and vibration. Wang et al. [101] have reported the fabrication of a self-powered multifunctional e-skin using a triboelectric mechanism. This e-skin monitors temperature and pressure and enables simultaneous material recognition. Additionally, they successfully synthesized an e-skin composed of a graphene/PDMS composite, resembling a sponge, exhibiting exceptional sensitivity to changes in both pressure and temperature. Similarly, Zhang et al. [102] demonstrated a pressure–strain sensor-based e-skin on a two-sublayer structure of carbon nanotubes and graphene oxide in hybrid 3D conductive networks. These networks are anchored on a thin, porous PDMS layer. The e-skin not only responded to stimuli such as wrist pulses, gentle feather scratching, and surfaces with varying roughness but also had the capability to monitor human breathing and music rhythm in a noncontact mode.

Zhao et al. [103] use a PEDOT: PSS/SWCNT sensor for flexible electronic skin. As shown in figure 2.14, the sensor comprises upper and lower PEDOT: PSS/SWCNT hybrid electrode arrays with a PDMS dielectric layer in between. The resulting electronic skin seamlessly adheres to the hand during diverse deformations such as folding, twisting, and stretching, demonstrating exceptional mechanical properties. Moreover, the electronic skin facilitates multi-point sensing for spatial pressure distribution and shape recognition in both stretched and non-stretched states. Electronic skin has shown considerable application in flexible robotics, human prosthetics, and artificial intelligence.

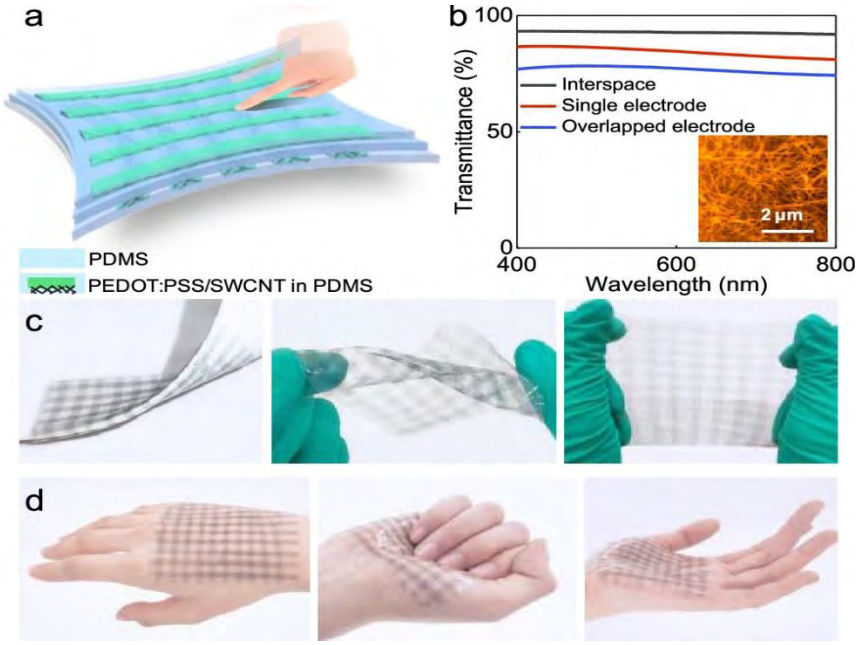

Figure 2.14. Highly stretchable and fully transparent pressure sensor under discriminable strain: (a) Schematic illustration of device design (b) Transmittance curves of the sensor (c) under folding, twisting, and stretching conditions (d) Conformability of the sensor on human hands [103].

Furthermore, Shideh Kabiri Amer et al. [104] designed and fabricated a tattoo-like graphene sensor seamlessly integrated with human skin using a cost- and time-effective "wet transfer, dry patterning" method. The sensor has a total thickness of 463 ± 30 nm, an optical transparency of ~85%, and more than 40% stretchability. The graphene electronic tattoo (GET) can be directly laminated on human skin, just like a temporary tattoo. A bare GET can stay attached to the skin for several hours without fracture or delamination. A GET may stay functional on the skin with liquid bandage coverage for several days.

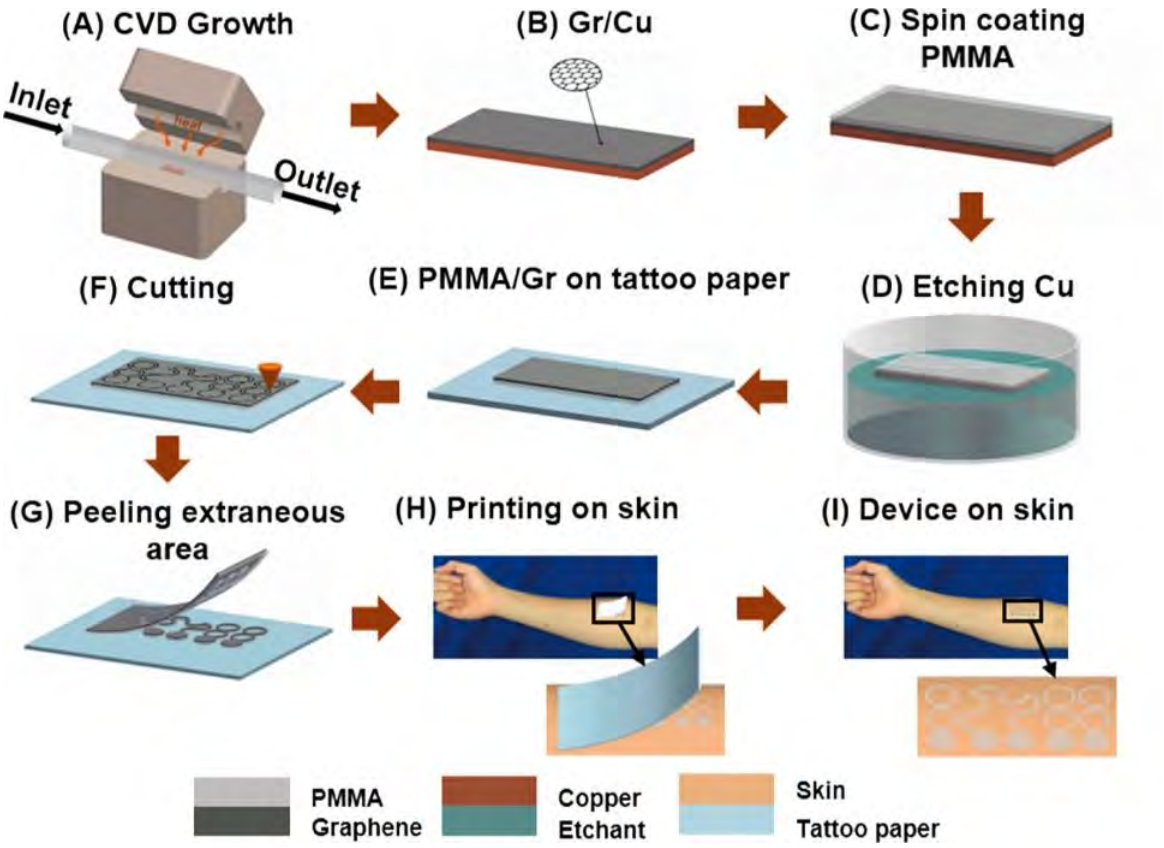

Figure 2.15. Fabrication process of GET. (A, B) Graphene was grown on copper foil using an atmospheric pressure chemical vapor deposition system (APCVD), (C) Less than 500 nm thick PMMA was spin-coated on graphene, (D) Copper was etched away, (E) Graphene/PMMA (Gr/PMMA) was transferred onto the tattoo paper, with PMMA touching the paper and graphene facing up, (F) Gr/PMMA was cut by a mechanical cutter plotter, (G) Extraneous Gr/PMMA was peeled off from the tattoo paper, (H) Mounting GET on the skin like a temporary transfer tattoo, (I) GET on skin [104].

E-skin faces challenges such as skin compatibility issues leading to discomfort and irritation, affecting long-term reproducibility. The changing elasticity of human skin with age creates noncompliance problems. Incorporating e-skin with body parts featuring complex contours is limited, causing potential stress at interfaces. Additionally, there's a concern about a mechanical mismatch between inherently stretchable e-skin and non-stretchable skin, impacting the application of e-skin-based sensors.

2.8.3 Electrophysiological signal detection

Electrophysiological signals capture and record the electrical activity resulting from physiological processes in living organisms. The techniques and equipment employed for signal detection vary based on the signal type and the study's specific context. Standard methods for detecting electrophysiological signal includes Electroencephalogram (EEG), Electromyogram (EMG), Electrocardiogram (ECG or EKG), Electroretinogram (EOG) and Event-Related Potential (ERP). Within these standardized methods, ECG and EMG serve as integral diagnostic tools, offering valuable insights into the functioning of the heart and muscles. Both ECG and EMG signals are measured using electrodes, acting as sensors to detect and capture the electrical activity associated with cardiac and muscular functions. These electrodes require high-quality and close contact with the skin. Electrodes should possess high conductivity and conformability over curved body surfaces to obtain good-quality signals without adversely affecting tissues.

ECG devices employ electrodes placed on the skin to detect and record the electrical impulses triggering each heartbeat. These ECG electrodes can be either wet or dry. Wet electrodes like Ag/AgCl offer good ionic mobility between the skin and the electrode, however, these gels cause skin irritations during long-term monitoring. Addressing this, dry electrodes have emerged, excelling in capturing accurate signals without the need for electrolytes [105]. In contrast, dry electrodes based on metal discs or files and metal clamps, historically rigid, do not fit to the skin. As a result of this, these electrodes produce high skin-electrode impedance and are highly susceptible to motion artefacts, resulting in poor signal quality [106]. Recent advances in flexible dry electrodes enable recording good quality electrophysiological signals compared to conventional dry electrodes as they conform over the body parts, thus minimizing the impedance and motion artefact.

The ECG signal is detected and recorded by applying electrodes on the body surface, enabling us to find and diagnose cardiovascular diseases. A typical functioning of the heart involves sequences of depolarization and repolarization and tracing the deflections of these waves, as shown in figure 2.16. The characteristic ECG signal waveform comprise of five segments: P, Q, R, S, and T. The QRS segments together form the characteristic spike in ECG signals, called the QRS complex. Physiologically, the P-wave corresponds to the initiation of atrial depolarization by the SA node, the QRS complex represents the ventricular depolarization begins at the apex

(atrial repolarization occurs), and the T wave corresponds to the ventricular repolarization beginning at the apex. The ECG signal contains all the heart's functioning information in similar fashions.

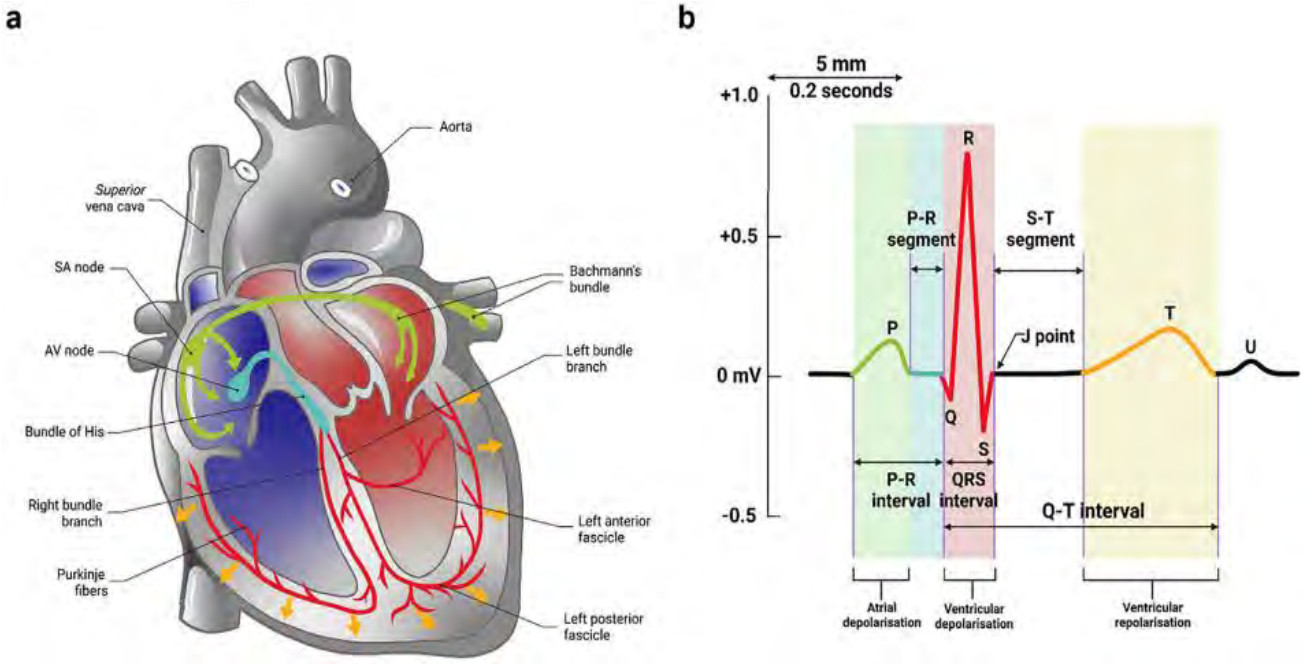

Figure 2.16. (a) Schematic showing the various sequences of depolarization and repolarization of the heart; (b) A typical electrocardiogram (ECG) waveform and its characteristic patterns (P and T waves, PR and ST segments, PR and QT intervals, and the QRS complex) [107].

On the other hand, an electromyogram (EMG) is a diagnostic test that measures the electrical activity generated by muscles during contraction and at rest. It involves applying electrodes to muscles to record muscle activity. The recorded EMG signal provides valuable information about muscle function, including the timing, strength, and pattern of muscle contractions. EMG is commonly used in medical settings to diagnose neuromuscular disorders, assess muscle activity, and aid in the development of treatment plans for conditions affecting the muscles and nerves.

Flexible dry electrodes are crucial in applications such as EEG and EMG. They are often developed by embedding the conductive materials (micro/nanomaterials and conductive polymers) into flexible polymers. These electrodes enhance the contact interface, allowing for a conformal fit even on curved surfaces. PDMS has attracted much attention among the various polymers due

to its transparency, biocompatibility, stretchability, and chemically resistive nature. Conductive micro or nanomaterials include carbon and its derivative, metal nanomaterials, and conductive polymers, and their hybrid composition has been widely used to fabricate flexible dry electrodes for acquiring electrophysiological signals. Flexible dry electrodes with high conductivity, bio-compatibility, conformability, and low skin-electrodes impedance are desirable for obtaining medical-grade electrophysiological signals.

Furthermore, flexible electrodes incorporate biocompatible materials, minimizing skin irritation for enhancing user comfort during prolonged wear. The evolution of flexible sensor technology extends to wearable applications, enabling continuous monitoring of electrophysiological signals in real-world environments. Wearable EEG and EMG devices with flexible electrodes offer insights beyond traditional laboratory settings by studying neural and muscular activity during dynamic activities.

Sajjad Asadi and his group [108] have developed graphene sponge-based elastomeric wearable dry electrodes to measure ECG signals. In their work, graphene sponge (GS) electrodes were produced via a freeze-casting process. They measured skin-electrode impedance and ECG signal using dry electrodes and compared them with conventional wet Ag/AgCl electrodes. The suggested graphene electrodes exhibit outstanding electrical properties, flexibility, wearability, and biocompatibility, offering a promising alternative for upcoming wearable sensors designed for real-time monitoring.

J.Y Baek et al. [109] developed a flexible dry electrode based on a Ti/Au metal layer on a thin PDMS substrate for electrophysiological signal acquisition. In their approach, metal films were deposited on the flexible substrate by e-beam evaporation, followed by photolithography and chemical etching. Finally, the metal pattern PDMS layer is bonded to the PDMS base substrate. They fabricated the forearm-wearable electrode by connecting the Velcro to the PDMS electrode, as shown in figure 2.18, for real-time measurements. They measured skin-electrode impedance and ECG signal using dry electrodes and compared them with conventional wet Ag/AgCl electrodes. After seven days of ECG monitoring, they investigated the feasibility of long-term monitoring of electrodes on the skin and showed better skin compatibility after long-term tests. However, the adhesion of deposited metal film on the PDMS substrate is the biggest challenge for continuous and long-term monitoring of signals.

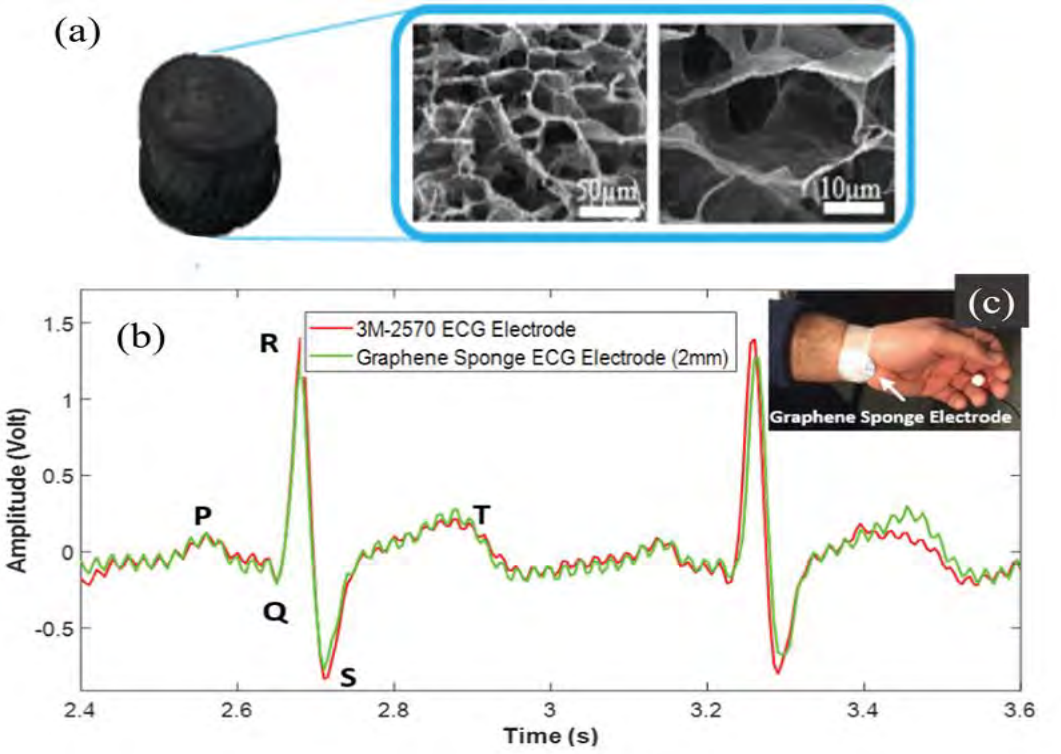

Figure 2.17. (a) Photograph of an uncompressed graphene sponge electrode and SEM images (top-view) of the electrodes, (b) the ECG signals measured by the graphene sponge and conventional (Ag/AgCl) electrode, (c) Demonstration of the GS electrode connection to the wrist by anti-allergic tape to measure ECG without any gel or electrolyte [108].

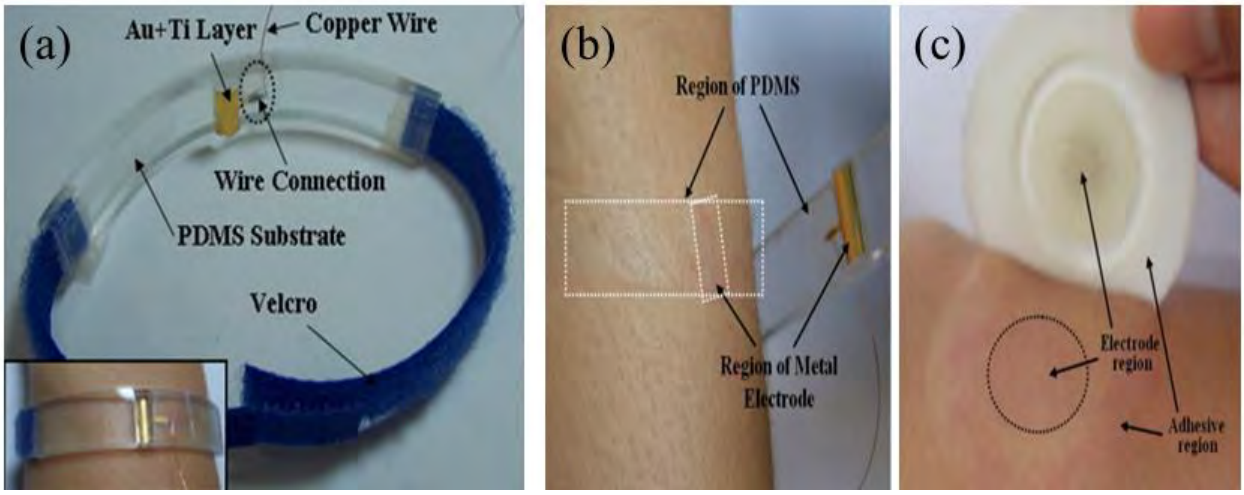

Figure 2.18. (a) Image of the fabricated electrode (inset: electrode wound around the forearm), (b) skin under the PDMS-based dry electrode after seven days of use, (c) skin under the Ag/AgCl electrode after two days of use [109].

Furthermore, Jie Yang et al. [110] developed a facile fabrication of robust and reusable PDMS-supported laser-induced graphene (LIG) dry electrodes for wearable electrocardiogram monitoring. The laser processing system easily patterned and produced the LIG/PDMS epidermal electrodes in batches. The LIG/PDMS dry electrode is washable, flexible, and reusable. With high-power ultrasonic treatments (5 h), as shown in figure 2.19, the as-prepared electrodes retained high electrical performance and excellent robustness, making them suitable for long-term monitoring. In collecting ECG signals, LIG/PDMS electrodes exhibit high performance comparable to commercial Ag/AgCl electrodes, and the epidermal electrode is also suitable for EMG monitoring.

Cunguang Lou et al. [111] fabricated graphene-based electrodes and a corresponding wireless ECG collection system. They developed different types of electrodes, such as graphene–PET, graphene paper and graphene textile, for ECG signal detection. The graphene textile electrode can more easily detect the highly sensitive ECG signals in all fabricated electrodes.

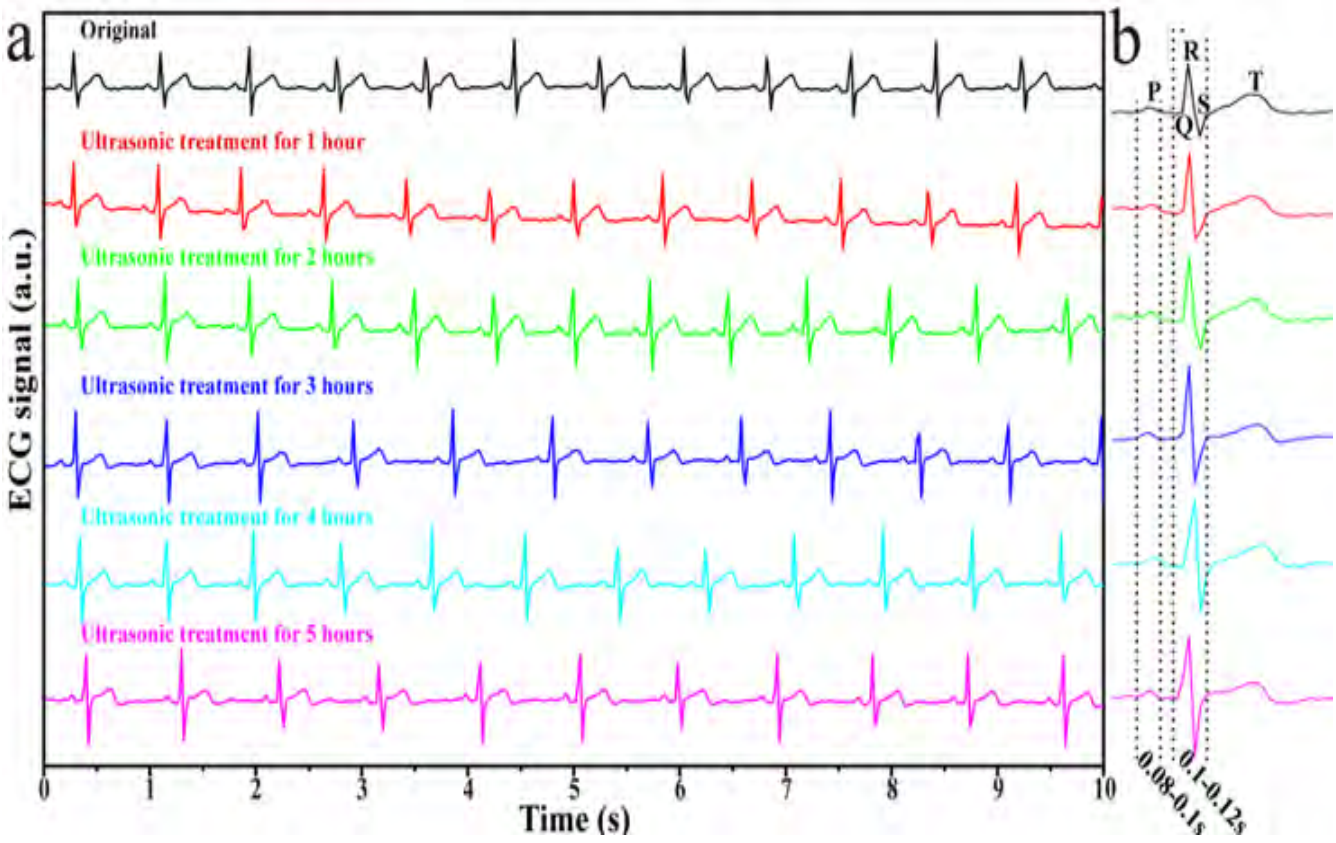

Figure 2.19. (a) Stability of LIG/PDMS electrodes, (b) ECG signals collected after different ultrasonic treatment cycles [110].

2.8.4 Human-machine interface

Human-machine interface (HMI) devices facilitate effective communication and interaction between humans and machines. The importance of HMI devices lies in their ability to enhance user experience, increase productivity, and enable seamless control and monitoring of complex systems. Wearable electronic devices with light mass, excellent flexibility, and mechanical properties have important research implications in future wearable HMI applications. Gestures are considered a linguistic communication technique that is intuitive, easy to use, and can be used as a special language to communicate with computers or robots.

Ling Zhang et al. [112] developed a self-protective and reproducible e-textile (SPRET) sensor. This sensor is composed of an entangled carbon nanotube (CNT) network, a combined polypyrrole-polydopamine-perfluorodecyltrlethoxysilane (PPy-PDA-PFDS) polymer layer and a textile substrate in a hierarchical manner. They implemented a human–robot interaction system utilizing a smart glove with the SPRET sensor array. As shown in figure 2.20, the SPRET glove pressure sensor accurately and reliably detects a wide range of physiological signals. In this innovative application, each finger of the robot synchronized with the human fingers, executing three sequential gestures that conveyed the message 'I love you'.

Furthermore, Sudeep Sharma et al. [113] designed and developed a stretchable, all-directional strain-insensitive electronic glove for HMI application. The electronic glove is fabricated using CNT-coated laser-engraved graphene (CNT/LEG), employing CO_2 laser engraving and electrospinning methods in its construction. The proposed e-glove has a ripple-like meandering sensing area and interconnections designed to stretch in response to the applied deformation without affecting the performance of the sensors, offering full mechanical stretchability. The e-glove, used as dry ECG electrodes, displayed high-quality ECG signals even under stretching conditions with typical PQRST wave peaks. The ECG recordings were comparable to the commercial Ag/AgCl gel electrodes. As shown in figure 2.21, the e-glove demonstrated the capability to control a robotic hand based on the gesture of human fingers.

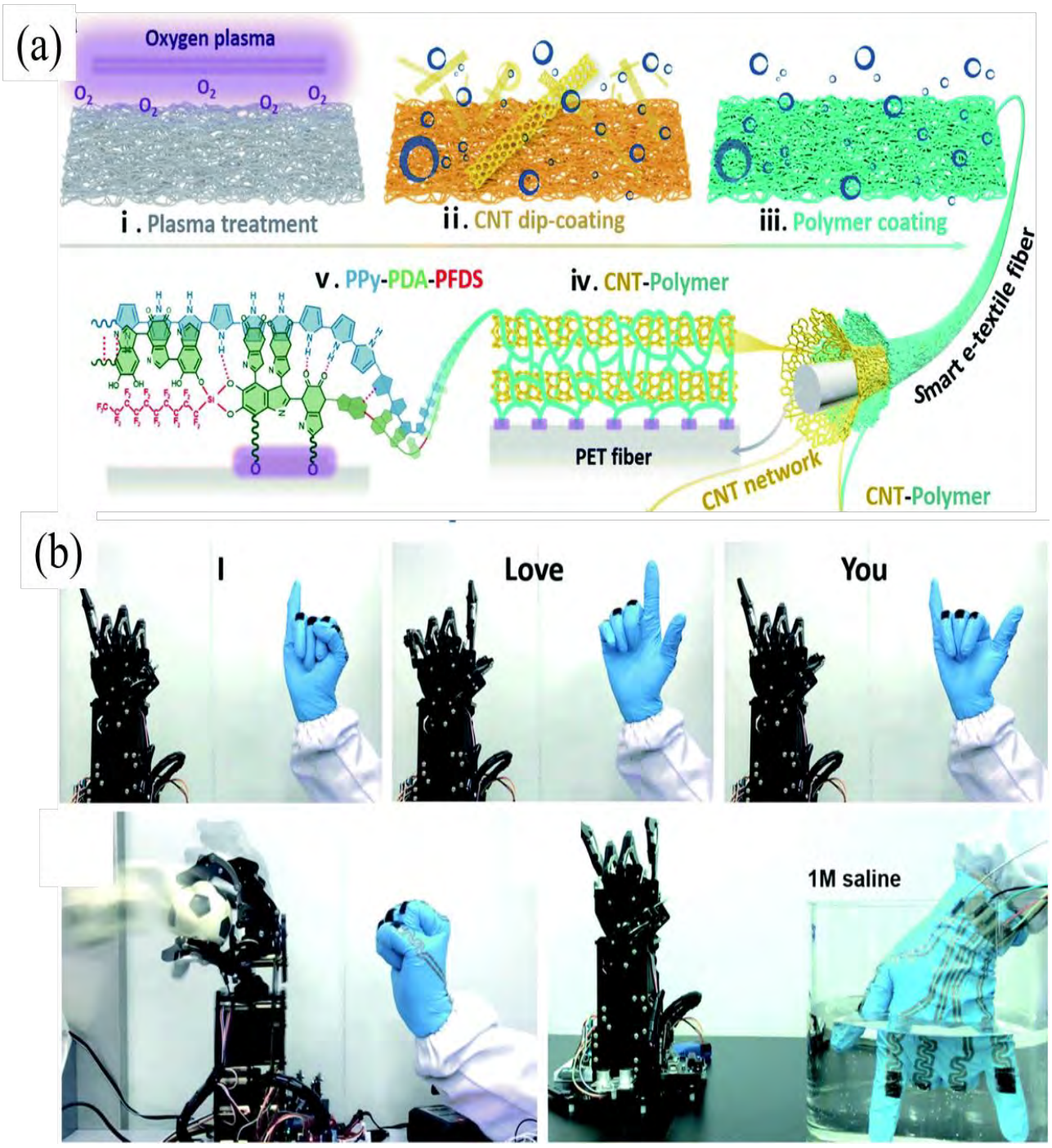

Figure. 2.20. (a) Schematic illustration of the preparation and structure of smart textile fibers with a "steel-concrete" layered structure. (b) Synchronized control of a robotic hand by human hand movements based on wearable smart textile sensors [112].

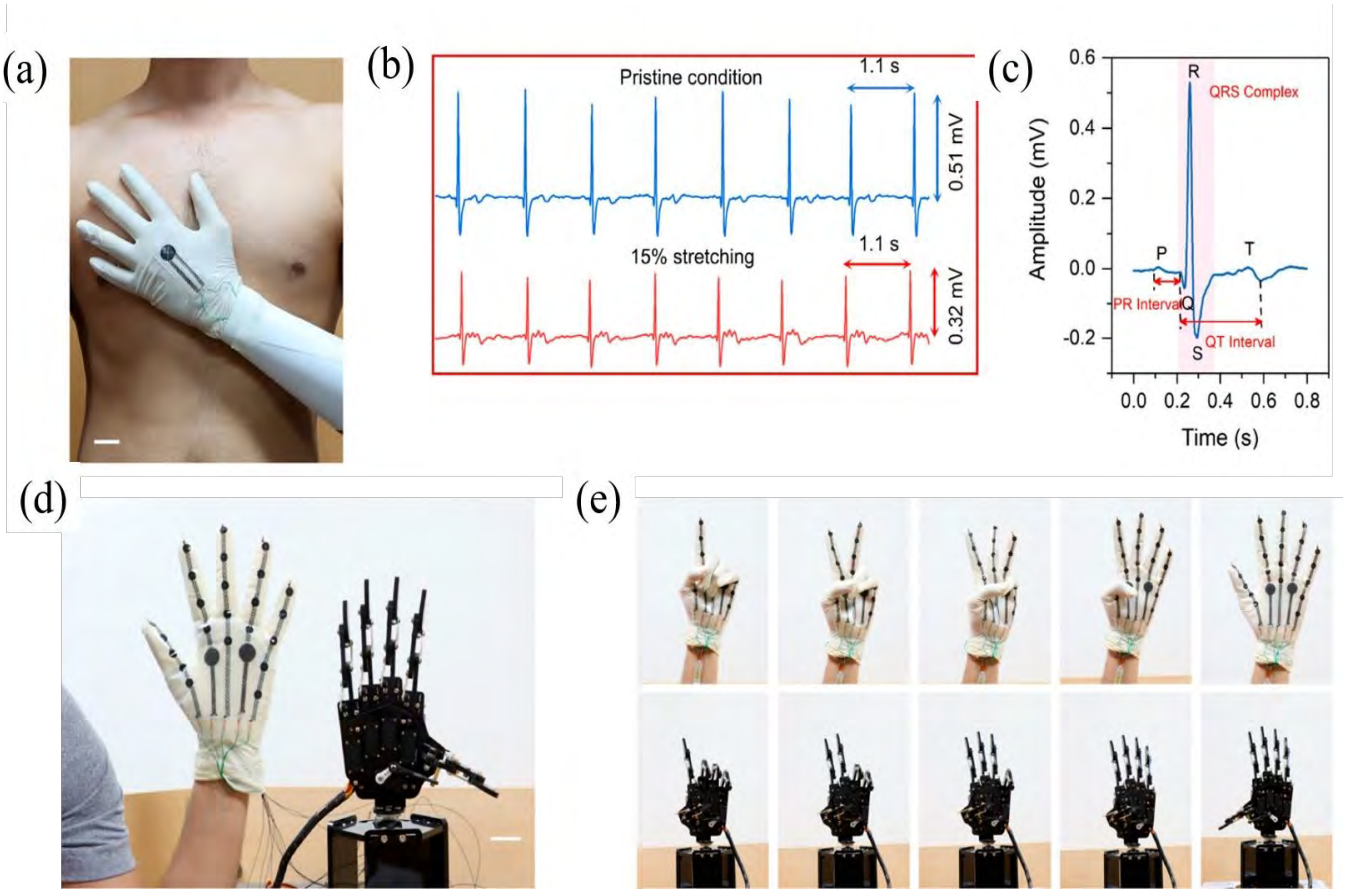

Figure. 2.21. (a) An optical image of the e-glove system in contact with the human chest for recording ECG signals, (b) ECG signals measured for eight continuous cycles from the chest at unstretched and 15% stretched, showing reduced amplitude under stretched conditions with noise introduction, (c) Characteristic peaks of the ECG waveform, encompassing P, Q, R, S, and T waves,(d) Photographs highlight the integration of the e-glove with a wired interactive robotic hand, (e) Real-time demonstrations of human–machine interactions are captured through photographs, showcasing the control of the robotic hand via the opening and closing of a human finger equipped with the e-glove [113].

2.9 Conclusions

In conclusion, flexible strain and pressure sensors are pivotal in health monitoring, human motion detection, and human-machine interface systems, boasting cost-effectiveness, scalability, easy fabrication, and ability to conform over arbitrary body surfaces and complex geometries. While conventional sensors excel in performance and stability, but they are rigid, planar, and lack flexibility and conformability. The fabrication of flexible sensors and dry

electrodes, employing materials like metal nanoparticles, carbon nanomaterials, and conductive polymers embedded in flexible substrates, demonstrates potential in wearable electronics.

Key parameters, including sensitivity and stretchability, working range, stability and durability, linearity, hysteresis, response and recovery time, depend on active elements, substrate material, and fabrication techniques. Despite notable achievements, challenges persist in achieving high stretchability, sensitivity, stability, durability, and comfort for detecting various human motions and vital signs. Achieving high conductivity with superior conformability is crucial for flexible dry electrodes, ensuring high-quality electrophysiological signals with low and stable skin-electrode impedance. Carbon nanomaterials like graphene and carbon nanotubes emerged as cost-effective solutions with exceptional properties, leading to their widespread use in flexible sensor fabrication. Subsequent chapters delve into the fabrication of flexible strain and pressure sensors and dry electrodes based on graphene and carbon nanotubes for various wearable electronic applications.

References

[1] P. Jiang, Z. Ji, X. Zhang, Z. Liu, and X. Wang, "Recent advances in direct ink writing of electronic components and functional devices," *Progress in Additive Manufacturing*, vol. 3, pp. 65-86, 2018.

[2] Y. Wang, J. Hao, Z. Huang, G. Zheng, K. Dai, C. Liu, and C. Shen, "Flexible electrically resistive-type strain sensors based on reduced graphene oxide-decorated electrospun polymer fibrous mats for human motion monitoring," *Carbon*, vol. 126, pp. 360-371, 2018.

[3] M. A. Saleh, R. Kempers, and G. W. Melenka, "A comparative study on the electromechanical properties of 3D-Printed rigid and flexible continuous wire polymer composites for structural health monitoring," *Sensors and Actuators A: Physical*, vol. 328, p. 112764, 2021.

[4] J. Wu et al., "Highly flexible and sensitive wearable e-skin based on graphite nanoplatelet and polyurethane nanocomposite films in mass industry production available," *ACS applied materials & interfaces*, vol. 9, no. 44, pp. 38745-38754, 2017.

[5] R. Yin, D. Wang, S. Zhao, Z. Lou, and G. Shen, "Wearable sensors-enabled human–machine interaction systems: from design to application," *Advanced Functional Materials*, vol. 31, no. 11, p. 2008936, 2021.

[6] F. Zhang et al., "A highly accurate flexible sensor system for human blood pressure and heart rate monitoring based on graphene/sponge," *RSC advances*, vol. 12, no. 4, pp. 2391-2398, 2022.

[7] Z. Deng, L. Guo, X. Chen, and W. Wu, "Smart Wearable Systems for Health Monitoring," *Sensors*, vol. 23, no. 5, p. 2479, 2023.

[8] L. Liza, M. H. Kabir, L. Jiang, S. Jerrams, and S. Chen, "The technology of wearable flexible textile-based strain sensors for monitoring multiple human motions: construction, patterning and performance," *Sensors & Diagnostics*, 2023.

[9] X. Zhou et al., "Superhydrophobic Flexible Strain Sensors Constructed Using Nanomaterials: Their Fabrications and Sustainable Applications," *Nanomaterials*, vol. 13, no. 19, p. 2639, 2023.

[10] J. C. Costa et al., "Flexible sensors—from materials to applications," *Technologies*, vol. 7, no. 2, p. 35, 2019.

[11] E. Liu et al., "An Overview of Flexible Sensors: Development, Application, and Challenges," *Sensors*, vol. 23, no. 2, p. 817, 2023.

[12] A. K. Yadav, N. Yadav, Y. Wu, S. RamaKrishna, and H. Zheng, "Wearable Strain Sensors: State-of-art and Future Applications," *Materials Advances*, 2023.

[13] F. Xu et al., "Recent developments for flexible pressure sensors: A review," *Micromachines*, vol. 9, no. 11, p. 580, 2018.

[14] C. V. N. Bhaskar, S. Pal, and P. K. Pattnaik, "Recent advancements in fiber Bragg gratings based temperature and strain measurement," *Results in Optics*, vol. 5, p. 100130, 2021.

[15] C. E. Campanella et al., "Fibre Bragg grating based strain sensors: Review of technology and applications," *Sensors*, vol. 18, no. 9, p. 3115, 2018.

[16] C. Covaci and A. Gontean, "Piezoelectric energy harvesting solutions: A review," *Sensors*, vol. 20, no. 12, p. 3512, 2020.

[17] J. Qin et al., "Flexible and stretchable capacitive sensors with different microstructures," *Advanced Materials*, vol. 33, no. 34, p. 2008267, 2021.

[18] C. Deng et al., "Highly stretchable vertical graphene electrodes for capacitive strain sensors," *Journal of Materials Chemistry C*, vol. 8, no. 16, pp. 5541-5546, 2020.

[19] D. Li et al., "Microstructure design and optimization of high-sensitivity interdigital capacitive humidity sensor based on uncertainty analysis," *Measurement*, vol. 178, p. 108993, 2022.

[20] A. Matin Nazar et al., "Skin-contact triboelectric nanogenerator for energy harvesting and motion sensing: Principles, challenges, and perspectives," *Biosensors*, vol. 13, no. 9, p. 872, 2023.

[21] H. Wang et al., "Triboelectric nanogenerators for human-health care," *Science Bulletin*, vol. 66, no. 5, pp. 490-511, 2021.

[22] N. Lu et al., "Highly sensitive skin-mountable strain gauges based entirely on elastomers," *Advanced Functional Materials*, vol. 22, no. 19, pp. 4044-4050, 2012.

[23] Q. Zheng et al., "Graphene-based wearable piezoresistive physical sensors," *Materials Today*, vol. 36, pp. 158-179, 2020.

[24] Y. Zhang et al., "Elastic fibers/fabrics for wearables and bioelectronics," *Advanced Science*, vol. 9, no. 35, p. 2203808, 2022.

[25] Y. Wang, J. Hao, Z. Huang, G. Zheng, K. Dai, C. Liu, and C. Shen, "Flexible electrically resistive-type strain sensors based on reduced graphene oxide-decorated electrospun polymer fibrous mats for human motion monitoring," *Carbon*, vol. 126, pp. 360-371, 2018.

[26] Y. Zheng et al., "The effect of filler dimensionality on the electromechanical performance of polydimethylsiloxane based conductive nanocomposites for flexible strain sensors," *Composites Science and Technology*, vol. 139, pp. 64-73, 2017.

[27] F. Zhang et al., "Synergism of binary carbon nanofibres and graphene nanoplates in improving sensitivity and stability of stretchable strain sensors," *Composites Science and Technology*, vol. 172, pp. 7-16, 2019.

[28] H. Souri and D. Bhattacharyya, "Highly stretchable and wearable strain sensors using conductive wool yarns with controllable sensitivity," *Sensors and Actuators A: Physical*, vol. 285, pp. 142-148, 2019.

[29] T. Li et al., "A flexible strain sensor based on CNTs/PDMS microspheres for human motion detection," *Sensors and Actuators A: Physical*, vol. 306, p. 111959, 2020.

[30] Y. R. Jeong et al., "Highly stretchable and sensitive strain sensors using fragmentized graphene foam," *Advanced Functional Materials*, vol. 25, no. 27, pp. 4228-4236, 2015.

[31] G. Shi et al., "Highly sensitive, wearable, durable strain sensors and stretchable conductors using graphene/silicon rubber composites," *Advanced Functional Materials*, vol. 26, no. 42, pp. 7614-7625, 2016.

[32] S. Chen et al., "A highly stretchable strain sensor based on a graphene/silver nanoparticle synergic conductive network and a sandwich structure," *Journal of Materials Chemistry C*, vol. 4, no. 19, pp. 4304-4311, 2016.

[33] M. Xu et al., "Highly stretchable strain sensors with reduced graphene oxide sensing liquids for wearable electronics," *Nanoscale*, vol. 10, no. 11, pp. 5264-5271, 2018.

[34] Y. Wang et al., "Ultra-stretchable, sensitive and durable strain sensors based on polydopamine encapsulated carbon nanotubes/elastic bands," *Journal of Materials Chemistry C*, vol. 6, no. 30, pp. 8160-8170, 2018.

[35] J. Z. Gul, M. Sajid, and K. H. Choi, "Retraction: 3D printed highly flexible strain sensor based on TPU–graphene composite for feedback from high speed robotic applications," *Journal of Materials Chemistry C*, vol. 8, no. 7, pp. 2597-2597, 2020.

[36] X. Guo et al., "Highly stretchable strain sensor based on SWCNTs/CB synergistic conductive network for wearable human-activity monitoring and recognition," *Smart Materials and Structures*, vol. 26, no. 9, p. 095017, 2017.

[37] J. Li et al., "Highly stretchable and sensitive strain sensor based on facilely prepared three-dimensional graphene foam composite," *ACS applied materials & interfaces*, vol. 8, no. 29, pp. 18954-18961, 2016.

[38] Y. Li et al., "Strain sensor with both a wide sensing range and high sensitivity based on braided graphene belts," *ACS applied materials & interfaces*, vol. 12, no. 15, pp. 17691-17698, 2020.

[39] X. Wang, J. Yu, Y. Cui, and W. Li, "Research progress of flexible wearable pressure sensors," *Sensors and Actuators A: Physical*, vol. 330, p. 112838, 2021.

[40] X. Wang, J. Yu, Y. Cui, and W. Li, "Research progress of flexible wearable pressure sensors," *Sensors and Actuators A: Physical*, vol. 330, p. 112838, 2021.

[41] Y. Xiong et al., "A flexible, ultra-highly sensitive and stable capacitive pressure sensor with convex microarrays for motion and health monitoring," *Nano energy*, vol. 70, p. 104436, 2020.

[42] T. Seesaard and C. Wongchoosuk, "Flexible and Stretchable Pressure Sensors: From Basic Principles to State-of-the-Art Applications," *Micromachines*, vol. 14, no. 8, p. 1638, 2023.

[43] W. J. Kim et al., "Piezoresistive Effect of Conductive and Non-Conductive Fillers in Bi-Layer Hybrid CNT Composites under Extreme Strain," *Materials*, vol. 16, no. 18, p. 6335, 2023.

[44] Y. Duan et al., "Recent progress in flexible pressure sensor arrays," *Nanomaterials*, vol. 12, no. 14, p. 2495, 2022.

[45] Y. Wang et al., "Highly sensitive and flexible tactile sensor with truncated pyramid-shaped porous graphene/silicone rubber composites for human motion detection," *Composites Science and Technology*, vol. 217, p. 109078, 2022.

[46] J. W. Zhang et al., "A flexible pressure sensor based on PEDOT coated polyester nonwoven fabric for low-pressure range," *Smart Materials and Structures*, vol. 31, no. 3, p. 035025, 2022.

[47] J. Jia et al., "Skin-inspired flexible and high-sensitivity pressure sensors based on rGO films with continuous-gradient wrinkles," *Nanoscale*, vol. 11, no. 10, pp. 4258-4266, 2019.

[48] X. Guo et al., "Human touch sensation-inspired, ultrawide-sensing-range, and high-robustness flexible piezoresistive sensor based on CB/MXene/SR/fiber nanocomposites for wearable electronics," *Composite Structures*, vol. 321, p. 117329, 2023.

[49] Y. Zhai et al., "Flexible and wearable carbon black/thermoplastic polyurethane foam with a pinnate-veined aligned porous structure for multifunctional piezoresistive sensors," *Chemical Engineering Journal*, vol. 382, p. 122985, 2020.

[50] M. Xu et al., "Flexible pressure sensor using carbon nanotube-wrapped polydimethylsiloxane microspheres for tactile sensing," *Sensors and Actuators A: Physical*, vol. 284, pp. 260-265, 2018.

[51] Y. Liu et al., "Flexible Pressure Sensor Based on Tetrapod-Shaped ZnO-PDMS Piezoelectric Nanocomposites," *IEEE Sensors Journal*, vol. 23, no. 4, pp. 3532-3540, 2023.

[52] T. Yang et al., "Hierarchically structured PVDF/ZnO core-shell nanofibers for self-powered physiological monitoring electronics," *Nano Energy*, vol. 72, p. 104706, 2020.

[53] J. Park et al., "Giant tunneling piezoresistance of composite elastomers with interlocked microdome arrays for ultrasensitive and multimodal electronic skins," *ACS nano*, vol. 8, no. 5, pp. 4689-4697, 2014.

[54] M. Jian et al., "Flexible and highly sensitive pressure sensors based on bionic hierarchical structures," *Advanced Functional Materials*, vol. 27, no. 9, p. 1606066, 2017.

[55] K.-H. Kang et al., "Wearable Resistive Pressure Sensor Based on Highly Flexible Carbon Composite Conductors with Irregular Surface Morphology," *ACS Applied Materials & Interfaces* Vol 9, no 20, pp. 17499-17507, 2017.

[56] P. Zhang et al., "Preparation and application of fabric-based interlocking microstructured flexible piezoresistive sensors," *Sensors and Actuators A: Physical*, vol. 363, p. 114740, 2023.

[57] H. Souri et al., "Wearable and stretchable strain sensors: materials, sensing mechanisms, and applications," *Advanced Intelligent Systems*, vol. 2, no. 8, p. 2000039, 2020.

[58] X. Zhang et al., "High-performance flexible strain sensors based on biaxially stretched conductive polymer composites with carbon nanotubes immobilized on reduced graphene oxide," *Composites Part A: Applied Science and Manufacturing*, vol. 151, p. 106665, 2021.

[59] X. Li et al., "Wearable strain sensing textile based on one-dimensional stretchable and weavable yarn sensors," *Nano Research*, vol. 11, pp. 5799-5811, 2018.

[60] J. Zhai et al., "Flexible waterborne polyurethane/cellulose nanocrystal composite aerogels by integrating graphene and carbon nanotubes for a highly sensitive pressure sensor," *ACS Sustainable Chemistry & Engineering*, vol. 9, no. 42, pp. 14029-14039, 2021.

[61] J. Zhou et al., "Multiscale and hierarchical wrinkle enhanced graphene/Ecoflex sensors integrated with human-machine interfaces and cloud-platform," *npj Flexible Electronics*, vol. 6, no. 1, p. 55, 2022.

[62] L. Shi et al., "Quantum effect-based flexible and transparent pressure sensors with ultrahigh sensitivity and sensing density," *Nature communications*, vol. 11, no. 1, p. 3529, 2020.

[63] Y. Li et al., "Hybrid strategy of graphene/carbon nanotube hierarchical networks for highly sensitive, flexible wearable strain sensors," *Scientific Reports*, vol. 11, no. 1, p. 21006, 2021.

[64] S. Zhang et al., "3D MXene/PEDOT: PSS composite aerogel with a controllable patterning property for highly sensitive wearable physical monitoring and robotic tactile sensing," *ACS Applied Materials & Interfaces*, vol. 14, no. 20, pp. 23877-23887, 2022.

[65] X. Su et al., "A highly conducting polymer for self-healable, printable, and stretchable organic electrochemical transistor arrays and near hysteresis-free soft tactile sensors," *Advanced Materials*, vol. 34, no. 19, p. 2200682, 2022.

[66] P. Xia et al., "Highly stretchable and sensitive flexible resistive strain sensor based on waterborne polyurethane polymer for wearable electronics," *Composites Science and Technology*, vol. 221, p. 109355, 2022.

[67] Y. Zhong et al., "Tunable wrinkled graphene foams for highly reliable piezoresistive sensor," *Sensors and Actuators A: Physical*, vol. 281, pp. 141-149, 2018.

[68] X. F. Zhao et al., "A skin-like sensor for intelligent Braille recognition," *Nano Energy*, vol. 68, p. 104346, 2020.

[69] Y. Long et al., "Molybdenum-carbide-graphene composites for paper-based strain and acoustic pressure sensors," *Carbon*, vol. 157, pp. 594-601, 2020.

[70] P. Wang et al., "Surface engineering via self-assembly on PEDOT: PSS fibers: Biomimetic fluff-like morphology and sensing application," *Chemical Engineering Journal*, vol. 425, p. 131551, 2021.

[71] Y. Kumaresan et al., "Multifunctional electronic skin with a stack of temperature and pressure sensor arrays," *IEEE Sensors Journal*, vol. 21, no. 23, pp. 26243-26251, 2021.

[72] K. Hu et al., "One-step construction of flexible conductive-piezoelectric nanoresistance network material for pressure sensing and positioning," *Colloids and Surfaces A: Physicochemical and Engineering Aspects*, vol. 641, p. 128592, 2022.

[73] F. L. Gao et al., "Integrated temperature and pressure dual-mode sensors based on elastic PDMS foams decorated with thermoelectric PEDOT: PSS and carbon nanotubes for human energy harvesting and electronic-skin," *Journal of Materials Chemistry A*, vol. 10, no. 35, pp. 18256-18266, 2022.

[74] Z. Tan et al., "Breathing-effect assisted transferring large-area PEDOT: PSS to PDMS substrate with robust adhesion for stable flexible pressure sensor," *Composites Part A: Applied Science and Manufacturing*, vol. 143, p. 106299, 2021.

[75] Y. Su et al., "Muscle fibers inspired high-performance piezoelectric textiles for wearable physiological monitoring," *Advanced Functional Materials*, vol. 31, no. 19, p. 2010962, 2021.

[76] K.I. Bolotin et al., "Ultrahigh electron mobility in suspended graphene," *Solid state communications*, vol. 146, no. 9-10, pp. 351-355, 2008.

[77] A.A. Balandin et al., "Superior thermal conductivity of single-layer graphene," *Nano letters*, vol. 8, no. 3, pp. 902-907, 2008.

[78] S.V. Morozov et al., "Giant intrinsic carrier mobilities in graphene and its bilayer," *Physical review letters*, vol. 100, no. 1, p. 016602, 2008.

[79] C. Lee et al., "Measurement of the elastic properties and intrinsic strength of monolayer graphene," *Science*, vol. 321, no. 5887, pp. 385-388, 2008.

[80] S. Bae et al., "Roll-to-roll production of 30-inch graphene films for transparent electrodes," *Nature nanotechnology*, vol. 5, no. 8, pp. 574-578, 2010.

[81] N. Selvakumar et al., "Enhanced optical absorption of graphene-based heat mirror with tunable spectral selectivity," *Solar Energy Materials and Solar Cells*, vol. 186, pp. 149-153, 2018.

[82] A. Kumar and C.H. Lee, "Synthesis and biomedical applications of graphene: present and future trends," *in Advances in graphene science*, pp. 5772-5578, 2013.

[83] K.S. Novoselov et al., "Electric field effect in atomically thin carbon films," *Science*, vol. 306, no. 5696, pp. 666-669, 2004.

[84] C. Mattevi et al., "A review of chemical vapour deposition of graphene on copper," *Journal of Materials Chemistry*, vol. 21, no. 10, pp. 3324-3334, 2011.

[85] J. Kim et al., "Formation of Graphene on Gold–Nickel Surface Alloys," *Journal of the American Chemical Society*, vol. 145, no. 11, pp. 6299-6309, 2023.

[86] S.I. Kim et al., "Electromagnetic interference shielding of graphene/PMMA composites depending on growth temperature of CVD-graphene," *Synthetic Metals*, vol. 299, p. 117464, 2023.

[87] B.R. Huang et al., "The Efficiency Study of Graphene Synthesis on Copper Substrate via Chemical Vapor Deposition Method with Methanol Precursor," *Nanomaterials*, vol. 13, no. 6, p. 1136, 2023.

[88] R.K. Gupta (Ed.), 2D Nanomaterials: Chemistry and Properties, *CRC Press*, 2022.

[89] S.J. Rowley-Neale et al., "An overview of recent applications of reduced graphene oxide as a basis of electroanalytical sensing platforms," *Applied Materials Today*, vol. 10, pp. 218-226, 2018.

[90] W. Norimatsu and M. Kusunoki, "Epitaxial graphene on SiC {0001}: advances and perspectives," *Physical Chemistry Chemical Physics*, vol. 16, no. 8, pp. 3501-3511, 2014.

[91] S. Iijima, "Helical microtubules of graphitic carbon," *Nature*, vol. 354, no. 6348, pp. 56-58, 1991.

[92] A.F. Ávila and G.S.R. Lacerda, "Molecular mechanics applied to single-walled carbon nanotubes," *Materials Research*, vol. 11, pp. 325-333, 2008.

[93] M.F. De Volder et al., "Carbon nanotubes: present and future commercial applications," *Science*, vol. 339, no. 6119, pp. 535-539, 2013.

[94] A.K. Lekawa-Raus et al., "Electrical properties of carbon nanotube based fibers and their future use in electrical wiring," *Advanced Functional Materials*, vol. 24, no. 24, pp. 3661-3682, 2014.

[95] H. Xu et al., "A multifunctional wearable sensor based on a graphene/inverse opal cellulose film for simultaneous, in situ monitoring of human motion and sweat," *Nanoscale*, vol. 10, no. 4, pp. 2090-2098, 2018.

[96] X. Xie et al., "A spirally layered carbon nanotube-graphene/polyurethane composite yarn for highly sensitive and stretchable strain sensor," *Composites Part A: Applied Science and Manufacturing*, vol. 135, p. 105932, 2020.

[97] S. Wang et al., "Wearable stretchable dry and self-adhesive strain sensors with conformal contact to skin for high-quality motion monitoring," *Advanced Functional Materials*, vol. 31, no. 5, p. 2007495, 2021.

[98] Q. Li et al., "Engineering of carbon nanotube/polydimethylsiloxane nanocomposites with enhanced sensitivity for wearable motion sensors," *Journal of Materials Chemistry C*, vol. 5, no. 42, pp. 11092-11099, 2017.

[99] M. Wang et al., "Highly Sensitive Flexible Sensors for Human Activity Monitoring and Personal Healthcare," *Langmuir*, 2023.

[100] T. Yang et al., "A wearable and highly sensitive graphene strain sensor for precise home-based pulse wave monitoring," *ACS Sensors*, vol. 2, no. 7, pp. 967-974, 2017.

[101] Y. Wang et al., "Hierarchically patterned self-powered sensors for multifunctional tactile sensing," *Science Advances*, vol. 6, no. 34, p. eabb9083, 2020.

[102] C. Mu et al., "Flexible normal-tangential force sensor with opposite resistance responding for highly sensitive artificial skin," *Advanced Functional Materials*, vol. 28, no. 18, p. 1707503, 2018.

[103] P. Zhao et al., "Strain-discriminable pressure/proximity sensing of transparent stretchable electronic skin based on PEDOT: PSS/SWCNT electrodes," *ACS Applied Materials & Interfaces*, vol. 12, no. 49, pp. 55083-55093, 2020.

[104] S. Kabiri Ameri et al., "Graphene electronic tattoo sensors," *ACS nano*, vol. 11, no. 8, pp. 7634-7641, 2017.

[105] V. Ravichandran et al., "Characterizing the Impedance Properties of Dry E-Textile Electrodes Based on Contact Force and Perspiration," *Biosensors*, vol. 13, no. 7, p. 728, 2023.

[106] Y.H. Chen et al., "Soft, comfortable polymer dry electrodes for high quality ECG and EEG recording," *Sensors*, vol. 14, no. 12, pp. 23758-23780, 2014.

[107] P.F.M. Elango et al., "Dry electrode geometry optimization for wearable ECG devices," *Applied Physics Reviews*, vol. 10, no. 4, 2023.

[108] S. Asadi et al., "Graphene elastomer electrodes for medical sensing applications: Combining high sensitivity, low noise and excellent skin compatibility to enable continuous medical monitoring," *IEEE Sensors Journal*, vol. 21, no. 13, pp. 13967-13975, 2020.

[109] J.Y. Baek et al., "Flexible polymeric dry electrodes for the long-term monitoring of ECG," *Sensors and Actuators A: Physical*, vol. 143, no. 2, pp. 423-429, 2008.

[110] J. Yang et al., "Facile fabrication of robust and reusable pdms supported graphene dry electrodes for wearable electrocardiogram monitoring," *Advanced Materials Technologies*, vol. 6, no. 9, p. 2100262, 2021.

[111] C. Lou et al., "Flexible graphene electrodes for prolonged dynamic ECG monitoring," *Sensors*, vol. 16, no. 11, p. 1833, 2016.

[112] L. Zhang et al., "A self-protective, reproducible textile sensor with high performance towards human–machine interactions," *Journal of Materials Chemistry A*, vol. 7, no. 46, pp. 26631-26640, 2019.

[113] S. Sharma et al., "Stretchable and All-Directional Strain-Insensitive Electronic Glove for Robotic Skins and Human–Machine Interfacing," *ACS nano*, vol. 17, no. 9, pp. 8355-8366, 2023.

Chapter: 3 PDMS and Graphene: Development, Synthesis and Characterizations

This chapter discusses the synthesis methods and techniques employed to fabricate flexible strain/pressure sensors. We commence by delving into the development of a flexible polydimethylsiloxane (PDMS) substrate. Following that, reduced graphene oxide (rGO) was synthesized using a modified hummer's method. A multilayer graphene growth is achieved through the low-pressure chemical vapor deposition (LPCVD) method. Here, we present an in-depth analysis of the LPCVD approach, including the growth process and its outcomes. Next, we focus on creating flexible strain sensors by multilayer graphene transferred onto the PDMS substrate. Finally, we thoroughly examine the materials and devices in a rigorous characterization process.

3.1 Materials

PDMS (PDMS base and curing agent, Sylgard 184 Silicone) were obtained from Dow Corning, USA. Carbon fiber, PET, polyimide and epoxy glue were purchased from a commercial source. A copper foil (98.5 % pure, thickness 0.2 mm) was purchased from Sigma Aldrich, and silver conductive adhesive paste from Thermo Fisher Scientific. Graphite powder, Sulfuric acid (H_2SO_4), Potassium permanganate ($KMnO_4$), and hydrochloric acid (HCl) were purchased from Molychem, hydrogen peroxide (H_2O_2), and hydrazine hydrate were purchased from RENKEM.

3.2 Polydimethylsiloxane (PDMS): a flexible substrate

The fabrication of flexible sensors typically involves integrating conductive nanomaterials with flexible substrates. The flexible substrates often include PET, PDMS, PEN, polyimide, kapton, ecoflex, fabric, and paper. Over the last decade, there has been a significant upsurge in interest in PDMS because of its wide-ranging applications, which include flexible sensors, electronic skin (E-skin), soft robotics, biomedical, microfluidics, and wearable electronics [1-4]. PDMS is a versatile and widely used silicon-based organic polymer of the siloxane family [5]. PDMS is an excellent choice for flexible substrate due to its organic polymer nature based on

silicon with unique elastomeric properties. Its valuable elastomeric properties, such as allowing for gas permeability, optical transparency, effortless self-bonding, biocompatibility and a notable degree of chemical resistance, render it indispensable for both research and industrial purposes [6-9]. There is also excellent potential for PDMS moulds to produce complex shapes. PDMS is widely used as the polymer matrix in electronics due to its flexibility and processability [10]. In addition to these properties, it's cost-effectiveness, rapid manufacturing, and appropriate tailing property are key advantages.

Furthermore, PDMS substrates exhibit exceptional elasticity, allowing deformation without compromising their structural integrity, thus making them suitable for stretchable and flexible device applications [11]. PDMS is renowned for its inert, non-toxic, and non-flammable nature [12, 13]. Its biocompatibility and minimal toxicity have led to extensive use in various medical implants and biomedical devices. Its compatibility with biological systems and non-reactive characteristics make it a valuable asset in biomedical research and healthcare [14].

PDMS molecules exhibit a high degree of flexibility, forming an amorphous material. Like many polymers, PDMS primarily assumes an amorphous solid state because topological constraints, such as crosslinking and variations in chain lengths, impede crystallization. The empirical formula reflects the simplest ratio of atoms in the compound, whereas the chemical formula delineates the precise number of each element within the compound. In contrast, the structural formula provides a detailed representation of the molecule's structure. The empirical formula for PDMS [15] is:

$$(C_2H_6OSi)_n \quad \textbf{…(3.1)}$$

The above formula represents the simplest whole-number ratio of carbon (C), hydrogen (H), oxygen (O), and silicon (Si) atoms in the polymer chain. The "n" signifies that the polymer consists of repeating units, and the actual size of "n" can vary depending on the specific formulation and requirements. Here, "n" is the number of times the monomer is repeated; if it is low, the PDMS will be liquid. If "n" is high, it will be semi-solid. The chemical formula of the PDMS [16] is:

$$(H_3C)_3\ Si[Si(CH_3)_2O]nSi(CH_3)_3 \quad \textbf{…(3.2)}$$

The chemical structure of PDMS consists of a (Si) atom that forms bonds with two methyl (CH_3) groups and two oxygen (O) atoms. These repeating siloxane units can be arranged to create a flexible, linear, or crosslinked polymer chain. As a polymer, the structure consists of a monomer unit ($[SiO(CH_3)_2]$) repeated "n" times. PDMS, often called silicone, is a synthetic polymer composed of these recurring dimethylsiloxane units. Its structural formula is shown in figure 3.1.

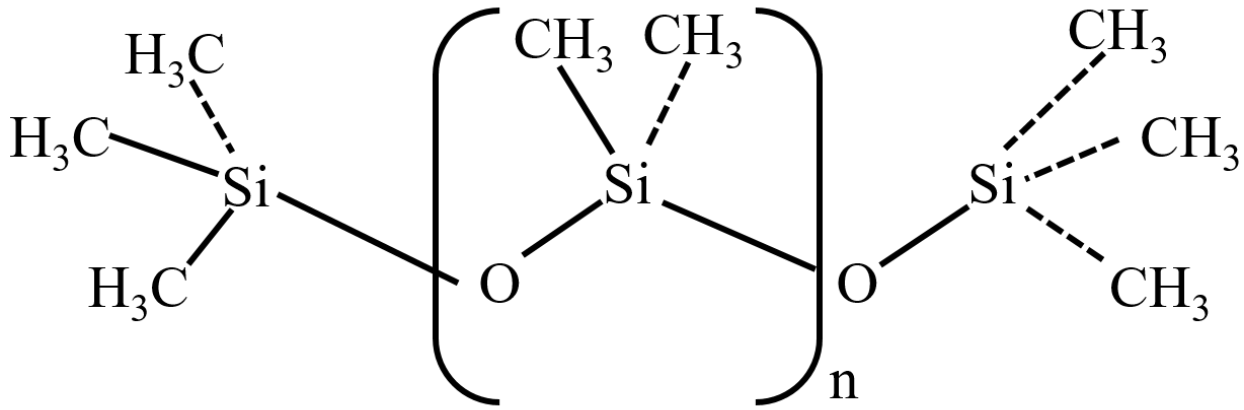

Figure 3.1. Chemical structure of polydimethylsiloxane (PDMS) [17].

3.3 Development of PDMS substrate

In the development process of PDMS, firstly, the silicon elastomer base and silicon elastomer curing agent were mixed in a ratio of 10:1. To eliminate air bubbles, the mixture was placed in a desiccator until all bubbles disappeared. A circular Teflon mould is utilized to place a silicon wafer on its surface. Subsequently, the mixture was poured onto a circular wafer and left to settle for 10 minutes. After this settling period, the PDMS mixture with the wafer was baked at a temperature of 80°C for 45 minutes. The development steps of PDMS are depicted in figure 3.2. Circular PDMS samples were then cut into rectangular pieces of various dimensions, as required for different measurements and applications.

The FESEM images of the plain PDMS material are shown in figure 3.3. The morphology of the PDMS is very homogenous and smooth, and there were no observable discrepancies at the 30 μm scale. This homogenous and smooth characteristic of PDMS is advantageous for screen printing. The absence of discrepancies is beneficial for fabricating flexible sensors, where PDMS is used as a flexible substrate.

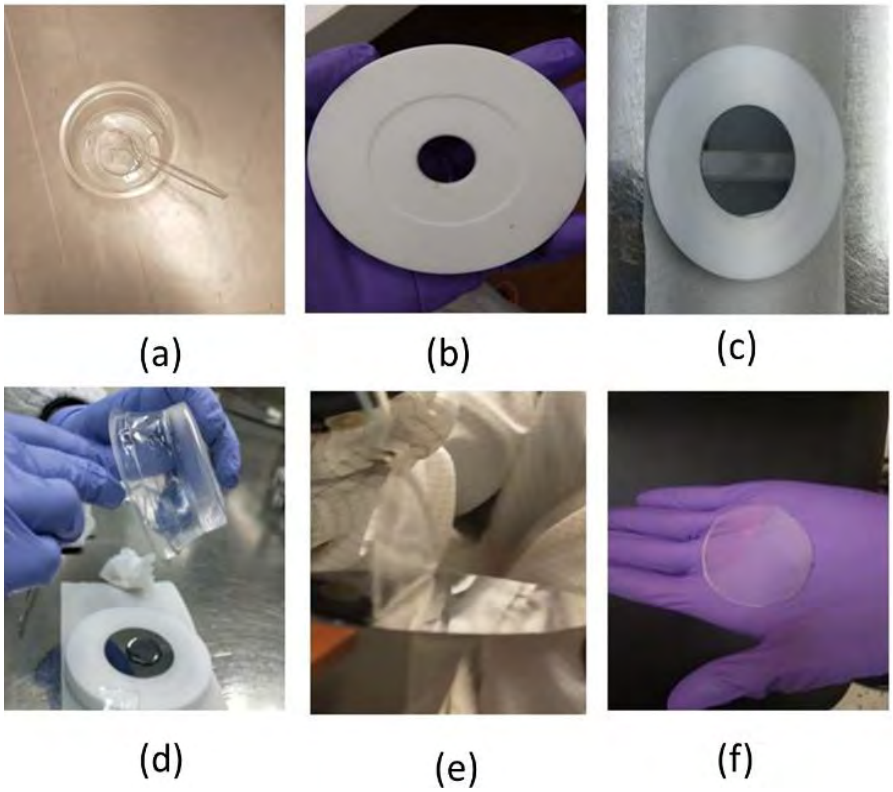

Figure 3.2. Optical photographs of the fabrication steps of PDMS Substrate (a) mixed silicon elastomer base and silicon elastomer curing agent (b) Teflon boat (c) silicon wafer on Teflon boat (d) drop mixed solution on wafer (e) peel of PDMS (f) obtained flexible PDMS substrate.

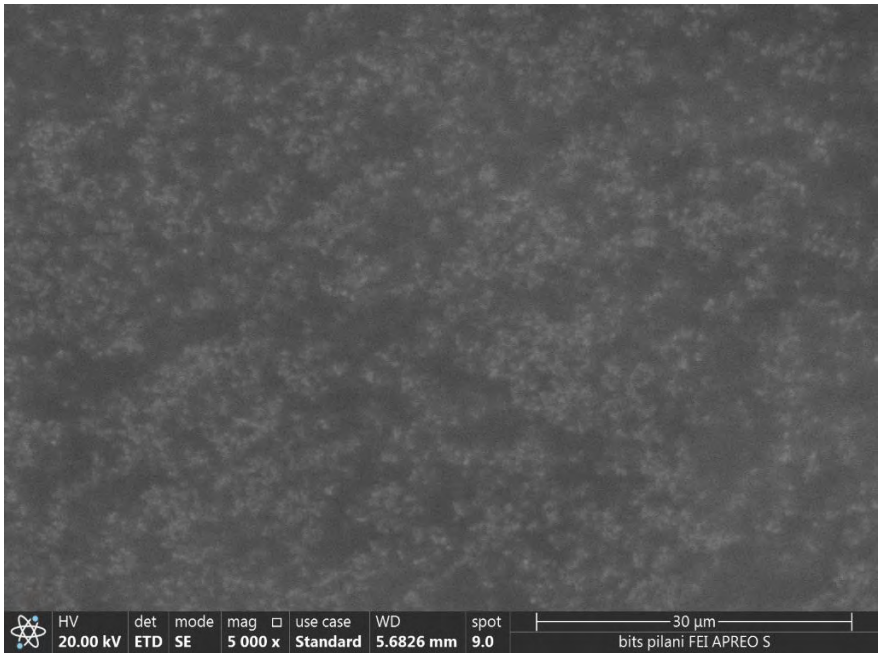

Figure 3.3. Field emission scanning electron microscopy (FESEM) images of obtained PDMS.

3.4 Mechanical properties of developed PDMS substrate

The mechanical properties of PDMS with different cross-linker ratios were investigated to assess the elasticity of the samples. PDMS has a low Young's modulus, making it a soft and compliant material. This property is helpful in applications that require deformation under mechanical stress. Acrylic mould was developed using a Mini-CNC machine model – UNI-FRAES V3 made by The Cool Tool (Austria) to obtain mechanical flexibility of fabricated PDMS. For tensile testing, a dumbbell-shaped acrylic mould with a width of 5 mm, a length of 30 mm, and a thickness of 2 mm was prepared and is shown in figure 3.4. (a). The Mini-CNC milling machine produces the dumbbell shape with the help of built-in software. We have done the programming to obtain the desired structure using G and M codes. These codes are used to cut the acrylic sheet in the XYZ plane and control the servo motor in the respective direction. Basically, these codes are exactly similar to the actual CNC machine. The dumbbell-shaped fabricated PDMS sample for the tensile test is shown in figure 3.4. (b).

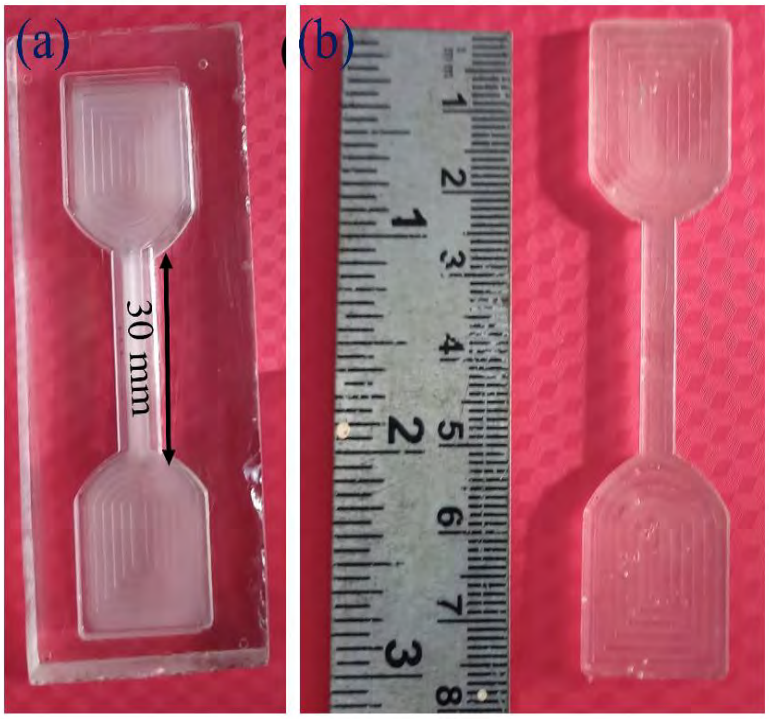

Figure 3.4. (a) Design of the acrylic moulds for the mechanical testing of PDMS with their parameters (b) fabricated plain PDMS.

Tensile tests are performed using a Mark-10 digital force gauge, as shown in figure 3.5. This test was conducted to determine the strength and behavior of PDMS under tension. PDMS samples were fabricated with the same dimensions to understand the stress-strain behavior of developed PDMS with different concentrations of cross-linker, i.e. silicon elastomer base and silicon elastomer curing agent in a ratio of 5:1, 10:1, 15:1, 20:1, 25:1. This set of samples, each with a different cross-linker concentration enables a systematic study of how formulation changes affect the tensile behavior of PDMS. This intern help to determine the optimal composition for specific applications and understand the material's performance across different conditions. The broader end of both sides of PDMS sample was clamped into the test setup. At the same time, the middle part was used for tensile testing, and subsequently, the samples were stretched at a constant elongation speed of 40 mm/min until the rupture of the samples. Each test was performed several times to obtain the repeatability and accuracy of the samples. First, the initial length was recorded for fabricated samples to obtain stress-strain curves, which gives the information about Young's modulus and elastic limit of each sample. The obtained results from each of the five samples for different curing agent/base weight ratio concentrations are shown in figure 3.6. The stress versus strain plot manifested linear elastic region up to a minimum strain value of 70 % and maximum strain value of 130 % for all samples before breakdown. The data reveals that the maximum strain of the sample directly corresponded to the curing agent/base weight ratio concentrations.

Figure 3.5. Mark-10 instrument setup for tensile testing.

We obtained Young's modulus (Elastic modulus) using Hook's law [18], as given by

$$\sigma = \varepsilon E \quad \textbf{…(3.3)}$$

where σ is the stress, ε is the strain, and E is Young's modulus. The slope value of the stress-strain curve represents Young's modulus. Comparing each Young's modulus of plain PDMS for the same curing conditions, it is clear that the value of the Young's modulus of PDMS is related to the amount of the elastomer base in PDMS. It is observed that with the increase in the amount of the elastomer base, the value of Young's modulus decreases from 2.82 MPa to 1.29 MPa. Tensile strength follows a similar trend, i.e. decreases from 3.38 MPa to 1.86 MPa. It was experimentally observed that an increased elastomer base can lead to a more flexible PDMS. The 10:1 PDMS sample was chosen to fabricate flexible strain sensors and dry electrodes because it exhibits a promising Young's modulus, and provides good flexibility and mechanical strength. The specific mechanical parameters, including elongation break, Young's modulus and tensile strength, can be calculated from the strain-stress curves. Table 3.1 summarizes the mechanical properties of various PDMS samples.

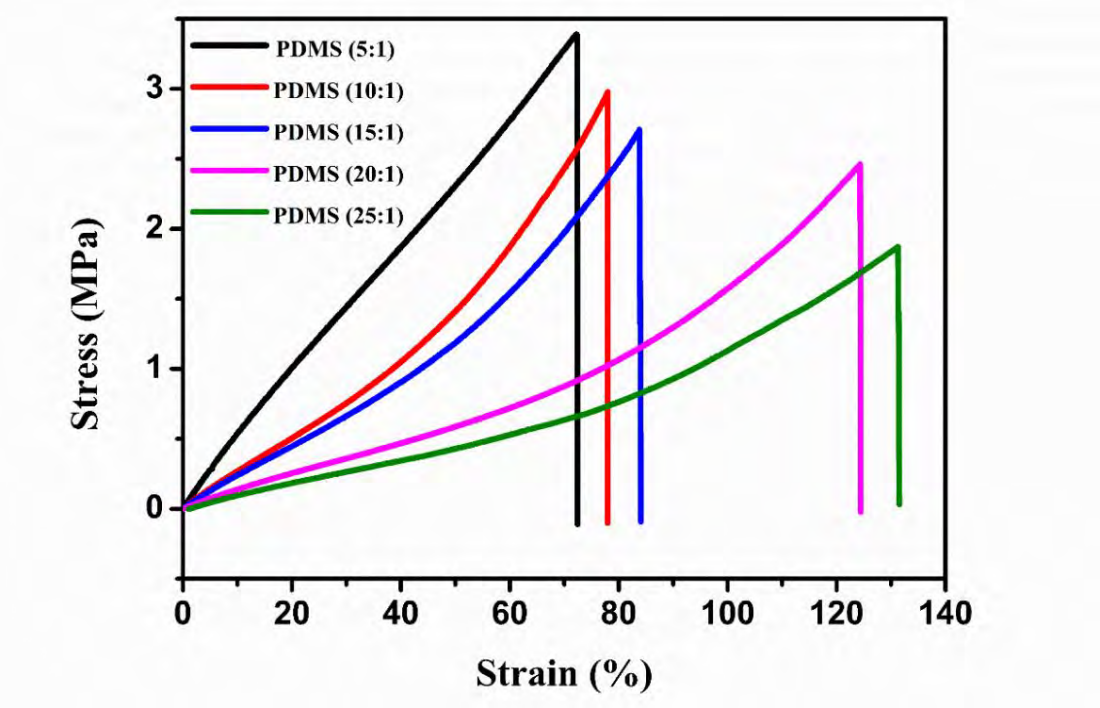

Figure 3.6. Typical tensile stress-strain curves for PDMS Samples with different amounts of crosslinking.

Table 3.1 Mechanical properties of PDMS Samples with different amounts of Crosslinking.

Material (PDMS)	Elongation break (mm)	Young's Modulus (MPa)	Tensile Strength (MPa)
PDMS 5:1	21.60	2.82	3.38
PDMS 10:1	23.40	2.26	2.98
PDMS 15:1	25.20	1.89	2.71
PDMS 20:1	37.20	1.68	2.48
PDMS 25:1	39.30	1.29	1.86

3.5 Reduced graphene oxide (rGO) synthesis

First, graphene oxide (GO) was synthesized from pure graphite fine powder using modified Hummer's method [19]. For this, sulfuric acid and phosphoric acid were mixed in a 9:1 volume ratio under continuous stirring, and 2 gm graphite powder was added to the solution. Then, 5 gm of oxidizing agent, potassium permanganate ($KMnO_4$), was added slowly, and the solution was stirred for 5 hours. To remove excess $KMnO_4$ from the solution, 10 mL hydrogen peroxide (H_2O_2) was added slowly and stirred for 20 minutes. Then, 15 mL of hydrochloric acid (HCl) and 30 mL of distilled water were added and the solution was centrifuged for 10 minutes. The excess solution was decanted away, and the residual was rewashed with HCl and distilled water five times. Then, the washed solution was dried at room temperature for 24 hours to produce the GO powder. To obtain rGO, the above suspension was again sonicated for two hours in the presence of Hydrazine hydrate, and the reduction was performed at 90°C for one hour. The resultant solution was filtered by cellulose filter paper and washed with HCl and distilled water. Finally, the filtrate was dried at room temperature for 24 hours to obtain rGO.

Two characteristic bands, namely the D and G bands, were observed at 1326 cm^{-1} and 1584 cm^{-1} respectively, confirming the presence of a graphite-like material in the obtained powder and are in good agreement with previous literature [20]. Additionally, the absence of a 2D band and the relation between the relative intensities ($I_D/I_G \approx 1.5$) confirmed the formation of rGO using the modified Hummer's method, as shown in figure 3.7. To study the surface morphology of rGO, FESEM was employed. Figure 3.8 (a,b) shows the recorded image of the synthesized rGO,

showcasing randomly distributed clusters of rGO and the presence of reduced graphene oxide nanosheets.

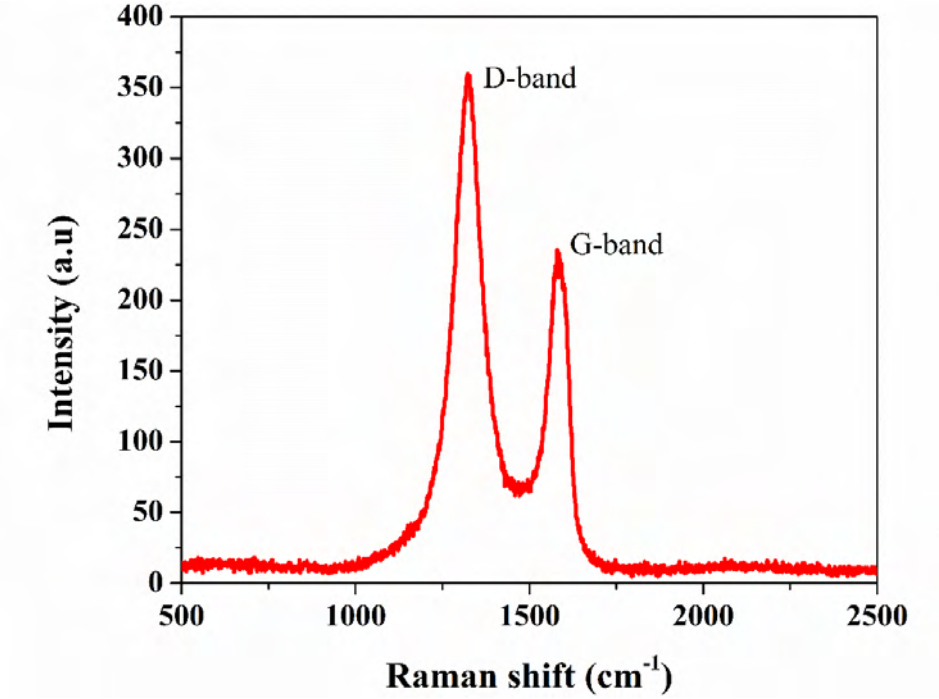

Figure 3.7. Raman spectrum of rGO synthesized using modified Hummer's method.

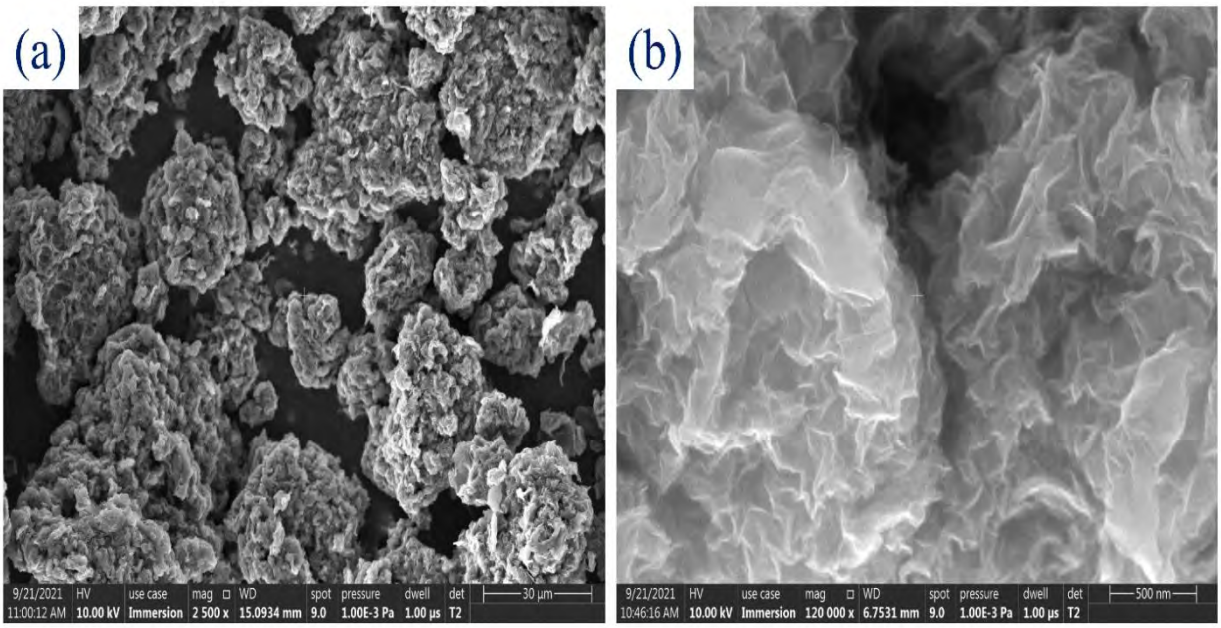

Figure 3.8. Field emission scanning electron microscopy (FESEM) of the reduced graphene oxide: (a) at the 30 µm scale and (b) at the 500 nm scale.

3.6 Multilayer graphene growth by low-pressure CVD (LPCVD) method

A copper (Cu) substrate was employed to synthesize a graphene film through low-pressure chemical vapor deposition (LPCVD). The copper foil was chosen as the catalyst due to its widespread use as a substrate for uniform single or multilayer graphene growth [21,22]. This preference stems from its low carbon solubility at or below the growth temperature. The CVD growth process for multilayer graphene generally involves four consecutive steps: heating, thermal annealing, growth, and cooling. To initiate the procedure, 0.2 mm thick copper foil with a purity of 98.5% was cut into dimensions of 1x1 cm^2 and 2x2 cm^2. Before the graphene growth, these copper pieces underwent a cleansing regimen. Initially, they were immersed in a dilute HCl solution (10%) for one minute. The copper pieces were rinsed in deionized (DI) water for a few minutes, subjected to a pure ethanol bath for five minutes and finally dried using nitrogen. Employing this sequence of baths effectively eliminated common impurity particles from the copper pieces, resulting in a pristine, continuous, and high-quality graphene formation. The pre-treated and dried copper pieces were then positioned within an alumina boat placed in a quartz furnace. The temperature was raised to the growth temperature of 1000 ℃, facilitating the decomposition of the hydrocarbon source.

The synthesis of multilayer graphene was carried out using a low-pressure CVD setup (LPCVD), with a gas mixture comprising argon (Ar), hydrogen (H_2), and methane (CH_4). Once the temperature reached a stable 1000 ℃, heating was sustained under a pressure of 1.5 Torr. Argon (Ar) gas flowed at a rate of (100-200) sccm (standard cubic centimetres per minute) for 90 minutes. Subsequently, hydrogen (H_2) was introduced into the furnace, and the copper pieces were held at 1000 °C with the concurrent flow of Ar (100-200) sccm and H_2 (50-100) sccm for 30 minutes. This annealing process aimed to refine the metal substrate. The next step involved introducing (25-50) sccm of methane gas into the system at 1000 °C. This step spanned a 30-minute interval, during which multilayer graphene was synthesized. Upon completion of the growth process, the sample within the quartz tube was allowed to cool down to room temperature naturally. This cooling was facilitated by an argon gas flow of (100-200) sccm. The temperature profile as a function of the time of the multilayer graphene growth conditions is shown in figure 3.9.

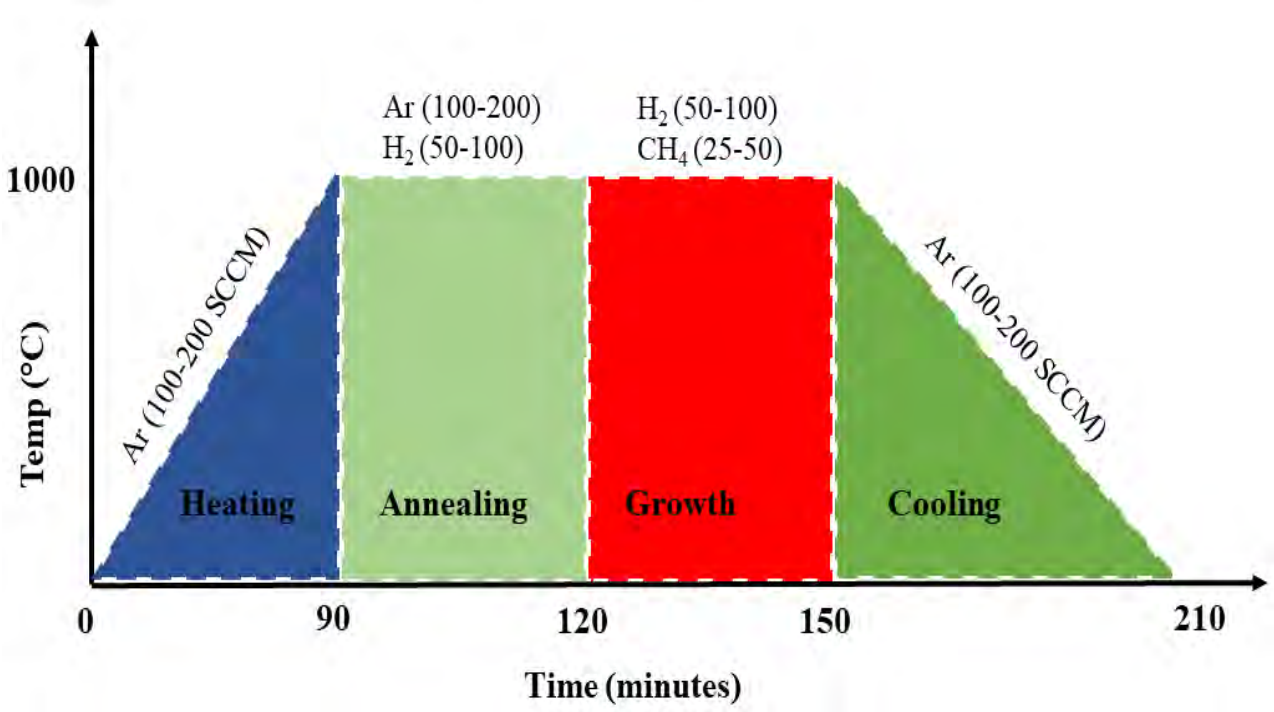

Figure 3.9. Temperature profile as a function of the time of graphene growth by the LPCVD system.

3.7 Fabrication of multilayer graphene/PDMS-based flexible strain sensor

The graphene transfer process and sensor fabrication steps are shown in figure 3.10. A PDMS mixture was prepared by combining silicon elastomer base and silicon elastomer curing agent in a 10:1 ratio. Subsequently, CVD-grown graphene on a copper foil was affixed to a silicon wafer using a highly adhesive thin double-sided tape. The PDMS mixture was applied onto the sample, and the sample was spin-coated with PDMS. The entire assembly was then placed in a hot oven at 80°C for 30 minutes, allowing the PDMS substrate to solidify along with the sample. After the curing process, the fully cured PDMS with graphene/copper was immersed in copper etchant for five hours. Then, the setup was placed in a water bath for half an hour after the copper etching to eliminate any chemical residue on the graphene or PDMS surface. After thoroughly washing, it was heated inside a hot-air oven for a few minutes to complete the drying process. The fabricated graphene/PDMS strain sensor was tested using a Keithley 2450 source meter, and the connections were made with an alligator clip.

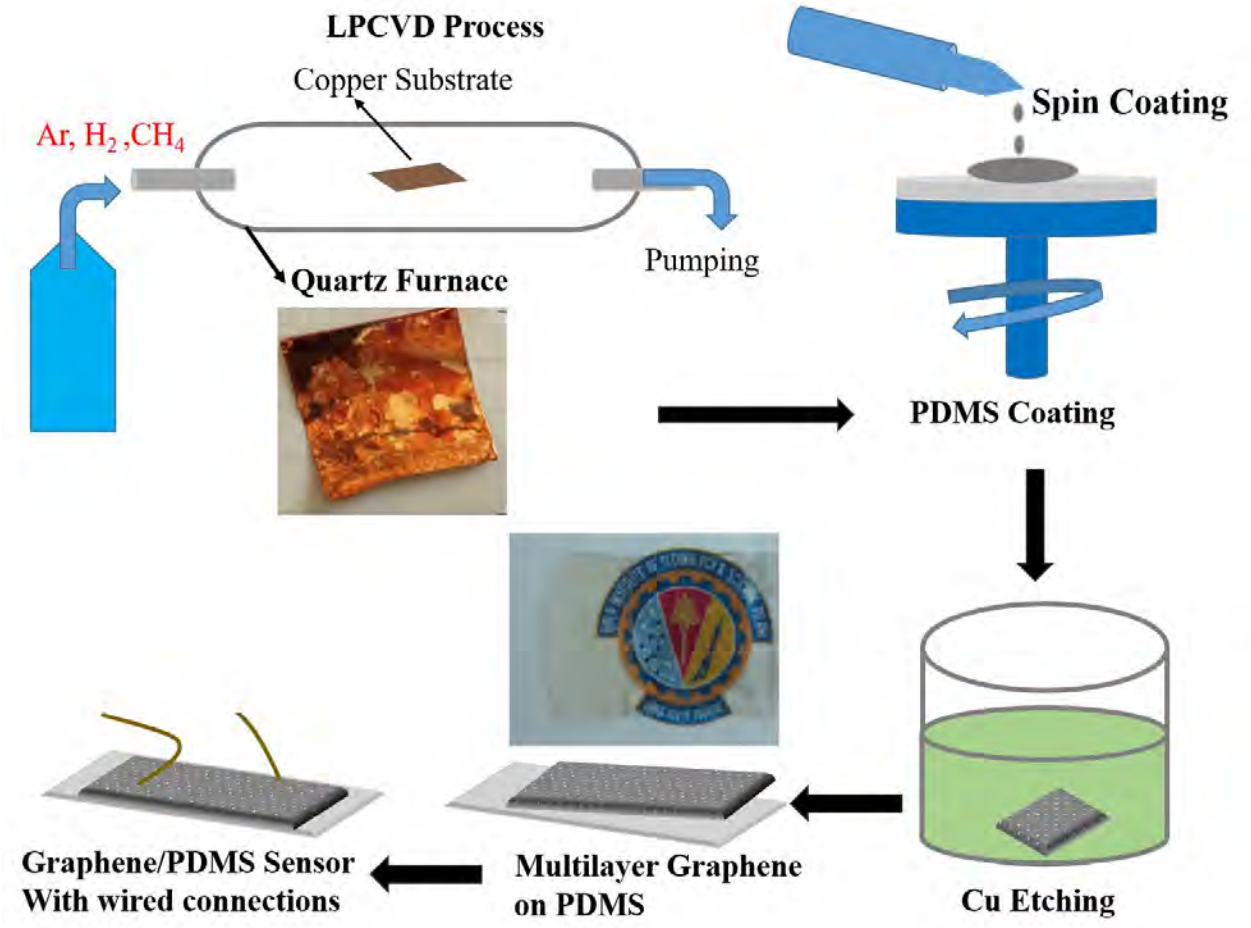

Figure 3.10. Schematic of graphene transfer process using a simple wet transfer method and multilayer graphene/PDMS-based flexible strain sensor fabrication.

We utilize Raman spectroscopy to characterize transferred CVD-grown graphene on PDMS. In figure 3.11, the Raman spectrum reveals three distinctive peaks: two primary Raman peaks and an additional peak related to the disorder. The two main Raman peaks encompass a doubly-degenerate in-plane sp^2 C-C stretching mode known as the G-band at 1582.07 cm^{-1}, Raman-active phonon mode involving the displacement of carbon atoms in a breathing-like motion within the hexagonal lattice structure denoted as the 2D-band at 2694.80 cm^{-1}. The additional disorder-related peak, the D-band, emerges at 1348.63 cm^{-1}. This mode is induced by symmetry disruptions in the graphene lattice, such as defects, vacancies or impurities. The Raman analysis indicates the successful transfer of graphene onto PDMS. The FESEM image reveals the transferred graphene on the PDMS substrate, as shown in figure 3.12. The graphene surface appears smooth, with some minor cracks and micro-wrinkles.

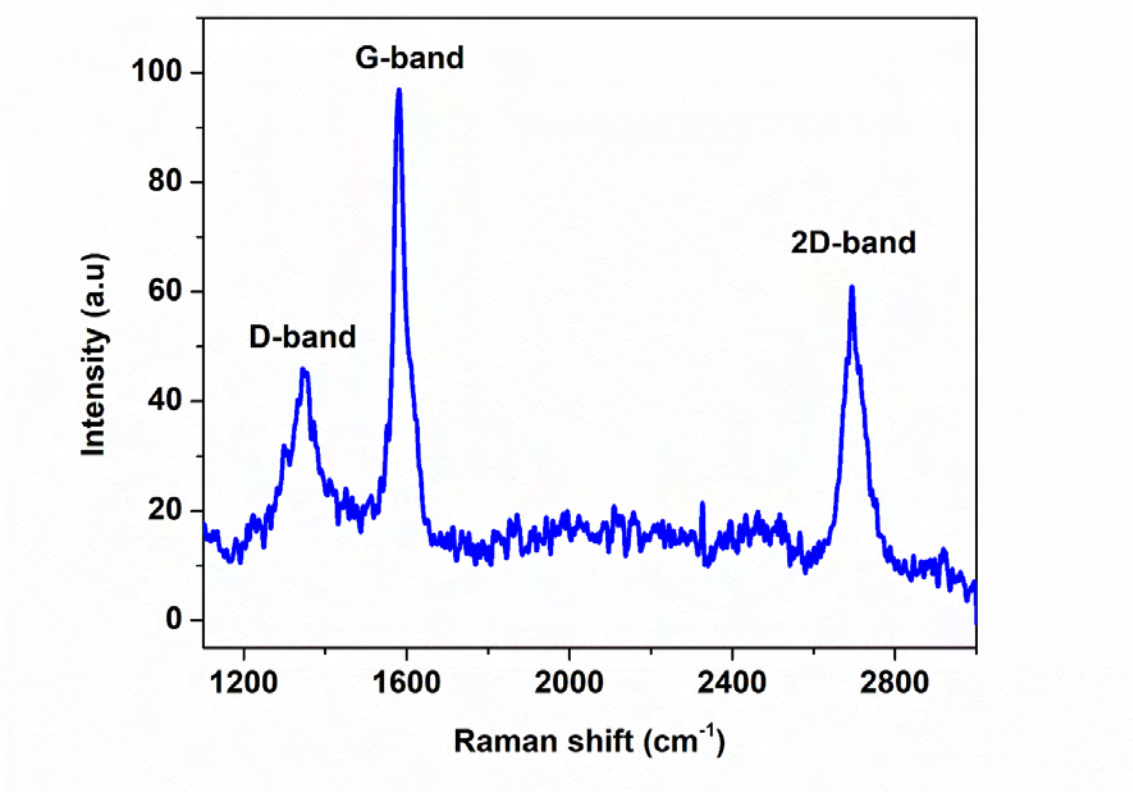

Figure 3.11. Raman spectra of transferred graphene with the laser wavelength of 532 nm.

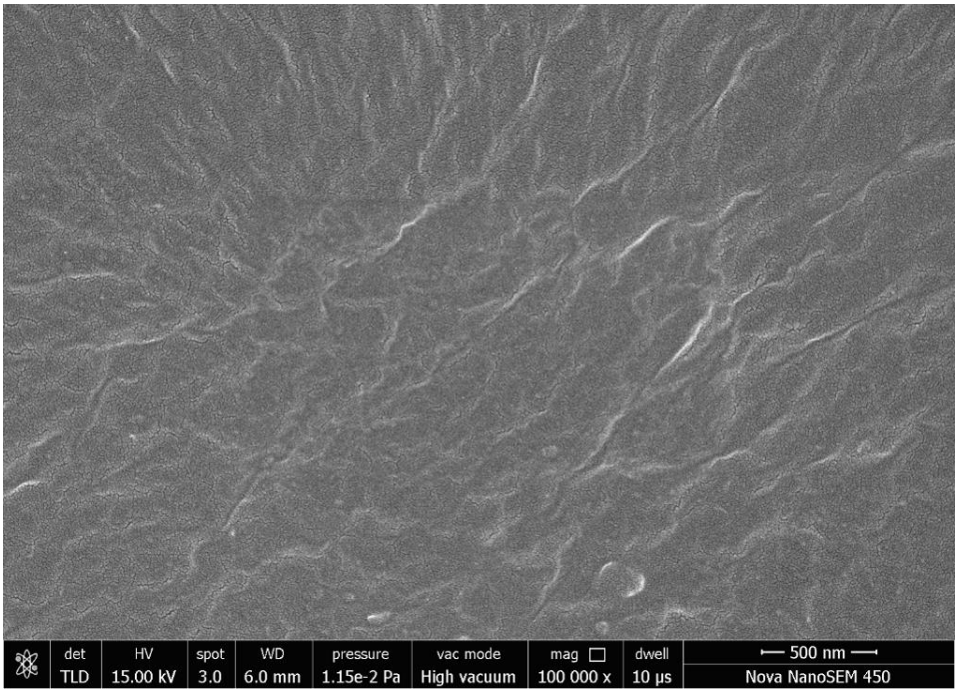

Figure 3.12. FESEM image of the transferred graphene on the PDMS substrate.

The X-ray photoelectron spectroscopy (XPS) spectra are shown in figure 3.13. The C 1s peak in graphene XPS spectra is observed. After deconvoluting into multiple peaks, the sp^2 carbon (graphitic) at a binding energy of 282.6 eV to 286.2 eV is present. The remaining spectra consist of sp^3 carbon (defects or functional groups). The hydroxyl C-OH and carbonyl C=O groups are also present at higher binding energy. The XPS analysis confirms the presence of transferred graphene on PDMS, with a detailed breakdown of carbon. The sp^2 carbon peaks suggest the presence of graphitic carbon, while the sp^3 carbon peaks indicate the existence of defects or functional groups.

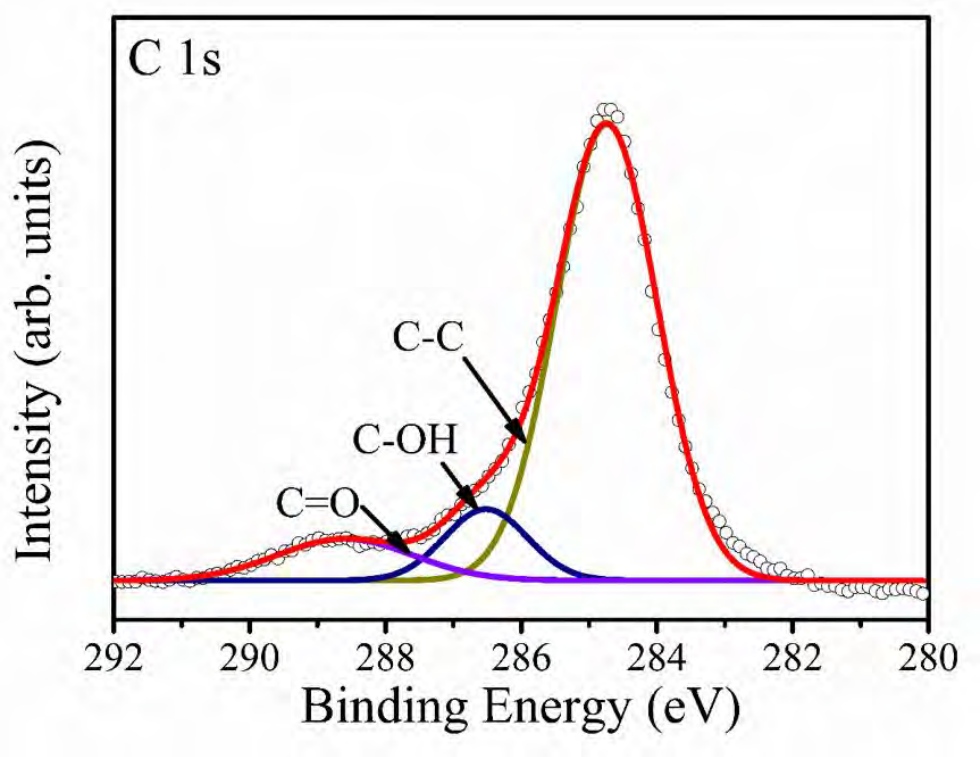

Figure 3.13. Obtain XPS spectra of transferred graphene.

3.8 Conclusion

In conclusion, the development of a flexible polydimethylsiloxane (PDMS) substrate was successfully achieved through a simple peel-off method. The synthesis of rGO was achieved using a modified Hummer's method, which is confirmed by the presence of both the D band at 1326 cm^{-1} and the G band at 1584 cm^{-1}. The FESEM imaging illustrated randomly distributed clusters of rGO and the existence of rGO nanosheets in the synthesized material. Additionally, the production of high-quality multilayer graphene was successfully synthesized using the low-pressure chemical

vapor deposition (LPCVD) technique on copper foil, followed by its transfer onto the flexible PDMS substrate. Quality verification of the transferred graphene was carried out through standard Raman spectroscopy, with the I_{2D}/I_G ratio confirming the multilayer graphene structure. Further validation through FESEM analysis confirmed the high-quality multilayer graphene on the PDMS substrate. Complementing these analyses, XPS analysis reinforced the overall assessment of the graphene's excellent quality.

References

[1] J. Wen, W. Wu, Z. Xie, and J. Wu, "Development of Piezoelectric Elastomers and Their Applications in Soft Devices," *Macromolecular Materials and Engineering*, vol. 230, p. 2300101, 2023.

[2] Q. Zheng, J.H. Lee, X. Shen, X. Chen, and J.K. Kim, "Graphene-based wearable piezoresistive physical sensors," *Materials Today*, vol. 36, pp. 158-179, 2020.

[3] Y. Dong, H. Zhong, Y. Wu, and J. Deng, "Preparation and Applications of Polydimethylsiloxane-Based Fluorescent Materials," *Macromolecular Rapid Communications*, vol. 44, no. 14, p. 2300106, 2023.

[4] S. Khan, S. Tinku, L. Lorenzelli, and R.S. Dahiya, "Flexible tactile sensors using screen-printed P (VDF-TrFE) and MWCNT/PDMS composites," *IEEE Sensors Journal*, vol. 15, no. 6, pp. 3146-3155, 2014.

[5] S.J. Vella and C. Moorlag, "Hydrophilic imaging member surface material for variable data ink-based digital printing systems and methods for manufacturing hydrophilic imaging member surface materials," *U.S. Patent* 9,630,423, 2017.

[6] G.K.M. Kabandana, T. Zhang, and C. Chen, "Emerging 3D printing technologies and methodologies for microfluidic development," *Analytical Methods*, 2022.

[7] S. Torino, B. Corrado, M. Iodice, and G. Coppola, "PDMS-based microfluidic devices for cell culture," *Inventions*, vol. 3, no. 3, p. 65, 2018.

[8] G. Dandegaonkar, A. Ahmed, L. Sun, B. Adak, and S. Mukhopadhyay, "Cellulose based flexible and wearable sensors for health monitoring," *Materials Advances*, vol. 3, no. 9, pp. 3766-3783, 2022.

[9] A. Tony, I. Badea, C. Yang, Y. Liu, G. Wells, K. Wang, R. Yin, H. Zhang, and W. Zhang, "The Additive Manufacturing Approach to Polydimethylsiloxane (PDMS) Microfluidic Devices: Review and Future Directions," *Polymers*, vol. 15, no. 8, p. 1926, 2023.

[10] D.C. Kim, H.J. Shim, W. Lee, J.H. Koo, and D.H. Kim, "Material-based approaches for the fabrication of stretchable electronics," *Advanced Materials*, vol. 32, no. 15, p. 1902743, 2020.

[11] W. Lee, H. Yun, J.K. Song, S.H. Sunwoo, and D.H. Kim, "Nanoscale materials and deformable device designs for bioinspired and biointegrated electronics," *Accounts of Materials Research*, vol. 2, no. 4, pp. 266-281, 2021.

[12] Z. Lou, L. Wang, K. Jiang, Z. Wei, and G. Shen, "Reviews of wearable healthcare systems: Materials, devices and system integration," *Materials Science and Engineering: R: Reports*, vol. 140, p. 100523, 2020.

[13] R. Dahiya, G. Gottardi, and N. Laidani, "PDMS residues-free micro/macrostructures on flexible substrates," *Microelectronic Engineering*, vol. 136, pp. 57-62, 2015.

[14] A. Singh, A. Ahmed, A. Sharma, and S. Arya, "Graphene and its derivatives: Synthesis and application in the electrochemical detection of analytes in sweat," *Biosensors*, vol. 12, no. 10, p. 910, 2022.

[15] K. Izdihar, H.R. Abdul Razak, N. Supion, M.K.A. Karim, N.H. Osman, and M. Norkhairunnisa, "Structural, mechanical, and dielectric properties of polydimethylsiloxane and silicone elastomer for the fabrication of clinical-grade kidney phantom," *Applied Sciences*, vol. 11, no. 3, p. 1172, 2021.

[16] E. Toth, K. Iván, P. Furjes, Z. Fekete, and E.G. Holczer, "Design, realisation and validation of microfluidic stochastic mixers integrable in bioanalytical systems using CFD modeling," *IEEE Biomedical Circuits and Systems Conference* (BioCAS), 2013, pp. 266-269.

[17] S. Marchioretto, I. Vervier, I. Van Reeth, K. Plotzke, and B. Johnson, "The Power of Silicones in Cosmetic Applications: The Science behind the Performance," *SOFW Journal*, vol. 147, no. 12, 2021.

[18] Z. Wang, A.A. Volinsky, and N.D. Gallant, "Crosslinking effect on polydimethylsiloxane elastic modulus measured by custom-built compression instrument," *Journal of Applied Polymer Science*, vol. 131, no. 22, 2014.

[19] S.N. Alam, N. Sharma, and L. Kumar, "Synthesis of graphene oxide (GO) by modified hummers method and its thermal reduction to obtain reduced graphene oxide (rGO)," *Graphene*, vol. 6, no. 1, pp. 1-18, 2017.

[20] G. Rajitha and R.K. Dash, "Optically transparent and high dielectric constant reduced graphene oxide (RGO)-PDMS based flexible composite for wearable and flexible sensors," *Sensors and Actuators A: Physical*, vol. 277, pp. 26-34, 2018.

[21] D. Luo, M. Wang, Y. Li, C. Kim, K.M. Yu, Y. Kim, H. Han, M. Biswal, M. Huang, Y. Kwon, and M. Goo, "Adlayer-free large-area single crystal graphene grown on a Cu (111) foil," *Advanced Materials*, vol. 31, no. 35, p. 1903615, 2019.

[22] M. Huang and R.S. Ruoff, "Growth of single-layer and multilayer graphene on Cu/Ni alloy substrates," *Accounts of Chemical Research*, vol. 53, no. 4, pp. 800-811, 2020.

Chapter: 4 Graphene-based Flexible Sensors: Design, Development and Applications

This chapter details the fabrication of a graphene-based flexible strain sensor and dry electrodes. The initial section focuses on the development and analysis of a flexible piezoresistive strain sensor using graphene nanoplatelets (GNPs) as an active layer and polydimethylsiloxane (PDMS) as a substrate for health monitoring applications. The subsequent section delves into the fabrication of a multilayer graphene/PDMS-based flexible strain sensor for human motion detection. In clinical and research settings, electrophysiological signals are pivotal, providing valuable insights into the functionality of various physiological systems. They are crucial for diagnosing, treating and understanding various health conditions and biological processes. The advancement of dry electrodes is significant, complementing the importance of electrophysiological signals. Unlike traditional wet electrodes, dry electrodes offer advantages by eliminating the need for a conductive gel to enhance signal quality. In this chapter, we focussed on the fabrication of flexible dry electrodes using rGO-PDMS to monitor electrophysiological signals. It was also demonstrated that dry electrodes perform better than conventional wet electrodes.

4.1 Graphene nanoplatelets (GNP)-based piezoresistive strain sensor

The rapid development of flexible electronics has raised tremendous interest in recent years to pave the way for the next generation of wearable devices [1]. Flexible and stretchable sensors have attracted extensive research owing to their applications in converting physiological signals into electrical data for health monitoring purposes, encompassing various functions like tracking joint movements, measuring blood pressure, and monitoring heartbeats [2-3]. Flexible strain sensors offer distinct advantages over metallic and semiconductor-based counterparts [4]. These sensors exhibit high sensitivity, stretchability, and biocompatibility in real-time monitoring applications. In addition, these sensors can conform to irregular or curved surfaces. These advantages make them well-suited for effectively capturing physiological data in health monitoring applications [5-7].

Flexible strain sensors are comprised of three essential components: flexible substrate, sensing layer and electrical connections. Among these components, the functional sensing layer is fabricated mainly by

using conductive materials such as metallic nanoparticles, nanowires, carbon nanotubes (CNTs), graphene and conducting polymeric materials [8-13]. These materials are chosen for their distinctive qualities, including electrical conductivity, mechanical strength, and structural compatibility. For the fabrication of strain sensors, large stretchability and a high sensitivity with a wide detection range have been the key parameters [14]. One such material that has captured significant attention is graphene nanoplatelets (GNPs), derived from the remarkable two-dimensional carbon allotrope, i.e. graphene. These graphene nanoplatelets are three-dimensional structures composed of multiple graphene layers. They have garnered substantial interest due to their exceptional electrical conductivity, mechanical strength, and unique piezoresistive characteristics, making them promising candidates for strain sensing [15-17].

Most of the reported strain sensors were fabricated on flexible substrates such as polydimethylsiloxane (PDMS), polyethylene terephthalate (PET), Ecoflex, polyimide (PI), natural rubber and PEDOT: PSS [18-22]. PDMS, a widely used elastomeric polymer in these flexible substrates, is an ideal substrate for flexible strain sensors. PDMS possesses a high degree of flexibility, excellent biocompatibility, and ease of processability, making it an ideal candidate for accommodating graphene and creating flexible strain sensors [23-24]. This chapter proposes a novel way to fabricate GNP-based piezoresistive strain sensors for human motion detection and health monitoring in wearable applications. Experimental studies indicate that the proposed device has high sensitivity, long-term stability, reproducibility and durability. These features are attractive for human motion detection devices, health monitoring and electronic skin applications.

4.2. GNP fabrication on PDMS

We have fabricated GNP-based strain sensors on PDMS and other flexible substrates, including polyethylene terephthalate (PET), polyimide and carbon fiber. Firstly, purchased GNP from Alfa-Aesar was mixed in 10:1 of elastomer base and curing agent by weight percentage, constituting 40 % of the total solution. After this, the composite has been mixed thoroughly for 20 minutes. The obtained composite was deposited on bare PDMS by screen printing, i.e., directly coated on the substrate with fine paint brush and deposited on other flexible substrates using the same method. Further samples were baked at 90° C for 90 minutes. After that, the obtained GNP/PDMS sample is used for different measurements. This work has followed the same process for other flexible substrates using GNP. Figure 4.1 shows optical photographs of a fabricated GNP/PDMS strain sensor that is stretchable, foldable and twistable. These properties of the fabricated sensor make it a suitable candidate for wearable applications.

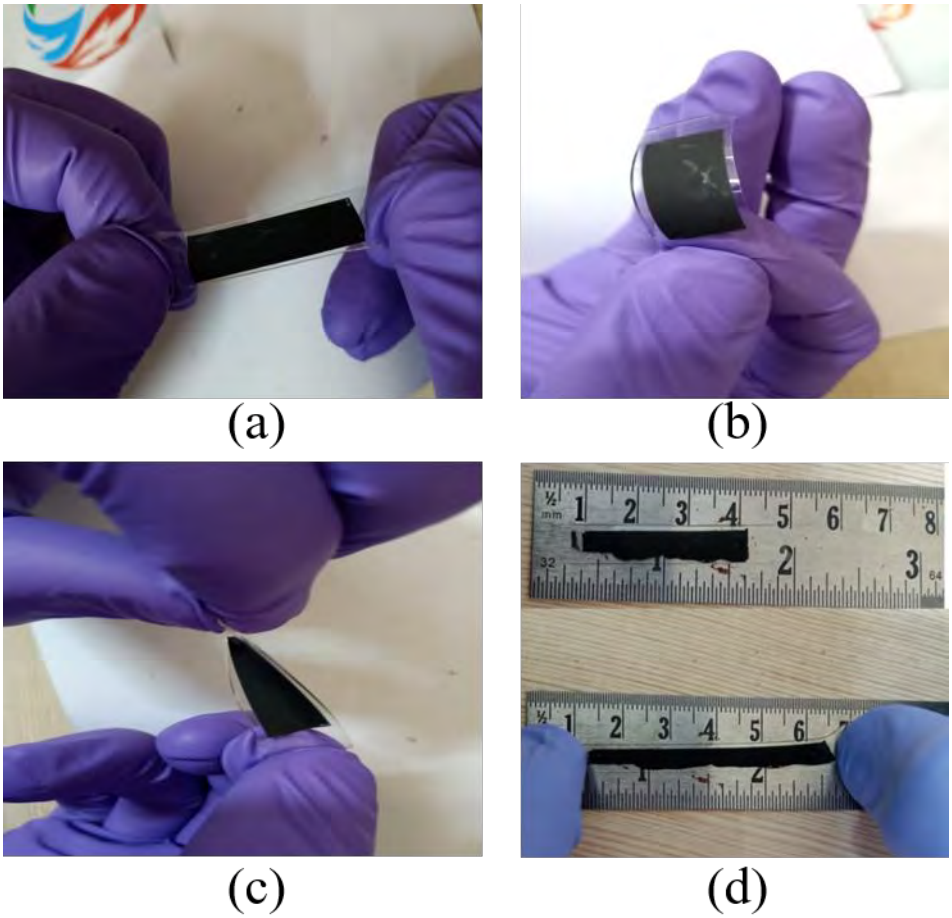

Figure 4.1. Optical photographs of fabricated GNP/PDMS strain sensor at (a) stretchable, (b) foldable, (c) twistable, (d) demonstration of fabricated GNP strain sensor having stretchability up to 65%.

The Raman spectra were obtained with a RENISHAW inVia Raman microscope with a laser excitation wavelength of 532 nm at room temperature. Figure 4.2**.** elucidates Raman spectra of GNP on PDMS substrate. Raman spectra contain three peaks at 1341.89 cm^{-1}, 1566.21 cm^{-1} and 2682.15 cm^{-1}, representing D, G and 2D peaks, respectively for GNP. The surface morphology of the graphene fabricated on different substrates is analyzed by FESEM (Quanta FEG 250). The recorded image of the purchased GNP is shown in figure 4.3 (a), which contains nanoplatelets and graphene microparticles. The average diameter and length of the nanoplatelets were found to be in the range of 40-60 nm and 200-400 nm, respectively. Figure 4.2 (b) shows the GNP coated on the PDMS substrate, indicating the proper adhesion of GNP in the form of uniform particles. The surface morphology of GNP-coated carbon fiber with different magnifications is shown in figure 4.3 (c, d). These FESEM images show a uniform coating of the GNP on the carbon fiber surface, indicating good adhesion.

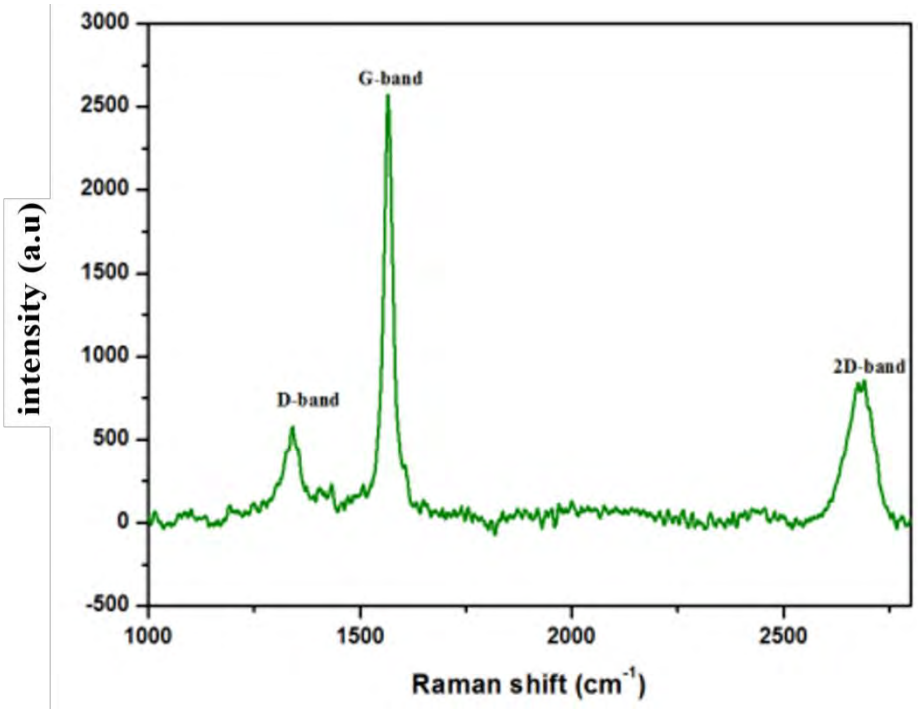

Figure 4.2. Obtained Raman spectra of fabricated GNP/PDMS.

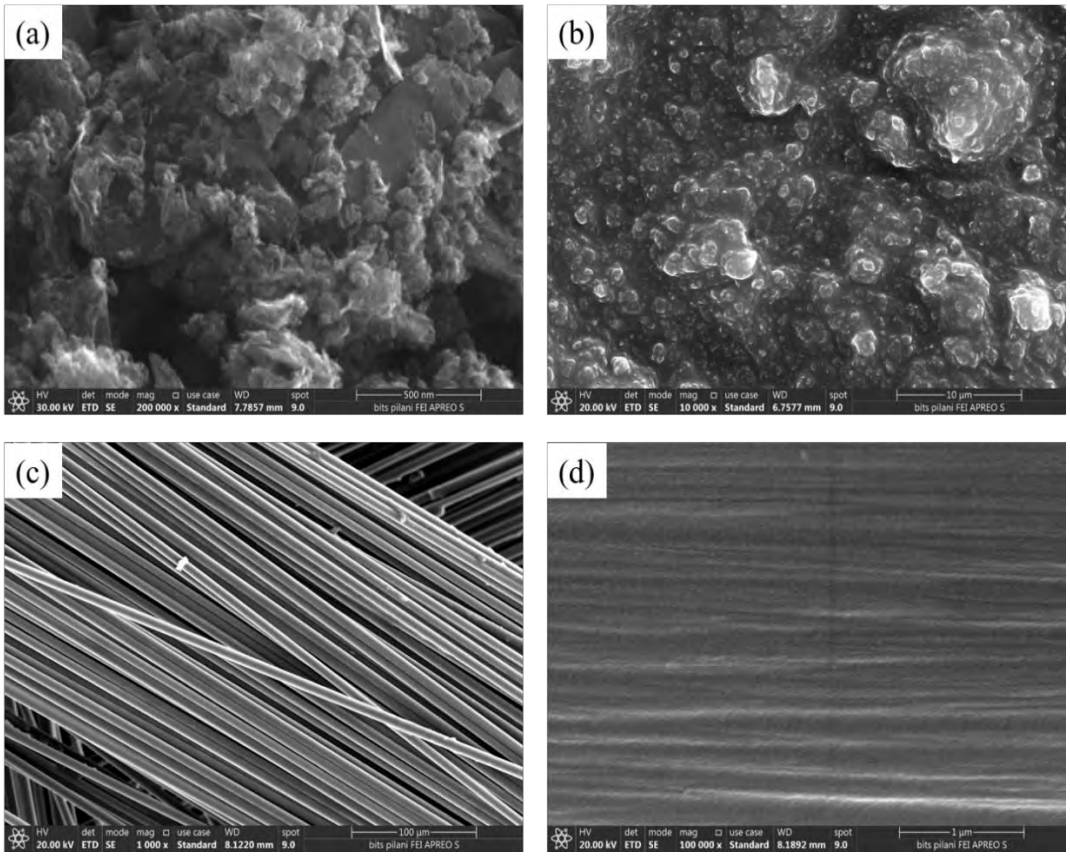

Figure 4.3. FESEM images of (a) purchased GNP, (b) fabricated GNP on PDMS, (c) fabricated GNP on carbon fiber with 100 µm scale, and (d) fabricated GNP on carbon fiber with 1 µm scale.

4.2.1 Measurement of GNP-based strain sensor

The graphene as a sensing layer was deposited by a manual printing method, and contacts were made with silver epoxy and copper wires. The testing of the strain sensor was measured with a self-made mechanical setup and digital Keysight B2901A multimeter. When a strain is applied to it, a change in the resistance was observed. Firstly, the sensor was stretched and then released and after that, the piezoresistive and strain behavior of GNP was analyzed. The piezoresistive effect in GNPs arises from the alteration in their electrical conductivity when subjected to mechanical deformation. This effect is primarily attributed to changes in the interlayer spacing within the nanoplatelets under strain, which influences electron transport between layers.

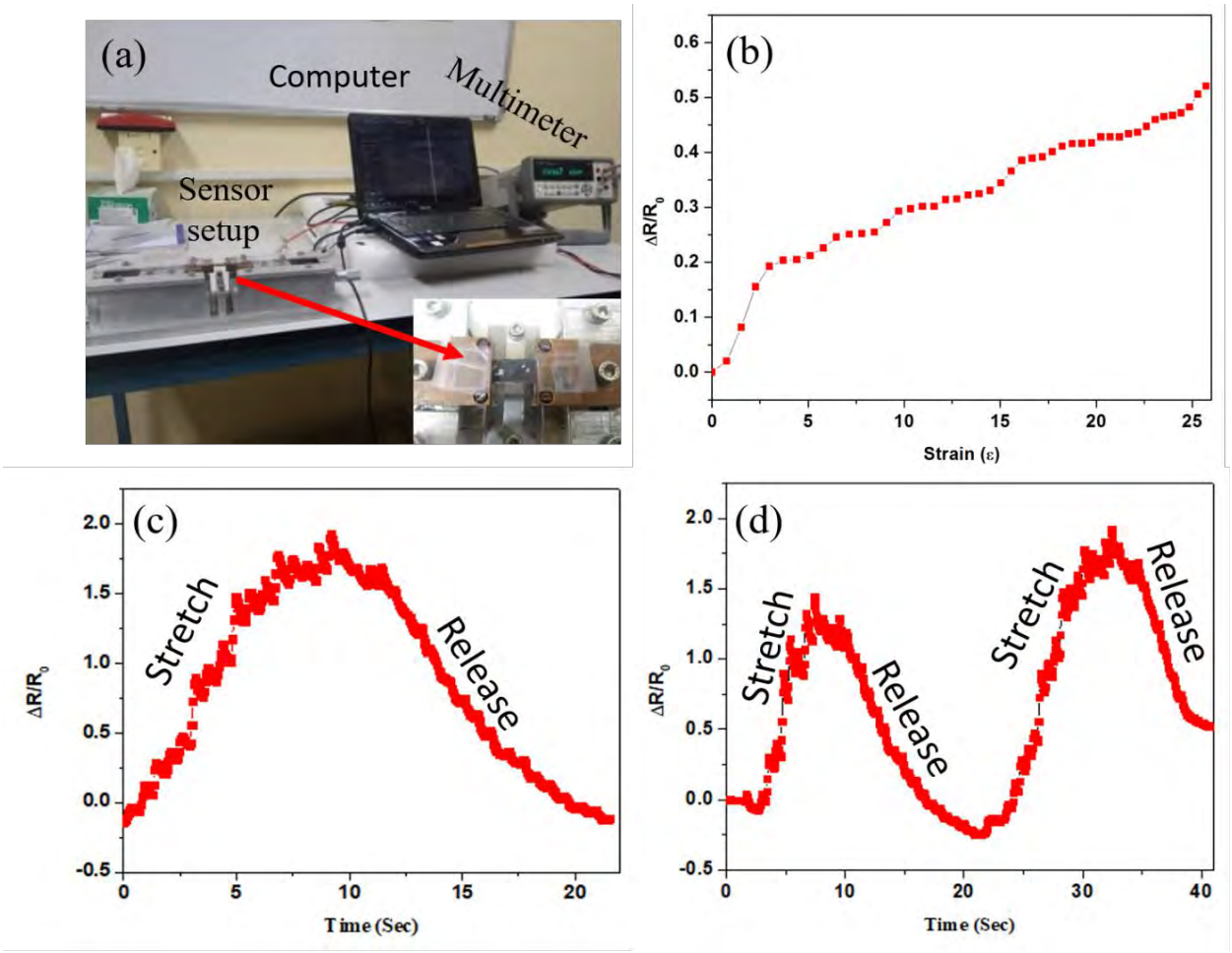

Figure 4.4. Experimental strain sensor setup where the inset shows the attached GNP sensor, (b) ΔR/R0 versus strain curves of the GNP/PDMS strain sensor. Relative resistance changed when the strain was applied from zero to 25 %, (c, d) graphene-based strain sensor showing the significant change in resistance upon stretching and releasing for one cycle and two cycles with time.

Figure. 4.4 (a) shows the experimental setup of GNP-based strain sensor measurements. Figure. 4.4 (b) shows the effect of applied strain on the resistance of the fabricated GNP/PDMS strain sensor. It has been observed that under applied strain ranging from zero to 25 %, the change in relative resistance increases and shows good linearity (figure 4.4 b). Based on the relationship between the changes in applied strain and change in resistance, the GNP/PDMS-based sensor's gauge factor was calculated as 62.5. Figure 4.4 (c, d) shows the relative resistance change versus time when the sensor stretches and releases for 1 and 2 cycle measurements, respectively. It is observed that resistance increases with stretching and decreases while releasing in both cycles. After completing the first cycle, the resistance of the strain sensor reverted to its initial value, and this pattern persisted in the subsequent cycle, mirroring the observations from the initial cycle.

4.2.2 GNP-based wrist pulse sensor

A wearable pulse sensor has been investigated based on graphene and implemented on various flexible substrates, including PDMS, PET, polyimide, and carbon fiber. An analysis was carried out to evaluate and compare their performance and suitability for pulse sensing applications. The human wrist pulse provides useful and valuable information for non-invasive medical diagnosis. Wrist pulse waves are vital physiological signals for cardiovascular effects and strongly correlate with serious diseases arising from the heart and blood [25]. Thus, it has been successfully demonstrated using GNP/PDMS, GNP/PET, GNP/Polyimide and GNP/Carbon fiber strain sensors to detect human wrist pulse. The fabricated sensor shows an excellent response for wrist pulse detection.

Figure 4.5 shows that a single wrist pulse is composed of three peaks, which correspond to the percussion wave (P wave), tidal wave (T wave), and dicrotic wave (D wave) of a wrist pulse waveform. This confirms that fabricated GNP strain sensors can detect wrist pulses. The different GNP strain sensors were mounted onto the wrist to detect real-time pulse signals. The output signals were stable and periodic; therefore, all fabricated graphene strain sensors can detect weak body signals, i.e. wrist pulse, due to their high flexibility, excellent stability, sensibility and repeatability. The result suggests that the GNP/PDMS strain sensor gives the best result among all other sensors due to its high stretchability and flexibility.

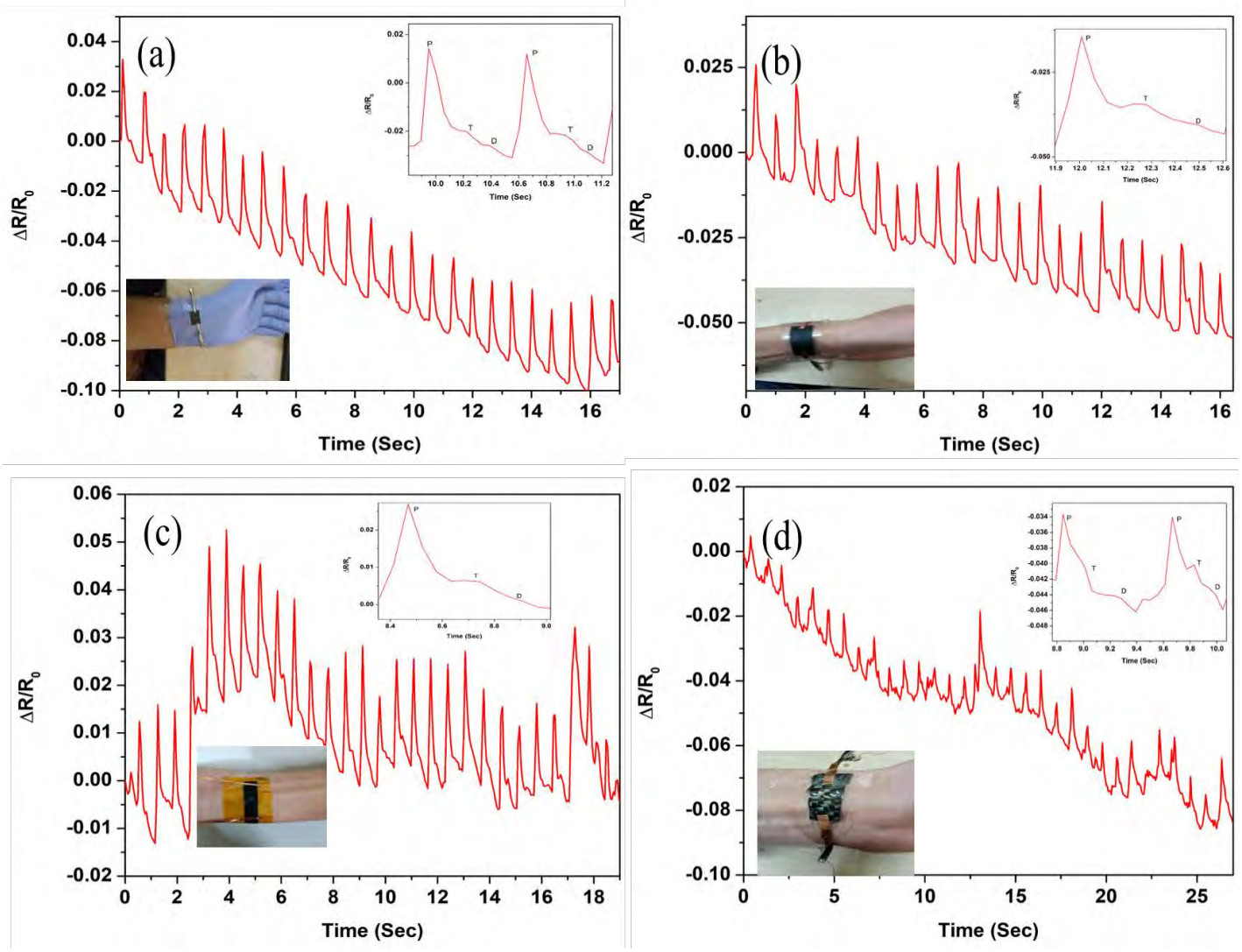

Figure 4.5. Wrist pulse response with different substrates (a) GNP/PDMS pulse sensor; the top inset has two single pulses (b) GNP/PET pulse sensor; the top inset is a single pulse, (c) GNP/Polyimide pulse sensor; the top inset is a single pulse, (d) GNP/Carbon fiber pulse sensor; the top inset has two single pulses.

4.2.3 GNP-based strain sensor under bending

In addition to monitoring wrist pulse, the GNP strain sensor can also detect other human motions like finger bending at different angles. In Figure 4.6 (a, b), the results show that the GNP sensor can efficiently and accurately detect small and big angles. When the strain sensor bends at different angles, 0°, 30° and 90° (in inset 4.6 a), the resistance changes compared to its initial value. Similarly, when the sensor is released at 0°, 30°, and 90° (inset 4.6 b), the resistance becomes almost double its initial value. Figure 4.6 (c) shows a photograph in which a GNP strain sensor was attached to a flexible plastic pipe. When the flexible pipe was

bent and unbent, the result shows that the change in relative resistance was small. This is due to the softness of PDMS between the flexible pipe and the sensor. Figure 4.6 (d) shows the repeatable signals measured by the PET/GNP strain sensor when the sensor is in folded and unfolded positions. The generated signals can be easily distinguished corresponding time. A repeatable two-peak pattern was observed. Thus, the strain sensor shows stability and reproducibility to folded and unfolded positions with relative resistance changes of approximately 30-35%.

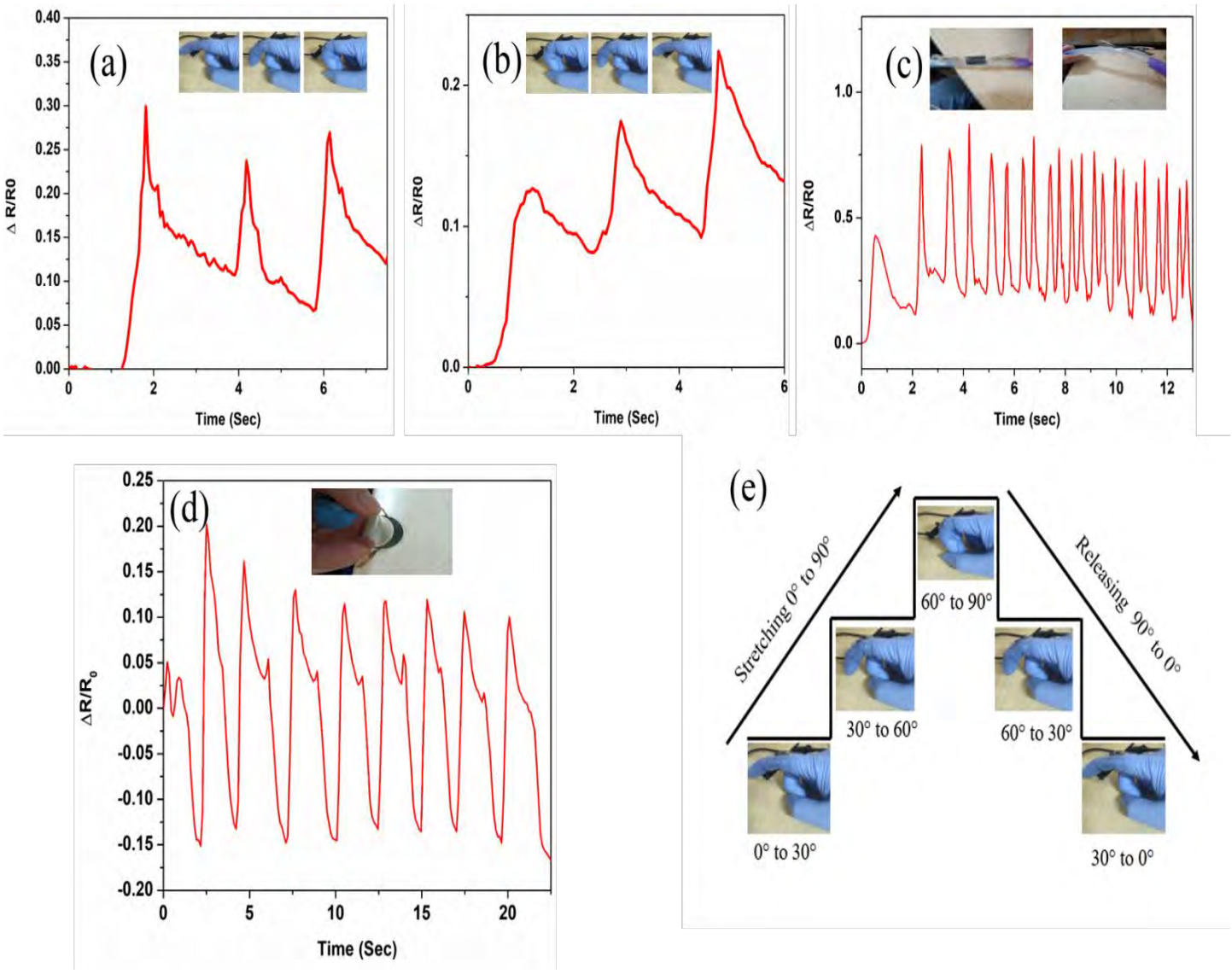

Figure 4.6. The GNP sensor shows relative change in resistance under different finger bending angles 0◦, 30◦ and 90◦. (a) corresponding signals of the bending of the finger, (b) unbending of the finger, (c) bending of flexible pipe, (d) signals of PET/GNP strain sensor, (e) step response of each finger bending figure (6a and 6b) at different angles.

Moreover, the PET/GNP strain sensor could be expected to detect the change in the bending angle when it is folded and unfolded at 180°. This confirms that the proposed strain sensor can be used for human/machine interface and in the field of robotics. Figure 4.6 (e) shows the step response of each finger bending at different angles. When the sensor bends at different angles from 0°to 30° then, resistance is increased, and when holding the sensor for a while, the signal tries to settle and again bend the finger from 30° to 60° and 60° to 90° same phenomenon is observed.

4.2.4 GNP-based resistive touch sensor

A GNP-based resistive touch sensor is a touch-sensitive device that incorporates graphene nanoplatelets in its fabrication. The bottom layer comprises of a flexible PDMS substrate, while the upper layer comprises of a thin conducting GNP layer. This advanced touch sensor operates in the principle of changes in electrical resistance upon touch, offering a responsive and versatile interface for various applications. The integration of graphene nanoplatelets enhances the sensor's conductivity and mechanical flexibility, making it a promising technology for sensitive and durable touch-sensitive systems.

The detection of finger tapping is shown in figure 4.7. The result shows that this sensor can also be used as a resistive touch sensor because the response signals exhibited excellent stability and high sensitivity. When the GNP/PDMS sensor is tapped (pressed) and untapped (released) for different intervals, its response changes with the tapping time. Figure 4.7 (a-e) shows the variation of $\Delta R/R_0$ versus strain for different press/release times, i.e. 1, 1.5, 2, 4, and 8 seconds respectively. Notably, the proposed strain sensor (in figure 4.7 f) exhibited exceptional stability and durability after undergoing intensive loading–unloading cycles for 5-sec press/release time. Figure 4.7 (f) shows that the tapping time goes around 90 secs, and its response relative resistance is the same. The proposed resistive touch sensor achieved remarkable performance with high sensitivity and excellent stability. The fabricated resistive touch sensor can be used in touch-based flexible screens.

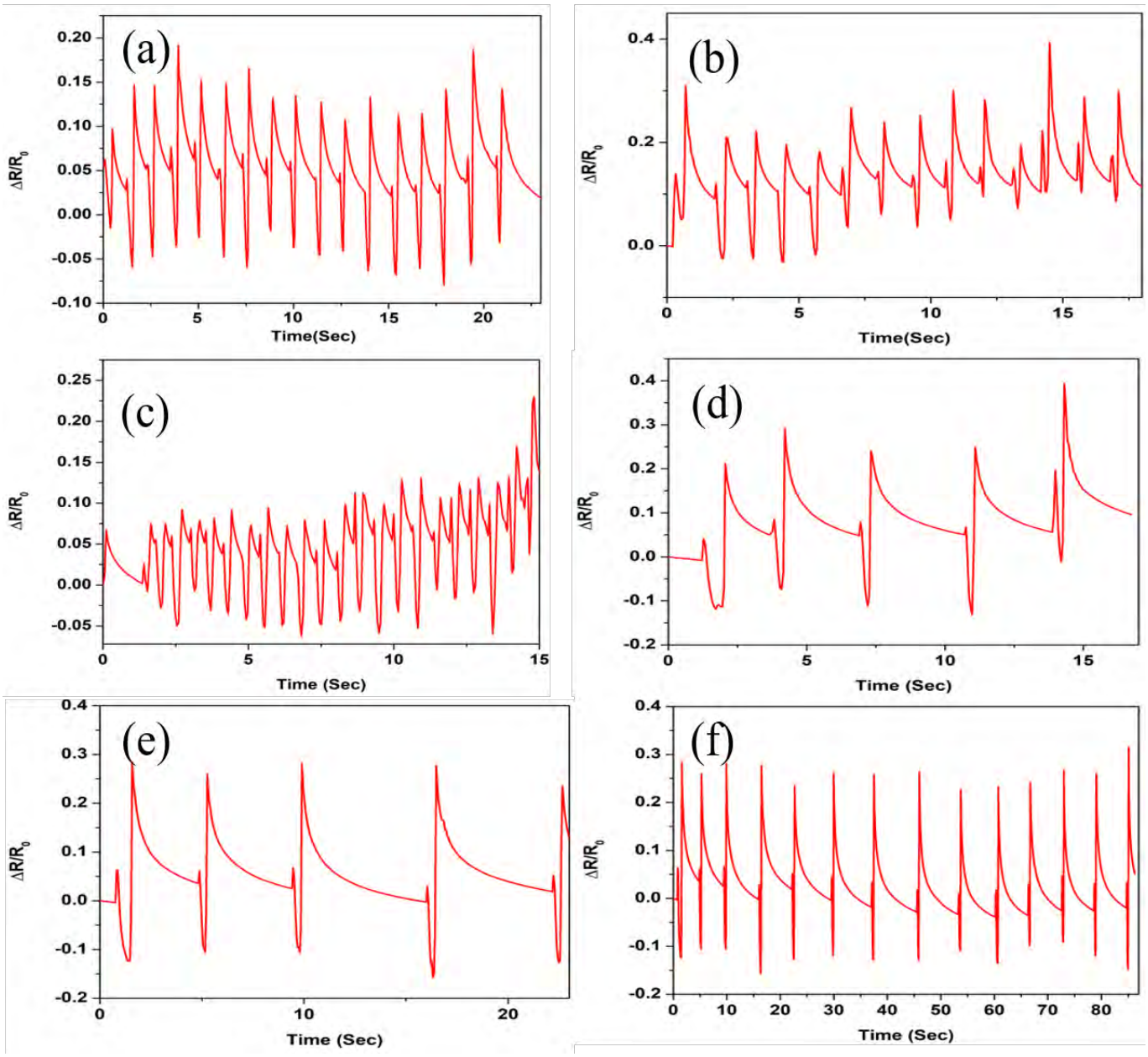

Figure 4.7. Real-time monitoring of resistance responses of GNP/PDMS for press/release of an index finger on GNP/PDMS sensor with various press/release times (a) 1 sec, (b) 1.5 sec, (c) 2 sec, (d) 4 sec, (e) 8 sec, (f) after undergoing intensive loading-unloading cycles for 5-sec press/release time for longer period.

4.3 Multilayer graphene/PDMS-based flexible sensor for human motion detection

As the PDMS substrate is stretched or compressed, the graphene layer experiences strain. This strain induces changes in the graphene's electronic structure, leading to alterations in its electrical conductivity. The change in resistance or conductivity of the graphene layer is proportional to the amount of strain applied to

the PDMS substrate. The resistance versus time characteristics taken from the Kiethley 2450 source meter are shown in figure 4.8. The fabricated graphene/PDMS strain sensor has broad application prospects in human motion detection. Figure 4.8 (a) shows that the resistance changed significantly when the sensor was connected to the elbow. The strain sensor responds well to elbow bending with larger resistance change compared to the sensor onto the finger and wrist, as shown in figure 4.8 (b) and (c). The relative resistance change depends on the deformation strain formed by the motions. The stronger the motion is, the larger the strain is, and the motion signals can be recorded. The flexible strain sensor can continuously monitor the bending of the finger and the wrist when the finger and wrist are bent. All the above human motion detection results show that the proposed strain sensor can detect small or large-scale human motion signals. This confirms that the designed flexible strain sensor based on multilayer graphene/PDMS has diverse potential applications in human motion monitoring and wearable electronics.

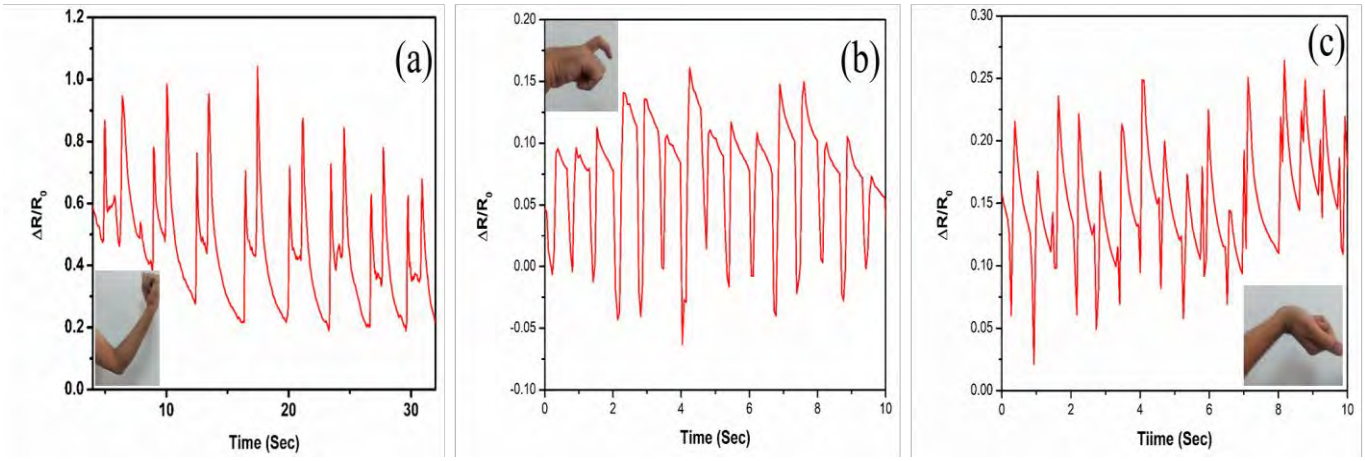

Figure 4.8. Application of the strain sensor for human motion detection: (a) recognition of elbow bending, (b) recognition of finger bending and (c) recognition of wrist bending.

4.4 Graphene-based dry electrodes

The rapid development of wearable electronics has advanced the biomedical field by recording, transmitting and monitoring real-time bio-potential signals such as ECG, EEG and EMG. Long-term electrocardiogram (ECG) signal monitoring is vital for early diagnosis and prevention of cardiovascular diseases [26-29]. Consequently, there is a growing demand for flexible electrodes with high performance and suitable for long-term ECG monitoring. However, the conventional wet gel Ag/AgCl electrodes currently used in hospitals are unsuited for these long-term recordings. Using a conductive gel evaporates over time, resulting in poor signal quality for a longer period [30-32]. The conductive gel causes irritation that might trigger allergic reactions in the skin and discomfort to the patients during long-term recordings [33-34].

In response to these limitations, substantial efforts have been dedicated to devise alternatives that fulfill the extended requirements of ECG monitoring [35-37]. The pursuit is for high-performance dry electrodes capable of ensuring superior contact quality without the need for gelling or skin preparation. Essential attributes, such as reusability, flexibility, softness, adhesion, and biocompatibility, are highly sought after [38-40]. Dry electrodes, often based on rigid metallic materials like Ag, Au, Al, and Ti, have been documented [41-43]. However, their limited flexibility, softness, elevated electrode-to-skin impedance, and insufficient biocompatibility impede their applicability in mobile and wearable health monitoring devices.

Given these challenges, carbon nanomaterials, such as carbon nanotubes and graphene, integrated into polymeric matrices, emerge as promising candidates for bioelectrode design due to their superior conductivity, biocompatibility, and conformity [44-45]. Graphene-based dry electrodes, especially in ECG monitoring applications, have garnered considerable attention in recent years. Their remarkable specific surface area, electrical conductivity, mechanical properties, and thermal stability create opportunities for innovation [46-48].

The fabrication of dry electrodes for ECG and EMG monitoring involved utilizing a reduced graphene oxide (rGO) active material on a polydimethylsiloxane (PDMS) substrate. PDMS, chosen for its biological and chemical inertness, flexibility, and robustness, holds innovation potential through its thermal stability, high transparency, and suitability for micro-moulding [49]. Employing a spray coating method, the dry electrodes were produced by depositing rGO onto a PDMS substrate. To evaluate the performance of the fabricated dry electrodes, we conducted measurements and analyses of the electrode-skin interface impedance, assessed the quality of ECG signals, and compared the results with commercial Ag/AgCl electrodes. The electrodes' capability to capture high-quality electromyogram (EMG) signals is also discussed. Our analysis of the rGO-PDMS dry electrodes reveals their significant potential for application in long-term health monitoring systems and wearable devices.

4.4.1 Fabrication of rGO -PDMS dry electrodes

In this work, a simple and facile method has been employed for fabricating rGO-PDMS dry electrodes. These electrodes are comprises of PDMS substrate and an active sensing rGO layer. The dry electrodes were fabricated using a spray-coating technique by depositing reduced graphene oxide (rGO) on a polydimethylsiloxane (PDMS) substrate.

The fabrication process of rGO-PDMS dry electrodes is demonstrated in figure 4.9. The synthesized rGO powder was ultrasonically dispersed in an N-methyl pyrrolidone (NMP) solution using a sonicator for one hour at 40 kHz at 100 W power. Using a spray gun, the rGO-NMP suspension was then cast on the backside of the PDMS substrate with a male snap button. To remove the NMP, the sample was dried using a hot air dryer. To ensure uniformity of the rGO film, the spraying and drying process is repeated several times.

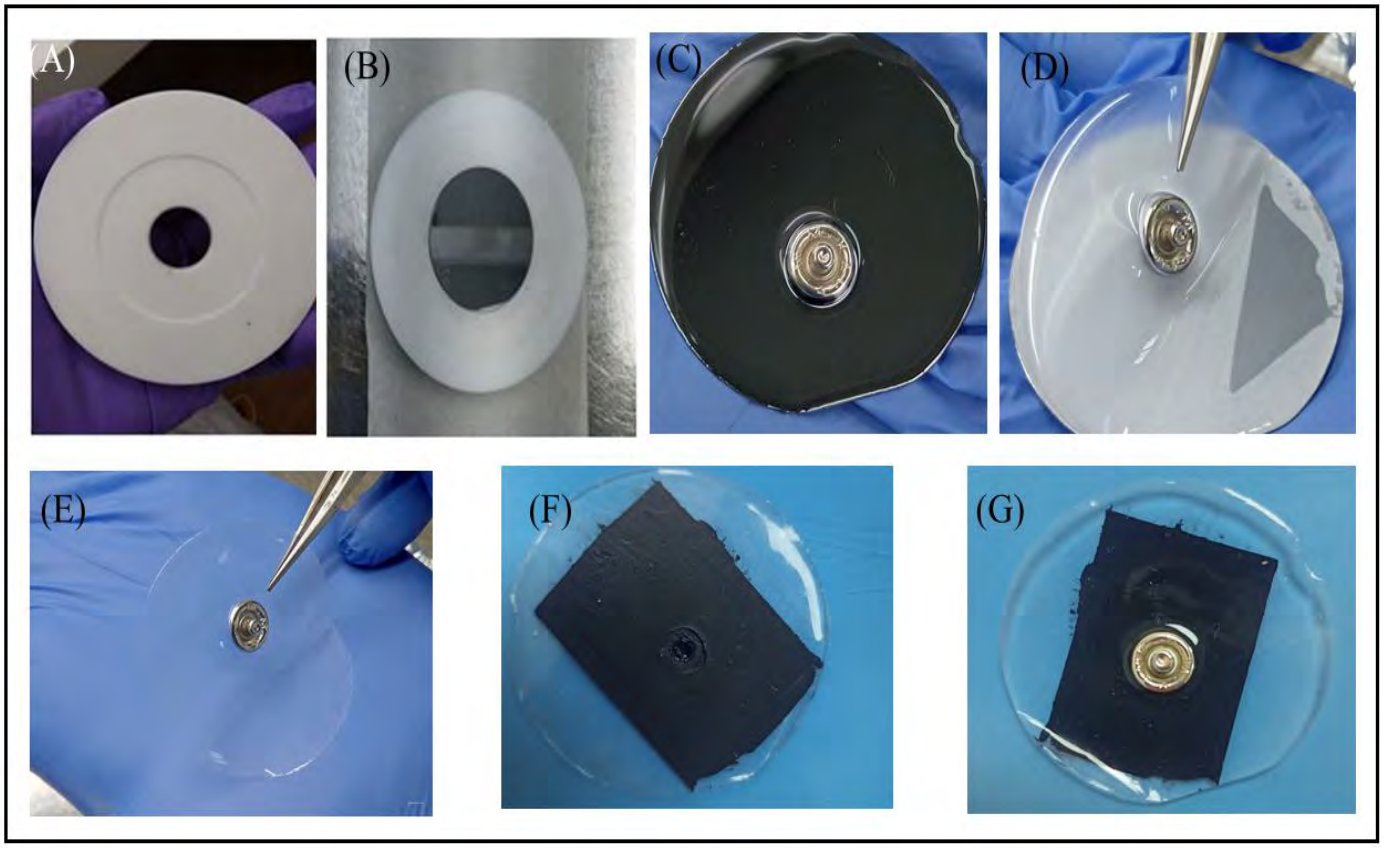

Figure 4.9. The steps of fabrication of the rGO-PDMS dry electrodes: (A) Teflon mould (B) silicon wafer on Teflon mould (C) PDMS mixture spread on the wafer and a male snap button placed at the centre of the wafer (D, E) peel of PDMS with the male snap button (F) back-view and (G) front-view of obtained rGO-PDMS dry electrode.

Figure 4.10. illustrates the FESEM image of a fabricated PDMS-rGO dry electrode with the rGO flakes uniformly distributed over the PDMS surface. Thus, a rectangular 3.58±0.2×2.53±0.2 cm^2 film of rGO, of a size comparable to that of the Biopac Ag/AgCl electrodes, was successfully fabricated.

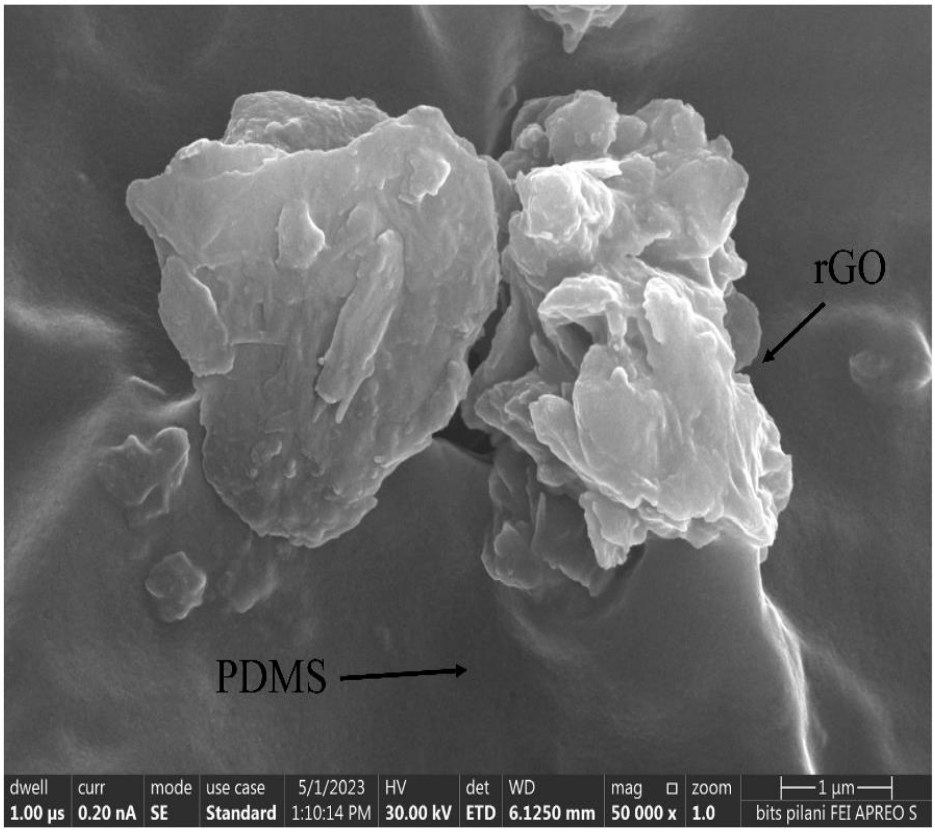

Figure 4.10. FESEM image of rGO/PDMS dry electrode at 1µm scale bars showing rGO flakes deposited over PDMS.

4.4.2 Impedance measurement and electrode modelling

The electrode-skin interface (ESI) is critical to the performance of the fabricated dry electrode. Ionic currents underneath the skin diffuse through this interface and interact with the electrodes. The exchange of electrons between the ions and electrode constitutes the biopotential signals. Care must be taken to optimize the electrode contact quality and minimize the impedance observed to record high-quality signals with minimal distortion and noise [50]. In this work, we propose an approach to directly compare the impedance of the electrode-skin interfaces formed by the fabricated electrode against that of the Ag/AgCl electrode. First, electrodes were placed on the subject's forearm with 4 cm and 8 cm spacings, and measurements were taken using a GwINSTEK 6300 LCR-Q meter over a frequency range of 10 Hz to 1 kHz. Representative samples are shown in figure 4.11.

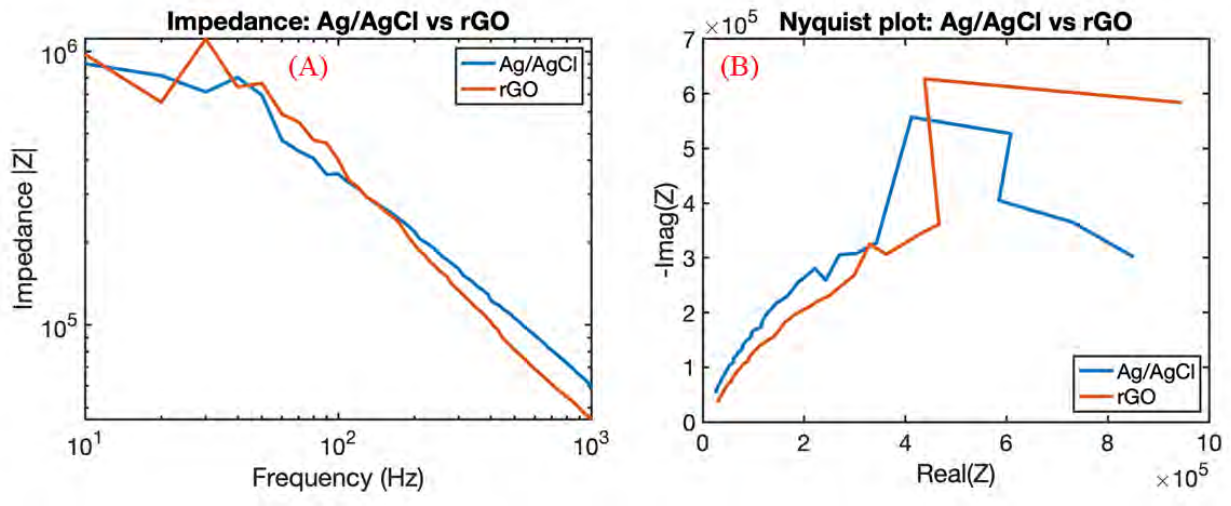

Figure 4.11. (A) Measured electrode impedance for the Ag/AgCl and fabricated rGO-PDMS electrodes and its (B) Nyquist plot form.

The skin-impedance measurements include contributions from the epidermis, dermis, deeper tissues and bodily fluids, as shown in figure 4.12.

$$Z_{tot,\ 4cm} = Z_{ESI} + Z_{ESI'} + Z_{4CM} \quad \textbf{...(4.1)}$$

$$Z_{tot,\ 8cm} = Z_{ESI} + Z_{ESI''} + Z_{8CM} \quad \textbf{...(4.2)}$$

To progress, simplifying assumptions were made. Z_{ESI} , $Z_{ESI'}$ and $Z_{ESI''}$ were assumed to be identical, and the approximation $Z_{8CM} \approx 2Z_{4CM}$ was assumed. Thus, Z_{4CM} could be approximated as $Z_{tot,8CM} - Z_{tot,4CM}$ and could be removed from the picture. For every pair of measurements $(Z_{tot,4CM}, Z_{tot,8CM})$, we can hence estimate Z_{ESI} in 2 ways: as $Z_{tot,4CM} - Z_{4CM}$ and as $Z_{tot,8CM} - 2Z_{4CM}$. Two 4cm and 8cm measurements were taken for both rGO and Ag/AgCl electrodes, and four pairings were formed. The rGO electrodes were reused throughout the process, while Ag/AgCl electrodes were replaced after use. Hence, eight estimates for $Z_{ESI}(f)$ were obtained. The simplified circuit model shown in figure 4.12 (B) was developed using the MATLAB ZfitGUI script. The circuit parameters of Ag/AgCl and rGO are shown in Table 4.1.

Table 4.1 Equivalent circuit model parameters of the electrode-skin interfaces formed.

	Rp (kΩ)	*Cp (nF)*	*Rs (kΩ)*
Ag/AgCl	213 ± 13	1.20 ± 0.01	9.68 ± 0.44
rGO	322 ± 52	0.85 ± 0.21	28.3 ± 7.61

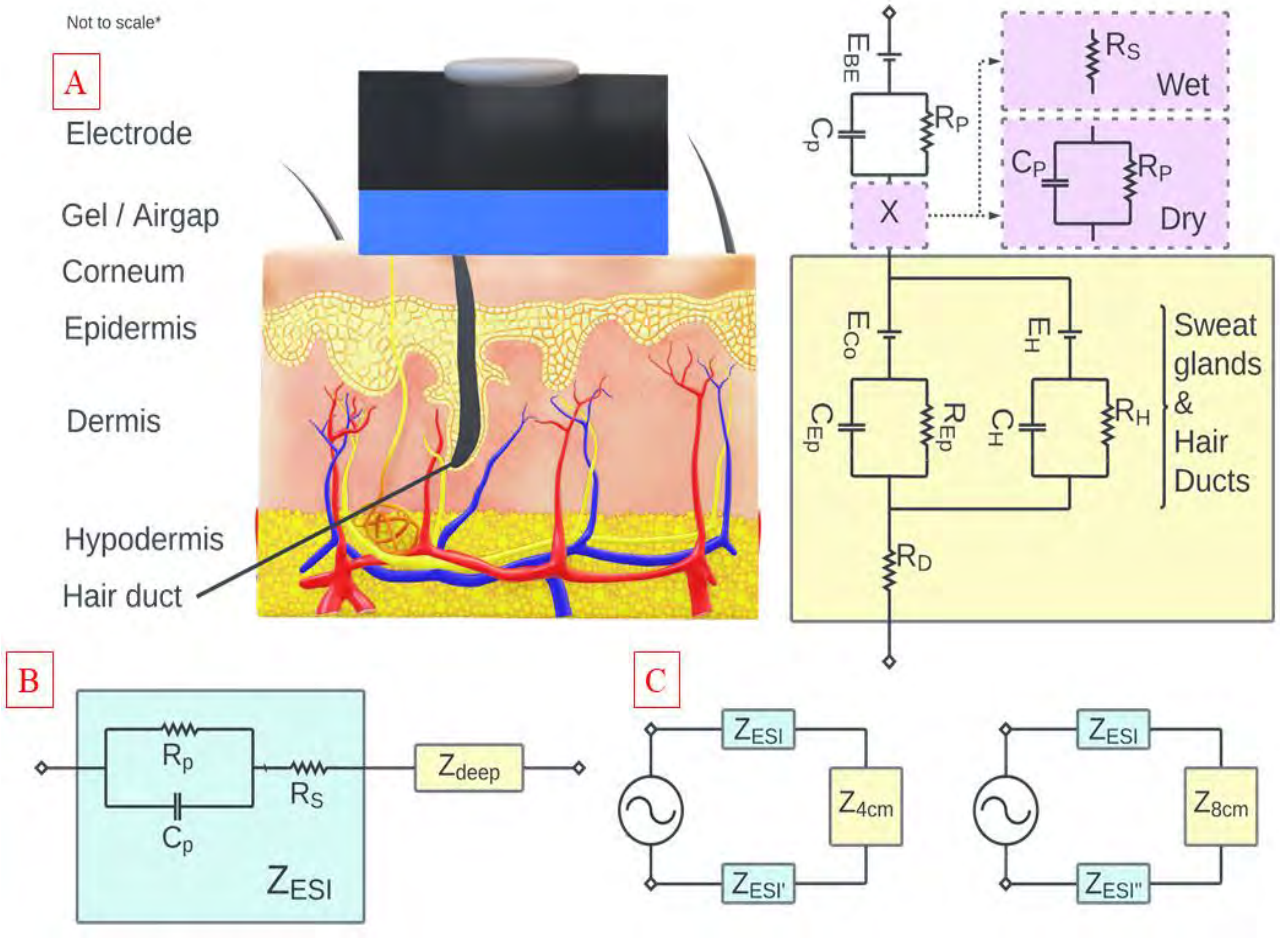

Figure 4.12. (A) The electrode skin interface and its circuit model [50-52], (B) simplified circuit model [53] and (C) circuit models for the measurements performed.

Figure 4.11 shows that the impedance offered by the rGO electrode is of the same order of magnitude as the Ag/AgCl electrode despite being a dry electrode. Table 4.1 presents a finer breakdown of the electrode behavior. It can be observed that, on an average, R_P and $1/C_P$ of the rGO electrode are about 1.5 times higher, and the R_S about 3 times higher than that of the Ag/AgCl electrode. The absence of an electrolyte reflects strongly, especially in R_S, which models the ionic mobility across the electrode-skin interface. It must be noted that the high variations observed in the rGO electrodes case also be correlated with the measurement time. Lower impedances were observed at later timestamps, perhaps due to the buildup of sweat. Considering lower bounds, the R_P, $1/C_P$ and R_S differ by factors of 1.35, 1.13 and 2.25, respectively. The impedance tradeoff has thus been quantified, and the potential suitability for long-term measurements is highlighted.

4.4.3 Electrocardiogram acquisition

An ECG data acquisition pipeline was designed to sense and amplify biopotential in general and ECG and EMG signals in particular, as shown in figure 4.13 (a). A Vernier EKG-BTA module, incorporating a high-gain differential amplifier optimized for bio-signals, an electrical isolation circuit, and a BTA-ELV analog protoboard adapter, was employed to amplify and transmit the ECG signals. The sampling process was facilitated by an Arduino Uno R3, which sampled the module's output at 1 kHz and transmitted the samples to a computer through a serial interface. Sampling utilized the 10-bit ADCs provided by the ATmega328P, with data transfer facilitated by UART at a baud rate of 115200. A MATLAB script was executed on the computer side to receive and store data from the serial interface while maintaining a consistent sampling rate of 1 kHz. Irrespective of the electrodes utilized, the measurements were conducted on a healthy 28-year-old male subject at room temperature. The 3-electrode configuration depicted in figure 4.13 (b) was adopted. The measurements was performed in a relaxed sitting position, and no skin preparation procedures were carried out.

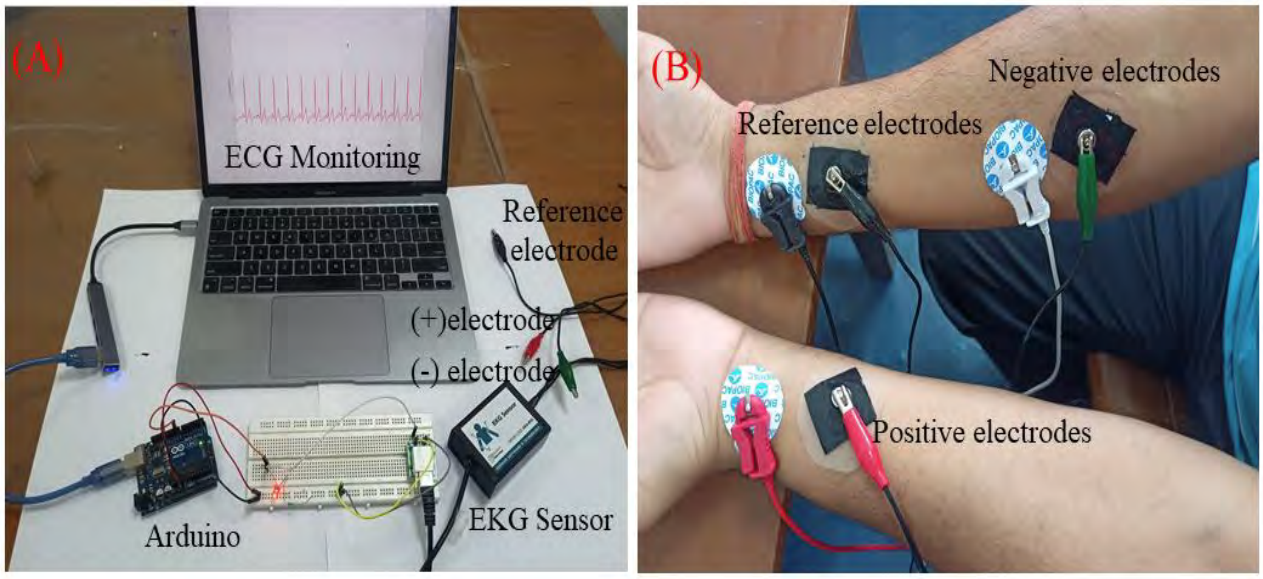

Figure 4.13. (A) The electronic ECG data acquisition system and the (B) 3-electrode configuration were used for the simultaneous ECG measurement using wet Ag/AgCl and dry rGO PDMS electrodes.

Figure 4.14 (A, B) shows ECG waveforms measured using standard wet Ag/AgCl electrodes and the developed rGO-PDMS dry electrodes and figure. 4.15 shows the zoom part of the ECG waveform measured using rGO-PDMS dry electrodes. It was observed that both electrodes measured ECG signals with similar signal amplitudes. In the recorded signals, the features of the ECG waveform essential for diagnosing

pathological conditions of the human heart, namely the P-wave, T-wave, and the QRS-complex, are clearly visible and undistorted. The features are easily extractable as well. For the recording shown in figure. 4.15, the P-R interval, QRS interval, Q-T interval, and heart rate were estimated to be 0.18s, 53.2ms, 0.38s, and 72.5 bpm, respectively. The electrodes can also be utilized for medical diagnosis due to the clarity of the signals and the extractability of critical ECG parameters.

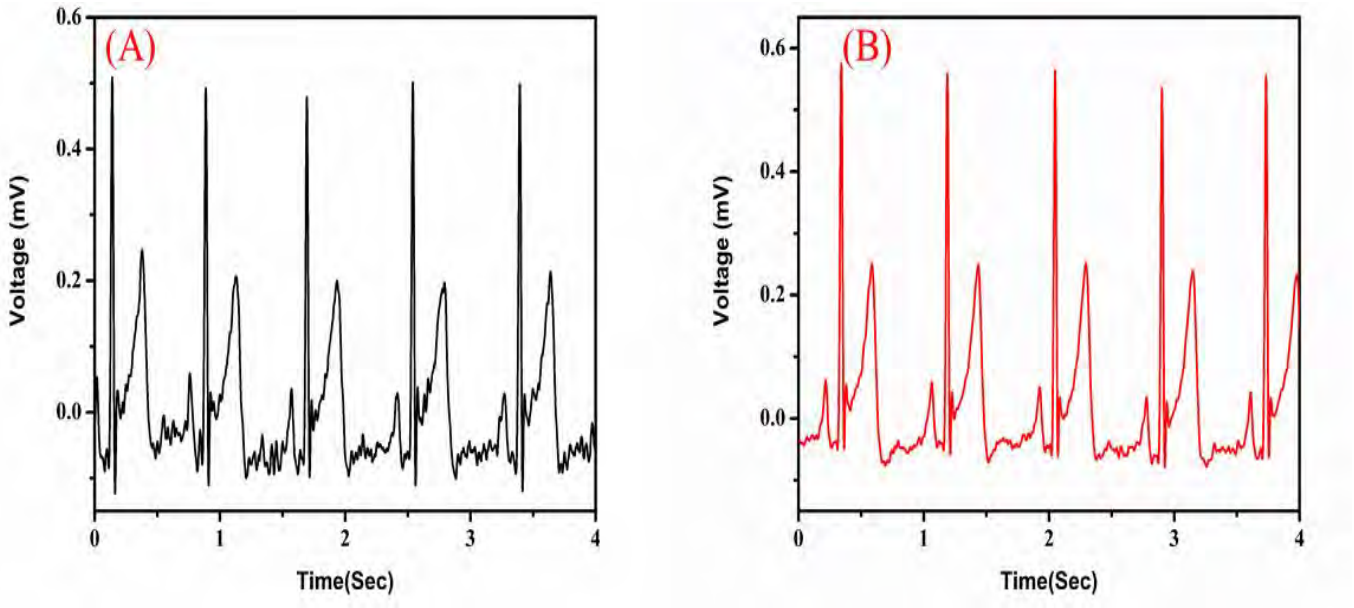

Figure 4.14. ECG signals were recorded using (A) Ag/AgCl electrodes and (B) fabricated rGO-PDMS dry electrodes.

Furthermore, the ECG signals recorded using rGO-PDMS electrodes contained less noise than those recorded using Ag/AgCl electrodes. The signal-to-noise ratio (SNR) of the recordings was computed by first estimating the peak-to-peak amplitudes of the P-wave, T-wave, and QRS-complex (*Vs*) and comparing it against the peak-to-peak deviations (*Vn*) observed in the respective regions of the waveform [54].

$$SNR\ (dB) = 20\ log10\frac{Vs}{Vn} \qquad \textbf{...(4.3)}$$

The waveforms recorded using the rGO-PDMS electrodes exhibit an average SNR of 27.2 dB, while those recorded using Ag/AgCl electrodes show an SNR of 25.7 dB. Thus, the rGO-PDMS electrodes can capture less noisy signals of similar amplitude as the Ag/AgCl electrodes, allowing for improved diagnosis quality.

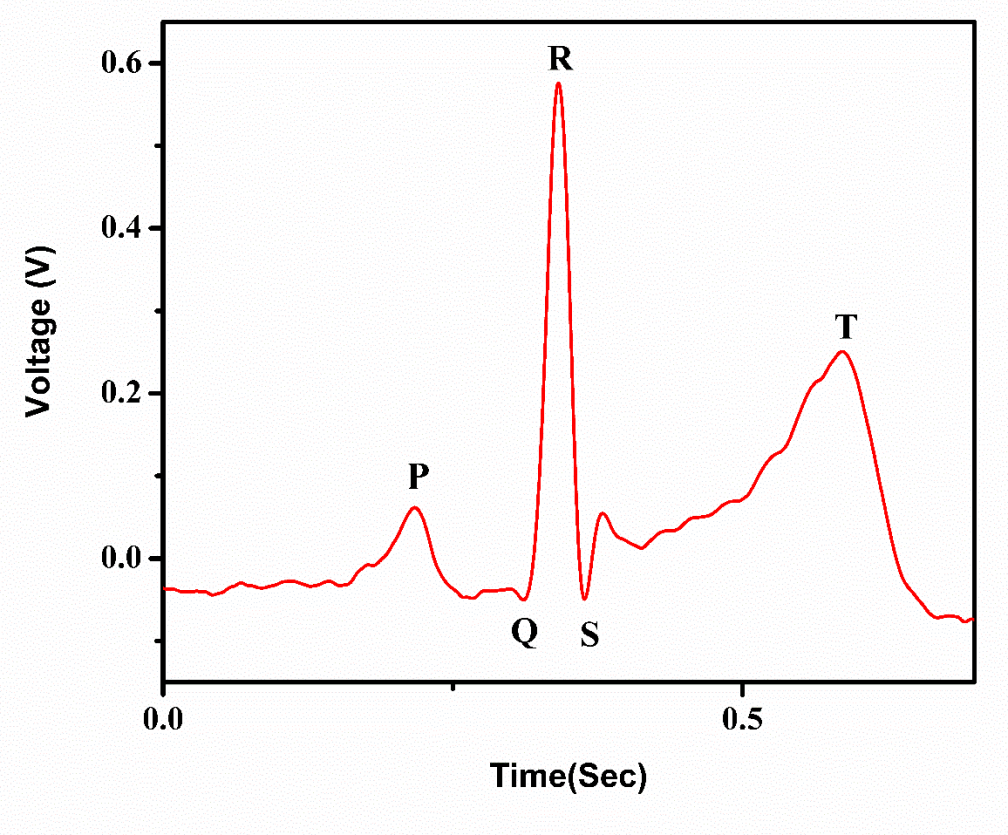

Figure 4.15. Obtained ECG cycle using the rGO-PDMS dry electrodes.

4.4.4 Electromyogram acquisition

Muscle cells generate electric potentials called electromyograms (EMG) on stimulation or activation. Analysis of EMG recordings would allow us to diagnose pathological conditions such as muscle-nerve discoordination and muscle fatigue [55]. To obtain EMG signals, two electrodes were placed across the bicep and one at the forearm without any skin preparation, and the same pipeline used to record ECG signals was utilized. EMG measurements of a 28-year-old healthy individual flexing his biceps at 3-second intervals were obtained using rGO and Ag/AgCl electrodes, as shown in figure 4.16. No significant difference in quality was observed in the measurements taken using rGO and Ag/AgCl electrodes. It is observed that the EMG recordings taken using the rGO-PDMS electrodes showed lower baseline variation, as compared to Ag/AgCl electrodes.

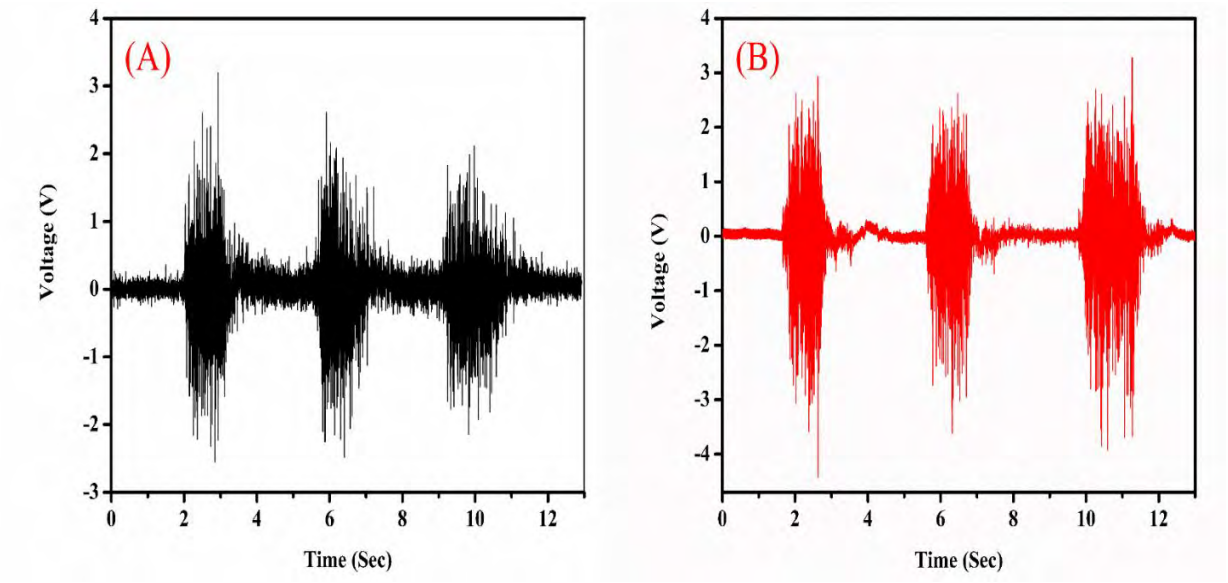

Figure 4.16. EMG signals were measured using (A) Ag/AgCl electrodes and (B) fabricated rGO-PDMS dry electrodes.

4.5 Conclusion

We successfully fabricated the flexible strain sensors based on graphene. The multilayer graphene/PDMS strain sensor effectively detects subtle human physiological signals, including elbow, finger and wrist. Based on its performance and facile fabrication, the proposed graphene strain sensor might have great potential in wearable electronics. We discussed a fabrication method for a wearable strain sensor using graphene nanoplatelets and PDMS. The resulting strain sensor exhibits high sensitivity, demonstrating perfect linearity in response to both stretching and releasing cycles when subjected to strain. Furthermore, the GNP strain sensor was also successfully used for human motion and wrist pulse detection. Notably, it accurately distinguishes all three positions of characteristic peaks (P, T, and D) in the wrist pulse spectrum. Its wide working range makes it a promising choice for wearable device applications.

The dry electrode was fabricated through a spray-coating method, involving the deposition of reduced graphene oxide (rGO) onto a polydimethylsiloxane (PDMS) substrate. The resulting dry electrode showcased uniformly distributed rGO flakes on the flexible PDMS surface, achieved through the spray-coating method. These electrodes demonstrated the capability to capture high-quality ECG and EMG signals. Compared to Ag/AgCl electrodes, the rGO-PDMS electrodes exhibited superior performance, recording ECG signals with higher signal-to-noise ratios and EMG signals with lower baseline variations. We employed circuit fitting techniques to analyze the electrode-skin interface impedance and quantified the tradeoff

associated with using the rGO-PDMS electrodes. The inherent advantages of dry electrodes, encompassing convenience, comfort, durability, and user-friendliness, position them as highly suitable for prolonged, unsupervised monitoring of ECG and EMG signals. The fabricated flexible rGO-PDMS electrodes showcased outstanding performance, making them a promising choice for wearable electronic devices and mobile healthcare technologies applications.

References

[1] S. Sun et al., "A wearable strain sensor based on the ZnO/graphene nanoplatelets nanocomposite with large linear working range," *Journal of materials science*, vol. 54, pp. 7048-7061, 2019.

[2] T. Q. Trung and N. E. Lee, "Flexible and stretchable physical sensor integrated platforms for wearable human-activity monitoring and personal healthcare," *Advanced materials*, vol. 28, no. 22, pp. 4338-4372, 2016.

[3] M. Ha et al., "Wearable and flexible sensors for user-interactive health-monitoring devices," *Journal of Materials Chemistry B*, vol. 6, no. 24, pp. 4043-4064, 2018.

[4] D. Corzo et al., "Flexible electronics: status, challenges and opportunities," *Frontiers in Electronics*, vol. 1, p. 594003, 2020.

[5] M. Cheng et al., "A review of flexible force sensors for human health monitoring," *Journal of advanced research*, vol. 26, pp. 53-68, 2020.

[6] T. Seesaard and C. Wongchoosuk, "Flexible and Stretchable Pressure Sensors: From Basic Principles to State-of-the-Art Applications," *Micromachines*, vol. 14, no. 8, p. 1638, 2023.

[7] J. Hu et al., "Recent progress in the flexible micro-pressure sensors for wearable health monitoring," *Nanoscale Advances*, 2023.

[8] M. A. Darabi et al., "Gum sensor: a stretchable, wearable, and foldable sensor based on carbon nanotube/chewing gum membrane," *ACS applied materials & interfaces*, vol. 7, no. 47, pp. 26195-26205, 2015.

[9] H. Dai et al., "Processing and characterization of a novel distributed strain sensor using carbon nanotube-based nonwoven composites," *Sensors*, vol. 15, no. 7, pp. 17728-17747, 2015.

[10] O. Kanoun et al., "Flexible carbon nanotube films for high performance strain sensors," *Sensors*, vol. 14, no. 6, pp. 10042-10071, 2014.

[11] L. Yang et al., "Development of a highly sensitive, broad-range hierarchically structured reduced graphene oxide/polyhipe foam for pressure sensing," *ACS applied materials & interfaces*, vol. 11, no. 4, pp. 4318-4327, 2019.

[12] W. Xu et al., "A sprayed graphene pattern-based flexible strain sensor with high sensitivity and fast response," *Sensors*, vol. 19, no. 5, p. 1077, 2019.

[13] T. Wang et al., "A self-healable, highly stretchable, and solution processable conductive polymer composite for ultrasensitive strain and pressure sensing," *Advanced Functional Materials*, vol. 28, no. 7, p. 1705551, 2018.

[14] B. Nie et al., "Flexible and transparent strain sensors with embedded multiwalled carbon nanotubes meshes," *ACS applied materials & interfaces*, vol. 9, no. 46, pp. 40681-40689, 2017.

[15] A. Mehmood et al., "Graphene based nanomaterials for strain sensor application—a review," *Journal of Environmental Chemical Engineering*, vol. 8, no. 3, p. 103743, 2020.

[16] S. Kashif Ur Rehman et al., "A review of microscale, rheological, mechanical, thermoelectrical and piezoresistive properties of graphene based cement composite," *Nanomaterials*, vol. 10, no. 10, p. 2076, 2020.

[17] P. Cataldi et al., "Graphene nanoplatelets-based advanced materials and recent progress in sustainable applications," *Applied Sciences*, vol. 8, no. 9, p. 1438, 2018.

[18] P. Cataldi et al., "Carbon nanofiber versus graphene-based stretchable capacitive touch sensors for artificial electronic skin," *Advanced Science*, vol. 5, no. 2, p. 1700587, 2018.

[19] R. Moriche et al., "Sensitivity, influence of the strain rate and reversibility of GNPs based multiscale composite materials for high sensitive strain sensors," *Composites Science and Technology*, vol. 155, pp. 100-107, 2018.

[20] D. Janczak et al., "Screen-printed resistive pressure sensors containing graphene nanoplatelets and carbon nanotubes," *Sensors*, vol. 14, no. 9, pp. 17304-17312, 2014.

[21] M. Zahid et al., "Strain-responsive mercerized conductive cotton fabrics based on PEDOT: PSS/graphene," *Materials & Design*, vol. 135, pp. 213-222, 2017.

[22] C. Yan et al., "Highly stretchable piezoresistive graphene–nanocellulose nanopaper for strain sensors," *Advanced materials*, vol. 26, no. 13, pp. 2022-2027, 2014.

[23] Y. Jeong et al., "Highly stretchable and sensitive strain sensors using fragmentized graphene foam," *Advanced Functional Materials*, vol. 25, no. 27, pp. 4228-4236, 2015.

[24] X. Wang et al., "Biocompatible and breathable healthcare electronics with sensing performances and photothermal antibacterial effect for motion-detecting," *npj Flexible Electronics*, vol. 6, no. 1, p. 95, 2022.

[25] K. Bayoumy et al., "Smart wearable devices in cardiovascular care: where we are and how to move forward," *Nature Reviews Cardiology*, vol. 18, no. 8, pp. 581-599, 2021.

[26] P. Rai et al., "Nano-bio-textile sensors with mobile wireless platform for wearable health monitoring of neurological and cardiovascular disorders," *Journal of The Electrochemical Society*, vol. 161, no. 2, p. B3116, 2013.

[27] M. Stoppa and A. Chiolerio, "Wearable electronics and smart textiles: A critical review," *sensors,* vol. 14, no. 7, pp. 11957-11992, 2014.

[28] K. Sel et al., "ImpediBands: Body coupled bio-impedance patches for physiological sensing proof of concept," *IEEE Transactions on Biomedical Circuits and Systems*, vol. 14, no. 4, pp. 757-774, 2020.

[29] C. Lou et al., "Flexible graphene electrodes for prolonged dynamic ECG monitoring," *Sensors*, vol. 16, no. 11, p. 1833, 2016.

[30] J. Y. Baek et al., "Flexible polymeric dry electrodes for the long-term monitoring of ECG," *Sensors and Actuators A: Physical*, vol. 143, no. 2, pp. 423-429, 2008.

[31] Y. Huang et al., "A novel wearable flexible dry electrode based on cowhide for ECG measurement," *Biosensors*, vol. 11, no. 4, p. 101, 2021.

[32] M. C. Barbosa et al., "Production of rGO-Based Electrospinning Nanocomposites Incorporated in Recycled PET as an Alternative Dry Electrode," *Polymers*, vol. 14, no. 20, p. 4288, 2022.

[33] N. T. Tasneem et al., "A low-power on-chip ECG monitoring system based on MWCNT/PDMS dry electrodes," *IEEE Sensors Journal*, vol. 20, no. 21, pp. 12799-12806, 2020.

[34] Y. Huang and C. W. Chiu, "Facile fabrication of a stretchable and flexible nanofiber carbon film-sensing electrode by electrospinning and its application in smart clothing for ECG and EMG monitoring," *ACS Applied Electronic Materials*, vol. 3, no. 2, pp. 676-686, 2021.

[35] Y. Bu et al., "The embedding of flexible conductive silver-coated electrodes into ECG monitoring garment for minimizing motion artefacts," *IEEE Sensors Journal*, vol. 21, no. 13, pp. 14454-14465, 2020.

[36] N. Celik et al., "Graphene-enabled electrodes for electrocardiogram monitoring," *Nanomaterials*, vol. 6, no. 9, p. 156, 2016.

[37] B. A. Reyes et al., "Novel electrodes for underwater ECG monitoring," *IEEE Transactions on Biomedical Engineering*, vol. 61, no. 6, pp. 1863-1876, 2014.

[38] A. S. Prasad and M. N. Jayaram, "Fabrication of GNR electrode for ECG signal acquisition," *IEEE Sensors Letters*, vol. 5, no. 9, pp. 1-4, 2021.

[39] H. Wang et al., "Robust tattoo electrode prepared by paper-assisted water transfer printing for wearable health monitoring," *IEEE Sensors Journal*, vol. 22, no. 5, pp. 3817-3827, 2022.

[40] Y. Yun et al., "Highly elastic graphene-based electronics toward electronic skin," *Advanced Functional Materials*, vol. 27, no. 33, p. 1701513, 2017.

[41] Y. Maithani et al., "Self-adhesive, stretchable, and dry silver nanorods embedded polydimethylsiloxane biopotential electrodes for electrocardiography," *Sensors and Actuators A: Physical*, vol. 332, p. 113068, 2021.

[42] S. Gong et al., "A gold nanowire-integrated soft wearable system for dynamic continuous non-invasive cardiac monitoring," *Biosensors and Bioelectronics*, vol. 205, p. 114072, 2022.

[43] M. Rodrigues et al., "Dry electrodes for surface electromyography based on architectured titanium thin films," *Materials*, vol. 13, no. 9, p. 2135, 2020.

[44] Y. Zhao et al., "Single-wall carbon nanotube-coated cotton yarn for electrocardiography transmission," *Micromachines*, vol. 9, no. 3, p. 132, 2018.

[45] S. Asadi et al., "Graphene elastomer electrodes for medical sensing applications: Combining high sensitivity, low noise and excellent skin compatibility to enable continuous medical monitoring," *IEEE Sensors Journal*, vol. 21, no. 13, pp. 13967-13975, 2021.

[46] S. Islam et al., "Fully printed and multifunctional graphene-based wearable e-textiles for personalized healthcare applications," *iScience*, vol. 25, no. 3, 2022.

[47] K. Murastov et al., "Flexible and water-stable graphene-based electrodes for long-term use in bioelectronics," *Biosensors and Bioelectronics*, vol. 166, p. 112426, 2020.

[48] P. S. Das et al., "Chemically reduced graphene oxide-based dry electrodes as touch sensor for electrocardiograph measurement," *Microelectronic Engineering*, vol. 180, pp. 45-51, 2017.

[49] Y. Huang et al., "Flexible capacitive pressure sensor based on laser–induced graphene and polydimethylsiloxane foam," *IEEE Sensors Journal*, vol. 21, no. 10, pp. 12048-12056, 2021.

[50] E. McAdams, "Bioelectrodes," *Encyclopedia of Medical Devices and Instrumentation, John Wiley & Sons*, Ltd, 2006.

[51] X. An and G. Stylios, "A Hybrid Textile Electrode for Electrocardiogram (ECG) Measurement and Motion Tracking," *Materials*, vol. 11, no. 10, pp. 1887, Oct. 2018.

[52] V. Alcan et al., "Investigation of graphene-coated Ag/AgCl electrode performance in surface electromyography measurement," *Biosensors and Bioelectronics*: Vol. X, no. 11, pp. 100193, 2022.

[53] R. Matsukawa et al., "Skin Impedance Measurements with Nanomesh Electrodes for Monitoring Skin Hydration," *Adv. Healthcare Mater*., vol. 9, no. 22, pp. 2001322, Nov. 2020.

[54] N. T. Tasneem et al., "Skin -potential variation insensitive dry electrodes for ECG recording," *IEEE Transactions on Biomedical Engineering*, vol. 64, no. 2, pp. 463-470, 2016.

[55] L. W. Lo et al., "Stretchable Sponge Electrodes for Long- Term and Motion-Artifact-Tolerant Recording of High-Quality Electrophysiologic Signals," *ACS nano*, vol. 16, no. 8, pp. 11792-11801, 2022.

Chapter: 5 Carbon Nanotubes-based Flexible Sensors: Design, Development and Applications

CNT nanocomposites offer a versatile and multifaceted set of properties, making them important in various applications, from advanced materials to wearable electronics and healthcare. As reported in chapter 2, polymer nanocomposites embedded with carbon nanotubes (CNTs) exhibit superior piezoresistivity, high flexibility and stretchability to potentially be the core material of the flexible and stretchable sensor in wearable electronics. Two types of CNTs exist: single-wall carbon nanotubes (SWCNTs) and multi-wall carbon nanotubes (MWCNTs). SWCNTs are often preferred for their excellent electrical conductivity, making them suitable for applications where electrical performance is crucial. In contrast, MWCNTs are more robust and have better mechanical properties than SWCNTs. These attributes make MWCNTs the preferred choice in scenarios where mechanical strength and long-lasting durability are paramount, especially in wearable device applications. This chapter presents two types of flexible sensors based on carbon nanotubes (CNTs). The initial sensor is a flexible pressure sensor based on a composite of MWCNTs for wearable electronic skin applications. The second is a flexible pressure strain sensor based on SWCNTs for human-machine interface (HMI) applications.

5.1 MWCNTs-based flexible pressure sensor

Flexible pressure sensors based on nanocomposite are most popular, receiving significant attention recently due to their great potential applications in wearable devices. These flexible sensors can be embedded into clothes or attached directly to the skin [1-2]. Owing to their many peculiar advantages compared with traditional sensors based on metals or semiconductors, including high sensitivity and stretchability, ease of fabrication, fast response, excellent stability, and lightweight. There is a rising interest in exploring novel materials to fulfill the growing demand for flexible pressure sensors. Researchers have delved into various conductive fillers that can be seamlessly integrated with polymers for this purpose. These fillers encompass a wide range of materials, including different types of nanoparticles, nanowires [3-4], graphene [5-6], carbon nanotubes (CNTs) [7-8], metal oxide [9] and conductive carbon black [10]. Carbon nanotubes

(CNTs) have gained prominence as a highly promising material, attributed to their exceptional electrical, mechanical, thermal, and chemical properties, along with notable features such as high flexibility, stretchability, sensitivity, and medical compatibility [11-14]. Carbon nanotube-based sensors have emerged as highly promising candidates for a wide range of applications such as wearable electronics, E-skin, human motion detection and structural health monitoring [15-18]. The percolation network structure formed by carbon nanotubes (CNTs) undergoes a notable transformation when the polymer nanocomposite, filled with CNTs, is exposed to varying levels of applied pressure. This transformation results in significantly enhanced piezo-resistive properties compared to other filler materials, owing to the curvilinear shape of CNTs. Additionally, when CNTs are combined with a highly elastic polymer, they enable the polymer matrix to maintain its exceptional stretchability as much as possible due to the entanglement of CNTs [19].

Therefore, the preliminary task for the preparation of desirable CNT nanocomposite is to make CNTs homogenously dispersed in the polymer matrix. With regards to the polymer matrix, Polydimethylsiloxane (PDMS) is considered to be the best choice for a flexible pressure sensor due to its high flexibility, biocompatibility, chemical and thermal stability, good transparency, ease of manufacturing and nontoxicity and so on, making it suitable for the wearable device. Furthermore, the cast moulding technique employed to fabricate nanocomposite with PDMS resin is simple and inexpensive. In this context, it has the ability to produce flexible conducting composites by adding CNT nanofillers.

This chapter focuses on the fabrication of a wearable resistive pressure sensor with a simple and low-cost method. The MWCNTs/PDMS nanocomposites-based resistive pressure sensor was designed and fabricated using different wt % of CNTs. The mechanical and electrical characteristics of the MWCNT nanocomposites are measured and studied. The FESEM morphologically observes the dispersion and distribution state of MWCNTs in the PDMS matrix. The fabricated pressure sensor obtains high sensitivity, stable data output at different pressure ranges and fast response time. Due to the excellent performance of fabricated MWCNT/PDMS, pressure sensor has broad application prospects in human motion detection, health monitoring, E-skin application and wearable electronic devices.

5.2. Fabrication of MWCNTs/PDMS pressure sensor

This chapter reports a simple and facile method to fabricate MWCNTs/ PDMS composite-based pressure sensor. For the fabrication of MWCNTs polymer composites, we need a suitable solvent for the dispersion of MWCNTs because they tend to agglomerate easily when dispersed in a solvent. The purchased MWCNTs with an average diameter of 25 nm, average length of 20 µm and 95% purity were mixed with Tetrahydrofuran (THF) for 20 minutes using magnetic stirring and ultrasonic for homogeneous mixing of MWCNTs. After this, the mixture of MWCNTs and THF was mixed on the PDMS elastomer base, followed by mechanical stirring for 20 minutes and ultra-sonication for 30 minutes. After that, the obtained composite mixture was heated at 90° C for 10 minutes to evaporate THF. In the final step, a silicon elastomer curing agent was added in a 10:1 ratio into the composite and degassed completely in a desiccator. This process is repeated several times to obtain a uniform dispersion of MWCNTs in the PDMS matrix. Figure 5.1 shows the schematic fabrication procedure of the MWCNTs/PDMS composite-based pressure sensor.

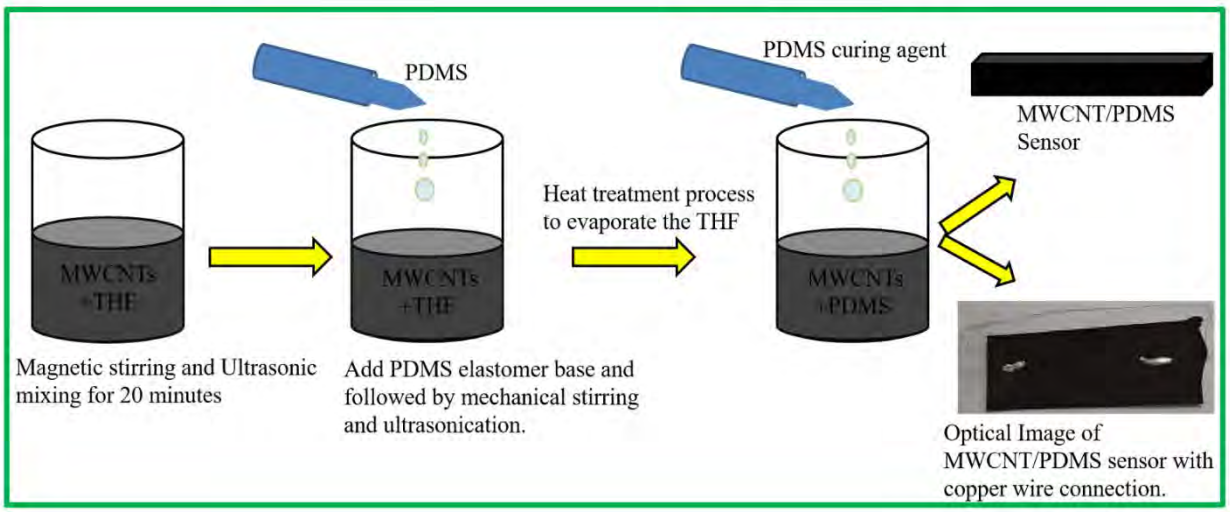

Figure 5.1. The schematic shows the fabrication procedure of the MWCNTs/PDMS pressure sensor.

The surface morphology characterization for MWCNTs/PDMS nanocomposite is done using FESEM. The recorded image of purchased MWCNTs at 500 nm resolution is shown in figure 5.2 (a), which contains randomly distributed bundles of MWCNTs. Figure 5.2 (b) elucidates the average diameter and length in the range of 20-30 nm and 20-40 µm, respectively.

Figure 5.2 (c) shows the fabricated MWCNTs/PDMS composite, indicating the homogeneous mixing, excellent dispersion quality with a large concentration of CNTs and complete evaporation of THF solvent. In addition, no free CNTs were observed on the MWCNT/PDMS composite surface, indicating that CNTs are fully dispersed in the polymer matrix. Including CNTs in an appropriate amount enhances electrical and mechanical properties.

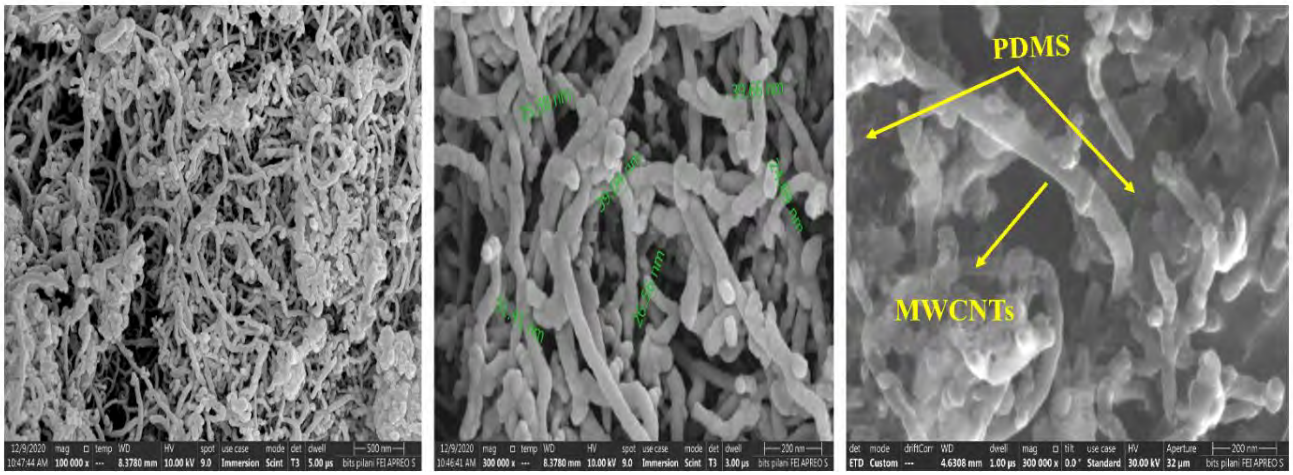

Figure 5.2. FESEM images showing (a) purchased MWCNTs at 500-nm scale bars, (b) MWCNTs at 200-nm scale bars with an average diameter and length of 25 nm and 20 µm, respectively, and (c) fabricated MWCNT/PDMS composite.

5.2.1 Mechanical tests of fabricated MWCNTs/ PDMS composites

It is well known that the incorporation of nanofillers into a polymer matrix can improve their strength and Young's modulus, which is related to mechanical strength. Tensile tests were implemented on all the fabricated nanocomposites, which were prepared using different concentrations of MWCNTs. The experimental procedure for creating MWCNTs/PDMS composite samples has been detailed in section 5.2, except for the increasing weight percentage of CNTs, i.e. (2%, 4 %, 6 %, 8 % and 10 %). The obtained MWCNT/PDMS mixture is deposited on a designed acrylic mould (detailed in figure 3.4) and placed inside an oven for curing. After that, the moulds were separated, and the MWCNTs/PDMS composite samples were obtained for mechanical measurements. Figure 5.3. shows the samples developed for measuring mechanical and electrical parameters. Each test was performed several times to obtain the repeatability and accuracy of the samples. First, the initial length was recorded for fabricated samples to obtain

stress-strain curves, which give information about the specific mechanical parameters, including elongation break, Young's modulus and tensile strength.

Figure 5.3. MWCNTS/PDMS composites for tensile and pressure sensor testing.

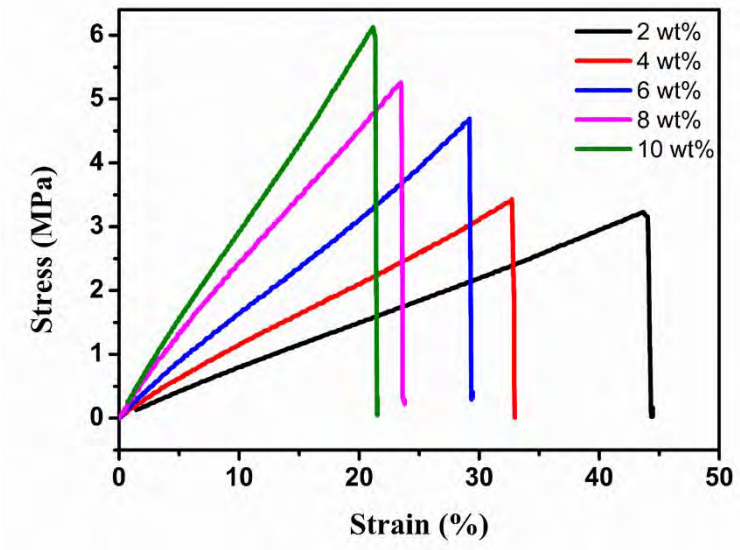

Figure 5.4. Tensile stress–strain curves for MWCNT/PDMS samples with their weight percentage.

The stress-strain behavior of MWCNT/PDMS composites for the different weight percentages at the same curing temperature is shown in figure 5.4. The Young's modulus of the tested samples was observed to be directly reliant on the weight concentration of CNTs. Figure 5.5 shows that as we start varying wt% of CNTs to the PDMS matrix, Young's modulus typically increases due to the stiff MWCNTs enhancing the composite's overall stiffness. However, the young modulus and tensile strength were highest for 10 wt% of CNTs; after that, it decreased due to the agglomeration of CNTs at their higher percentages.

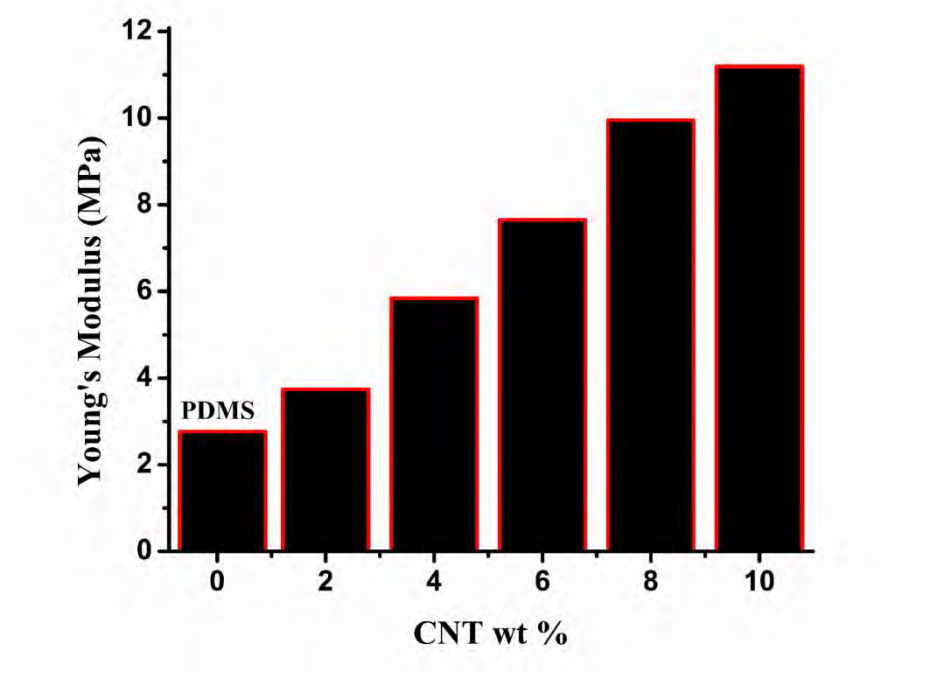

Figure 5.5. Variation of Young's modulus for PDMS and MWCNT/PDMS composites with varying CNT wt%.

Table 5.1 shows that Young's modulus of MWCNT/PDMS composites increases with the increase in the weight percentage of CNTs. The Young's modulus of pure PDMS was 2.26 MPa, while the Young's modulus of the 10-wt% MWCNTs/PDMS composites was nearly five times of the pure PDMS (i.e., 11.19 MPa). This is because the increase in weight % of CNTs enhances the Young's modulus of the composite.

Table 5.1. Mechanical properties of MWCNT/PDMS composites.

Material	Elongation break (mm)	Young's Modulus (MPa)	Tensile Strength (MPa)
PDMS	23.40	2.26	2.98
CNT 2wt%	13.20	3.74	3.19
CNT 4wt%	9.60	5.84	3.42
CNT 6wt%	8.70	7.65	4.66
CNT 8wt%	6.90	9.95	5.21
CNT 10wt%	6.30	11.19	6.11

5.2.2 Piezo-resistive properties of MWCNTs/PDMS composite in cyclic loading

Durability is an important piezo-resistive property of a pressure sensor that represents the endurance of long-term stretching/releasing cycles with excellent mechanical and electrical performance simultaneously. For this, a mechanical tensile cycling test was performed to obtain the electric stability and reproducibility of the MWCNTs/PDMS sensor. Figure 5.6. shows the variation of the relative change in resistance ($\Delta R/R_0$) of the MWCNTs/PDMS sample under tensile deformation. The pressure sensor was continuously stretched and released under a 15 % strain for 1,000 repeated loading–unloading cycles, and the $\Delta R/R_0$ was recorded. The relationship is linear, and the electrical resistance increases with the deformation. In addition, in the enlarged images (490–510) cycles, at the middle cycles (1465–1485) and for the (2560–2580) cycles, a constant $\Delta R/R_0$ of about 4.2 is observed. It is important to note that the small change in resistance of the composite is due to the applied stress and is not related to changes in the dimension or electromechanical properties of the MWCNTs/PDMS sensor. The resistance responses during all the loading–unloading cycles were highly symmetric, indicating negligible hysteresis of the sensor and displaying fast response and recovery characteristics. This response, together with the large values obtained for the gauge factor (GF), provides the suitability of these nanocomposites for

high-strain deformation sensors. The MWCNTs/PDMS sensor suggests very promising results, i.e. less response/ recovery time, reproducibility over 1000 cycles, high sensitivity and long-term stability. These fabricated samples shows great mechanical flexibility, which could be advantageous when applying sensors to uneven or curved surfaces.

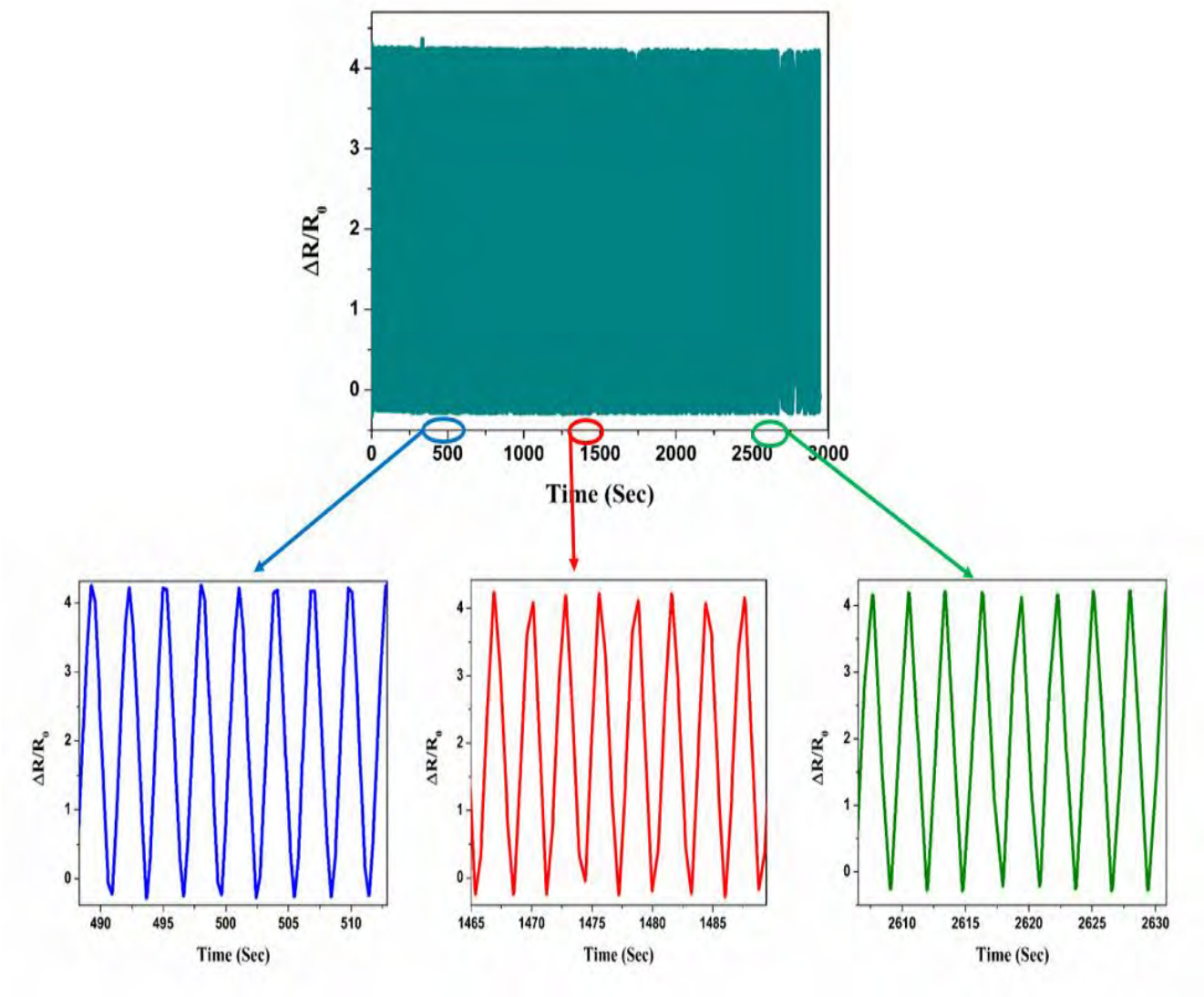

Figure 5.6. Variation of the electric resistance $\Delta R/R_0$ with time for the MWCNTs/PDMS composites for 1000 loading-unloading cycles.

5.2.3 Measurements of MWCNT/PDMS pressure sensor

The pressure sensor testing was performed using a Yantrika dead weight tester, as shown in figure 5.7. A Yantrika dead weight tester, hydraulic dead weight tester or pressure balance tester is an instrument used to measure the pressure, and it operates on the principle that the force applied to a confined fluid is directly proportional to the pressure generated. This instrument enables the accurate calibration of pressure-measuring devices by carefully balancing the forces with precisely calibrated weights.

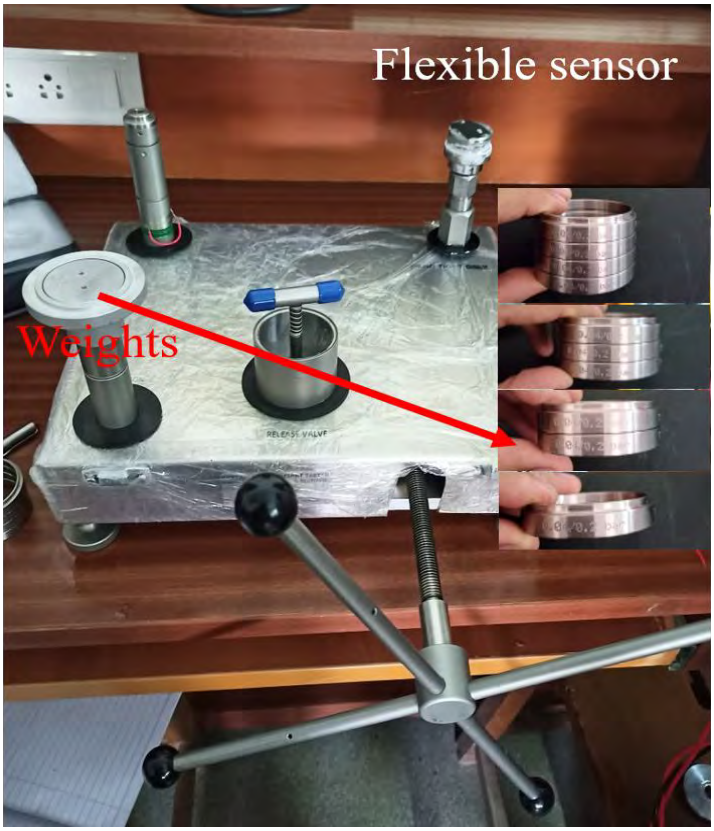

Figure 5.7. The pressure sensor testing setup: Yantrika dead weight tester.

A pressure sensor comprising MWCNTs/PDMS composites of a circular structure was designed and fabricated. Figure 5.8 describes the pressure sensor featuring a circular diaphragm with a 30-mm diameter and its behavior in both undeflected and deflected positions when subjected to applied pressure. MWCNTs are dispersed within the PDMS material. These nanotubes enhance the electrical conductivity of the diaphragm and allow for piezo-resistive sensing. When external pressure is applied, the diaphragm deforms, causing a change in the embedded CNTs' electrical resistance. This change results from the piezo-resistive effect, where

the diaphragm's electrical resistance varies with mechanical strain. This change in resistance is directly proportional to the applied pressure and the recorded resistance serves as the sensor's output signal.

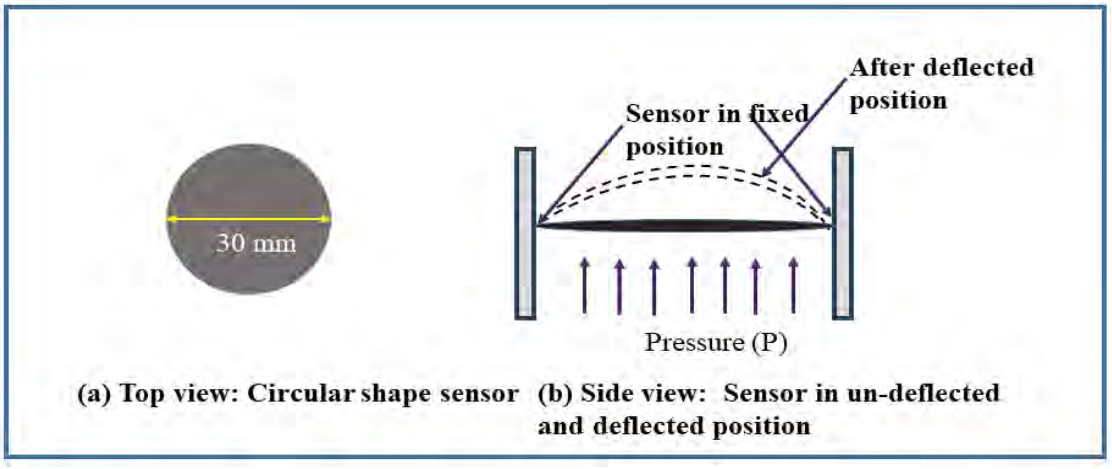

Figure 5.8. Typical geometry of an MWCNT/PDMS pressure sensor circular shape with 30-mm diameter, (b) pressure sensors undeflected and deflected position when pressure applied.

Figure 5.9 (a) shows an isolated diaphragm made of stainless steel, which is designed for applying pressure and serving as a flexible sensor base. This diaphragm was utilized for conducting pressure measurements. Figure 5.9 (b) shows that the sensor is affixed to the stainless steel diaphragm using gorilla glue and appropriate copper wire contacts.

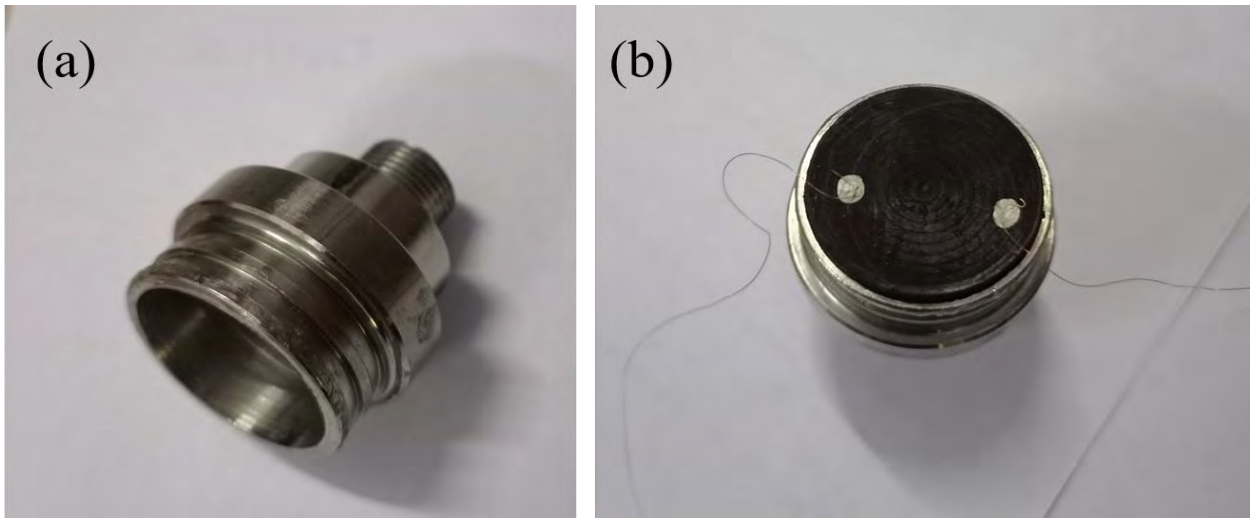

Figure 5.9. (a) Stainless steel-based isolated diaphragm, and (b) fabricated pressure sensor for measurements.

Figure 5.10 shows the variation of relative change in the resistance when the 2 wt%, 4 wt%, 6 wt%, 8 wt% and 10 wt% MWCNTs/PDMS composite samples were placed under pressure. It is observed that the change in resistance of the MWCNTs/PDMS composite increases with an increase in pressure due to the enhancement of CNTs concentration. These results are due to the resistive-dominant properties of the composites with a high density of CNTs. It was found that compositions with more wt% shows the conductive properties of CNTs. Increasing the pressure by more than 100kPa caused the composites to have a leakage problem in the sensor setup. Hence, it was chosen to keep the pressure range between 0.1 kPa to 100 kPa. To test the response of the MWCNTs/PDMS fabricated pressure sensor, the 0.1 kPa to 100 kPa pressure was loaded and unloaded.

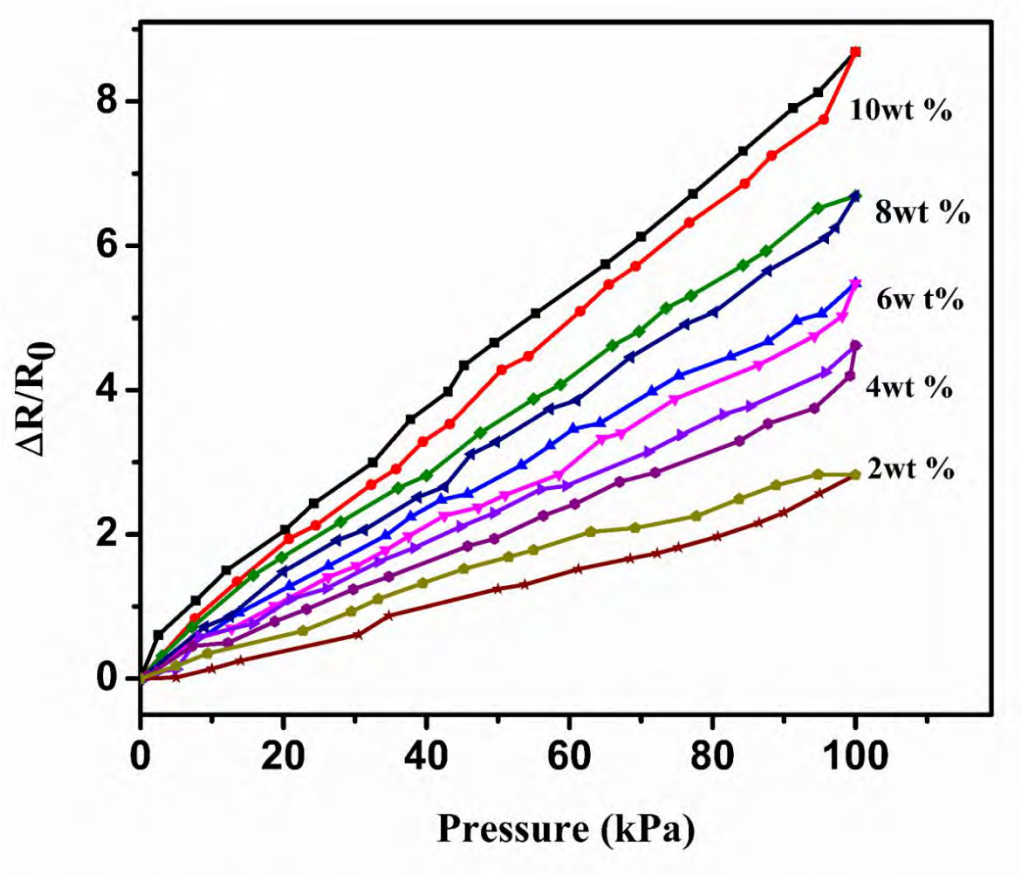

Figure 5.10. Piezo-resistive response of MWCNT/PDMS composites pressure sensor with an intermediate MWCNTs concentration of 2–10 wt%.

The sensitivity [20] can be expressed as:

$$S= \delta (\Delta R/R_0)/\delta P \quad \textbf{…(5.1)}$$

where $\Delta R=R-R_0$ and δP represent the variation of the applied pressure. The sensitivities of five different MWCNTs/PDMS-based pressure sensors were calculated with very low-pressure range (0.1–100 kPa).

Table 5.2. compares the proposed sensors with previous works based on CNTs/PDMS nanocomposites. It is evident that the proposed sensors exhibit high sensitivity and offer a broad pressure range. Consequently, they are well-suited for detecting biological signals. They can find applications in interactive wearable devices like electronic skin (E-Skin) and intelligent robotics.

Table 5.2. Comparison of recently reported carbon nanotube-based flexible pressure sensors.

Active Material	**Working range**	**Sensitivity**	**Ref.**
CNTs	0-50 kPa	0.25 kPa^{-1}	[21]
CNTs	0.25 kPa	1.39 kPa^{-1}	[22]
VACNTs	20 Pa-5 kPa	0.3-0.7 kPa^{-1}	[23]
MWCNTs	600 kPa	0.032 kPa^{-1}	[24]
MWCNTs	0-100 kPa	0.004 kPa^{-1}	[25]
MWCNTs	**0.1-100 kPa**	**0.0828 kPa^{-1}**	**This work**

The pressure sensors show high sensitivity and excellent linearity. It is observed in Fig. 5.11 that the sensitivity increases with the increase of the wt% of CNTs. The performance of the MWCNT/PDMS pressure sensors varies with weight percentage. When the weight of the CNTs increases, the sensitivity of the constructed sensors increases. The sensor is suitable for sensing a range of pressure (from 0.1 to 100 kPa) and shows five distinct sensitivities (0.02715, 0.04432,

0.05253, 0.06574, and 0.08283 kPa^{-1}) that gradually increase with the wt% of CNTs. The obtained sensitivities from the MWCNTs/PDMS pressure sensor (0.02715–0.08283 kPa^{-1}) are comparable with the sensitivity (0.018–0.078 kPa^{-1}) of human skin [26-27]. The 10-wt% MWCNTs/PDMS sensor suggested achieving the best piezo-resistive sensitivity (slope of the line) of 0.08283 kPa^{-1} in the linear range, and $\Delta R/R_0$ is also linearly related to pressure. More than 10 wt% of MWCNTs was not considered due to an increase in the hardness of the composite, which leads to the leakage problems in the sensor setup by applying the pressure.

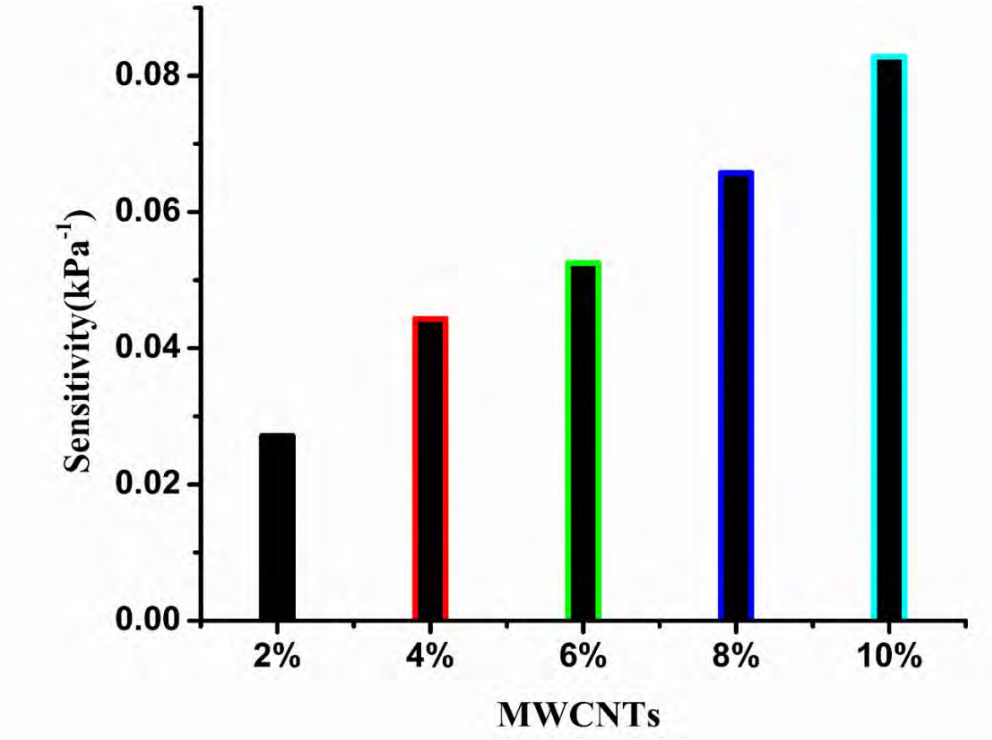

Figure 5.11. Shows the effect of CNT weight percentages increases the sensitivity.

5.2.4 Response of MWCNTs/PDMS pressure sensor for wrist pulse monitoring

The PDMS/MWCNT (10 wt. %) sensor is tightly attached to the human wrist to monitor the wrist pulse signal. The response of MWCNT/PDMS piezo-resistive pressure sensor is shown in figure 5.12. The response shows that the developed pressure sensor possesses the capability to capture and present a real-time wrist pulse waveform. This allows the monitoring of the radial artery pulse wave which is composed of three peaks. The top inset in figure 5.12 shows one single wrist pulse, which corresponds to the percussion wave (P wave), tidal wave (T wave), and dicrotic wave (D wave). Each signal wave exhibits a regular and repeatable response in the wrist pulse

waveform. The radial artery augmentation index (AIr = P_2/P_1) and Δt_{DVP} time delay between the percussion wave and tidal wave used as a measure of arterial stiffness are, respectively, calculated to be 74.41% and 0.17 sec, matching the reference data of a healthy adult man [28-29]. A decrease in Δt_{DVP} and an increase in AIr, which corresponds to the changes in amplitude and timing of pulse wave also affect the blood pressure. The results reveal the effectiveness of the sensor for clinical diagnosis and biomedical monitoring.

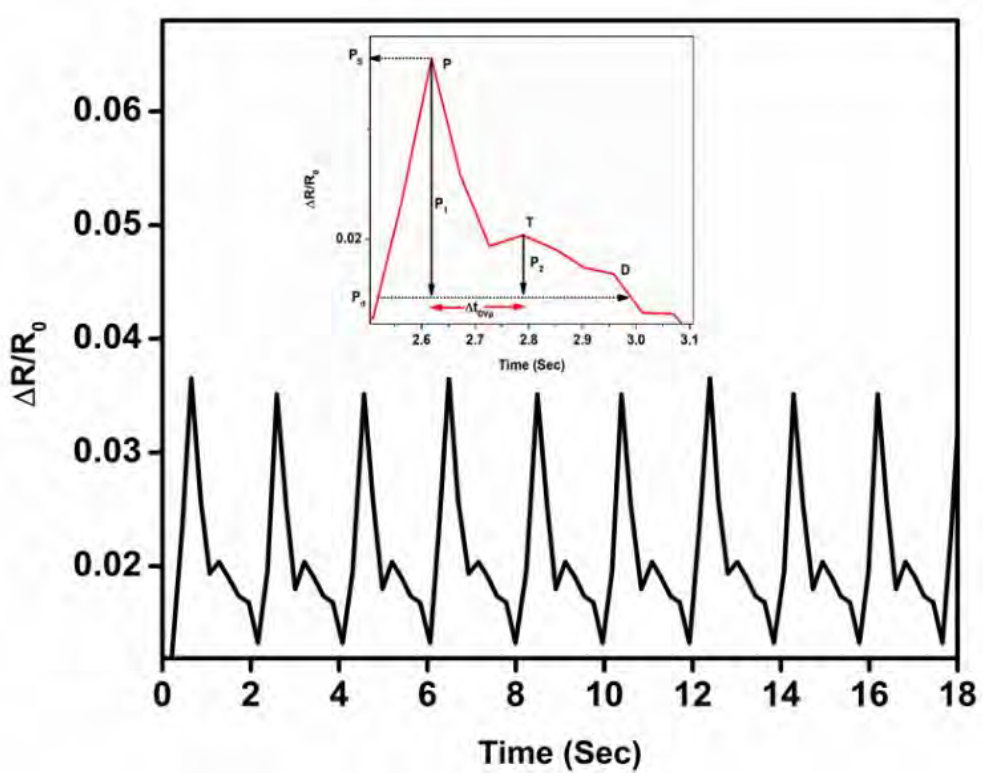

Figure 5.12. Response of MWCNTs/PDMS pressure sensor for wrist pulse monitoring.

5.3. SWCNTs-based flexible strain sensor

The development of wearable electronics has brought a revolutionary change in human-machine interaction (HMI) applications in recent years. Among the various wearable devices, an electronic glove (e-glove) embedded with flexible strain sensors holds significant potential to monitor hand gesture detection [30-32]. These gloves, equipped with embedded sensors and electronic components, enable seamless interaction between humans and machines through intuitive hand gestures, monitoring of vital sign signals, and touch-sensitive interfaces [33]. The

development of advanced strain sensors have emerged as a promising candidate to enhance the HMI device's sensitivity, flexibility and reliability. These sensors are strategically designed to demonstrate significant deformability, guaranteeing their ability to replicate the wearer's fingers intricate deformations accurately.

Traditional strain sensors based on metals and semiconductors have high sensitivity but a limited strain range, typically around 5%, which falls short of meeting the sensing demands of wearable devices. Moreover, they face challenges when mounting on curved surfaces, irregular shapes and are often incompatible with accommodating finger deformations. On the other hand, strain sensors based on carbon nanotubes, graphene, carbon black, and conductive polymers exhibit compatibility with finger deformations, enable interaction with irregular surfaces and can be seamlessly integrated into electronic gloves. Due to their exceptional electrical, mechanical, and thermal properties, single-walled carbon nanotubes (SWCNTs) have garnered significant attention in recent years [34-37]. These unique characteristics and their high aspect ratio make SWCNTs ideal candidates for strain-sensing applications. By exploiting the piezo-resistive effect, SWCNTs-based strain sensors can accurately convert mechanical deformations into electrical signals, enabling precise and dynamic monitoring of human movements.

In addition, it complements the advantageous properties of SWCNTs, providing mechanical flexibility and robustness to the strain sensor. PDMS is an excellent substrate for embedding SWCNTs and enhances the sensor's conformability to various surfaces, including electronic gloves [38]. The combination of SWCNTs and PDMS offers a synergistic effect, resulting in a highly sensitive and durable strain sensor for HMI applications. Their ability to accurately detect and quantify various strains, such as bending, stretching, and twisting, enables multiple applications, including motion tracking, gesture recognition and body motion detection.

Following this, we introduce a simple glove-based controller that utilizes SWCNTs/PDMS-based strain sensors for hand gesture detection in the context of HMI applications. The primary focus of this work is to design suitable flexible strain sensors and formulate a proper packaging plan for glove-based control. The robotic hand was assembled mechanically and electrically, and the resting and gripping positions of the motors were calibrated and fine-tuned. Controllability of all fingers was achieved, and a keyboard-based serial control

interface was implemented for testing the hand gesture. This characteristic enables the glove to trace finger deformations accurately.

5.3.1 Fabrication of SWCNTs/PDMS strain sensor

A thin SWCNTs/PDMS composite layer was deposited directly onto a PDMS substrate to create the flexible strain sensor. Firstly, the PDMS substrate was prepared using a similar technique explained in chapter 3. After that, the PDMS mixture was poured onto a rectangular acrylic mould and cured the PDMS in an oven at 80°C for half an hour. The SWCNTs were sonicated in toluene solvent for 5 hours to achieve a well-dispersed SWCNT solution. Here, toluene acts as a dispersant, breaking down the agglomerates of SWCNTs and promoting their dispersion. The obtained SWCNTs/toluene solution was combined with freshly prepared PDMS mixture in a 10:1 ratio and stirred gently to disperse the SWCNTs uniformly in the PDMS matrix; after that, the composite was placed in a hot drier to allow the toluene to evaporate because the absence of toluene is crucial for obtaining reliable and stable strain sensor's performance. After that, the thin composite layer was deposited onto the cured PDMS substrate and again cured at 80°C, enhancing composite adhesion on PDMS. At the final stage, electrical contacts were applied using conductive silver paste and copper wires.

In order to study detailed information about chemical structure, the Raman characterization is performed. Figure 5.13. shows the recorded Raman spectra for SWCNTs. There are four major Raman bands observed for the CNT: RBM bands around 150 cm^{-1}, D-band at 1325 cm^{-1}, G-band at 1594 cm^{-1}, and 2D-band at 2621 cm^{-1}. The Radial Breathing Mode (RBM) is a characteristic vibrational mode of SWCNTs, indicating CNTs presence. The RBM peak in the Raman spectrum is a prominent feature and is often used to determine the diameter (chirality) of the SWCNT. Different chiralities of SWCNTs have RBM peaks at different Raman shift frequencies. Smaller-diameter SWCNTs will have RBM peaks at higher Raman shift frequencies, while larger-diameter SWCNTs will have RBM peaks at lower Raman shift frequencies.

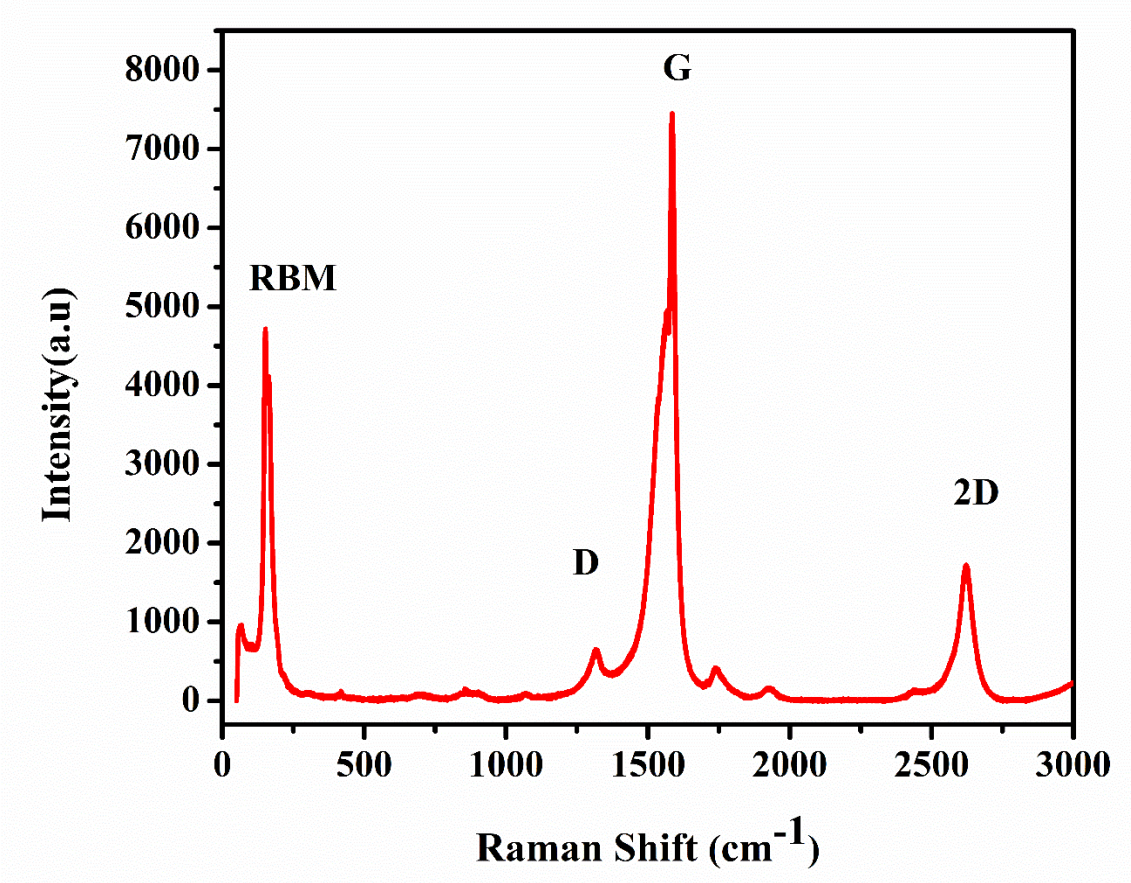

Figure 5.13. Shows recorded Raman spectra of SWCNTs.

D-band is a measure of the fraction of structural defects in CNTs, and it is often referred to as the "disorder" or "defect" band because it is associated with structural defects and disorder in the carbon lattice. The D band is typically observed at a lower Raman shift frequency than other spectrum features, such as the G band. It arises due to defects, such as vacancies, grain boundaries, and disordered carbon atoms in the material. These defects disrupt the perfect hexagonal lattice of carbon atoms and introduce phonon modes that give rise to the D band. The G band is associated with the E2g phonon mode in a pristine, ordered carbon lattice and typically appears at a higher Raman shift frequency. In SWCNT Raman spectra, the 2D band is often observed in addition to the RBM peak, and it provides valuable information about the chiral indices and structural properties of the nanotubes. The positions and relative intensities of the 2D bands indicate the nanotubes' specific chiralities and diameters.

The surface morphology of the SWCNTs strain sensor has been investigated by FESEM, and findings are displayed in figure 5.14. It is noted that SWCNTs appear more or less smooth, clean, long, straight, well aligned, and uniformly distributed, indicating a less defective wall of SWCNTs. Figure 5.15 shows optical photographs of a fabricated SWCNTs/PDMS-based flexible strain sensor that is stretchable and twistable. These properties of the fabricated sensor make it a suitable candidate for HMI applications.

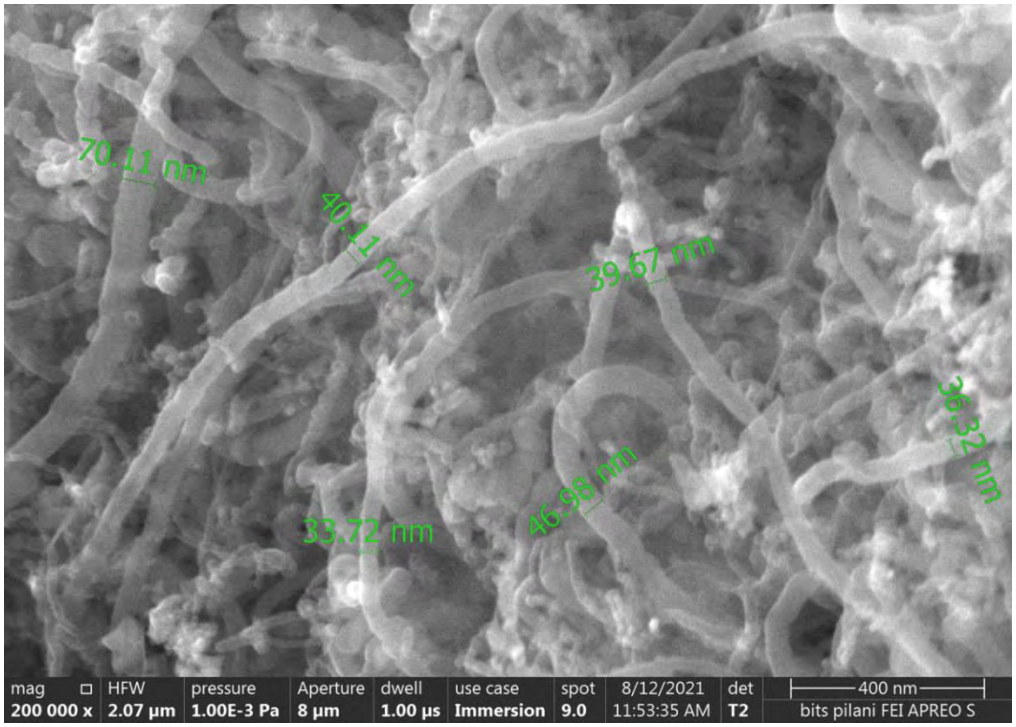

Figure 5.14. FESEM image of SWCNTs at 400-nm scale bars with an average diameter of 40 nm.

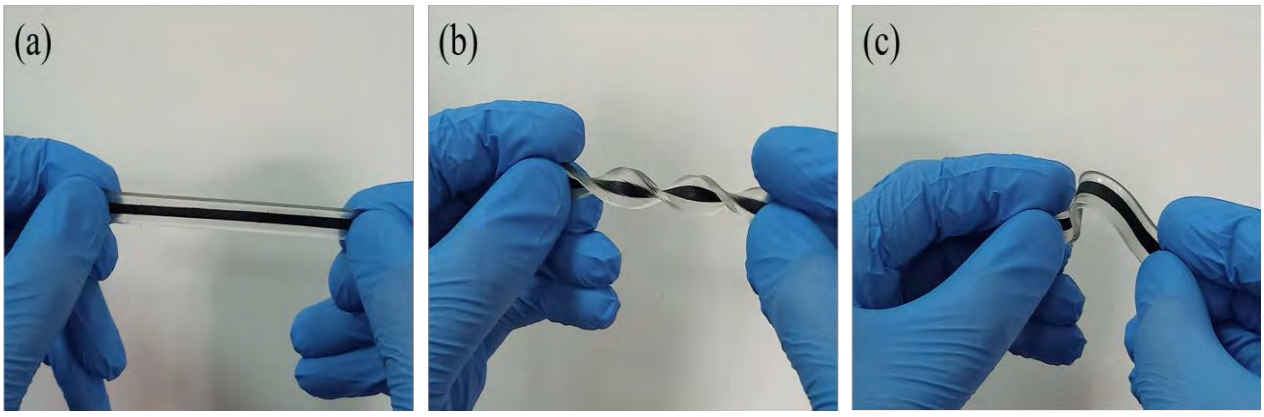

Figure 5.15. Optical photographs of fabricated SWCNTs/PDMS-based flexible strain sensor (a) stretchable, (b), twistable and (c) foldable.

5.3.2 Fabrication of electronic glove

In order to demonstrate the application of the human-machine interface, the fabricated SWCNTs/PDMS strain sensors were integrated onto the latex glove. However, a challenge arises due to the incompatibility of PDMS and latex gloves with adhesives such as cyanoacrylate-based superglues. To overcome this issue, we opted for a different approach to integrating sensors on the glove. We used an acrylic adhesive double-sided tape onto the latex glove, then placed a thin copper tape on top. The next step involved placing a small amount of PDMS mix onto the copper tape and the fabricated sensor carefully placed on the PDMS mix. To provide the electrical contacts thin copper wires are connected to the SWCNTs/PDMS composite using silver paste. The contacts are fragile, and hence, the sensor integration is done with utmost care. The sensors as a whole are shown in figure 5.16. Finally, the glove with sensors was cured using the hot oven, ensuring a stable and secure integration of the sensors onto the glove. This process was controlled and repeatable, ensuring consistency of sensor integration on the glove.

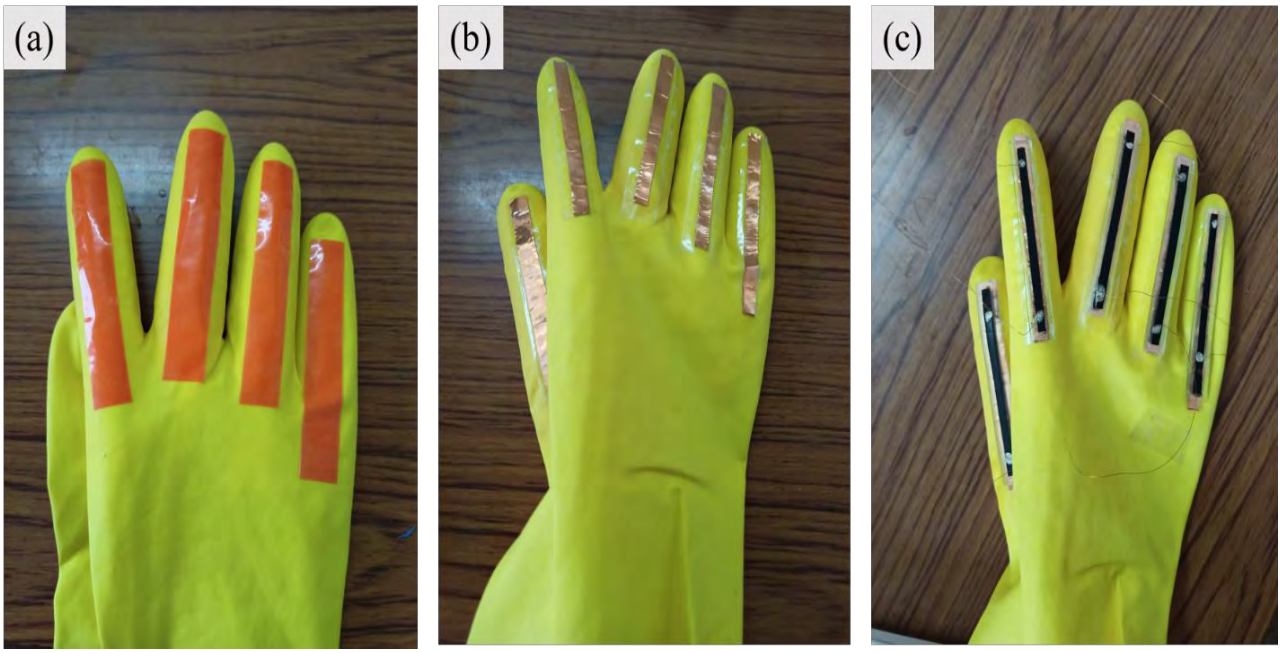

Figure 5.16. Optical photographs of the e-glove fabrication process: (a) acrylic adhesive double-sided tape onto the latex glove, (b) thin copper tape with liquid PDMS on the acrylic tape, and (c) the latex glove with SWCNTs/PDMS flexible strain sensors.

5.3.3 Development of robotic hand

Firstly, the STL files were sliced using Ultimaker Cura 5.1.0 and 3D-printed using an Ultimaker S5 with 0.2mm precision and 60% infill. The hand was printed using polylactic acid (PLA) in the AA 0.4mm core and its support structures with polyvinyl alcohol (PVA) in the BB 0.4mm core. The process required 80.3m of PLA, 12.3m of PVA and 58 hours of printing time.

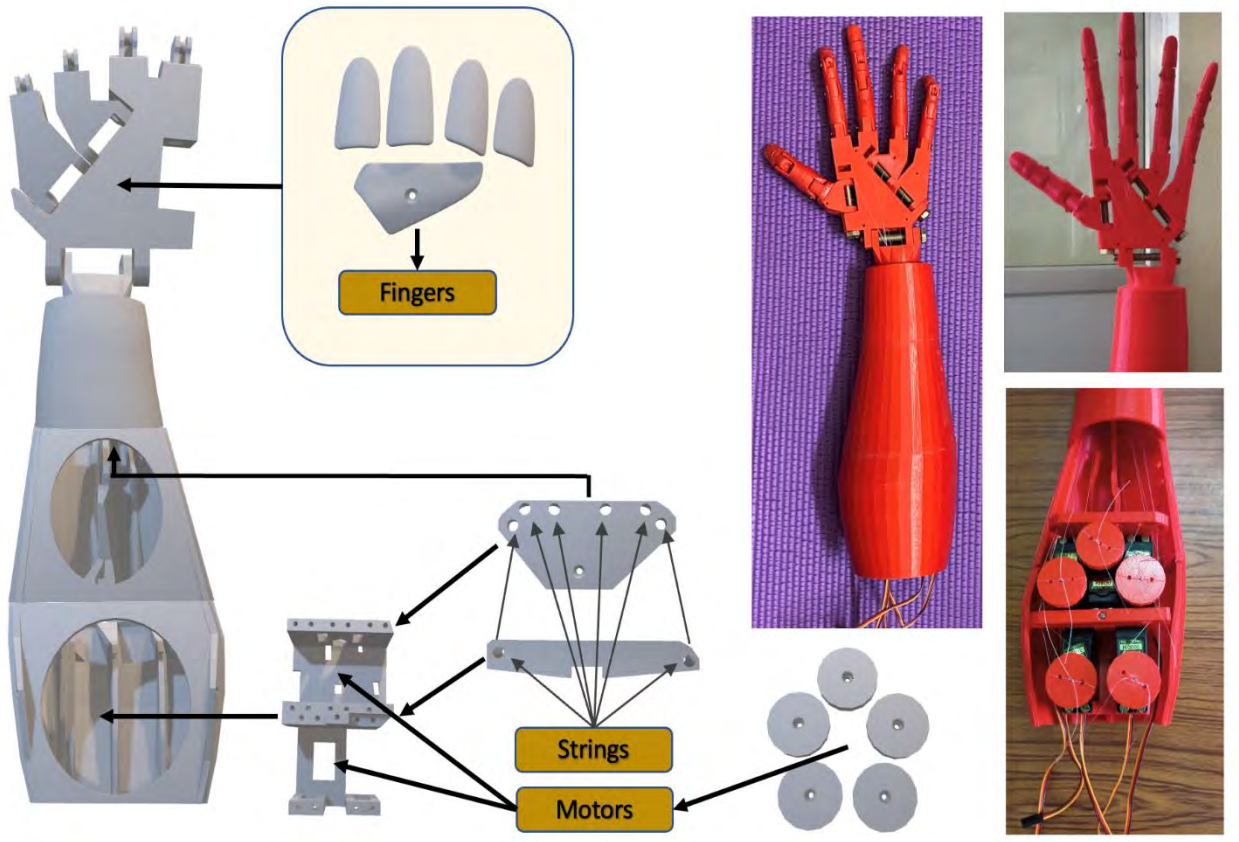

Figure 5.17. The procedure followed for assembling the robotic hand.

The PVA was dissolved in warm water, and the parts were smoothened with 220-grit sandpaper. The overall assembly process is described in figure 5. 17. Appropriate bolts and screws were fixed at all the design joints. The joints were glued together as appropriate. 0.3mm diameter high-strength Nylon strings were passed through each of the fingers and were fixed to the tip of each of the fingers from inside. One string was used per finger, and the two ends of each string were tied to MG946R servo motors. The motor was rotated to its 45-degree position when attaching the wrist end, with the finger resting position. Now, the motor is rotated to the 135-degree position, and the other end of the string is pulled till the hand reaches its gripping position.

The string is then tied firmly to the motor. This assembling methodology ensures the controllability of the fingers by the motors with sufficient margins. Further mechanical deviations can be accommodated at the software level. This process is repeated for all five fingers. The robotic hand was assembled mechanically and electrically, and the resting and gripping positions of the motors were calibrated and fine-tuned.

5.3.4 Electrical performance of SWCNTs/PDMS strain sensor

The electrical characteristics of SWCNTs/PDMS nanocomposites play a vital role in determining the performance of flexible and stretchable sensors, impacting their sensitivity and stability. As illustrated in Figure 5.18, the variable resistance value of the strain sensor has a linear relationship with the applied strain. It is seen that the variable resistance value is increased with the increasing strain. The gauge factor of the SWCNTs/PDMS strain sensor is 73 and exhibits remarkable sensitivity, making it highly suitable for detecting finger gestures.

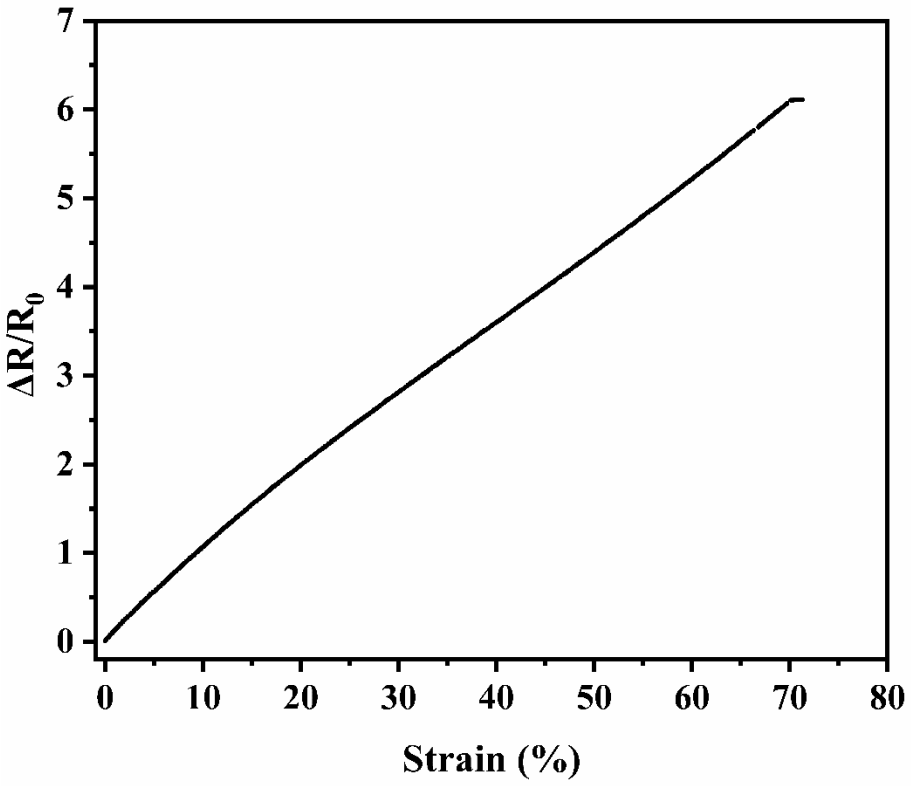

Figure 5.18. Shows the linear relationship between the variable resistance and the applied strain.

Figure 5.19 depicts the fatigue analysis of the flexible SWCNTs/PDMS strain sensor, validated by repeatedly loading and unloading for 850 seconds under a 30 % strain. The data reveals that the maximum strain value during repeated loading cycles remains the same, i.e. around 65. The e-glove embedded with SWCNTs/PDMS strain sensors proves to be exceptionally stable for continuous strain data collection, showcasing tremendous potential in applications related to finger gesture detection and human-machine interface (HMI).

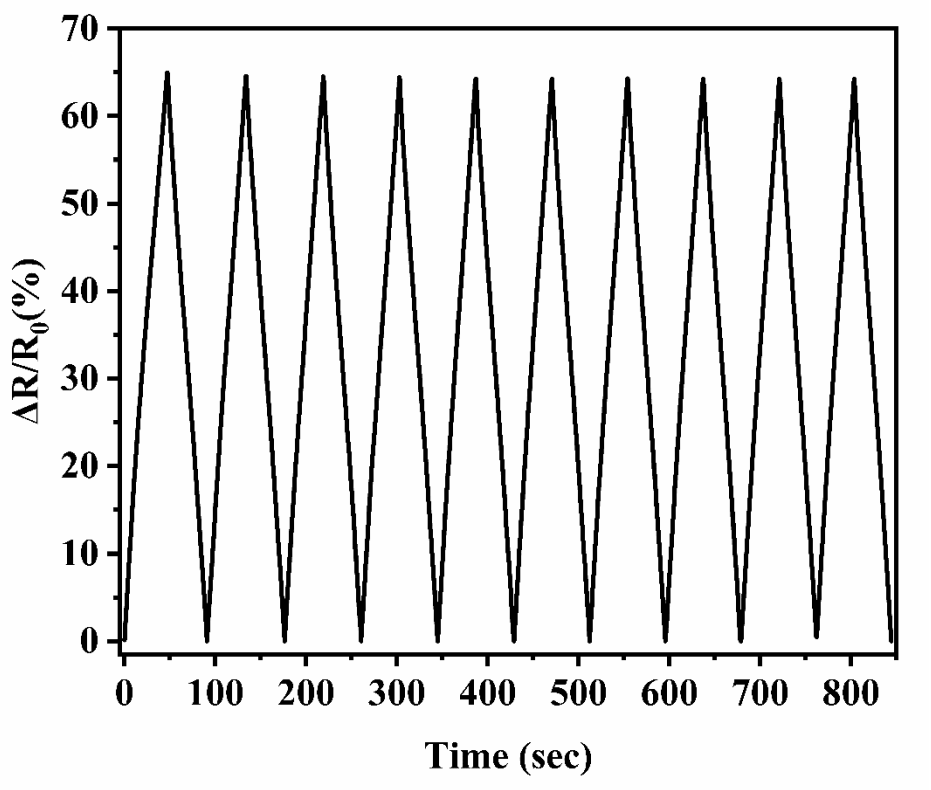

Figure 5.19. Fatigue test of the SWCNTs/PDMS strain sensor under repeated loading and unloading cycles.

5.3.5 Human robotic hand interaction and glove-based controllers

We discussed the importance of human-robotic interaction in chapter 2. Now, let us look at the importance of the glove-based controllers. These controllers provide the users with an intuitive means of controlling the robotic hands. Additionally, they play a crucial role in building extensive databases used to train models that can eventually replace human users. For example, these controllers may utilize pressure or strain sensors to convert finger motions into electrical signals.

The fundamental working principle of the SWCNTs-based strain sensor is rooted in the concept that the material resistance changes when contacts are formed or broken. Consequently, it can be asserted that resistivity is interconnected with the applied strain. This phenomenon is commonly known as piezoresistivity. These piezo-resistive sensors are integrated onto the latex gloves as described previously. The primary sensing element of the SWCNTs/PDMS strain sensor is a variable resistor. When it is stretched, the resistance changes. A generic voltage divider circuit was employed to measure the unknown resistance, as shown in figure 5.20. The circuit transduces the resistance changes into voltage changes. Mathematically, the circuit can be described by the following equation:

$$Vout = Vin \frac{R2}{R1+R2} \quad \textbf{...(5.2)}$$

where Vout is the output voltage, R_2 is the unknown resistance of the SWCNTs/PDMS strain sensor, R_1 is the known resistance, and Vin is a 5V input voltage. Vout was recorded using Arduino's 10-bit ADC. Hence, using equation 5.2, the resistance of the flexible sensors can be calculated from the ADC's readings. The 16-point averaging is applied to handle any spurious readings, such as loose contacts or accidental shorting due to external metallic objects. Similar steps are also implemented to protect the robotic hand from any danger as well. The voltage-converted resistance values of all sensors are sampled over 5 seconds at 100Hz, and the average reading is set to be the baseline voltage of the glove. This value is subtracted from all future readings, and mapping the resting position value to the 0 position is attempted.

Next, the glove state visualizer tool is utilized. The interface utilizes a pair of scripts based on MATLAB and Arduino. These scripts sample the hand's state at a rate of 100Hz and communicate the measurements to the MATLAB program through the serial interface. The program then plots the baseline-shifted voltages. This way, each finger can be tested and calibrated individually. The fingers are gripped one by one, and the peaks of the baseline-shifted voltage plots are noted. The gripping positions of all the fingers are assigned to be the corresponding peak values observed, establishing the baseline voltage and maximum deviation through calibration steps. The next step involves mapping these calibrated voltages to the observed motor positions. This mapping is inherently non-linear due to the non-linear variations in resistance and voltage as the fingers are slowly clenched.

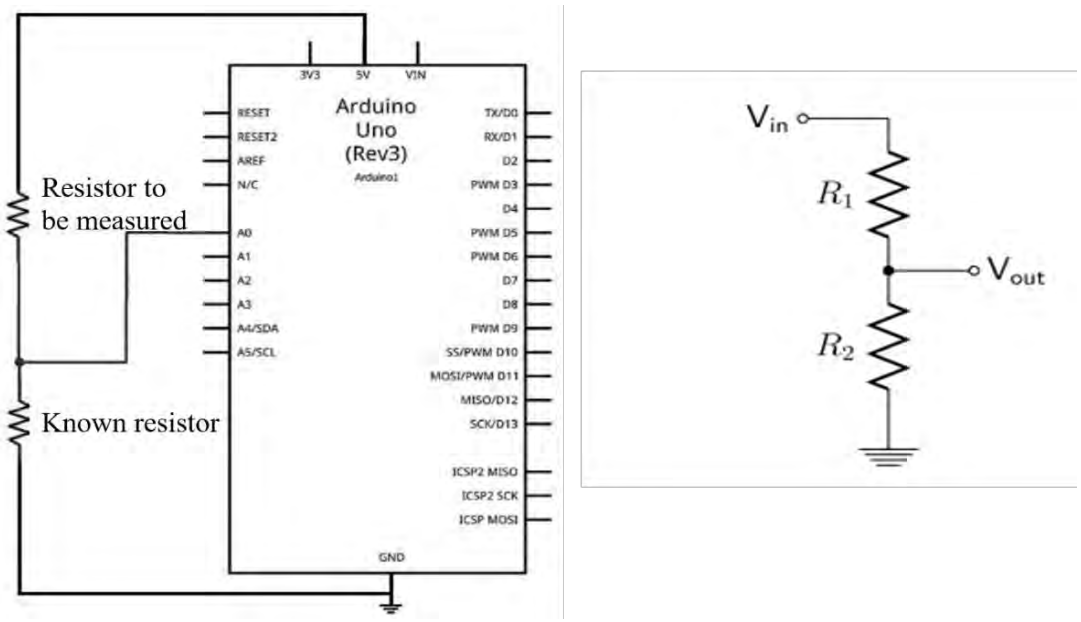

Figure 5.20. A generic voltage divider circuit to measure unknown resistance.

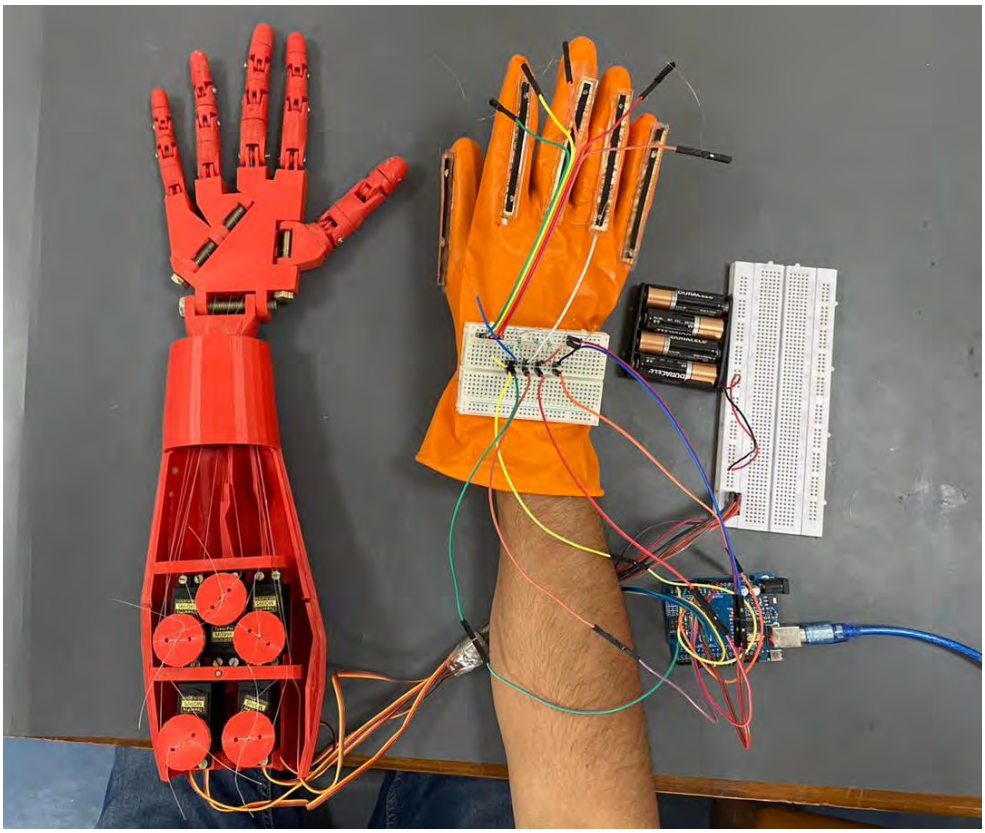

Figure 5.21. Electrical assembly of the glove-controlled robotic hand.

The glove-controlled robotic hand's electrical connections are shown in figure 5.21. Using five PWM pins, we use an Arduino Uno to read the glove's status and control the hand's servo motors. When the Arduino is powered via USB, it can only provide up to 500mA, which is not enough for all five servo motors. However, if the 9-12 V barrel jack powers the Arduino, it can give 800mA, but it is still close to the limit. Therefore, in order to meet power requirements, we used a 6V external battery and the servo motors were connected to a 6V battery pack with AAA batteries arranged in a 4S configuration.

The electrical assembly involves two breadboards designated for the glove and the robotic hand, as shown in figure 5.21. The wires from the electronic glove are connected with the known resistance and Arduino. The wires from the robotic hand were neatly packaged into a 3x5 grid and taped in place. The 6V battery's supply and ground are connected to the rails of the breadboard. Then, two arrays of 5 wires corresponding to supply and ground are taped together and connected into the slots in the 3x5 grid previously made. Lastly, another array is connected to the 3x5 grid, which branches into the PWM pins of the Arduino on the other side. This modular approach ensures a well-organized and efficient wiring setup for controlling the robotic hand.

5.3.6 Finger motion detection using electronic glove

Finger motion detection measurements were performed to verify the electronic glove's suitability for HMI applications. The e-glove is equipped with five SWCNTs/PDMS strain sensors, which track the deformation of finger bending actions to record strain data for each of the five fingers. In Figure 5.22, the strain response to various finger-bending actions is depicted as captured by the smart glove. Initially, one finger was bent and returned to its original position, repeating this process for all fingers. The recorded strain data corresponds to the thumb, index finger, middle finger, ring finger, and little finger. The e-glove and the SWCNTs/PDMS strain sensor can stretch and deform in response to finger movements. There is a noticeable variation in resistance linked to the bending of each finger. This phenomenon results from the sensor stretching as the finger bends, reducing the conduction pathway and increasing resistance. When returning to its original state, the sensor underwent compression, which expanded the conduction pathway and consequently led to a decrease in resistance.

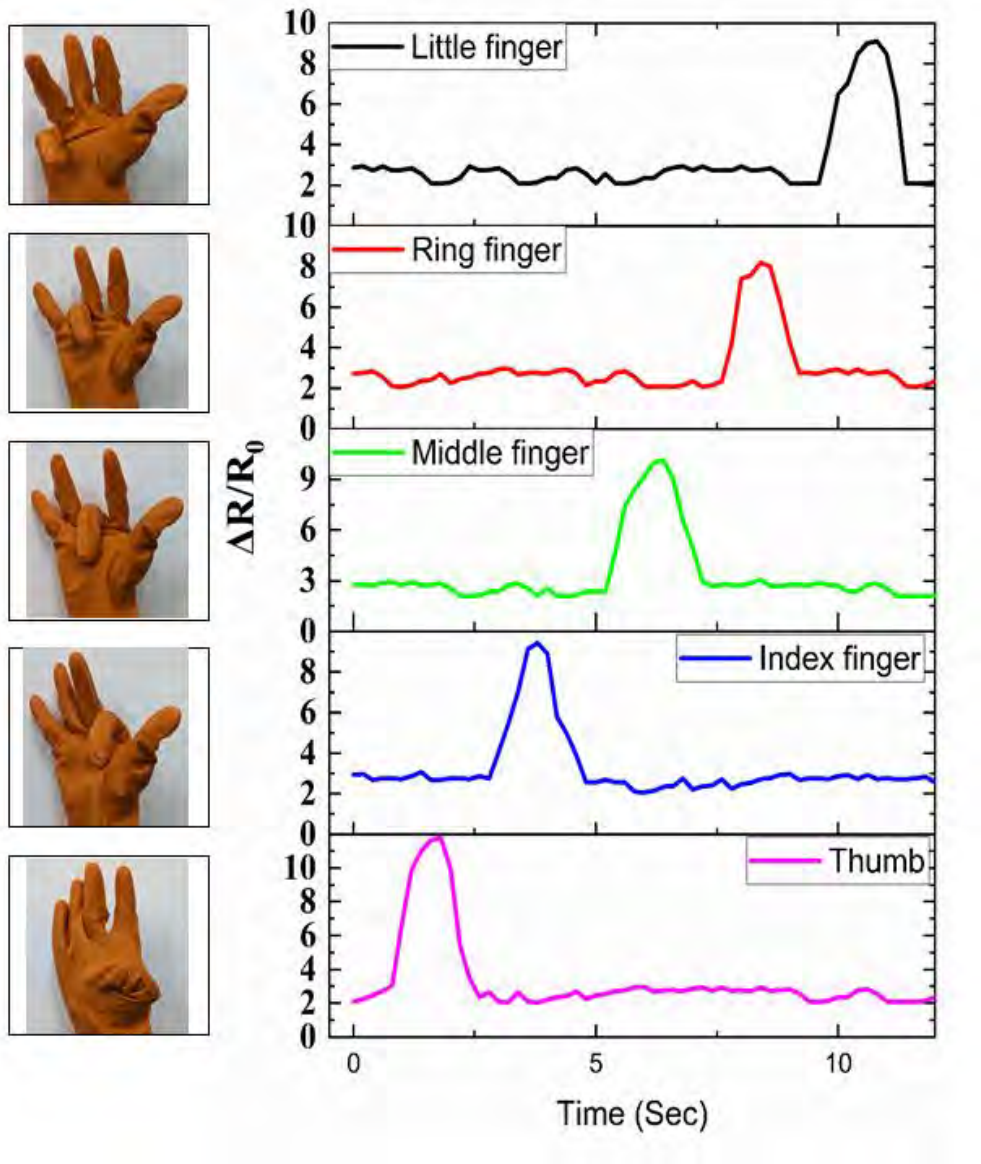

Figure 5.22. Strain data from the e-glove with different fingers bending.

Figure 5.23 illustrates the electronic glove's resistance changes, stemming from the SWCNTs/PDMS strain sensor's capability to detect and respond to the user's grip on the smiley face squeeze ball. When the glove wearer squeezes the ball, the strain sensor undergoes deformation, resulting in alterations in the electrical resistance within the SWCNT network. The resistance changes are measured through an electrical circuit integrated into the electronic glove. Increasing strain (while holding the ball) results in a noticeable rise in resistance while decreasing strain (when releasing the ball) reduces resistance. The strain data for each finger correlates with the bending radius of curvature of the strain sensors. Around 1.7 seconds, the strain data rises as

all five fingers exert pressure on the ball. The strain distribution across the fingers is uneven due to the varying pressures applied by different fingers to the ball. At 4 sec, the strain data decreases as the external pressure from all five fingers is released from the ball. These observations indicate that the e-glove based on SWCNTs/PDMS strain sensors can be used in soft robotics to provide real-time feedback and control for soft robots, making them more adaptive, responsive, and capable of handling a wide range of applications such as human-machine interface.

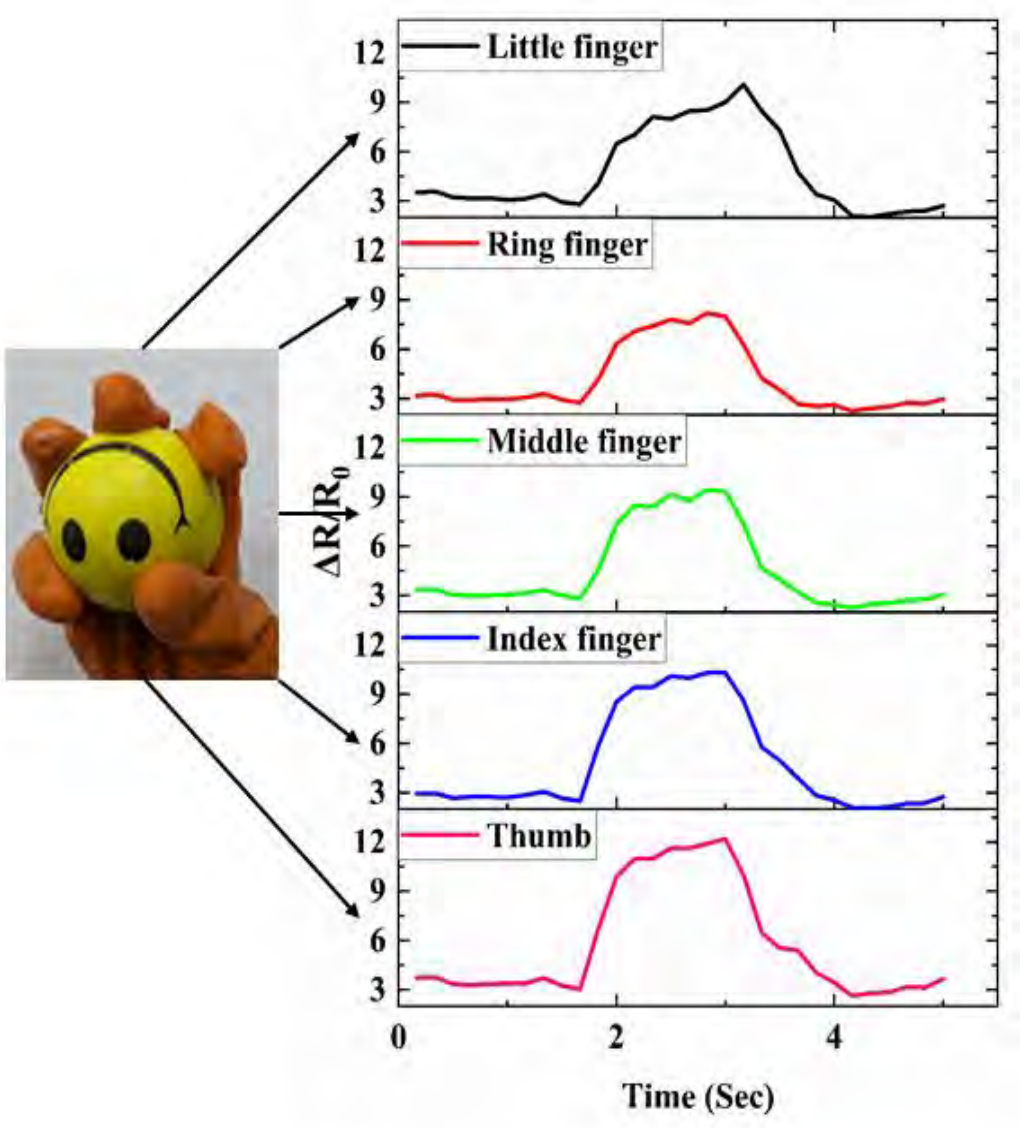

Figure 5.23. The resistance changes while holding and releasing the smiley face squeeze ball placed within the fingers of the glove.

5.3.7 SWCNTs/PDMS strain sensor for HMI application

The fabricated e-glove is worn on the right hand to record finger gesture via SWCNTs/PDMS-based strain sensor. It is shown in figure 5.24 (a-f) that the hand gestures successfully control the robot fingers. The successful dynamic control of the robot hand through human finger gestures demonstrates the practicality and potential of the e-glove that we have developed for human-machine interactions.

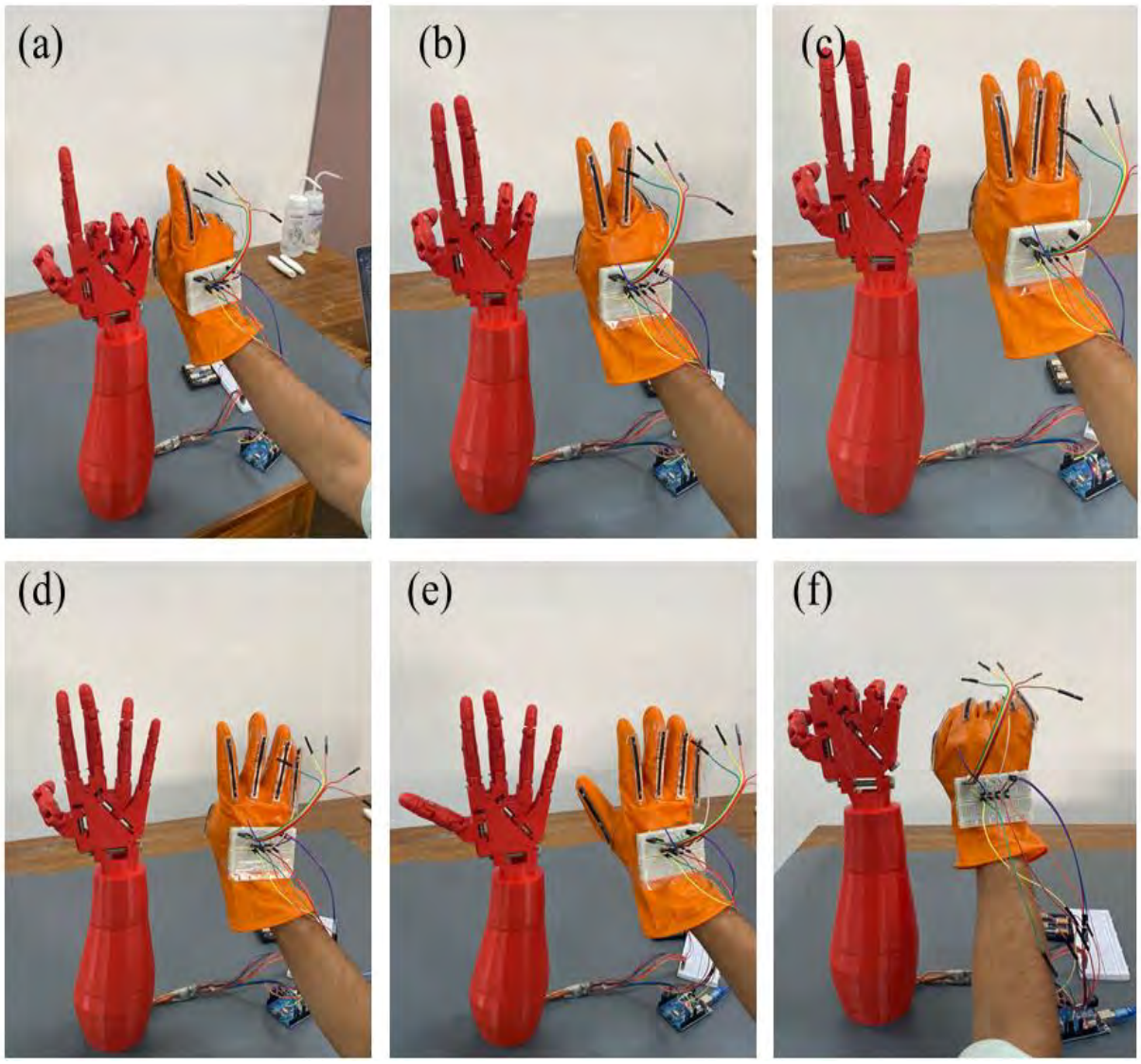

Figure 5.24. (a-f) Photographs were taken while showcasing real-time human-machine interactions of a robotic hand using an SWCNTs/PDMS-based electronic glove-controlled opening and closing of a human finger.

5.4 Conclusions

In this chapter, we presented the fabrication of flexible pressure/ strain sensors based on carbon nanotubes (CNTs). The first part of this chapter examined MWCNTs/PDMS composite properties at various CNT weight ratios (2–10 wt%). The flexible pressure sensor demonstrated high sensitivity (0.02715–0.08283 kPa^{-1}) across a broad pressure range (0.1 to 100 kPa), with the 10-wt% MWCNTs/PDMS variant being the most sensitive. In addition, it was demonstrated that the proposed pressure sensor can also detect human wrist pulse. This sensor offers high conductivity, excellent tensile strength, flexibility, and strain sensitivity for applications like e-skin, robotics, and wearable healthcare devices, with potential use in arterial stiffness index estimation via wrist pulse detection. The second part of this chapter focuses on developing a novel SWCNT/PDMS-based e-glove for Human-Machine Interface applications. The fabrication process, mechanical and electrical performance, and potential strain sensor applications are comprehensively discussed. The gauge factor of the strain sensor is 73, which shows that the sensor is sensitive enough for finger gesture detection. The strain distribution was recorded by the e-glove when holding or releasing the soft object. Experiment results demonstrated that the e-glove embedded with SWCNT/PDMS strain sensors can successfully control the robot finger.

References

[1] B. Zazoum, K. M. Batoo, and M. A. A. Khan, "Recent advances in flexible sensors and their applications," *Sensors*, vol. 22, no. 12, p. 4653, 2022.

[2] Z. Ma, Y. Zhang, K. Zhang, H. Deng, and Q. Fu, "Recent progress in flexible capacitive sensors: Structures and properties," *Nano Materials Science*, 2022.

[3] F. S. Irani et al., "Graphene as a piezoresistive material in strain sensing applications," *Micromachines*, vol. 13, no. 1, p. 119, Jan. 2022.

[4] M. Panth et al., "Flexible zinc oxide nanowire array/graphene nanohybrid for high-sensitivity strain detection," *ACS Omega*, vol. 5, no. 42, pp. 27359–27367, Oct. 2020.

[5] W. Xu et al., "A sprayed graphene pattern-based flexible strain sensor with high sensitivity and fast response," *Sensors*, vol. 19, no. 5, p. 1077, Mar. 2019.

[6] Y. Liu et al., "Flexible, stretchable sensors for wearable health monitoring: Sensing mechanisms, materials, fabrication strategies and features," *Sensors*, vol. 18, no. 2, p. 645, 2018.

[7] K. Leemets, U. Mäeorg, A. Aabloo, and T. Tamm, "Effect of contact material and ambient humidity on the performance of MWCNT/PDMS multimodal deformation sensors," *Sens. Actuators A, Phys.*, vol. 283, pp. 1–8, Nov. 2018.

[8] S. J. Lim, H. S. Lim, Y. Joo, and D.-Y. Jeon, "Impact of MWCNT concentration on the piezo-impedance response of porous MWCNT/PDMS composites," *Sens. Actuators A, Phys*., vol. 315, Nov. 2020.

[9] B. Wang et al., "Flexible and stretchable metal oxide nanofiber networks for multimodal and monolithically integrated wearable electronics," *Nature Commun*., vol. 11, no. 1, pp. 1–11, Dec. 2020.

[10] C. Ji et al., "Highly sensitive wearable flexible pressure sensor based on conductive carbon black/sponge," *IEEE Trans. Electron Devices*, vol. 68, no. 10, pp. 5198–5203, Oct. 2021.

[11] O.-N. Hur, J.-H. Ha, and S.-H. Park, "Strain-sensing properties of multiwalled carbon nanotube/polydimethylsiloxane composites with different aspect ratio and filler contents," *Materials*, vol. 13, no. 11, p. 2431, May 2020.

[12] X. Fu et al., "Stretchable strain sensor facilely fabricated based on multi-wall carbon nanotube composites with excellent performance," *J. Mater. Sci*., vol. 54, no. 3, pp. 2170–2180, Feb. 2019.

[13] H. Kim, S.-K. Hong, J.-K. Ryu, and S.-H. Park, "Effect of filler alignment on piezo-resistive and mechanical properties of carbon nanotube composites," *Materials*, vol. 13, no. 11, p. 2598, Jun. 2020.

[14] R. Ramalingame, N. Udhayakumar, R. Torres, I. T. Neckel, C. Müller, and O. Kanoun, "MWCNT-PDMS nanocomposite based flexible multifunctional sensor for health monitoring," *Proc. Eng*., vol. 168, pp. 1775–1778, Jan. 2016.

[15] J. Lee et al., "Transparent, flexible strain sensor based on a solution-processed carbon nanotube network," *ACS Appl. Mater. Interfaces*, vol. 9, no. 31, pp. 26279–26285, Jul. 2017.

[16] K. Thiyagarajan, G. K. Rajini, and D. Maji, "Flexible, highly sensitive paper-based screen printed MWCNT/PDMS composite breath sensor for human respiration monitoring," *IEEE Sensors J.*, vol. 21, no. 13, pp. 13985–13995, Jul. 2021.

[17] K. Huang et al., "Ultrasensitive MWCNT/PDMS composite strain sensor fabricated by laser ablation process," *Compos. Sci. Technol.*, vol. 192, May 2020, Art. no. 108105.

[18] S. Hong, S. Lee, and D.-H. Kim, "Materials and design strategies of stretchable electrodes for electronic skin and its applications," *Proc. IEEE*, vol. 107, no. 10, pp. 2185–2197, Oct. 2019.

[19] O. Kanoun et al., "Review on conductive polymer/CNTs nanocomposites based flexible and stretchable strain and pressure sensors," *Sensors*, vol. 21, no. 2, p. 341, 2021.

[20] Y. Liu et al., "High-performance and wearable strain sensors based on graphene microfluidics and serpentine microchannels for human motion detection," *Microelectronic Engineering*, vol. 231, p. 111402, 2020.

[21] Y. Duan et al., "Bioinspired spinosum capacitive pressure sensor based on CNT/PDMS nanocomposites for broad range and high sensitivity," *Nanomaterials*, vol. 12, no. 19, p. 3265, Sep. 2022.

[22] K.-H. Kim et al., "Wearable resistive pressure sensor based on highly flexible carbon composite conductors with irregular surface morphology," *ACS Appl. Mater. Interfaces*, vol. 9, no. 20, pp. 17499–17507, May 2017.

[23] T. M. de Rijk and W. Lang, "Low-cost and highly sensitive pressure sensor with mold-printed multi-walled carbon nanotubes dispersed in polydimethylsiloxane," *Sensors*, vol. 21, no. 15, p. 5069, Jul. 2021.

[24] Y. Su et al., "Piezoresistive electronic-skin sensors produced with self-channeling laser microstructured silicon molds," *IEEE Trans. Electron Devices*, vol. 68, no. 2, pp. 786–792, Feb. 2021.

[25] H. Zhong et al., "Large-area flexible MWCNT/PDMS pressure sensor for ergonomic design with aid of deep learning," *Nanotechnology*, vol. 33, no. 34, Aug. 2022.

[26] L. Yang et al., "Development of a highly sensitive, broad-range hierarchically structured reduced graphene oxide/PolyHIPE foam for pressure sensing," *ACS Appl. Mater. Interfaces*, vol. 11, no. 4, pp. 4318–4327, Jan. 2019.

[27] A. Chortos and Z. Bao, "Skin-inspired electronic devices," *Mater. Today*, vol. 17, no. 7, pp. 321–331, 2014.

[28] J. Qiu et al., "Rapid-response, low detection limit, and high-sensitivity capacitive flexible tactile sensor based on three-dimensional porous dielectric layer for wearable electronic skin," *ACS Appl. Mater. Interfaces*, vol. 11, no. 43, pp. 40716–40725, Oct. 2019.

[29] Q. Li et al., "Highly sensitive and flexible piezoresistive pressure sensors based on 3D reduced graphene oxide aerogel," *IEEE Electron Device Lett*., vol. 42, no. 4, pp. 589–592, Apr. 2021.

[30] F. B. Kadumudi et al., "The manufacture of unbreakable bionics via multifunctional and self-healing silk–graphene hydrogels," *Advanced Materials*, vol. 33, no. 35, p. 2100047, 2021.

[31] C. Yan et al., "Highly stretchable piezoresistive graphene–nanocellulose nanopaper for strain sensors," *Advanced Materials*, vol. 26, no. 13, pp. 2022-2027, 2014.

[32] S. S. Mechael et al., "Ready-to-wear strain sensing gloves for human motion sensing," *iScience*, vol. 24, no. 6, 2021.

[33] S. Lee et al., "A knitted sensing glove for human hand postures pattern recognition," *Sensors*, vol. 21, no. 4, p. 1364, 2021.

[34] M. Rani et al., "Recent advancement and challenges in multifunctional carbon nanotube buckypaper and its composites for energy storage and conversion applications," *Journal of Energy Storage*, vol. 73, p. 109063, 2023.

[35] I. V. Novikov et al., "Multifunctional elastic nanocomposites with extremely low concentrations of single-walled carbon nanotubes," *ACS Applied Materials & Interfaces*, vol. 14, no. 16, pp. 18866-18876, 2022.

[36] S. Zhu et al., "High-quality single-walled carbon nanotube films as current collectors for flexible supercapacitors," *Journal of Materials Chemistry A*, 2023.

[37] A. Khalid et al., "Single-chirality of single-walled carbon nanotubes (SWCNTs) through chromatography and its potential biological applications," *New Journal of Chemistry*, vol. 47, no. 3, pp. 992-1022, 2023.

[38] H. R. Lim et al., "Advanced soft materials, sensor integrations, and applications of wearable flexible hybrid electronics in healthcare, energy, and environment," *Advanced Materials*, vol. 32, no. 15, p. 1901924, 2020.

Chapter: 6 Conclusion and Future Work

This chapter consolidates the research findings, emphasizing the exploration of simple and cost-effective fabrication methods for developing flexible strain/pressure sensors and dry electrodes using carbon nanomaterials in the context of wearable electronic applications. The primary objective of this thesis is to investigate the fabrication methods, delving into critical aspects of the design and fabrication of graphene and carbon nanotube (CNT) based flexible sensors and dry electrodes. In this work, we have analyzed the performance of developed flexible devices, including sensors and dry electrodes, for various real-time sensing applications in wearable electronics.

6.1 Conclusion

Graphene and carbon nanotubes are anticipated to open a new era in wearable electronics due to their remarkable properties. These materials enable the production of flexible devices, sensors, dry electrodes, and a range of other products that are foldable, stretchable, and highly flexible, poised to make a significant impact in the market. In chapter 2, recent literature on flexible strain/pressure sensors and dry electrodes employing carbon nanomaterials and their applications in wearable electronics was thoroughly reviewed. A comprehensive analysis of the advantages and disadvantages highlighted in various studies was conducted, resulting in the development of a novel perspective on strain/pressure sensors utilizing graphene and carbon nanotubes.

In Chapter 3, the successful development of a flexible PDMS substrate and graphene synthesis by a simple and cost-effective method, achieved through the utilization of the modified Hummers method and chemical vapor deposition method, respectively, is detailed. A multilayer graphene PDMS-based flexible strain sensor was fabricated using the wet transfer method. In contrast, rGO/PDMS-based dry electrodes were fabricated using the spray coating. The resulting flexible PDMS substrate, strain sensors and dry electrodes were comprehensively characterized using various characterization techniques.

In chapter 4, we have successfully developed the graphene-based flexible strain sensors and dry electrodes. Subsequently, we showcased their practical applications in wearable electronics. The GNP/PDMS strain sensor exhibited good performance in terms of device parameters such as sensitivity, stability and repeatability, particularly in detecting human motions and wrist pulse. The GNP/PDMS strain sensor demonstrated the ability to capture gentle touch with high sensitivity, a feature highly coveted for applications such as flexible screens and human-machine interfaces. Furthermore, the potential applications of the developed flexible sensors were showcased by using a prepared multilayer graphene/PDMS flexible strain sensor in human motion detection. Integration of rGO as a flexible dry electrode with PDMS was achieved for monitoring electrophysiological signals. The fabricated electrodes revealed the excellent adhesion between the rGO and PDMS. The rGO dry electrodes were directly applied to the skin on healthy human arms without the need for skin preparation. Operating in conjunction with a data acquisition system, these rGO dry electrodes demonstrated the capability to acquire electrophysiological signals similar to the conventional Ag/AgCl electrodes, which are typically disposable and for single-time use. Finally, we have validated the continuous and long-term electrophysiological signal acquisition using the rGO electrodes, highlighting their potential for practical and sustainable applications in electrophysiological monitoring.

In chapter 5, we successfully developed carbon nanotube-based flexible sensors. Recognizing the well-known challenge of achieving uniform dispersion of CNTs in the PDMS matrix, we addressed this issue through a series of trial experiments, resulting in significant improvements to the conventional solution process fabrication methods for both MWCNTs/PDMS and SWCNTs/PDMS composites. A flexible pressure sensor based on MWCNTs/PDMS composite was fabricated to detect the human wrist pulse for electronic skin application. The mechanical and electrical properties of the MWCNT/PDMS composite at different weight ratios of CNTs (2, 4, 6, 8, and 10 wt %) were systematically determined. The pressure sensor was thoroughly characterized regarding sensing performance, including sensitivity, hysteresis, and durability. The pressure sensor exhibited ultrahigh sensitivity (0.02715–0.08283 $kPa^{-1)}$ over a large pressure sensing range from 0.1 to 100 kPa with linear sensing capability. The 10-wt% MWCNT/PDMS composite was found to exhibit the highest sensitivity to the pressure measurement. A novel SWCNT/PDMS-based e-glove was also successfully

fabricated for human-machine interface applications. The fabrication process, mechanical and electrical performance, and potential strain sensor applications are comprehensively discussed. The strain sensor demonstrated a gauge factor of 73, showcasing sensitivity sufficient for finger gesture detection. Furthermore, the glove's capability to record strain distribution when holding or releasing a soft object was demonstrated. Experimental results demonstrated that the e-glove embedded with SWCNT/PDMS strain sensors successfully controlled the robot finger, emphasizing the potential of this e-glove in enhancing human-machine interactions.

Table 6.1 summarizes the fabricated sensors and dry electrodes' materials, fabrication methods, and performance parameters. It summarises the developed flexible sensors and dry electrodes, highlighting their effectiveness in various applications, including health monitoring, human motion detection, electronic skin, human-machine interface, and electrophysiological signal monitoring.

Table 6.1 Summary of the developed flexible sensors, dry electrodes, materials, fabrication methods, performance parameters and applications developed and discussed in this thesis.

Fabricated Sensors	**Conductive Materials**	**Fabrication Method**	**Working Range**	**Sensitivity/ (GF)**	**Applications**
GNP/PDMS based strain sensor	GNP	Screen printing	65 % Strain	62.5	Health monitoring
LPCVD/PDMS graphene based strain sensor	Graphene	Wet – transfer method	------	------	Human motion detection
MWCNTs/PDMS based pressure sensor	MWCNT	Solution process method	0.1 to 100 kPa	0.0828 kPa^{-1}	Electronic-skin
SWCNTs/PDMS based strain sensor	SWCNT	Solution process and screen printing	70 % Strain	73	Human-machine interface
rGO/PDMS based dry electrode	rGo	Spray coating method	------	------	Electrophysiological signal monitoring

6.2 Future work

In this work, we successfully demonstrated the monitoring of various bio-signals such as human motion, wrist pulse, ECG and EMG using the fabricated flexible strain/pressure sensors and flexible dry electrodes. We have also proposed novel fabrication methods and strategies to enhance these devices wearable comfort, conducting a comprehensive analysis of the devices characteristics to evaluate their performance. Despite these achievements, the biggest challenge in advancing flexible electronics lies in developing facile, large-scale, cost-effective strategies for their practical applications in bio-signal monitoring. In order to continue and enhance the work presented in this thesis, there are various possibilities to improve the current work by the following suggestions for future work.

- The fabrication methods introduced in this thesis can also be utilized in the fabrication of different types of functional materials, such as flexible and wearable sensors, on different flexible substrates to expand the range of potential applications, such as bio-sensing and electrochemical sensing.

- Investigating the integration of smart materials into flexible devices to expand their capabilities. The exploration of materials featuring responsive attributes, such as self-healing properties or adaptive sensing, can substantially enhance these devices' robustness and functionality. A key focus for future research is improving the conductivity, stability, and durability of conductive carbon nanomaterials. This enhancement is poised to make them applicable across various future technologies, including flexible batteries, solar cells, supercapacitors, piezoelectric and triboelectric nanogenerators, wireless communications, and flexible antennas.

- Investigate the development of multimodal sensing systems that combine different types of sensors on a single platform. This could lead to more comprehensive and versatile wearable devices capable of simultaneously monitoring various physiological and electrophysiological parameters.

- The electrical connection between all developed sensors and the data logger was established through electrical wires, leading to certain measurement challenges like signal instability and difficulties in handling the wires when many sensors are tested simultaneously. To address these issues, future efforts will focus on designing a wireless unit to make reading out data from the sensor more straightforward and faster.

- The sensors and dry electrodes utilized in this thesis are fabricated through solution processes, screen printing, and spray coating methods for various applications in wearable electronics. However, the current methods involve multiple intermediate steps. To address this challenge, alternative fabrication techniques like inkjet printing will be explored to streamline the process.

- In order to achieve skin-friendly, hypoallergenic, and suitable wear for extended periods, the development of dry electrodes is crucial, particularly in medical and health monitoring contexts. Exploring the processing and analysis of electrophysiological signals, such as ECG and EMG, is essential for a deeper understanding of vital sign functionality and early disease detection. Emphasis should be placed on enhancing the biocompatibility of flexible dry electrodes to ensure prolonged and comfortable usage. Additionally, integrating power systems, data processing units, and wireless communication with advanced sensors and dry electrodes is necessary for enabling personalized, remote, and continuous monitoring of bio-signals within the healthcare system.

List of Patents/Publications

Patent filed:

1. **Suraj Baloda**, Sashank Krishna Sriram, Navneet Gupta "RGO-PDMS dry electrodes for long-term health monitoring" Indian Patent, Application no 202311058897, Filed on 05/09/2023.

Publication in Peer Reviewed Journals:

1. **S. Baloda**, Z. A. Ansari, S. Singh, and N. Gupta, "Development and Analysis of Graphene Nanoplatelets (GNP) Based Flexible Strain Sensor for Health Monitoring Applications," *IEEE Sensors Journal*, vol. 20, no. 22, pp. 13302-13309, 2020.
2. **S. Baloda**, N. Gupta, and S. Singh, "A Flexible Resistive Pressure Sensor based on Multi-Walled Carbon Nanotubes/ Polydimethylosiloxane Composite for Electronic-Skins Application," *IEEE Transactions on Electron Devices*, vol. 69, no. 12, pp. 7011-7018, 2022.
3. **S. Baloda**, S. Krishna Sriram, S. Singh, N. Gupta, "Reduced Graphene Oxide-Polydimethylsiloxane based Flexible Dry Electrodes for Electrophysiological Signal Monitoring" *IEEE Transactions on Nanotechnology (under review)*.
4. **S. Baloda**, S. Krishna Sriram, S. Singh, N. Gupta, "Development of SWCNTs/PDMS Composite Strain Sensors Integrated Smart Glove for Human-Machine Interface Applications" *IEEE Sensors Journal (under review)*.

Publication in Peer Reviewed Conferences:

1. **Suraj Baloda**, Zeeshan Alam Ansari, Sumitra Singh, Navneet Gupta, "Graphene nanoplatelets /PDMS based flexible strain sensors for wearable electronics", *Symposium on Nanomaterial Electronics (SCNE-2019)*, BITS-Pilani, Rajasthan, Nov. 8-9, 2019.
2. **S. Baloda**, N. Gupta, S. Singh "Chemical Vapor Deposited Graphene/PDMS based Flexible Strain Sensor for Human Motion Detection Application" In 2024 *IEEE Applied Sensing Conference (APSCON)*, Goa, India, 2024.
3. **S. Baloda**, N. Gupta, S. Singh "Silicone/Graphene Nanoplatelates based Flexible Strain Sensor for Wearable Electronics" In 2024 *IEEE Applied Sensing Conference (APSCON)*, Goa, India, 2024.

Brief Biography of the Candidate

Mr. Suraj Baloda received the M.Tech. degree in Nanoscience and Nanotechnology from the University of Delhi, India in 2017. During the second year of his M.Tech, he was awarded with a French government scholarship (CFIU-Nanotech) to pursue master's degree in nanophysics at the University of Joseph Fourier, Grenoble, France. In 2017, he qualified the all India CSIR-NET (Council of Scientific and Industrial Research - National Eligibility Test) and was awarded the Junior Research Fellowship (JRF). He joined Birla Institute of Technology and Science (BITS), Pilani as a full time research scholar in January, 2019. Currently, He is working as Senior Research Fellow (SRF) at the Department of Electrical and Electronics Engineering (EEE), BITS, Pilani.

His research interests encompass the fabrication of flexible pressure/strain sensors based on carbon nanomaterials, as well as the development of flexible dry electrodes for applications in structural health monitoring, electrophysiological signal monitoring, and human-machine interface. These sensors and dry electrodes are designed for use in flexible and wearable devices. Additionally, he contributes actively as a reviewer for the IEEE Sensors Journal and IEEE Transactions on Electron Devices.

.

Brief Biography of the Supervisor

Prof (Dr.) Navneet Gupta obtained M.Sc. in Physics-Electronics in 1995 from H.N.B Garhwal Central University (HNBGU), Srinagar with the first rank in the University. He received M.Tech in 1998 from Indian Institute of Technology (IIT-BHU) (formerly ITBHU). In 2005, he completed his doctorate in the area of semiconductor devices from HNBGU. Since 2005, Prof. Gupta has been associated with Birla Institute of Technology and Science (BITS), Pilani. Currently, he is Professor and Head of the Electrical and Electronics Engineering Department (EEE) at BITS-Pilani, Pilani campus, Rajasthan, India. He also served as the Associate Dean of the Sponsored Research and Consultancy Division at the same institute during 2018 to 2022.

Prof. Gupta's research interests encompass the modeling of Micro/Nano Electronic Devices, Flexible and Wearable Electronics, Computational Material Science, and Electromagnetics and Antennas. He has authored 75+ research papers in high-repute international journals and presented 65+ papers at various conferences in India and abroad. He has successfully guided eight PhD students, one National Post-Doctoral Fellow (NPDF), and is currently supervising two PhD candidates. Prof. Gupta has secured research funding from various government agencies, including UGC, DST, SERB, DRDO, and MHRD. Additionally, he has authored five textbooks in the field of Electrical Engineering, Engineering Physics, and Materials Science, published by international and national publishers.

Prof. Gupta received several awards, including the *Prof. S. S. Ranganthan Memorial Teaching Excellence Award 2022* by BITS Pilani, the *Outstanding Engineering Services to Society Award* by the Institution of Engineers (India), Rajasthan State Centre, and the DST *Young Scientist Award* in Physical Sciences. He holds a Gold Medal in Master's degree and has been honored with the *Bharat Jyoti Award*. He is a Fellow of the Institution of Engineers (India), a Senior Member of IEEE, and a life member of renowned professional bodies such as the Semiconductor Society of India, Material Research Society of India (MRSI), and Optical Society of India (OSI). Prof. Gupta serves as an expert reviewer for many reputed international journals, including IEEE, Springer, Elsevier, and IE (I).

Brief Biography of the Co-Supervisor

Dr. Sumitra Singh is Principal Scientist in the Semiconductor Sensors and Microsystems Group at the Council of Scientific and Industrial Research–Central Electronics Engineering Research Institute (CSIR–CEERI) in Pilani, Rajasthan. Previously, she was associated with the Flexible and Non-Silicon Electronics Group at CSIR-CEERI, Pilani. She obtained Ph.D. from Devi Ahilya Vishwavidyalaya (DAVV), Indore, in 2010, and she possesses over 16 years of research experience. Dr. Singh has authored and presented more than 60 papers in reputable journals and conferences, focusing on GaN/InGaN LEDs/Solar cells and flexible sensors. Her research interests include Graphene-based flexible electronics, Nano-biosensors, Organic semiconductors, thin-film solar cells, and III-V semiconductor devices. Currently, she is dedicated to the field of flexible electronics for human health monitoring and robotic applications.

Dr. Singh has successfully led and completed various research projects, including "Fabrication of Silicon Carbide Power Diodes," funded by RIC-DRDO, and "Development of new generation nano metal-oxide/graphene-polymer composite materials for use in wearable electronics," funded by CSIR. She is currently involved in an ongoing research project titled "Development of Graphene-Based Flexible and Wearable Strain Sensors for Prosthetic Hand Application," funded by SERB (Power Grant). Additionally, Dr. Sumitra Singh is a life member of several esteemed professional societies, including the Metrology Society of India (MSI), Optical Society of India (OSI), Indian Physics Association (IPA), Semiconductor Society of India (SSI), and the Institution of Electronics and Telecommunication Engineers (IETE).